DATA-DRIVEN DISTRIBUTIONALLY ROBUST OPTIMIZATION FOR RESILIENT MARITIME LOGISTICS SYSTEMS UNDER UNCERTAINTY

XU XIN

PhD

The Hong Kong Polytechnic University

This programme is jointly offered by

The Hong Kong Polytechnic University

and

Tongji University

2025

The Hong Kong Polytechnic University
Department of Logistics and Maritime Studies

Tongji University
School of Economics and Management

Data-driven distributionally robust optimization for resilient maritime logistics systems under uncertainty

Xu Xin

A thesis submitted in partial fulfilment of
the requirements for the degree of
Doctor of Philosophy

September 2025

Certificate of Originality

I hereby declare that this thesis is my own work and that, to the best of my knowledge and belief, it reproduces no material previously published or written, nor material that has been accepted for the award of any other degree or diploma, except where due acknowledgement has been made in the text.

_______________________________(Signed)

_________XIN Xu_________(Name of student)

Dedication

I would like to dedicate this thesis to my parents,

who were there when no one was.

I also dedicate this thesis to all

who have loved, guided,

and believed

in me.

Abstract

The maritime industry is intricately linked to global political and economic conditions, making its inherent uncertainties a central concern for both academia and industry. Recent years have seen a surge in unforeseen events (e.g., the COVID-19 pandemic), frequently subjecting stakeholders to volatile container transportation demand, port congestion, and shipment delays. In this context, the development of a maritime logistics system capable of maintaining an acceptable level of maritime service continuity in the face of uncertainty—or, more specifically, the establishment of a *resilient maritime logistics system*—has become a critical measure for enhancing global supply chain resilience.

Motivated by the above background, this thesis addresses the crucial challenge of improving the resilience of maritime logistics systems under two primary uncertain factors: (1) *uncertain vessel delay times* and (2) *uncertain container transportation demand*. In order to comprehensively enhance the resilience of various elements within the maritime logistics system (i.e., ports and shipping routes), this thesis investigates three distinct problems. The first problem is berth allocation (landside problem), with a focus on improving port operation resilience. The second problem is liner fleet deployment (seaside problem), with a focus on improving shipping route resilience. The third problem is the joint optimization of liner fleet deployment and slot allocation (seaside problem), with a focus on improving shipping route resilience. Through three interconnected studies, detailed in Chapters 3 to 5, we develop novel distributionally robust optimization (DRO) frameworks that effectively mitigate the limitations of traditional stochastic programming (SP) and robust optimization (RO) modeling approaches. Furthermore, we design customized algorithms and acceleration strategies to efficiently solve large-scale problems.

First, we present a distributionally robust chance-constrained (DRCC) model with a type-1 Wasserstein ambiguity set to address the landside berth allocation problem under vessel arrival time uncertainty in Chapter 3. This model

overcomes the conservatism of robust optimization and eliminates the distributional assumption requirement of stochastic programming. Numerical experiments validate that introducing acceleration strategies, i.e., sample average approximation constraints and coefficient strengthening techniques, significantly reduce program running time. Extensive sensitivity analyses reveal how pre-defined service levels in the chance constraint and ambiguity set radii impact operational decisions. We also compare the effects of employing a joint chance constraint versus several independent chance constraints on the solution. The out-of-sample analysis results demonstrate the strong out-of-sample performance of our DRCC model while meeting port service requirements.

Then, for the seaside liner fleet deployment problem under container transportation demand uncertainty, we propose a data-driven DRCC model also adopting a type-1 Wasserstein ambiguity set in Chapter 4. This approach minimizes the total operational costs for liner companies while ensuring that the capacity deployed to each route meets transportation demand through a joint chance constraint. We reformulate the DRCC model into a mixed integer programming model, accelerating its solution through introducing sample average approximation constraints and several valid inequalities. Sensitivity analysis on the ambiguity set radius and the pre-defined service level in the joint chance constraint is conducted. Moreover, we compare the optimal solutions obtained by stochastic programming and robust optimization with solution obtained by the DRCC model. The out-of-sample test results confirm that liner companies can achieve a higher rate of transportation demand fulfillment based on the DRCC model, and our DRCC model outperforms robust optimization model (by avoiding excessive conservatism) and stochastic programming model (by preventing optimization bias).

Finally, to jointly optimize liner fleet deployment and slot allocation under container transportation demand uncertainty, we establish a two-stage distributionally robust model with two ellipsoidal ambiguity sets in Chapter 5. Similar to the model in Chapter 4, this distribution-free framework also

incorporates a joint chance constraint to ensure that the weekly container transportation demands of contract shippers are met to a given service level. We reformulate the original model into a second-order cone model (SOCM), which is efficiently solved via a customized outer approximation algorithm. Sensitivity analyses are performed on several key parameters, including the ambiguity set radius, the mean and covariance of contract demand, and liner capacity. Out-of-sample comparisons empirically verify the superiority of our DRO model.

Collectively, these studies contribute to the field of maritime logistics system by providing cutting-edge modelling tools and DRO frameworks to address critical operational challenges under uncertainty. The developed models and algorithms offer practical solutions for enhancing the resilience of maritime logistics systems, directly supporting stakeholders in navigating volatile market conditions and improving the robustness of global maritime supply chains.

Keywords: liner shipping; fleet deployment; slot allocation; berth allocation; demand uncertainty; vessel arrival uncertainty; distributionally robust optimization; joint chance constraints; outer approximation algorithm; sample average approximation constraints; valid inequalities

Publications arising from the thesis

1. Chen, K., Guo, J., **<u>Xin, X.</u>**, Zhang, T., & Zhang, W. (2023). Port sustainability through integration: A port capacity and profit-sharing joint optimization approach. *Ocean & Coastal Management*, *245*, 106867.
2. Chen, K., Yi, X., **<u>Xin, X.</u>**, & Zhang, T. (2023). Liner shipping network design model with carbon tax, seasonal freight rate fluctuations and empty container relocation. *Sustainable Horizons*, *8*, 100073.
3. Gao, L., Wang, X., & **<u>Xin, X.</u>** (2025). Channel Selection Strategies of Chinese E-Commerce Supply Chains Under Green Governmental Subsidies. *Systems*, *13*(3), 172.
4. Li, Z., Wang, L., Wang, G., **<u>Xin, X.</u>**, Chen, K., & Zhang, T. (2024). Investment and subsidy strategy for low-carbon port operation with blockchain adoption. *Ocean & Coastal Management*, *248*, 106966.
5. Liu, M., **<u>Xin, X.</u>**, Wang, X., Zhang, T., & Chen, K. (2025). Dual-channel slot sales strategy for container liner shipping companies with blockchain technology adoption. *Transport Policy*, *162*, 200–220.
6. Xiang, Z., **<u>Xin, X.</u>**, Zhang, T., Chen, K., & Liu, M. (2025). Asia–Europe liner shipping network design model considering Arctic route and black carbon tax. *Ocean & Coastal Management*, *261*, 107492.
7. **<u>Xin, X.</u>**, Wang, S., & Zhang, T. (2025). Truck-drone supported humanitarian relief logistics network design: A two-stage distributionally robust optimization approach. *Transportation Research Part C: Emerging Technologies*, Accepted.
8. **<u>Xin, X.</u>**, Zhang, T., Wang, X., He, F., & Wu, L. (2025). Risk-averse distributionally robust optimization for construction waste reverse logistics with a joint chance constraint. *Computers & Operations Research*, *173*, 106829.
9. **<u>Xin, X.</u>**, Zhang, T., Xiang, Z., & Liu, M. (2025). Battery electric vehicle

transportation network robust pricing-infrastructure location model with boundedly rational travelers. *Applied Energy*, *386*, 125606.

Acknowledgements

Completing this doctoral journey has been a profound experience, and it is with deep gratitude that I acknowledge those who made this achievement possible.

First and foremost, I extend my sincerest appreciation to my doctoral supervisors, Prof. Shuaian (Hans) Wang of the Department of Logistics and Maritime Studies at The Hong Kong Polytechnic University, and Prof. Xiaoli Wang of the School of Economics and Management at Tongji University. Prof. Shuaian (Hans) Wang, whom I deeply respect, embodies academic excellence through his rigorous scholarship, innovative thinking, and exceptional efficiency. His prompt and insightful responses to my queries, coupled with his meticulous and constructive revisions of my several manuscripts, have been invaluable to my growth. He leads by example, demonstrating that "*actions speak louder than words*," and has inspired me to strive for excellence in all endeavors. To Prof. Xiaoli Wang, my supervisor since I joined Tongji University in 2018: Thank you for continually guiding me toward compelling research directions and thought-provoking research questions. Beyond academia, your genuine care for my well-being—especially your reminders to prioritize health amidst the demands of doctoral studies—has touched me deeply. Your unwavering support has shaped both my academic and personal journey.

I owe immense gratitude to mentors and peers who illuminated my path. My profound thanks go to Prof. Zhongzhen Yang (Faculty of Maritime and Transportation, Ningbo University, China), my earliest academic guide. Prof. Yang, when you were still at Dalian Maritime University, your earnest mentorship during the *11th National Competition of Transport Science and Technology for Students* (NACTranS) in 2016 and the *12th NACTranS* in 2017 opened a window to the world of scholarly pursuit—an inspiration that directed my future trajectory. To Prof. Kang Chen (School of Maritime Economics and Management, Dalian Maritime University, China): Your patient instruction, beginning in my sophomore year, fundamentally shaped my academic literacy. Through your meticulous guidance on academic writing and data visualization, you equipped me with foundational skills indispensable to research. Without both professors' nurturing, I would never have embarked on this scholarly journey. I also thank Tao Zhang (School of Economics and Management, Tongji University, China), my peer and indispensable collaborator. Countless ideas crystallized through our vibrant discussions, and our collaboration over recent years has resulted in more than a dozen co-authored publications. Your intellectual companionship has broadened my horizons and enriched this journey. I would also like to thank my classmate Miaohui Liu (School of Economics and Management, Tongji University, China), who is also a PhD student supervised by Prof. Xiaoli Wang in Tongji. Our collaborative work on blockchain applications in maritime shipping supply chains introduced me to transformative methodologies and opened new avenues of inquiry.

Finally, my deepest love and gratitude belong to my family. Throughout the pressures of my doctoral studies, my parents and grandparents never added to my burdens. Instead, they provided constant encouragement, understanding, and a nurturing home environment that allowed me to thrive. Your unconditional love has been the bedrock of my resilience and the driving force behind my pursuit of knowledge. You are my eternal pillars of strength.

As this seven-year chapter draws to a close, words feel insufficient to express the depth of my appreciation. I dedicate this dissertation as a humble token of gratitude to all who have loved, guided, and believed in me.

Table of contents

List of figures

List of tables

Chapter 1: Introduction

1.1. Background

Maritime transportation plays a major role in global trade, representing approximately 70% of the global trade value and over 80% of the total number of traded goods (Meng et al., 2014). Its inherent economies of scale and comparatively lower carbon intensity per ton-mile reinforce its dominance in transcontinental logistics networks (Li et al., 2024b; Meng & Wang, 2012). Even during the COVID-19 pandemic, world container transportation volume declined by only 1.2% (Notteboom et al., 2021). The freight rate of container liner shipping between ports in China and Europe reached a 4-year record in the second half of 2020. Currently, cargos can be picked up and delivered to nearly all corners of the world efficiently. Thus, it is not surprising that scientific maritime logistics systems design has become a focus of attention in recent years in both academia and industry (Christiansen et al., 2020).

However, since the maritime industry is often involved in transporting cargo across continents, its rise and fall are usually highly correlated with the world's political and economic situation (Zhang et al., 2025). Over the past three years, the majority of maritime stakeholders have encountered a series of challenges, including fluctuating transportation demand and shipment delays (especially during the COVID-19 pandemic). In this context, how to fully respond to the inherent uncertainties in maritime transport and achieve the *resilience*[1] of port and shipping services has become an important topic of concern to academia and industry (Zhang et al., 2025).

Motivated by the above background, the research objective of this thesis is to achieve a design of resilient maritime logistics systems considering several inherent uncertain factors. The maritime logistics system is a vehicle for the realization of maritime transportation of goods, consisting of several nodes (i.e., ports) and edges (i.e., shipping routes). The cargos produced in the hinterland are loaded onto vessels through the port, a key node connecting the landside and the seaside, and then complete spatial displacement through the vessel traveling on the shipping route and arrive at the destination port. This shows that to enhance the resilience of the maritime logistics system, we can (1) start from the optimization of port operations on the landside, or (2) from the optimization of shipping route operations on the seaside.

Following this idea, this thesis conducts a series of studies. First, this thesis focuses on the berth allocation problem (BAP) considering uncertainty. In practice, vessel berthing operations frequently encounter various uncertainties, such as weather conditions (Luo et al., 2024) and mechanical failures (Lv & Gao, 2023). These uncertainties can easily cause delays in vessel arrivals and cargo operations, which may lead to port congestion and, in severe cases, terminal

[1] Here, “resilience” refers to the ability of operational decisions made by decision makers in ports and shipping services to withstand uncertainty factors.

closures (Wang & Meng, 2012a; Xu et al., 2012). Therefore, our focus is to address the BAP with full consideration of the uncertainty in the vessel arrival time to enhance the resilience of the nodes (i.e., ports) in the maritime logistics system. Second, this thesis focuses on the optimization of shipping route operations on the seaside. Since container transportation accounts for more than 60% of the cargo value (Stopford, 2008), we discuss a fleet deployment problem (LFDP) using container liner shipping as a research object to achieve resilience enhancement of edges (i.e., shipping routes) in the maritime logistics system. Regarding the uncertainties to be considered, we focus more on the uncertainty in container transportation demand that has also garnered significant attention from the academic community. Third, in light of the necessity for liner companies to allocate suitable slots in accordance with their deployed fleet, this thesis concludes with a further emphasis on the liner fleet deployment and slot allocation problem (LFDP-SAP) considering container transportation demand uncertainty. In addition to enabling liner companies to achieve reasonable liner fleet deployment, solving this problem can further help them achieve profitability through slot allocation. Overall, by studying the abovementioned three aspects, this thesis can eventually realize the enhancement of nodes and edges resilience in maritime logistics systems by fully considering uncertainty caused by time and container transportation demand.

Currently, to model the abovementioned multiple sources uncertainties, the mainstream idea of existing research is to adopt stochastic programming (SP) and robust optimization (RO) methods. The premise of using the former method is that the distribution functions of the uncertain parameters must be known. In this way, a series of scenarios can be generated based on known distribution functions, thereby transforming a problem with uncertain parameters (i.e., random variables) into a deterministic one. The method of transforming the SP model by constructing scenarios using samples drawn from a known distribution function is also called the sample average approximation (SAA). However, doing so often results in a phenomenon known as optimization bias. This phenomenon refers to the model's solution performing well only on generated samples (scenarios) but performing poorly under the uncertainty of the real world. The RO method assumes that the values of uncertain parameters are in an uncertain set. The idea of modeling using the RO method focuses on the optimization of the worst-case scenario produced by the uncertain set and often results in overly conservative solutions.

Fortunately, the theory of distributionally robust optimization (DRO) has grown considerably in recent years. Unlike scenario-based SP methods, the DRO technique assumes that the distribution function of a random variable is not clear but is in an ambiguity set (Bertsimas et al., 2019). Moreover, the DRO technique focuses on the optimization of the worst distribution scenario, which can avoid producing overly conservative solutions like the RO method. Overall, the DRO method offers several advantages: (1) This method does not require full information about the distribution function of uncertainty parameter, which can avoid the difficulty of scenario recognition (Snyder, 2006). (2) DRO can use the data at hand to limit the range of random variables (Zhao et al., 2022), which can prevent overly conservative decision-making compared with scenario-based SP and robust optimization (RO) techniques (Xin et al., 2025b; Zhang et al., 2025).

In summary, the research objective of this thesis is to address the inherent uncertainties (i.e., uncertainties time and transportation demand) in maritime logistics systems based on the DRO theory in order to enhance the resilience of both landside system elements (ports) and seaside system elements (shipping routes) of the logistics systems. The relevant results can provide the necessary theoretical basis and decision support for the daily operation of ports and liner companies.

1.2. Thesis outline

The remainder of the thesis is organized as follows. The second chapter of this thesis is a literature review. Through a systematic review of the landside BAP, and the seaside liner shipping network design problem, we identify the current research gaps. Chapter 3 discusses how to use DRO theory to establish an optimization model to address BAP in order to enhance landside resilience of maritime logistics systems. Chapters 4 and 5 focus on the improvement of seaside resilience of maritime logistics systems and model the LFDP and the joint optimization of LFDP and SAP based on the DRO theory. Finally, Chapter 6 concludes this thesis and proposes several future research directions.

Chapter 2:
Literature review

As mentioned in Chapter 1, this thesis considers enhancing the resilience of the maritime logistics system under uncertainty from both the landside and seaside. Therefore, in Chapter 2, we first review the literature related to berth allocation under uncertainty in Section 2.1, since ports and berths are the most typical components of the maritime logistics system on the landside. Then, in Section 2.2, we shift our focus to the seaside. By reviewing the literature associated with liner shipping network design, we explore how current research considers enhancing route resilience under container transportation demand uncertainty.

2.1. Research on berth allocation problem

As a classic problem, the initial research on the berth allocation problem (BAP) discussed in this thesis can be found in Lim (1998). The port terminal layout can be classified into three categories, as proposed by Bierwirth and Meisel (2010), which are illustrated in Fig. 2.1. These categories are discrete BAP, continuous BAP, and hybrid BAP. In the first case, the port has limited berths, and each vessel can choose only one berth. In the continuous case, each vessel can select any position on the wharf for berthing, although a position is typically allocated for vessels with the lowest berthing costs. This approach enables the optimization of wharf space utilization. The hybrid BAP allows multiple vessels to berth at one berth simultaneously, and a large vessel may also occupy multiple berths at the same time. In discrete and hybrid BAP scenarios, the introduction of additional binary variables is typically necessary to ensure the accurate representation of the berth allocation operation of the port terminal.

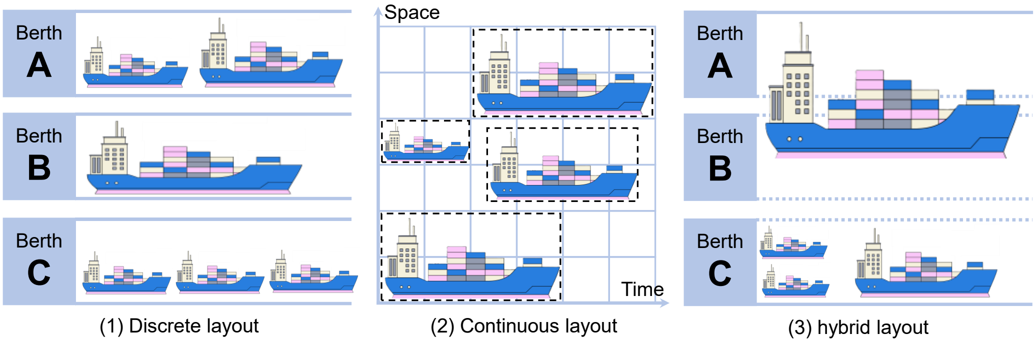

Fig. 2.1 Three types of layouts usually applied in port terminals

BAPs are NP-hard even in a deterministic setting (Agra & Rodrigues, 2022), and the introduction of uncertainty factors makes the solution of such problems even more difficult. A seminal study that focused on BAPs with uncertainty factors was conducted by Moorthy and Teo (2006). For a comprehensive review of the development of BAP research, interested readers may also refer to Bierwirth and Meisel (2010), Rodrigues and Agra (2022) and Li et al. (2024a). According to the above review papers, scholars have expressed the greatest concern with uncertainty factors pertaining to *vessel arrival time* and *cargo handling time* (also known as vessel operation time; see Fig. 4 in Li et al. (2024a)), and this thesis considers only the former as the uncertain parameter. In Chapter 3, we make this setting on the basis of the following three considerations: (i) our deterministic assumption of cargo handling (or vessel operation) times does not affect the model framework, as delays in cargo handling times either have no impact on berthing schedules or can be equivalently converted into delays in vessel arrival times; (ii) considering only one type of time as a random parameter simplifies the use of mathematical notation; and (iii) we can easily adopt a chance-constrained approach to reasonably control the service level of the port by assuming that there is uncertainty in the vessel arrival time.

The approaches for addressing uncertainty in BAPs can be broadly categorized into three groups: (i) the proactive approach, (ii) the reactive approach, and (iii) a combination of the two (also known as the proactive/reactive approach). This categorization is based on how the port manager responds to each type of uncertainty. The proactive approach makes a priori decisions before the start of the planning period (i.e., vessel arrival in the BAP), with the objective of optimizing the berthing schedule by accounting for uncertain parameters. For example, if the port manager formulates a berthing schedule that is feasible under all realizations of uncertain parameters, then this constitutes a proactive approach. Notable studies that employ this approach include those of Zhen (2015), Jia et al. (2020), and Wu and Miao (2021). The reactive approach refers to port managers taking remedial actions after the emergence of unpredicted events, focusing on rescheduling adjustments to mitigate disruption costs when deviations from the baseline plan occur (see Al-Refaie and Abedalqader (2022) for an example). Finally, the proactive/reactive approach divides the port manager’s decision into two stages: the planning stage and the reactive stage. In the planning stage, decision makers consider the impact of uncertainty parameters when designing the berthing schedule and take remedial measures when such uncertainty is discovered in the reactive stage. Overall, proactive approaches usually avoid constant adjustments to the original vessel berthing schedule; passive approaches are more flexible but may result in frequent adjustments to the original schedule. The distributionally robust chance-constrained (DRCC) model we develop in Chapter 4 can be seen as a proactive approach and allows the service level and cost reliability to be balanced by the introduction of the chance constraint.

In terms of modeling methodologies, developing stochastic programming (SP) models and robust optimization (RO) models is a popular choice for modeling BAPs while considering uncertainty, and a small number of papers have adopted (fully) fuzzy programming models (Pérez-Cañedo et al., 2020; Segura et al., 2017) and deterministic models (Lv et al., 2020; Xiang et al., 2018; Zeng et al., 2011a; Zeng et al., 2011b; Zhang et al., 2016). Here, we review the research on mainstream modeling formulations. Moorthy and Teo (2006) established an SP model to optimize berth positions while considering vessel arrival delay. This marks the earliest documented discourse on BAP under uncertainty. To solve this problem, the authors designed a simulated annealing (SA) algorithm based on sequence pairs. In the same year, Zhou et al. (2006) considered vessel arrival time and handling time as stochastic parameters and developed an SP model. The authors assumed that the above random parameters follow a normal distribution, and an algorithm based on the framework of the genetic algorithm was designed to explore the approximate optimal solution to the model. Golias (2011) took service time and vessel delay risk as the bi-objectives of the model and used a heuristic approach (i.e., the 2-PPM algorithm) proposed by Lemesre et al. (2007) to solve the model. Jia et al. (2020) divided vessels into sea vessels and feeders and considered that the service times of the feeders are random parameters. By assuming that the probability density functions (PDFs) of the abovementioned random parameters are known, the authors developed a novel simulation optimization algorithm to solve the model. Unlike previous studies where uncertainty was only used to evaluate solutions, Du et al. (2010) pioneered the first attempt to optimize berth schedules by incorporating uncertain parameters. The authors employed the SA algorithm to solve the deterministic BAP, thereby obtaining a feasible solution. They then calculated the inconsistent cost of vessels and modified the buffer size of vessels in the subsequent iteration. This has led to extensive exploration of the proactive/reactive approach for the BAP in academia, which has given rise to the idea of constructing a two-stage SP to formulate a BAP with uncertainty. For example, Zhen et al. (2011) considered the arrival time of vessels and operation time as uncertain parameters and proposed a meta-heuristic method for large-scale BAP to solve the above problems in large-scale real-world environments. Sheikholeslami and Ilati (2018) discussed a similar research question, but the difference is that the authors integrated tidal factors into the model framework and constructed a two-stage SP model. Under the assumption that the random parameters (i.e., vessel arrival time) follow a lognormal distribution, the authors converted the SP model into a deterministic model via SAA.

One can see that the theoretical basis of constructing the series of SP models in the above studies is to assume that the distribution information of the uncertainty parameters (e.g., vessel arrival time and cargo handling time) is known (or assumed to be known). However, in many cases, it is impossible for decision makers to obtain (or predict) accurate probability information. Therefore, some scholars use the RO method for modeling to avoid inputting the distribution information of random parameters. For example, Xu et al. (2012) established an RO that considers the uncertainties associated with the vessel arrival delay and handling time and designed an algorithm by integrating the SA algorithm and branch-and-bound algorithm. To further consider the trade-offs between different management objectives that decision makers may consider, Zhen and Chang (2012) considered the uncertainty of vessel arrival time and operation time, constructed an RO with two objectives (cost minimization and robustness maximization) and proposed a meta-heuristic to address large-scale instances. Similarly, Xiang et al. (2017) developed a bi-objective RO, but the aim was to balance economic performance and service level. The authors considered arrival and operation times as uncertainties, and an adaptive gray wolf (AGW) algorithm was designed. Xiang and Liu (2021) established an expanded robust optimization model to utilize operation data effectively. It differs from the classic RO in that it introduces multiple uncertainty sets constructed via the *K*-means clustering approach. A customized column-and-constraint generation algorithm was designed by the authors. Some scholars were influenced by Du et al. (2010) and constructed two-stage RO models. For example, Liu et al. (2020) expanded the BAP from one stage to two stages. On the basis of Agra and Oliveira (2018), the authors designed a rolling horizon heuristic (RHH) algorithm to address real-world problems. In Qu et al. (2023), the authors considered tidal and environmental factors (i.e., carbon emissions from different port equipment and vessels) and developed a two-stage RO model.

Recently, scholars have begun to extend DRO theory to BAP modeling to balance the defects of the SP and RO methods. DRO theory was first described in Scarf et al. (1957), but its development has only begun in the last decade. Along with the introduction of chance constraints, constructing DRCC models has gradually become a popular approach to address uncertainty in decision-making problems. Readers interested in DRCCs can refer to Küçükyavuz and Jiang (2022) to learn more about this theory. The assumption of using the DRO-based method is that although the PDF of uncertain parameters is difficult to obtain (or assume), some partial knowledge associated with uncertain parameters can be obtained by collecting daily operating data. On the basis of the above knowledge (e.g., information regarding uncertainty parameters), an ambiguity set can be constructed, which contains a series of distributions of uncertainty parameters. If the cardinality of the ambiguity set is 1, that is, it contains only one possible probability distribution, then the DRO model reduces to the SP model. For a given support, if the constructed ambiguity set incorporates all potential distributions, the DRO model is equivalent to the RO model. Therefore, the SP model and RO model are generalized by the DRO model (Lin et al., 2022; Rahimian & Mehrotra, 2022). Nevertheless, the key to using this method is to choose the ambiguity set appropriately. In this thesis (see Chapter 3), we adopt an ambiguity set based on the statistical distance, which is called the type-1 Wasserstein ambiguity set. The advantages of the Wasserstein ambiguity set and the type-1 Wasserstein metric are discussed in Gao and Kleywegt (2023) and Ho-Nguyen et al. (2023). From a theoretical point of view, adopting the type-1 Wasserstein ambiguity set has the following advantages. First, it inherently accounts for tail events by restricting distributions within a Wasserstein ball around the empirical distribution. This ensures robustness against rare but impactful delays, even if their historical occurrence is limited. Second, vessel delays often follow complex, multimodal distributions influenced by heterogeneous factors (e.g., weather, congestion), which are poorly captured by parametric assumptions. Constructed directly from historical data, Wasserstein sets avoid restrictive parametric assumptions, making them suitable for multimodal or hybrid delay patterns. From a practical point of view, port managers usually require intuitive risk communication (e.g., what worst-case scenarios are considered?). The Wasserstein radius directly quantifies the maximum allowable deviation from historical data. Moment-based uncertainty intervals lack intuitive connections to real-world delay impacts. Notably, the approach developed in this thesis can also be generalized to a moment information-based ambiguity set.

To the best of our knowledge, the paper most similar to Chapter 3 is Agra and Rodrigues (2022), in which the authors regarded the cargo handling time as an uncertain parameter and constructed a two-stage DRO model based on a type-1 Wasserstein ambiguity set (i.e., the so-called Kantorovich ambiguity set in Agra and Rodrigues (2022)). Although the authors attempted to use DRO to conduct a preliminary exploration of BAP, this paper still has the following shortcomings. First, the authors ignore the impact of vessel berthing location on operating costs. In other words, the objective function in Agra and Rodrigues (2022) does not include costs associated with the vessel berthing position. This is equivalent to assuming that each vessel can berth at any position of the wharf, which limits the generalization of the model when discussing discrete and hybrid BAPs (see Fig. 2 in Rodrigues and Agra (2022)). Second, the modeling and solution methods proposed by the authors can be applied only to continuous BAPs. The authors also explain this in their conclusion. If we want to discuss discrete or hybrid BAPs (or consider practical factors, such as tides), the method proposed by the authors is not applicable due to the existence of integer variables. Finally, the algorithm designed by the authors requires calculating the second-stage model corresponding to each scenario in each iteration, which is very time-consuming. In Chapter 3, we address the aforementioned research gaps by focusing on the following aspects: (i) We consider the penalty cost associated with vessel berthing location in the process of model establishment and use the introduced joint chance constraint to achieve a trade-off between the service level and cost. (ii) We propose a standard DRCC model that can be easily extended to model BAPs with discrete layouts. (iii) We design several acceleration strategies to achieve efficient solutions of the DRCC model.

2.2. Research on liner shipping network design

The academic community currently divides the liner shipping network design problem into three interrelated and interacting sub-problems (Wang & Meng, 2017). The first subproblem is called the liner fleet deployment problem (LFDP), which requires liner companies to deploy appropriate classes and numbers of liners for each route. This is a tactical-level decision-making problem. In addition, liner companies may consider optimizing the speed of their liners, chartering in and out, and optimizing the status of their liners (i.e., whether they are in service or in storage). The second sub-problem is known as the service network design problem (SNDP), which is also a tactical-level decision-making problem in which liner companies optimize the port of call and calling sequence of their fleet. The third sub-problem is the slot allocation problem (SAP) at the daily operational level. Liner companies need to make acceptance-rejection decisions on daily orders to accommodate limited liner slots. At first, scholars often studied one of the sub-problems in isolation. Subsequently, with an in-depth understanding of the problem, many studies considering the joint optimization of two or even three sub-problems have been proposed. Readers interested in further information are encouraged to consult the following review paper and references therein: Wang and Meng (2017), Christiansen et al. (2013), and Christiansen et al. (2020). In this thesis, the problem involved in Chapter 4 is LFDP. The problem involved in Chapter 5 is the composite problem of LFDP and SAP. Therefore, this section mainly reviews the research on these two sub-problems and the composite problem composed of different sub-problems.

2.2.1. Research on liner fleet deployment problem

The earliest research on the liner fleet deployment problem dates back to the 1990s. The initial research idea of scholars was based on the fact that container transportation demand was known. In 1991, Perakis and Jaramillo (1991) and Jaramillo and Perakis (1991) were published, indicating that the problem was formalized by the academic community. In Perakis and Jaramillo (1991), the authors abstracted this planning problem as a linear programming problem, while a integer linear programming model was proposed by the same authors in Jaramillo and Perakis (1991). Subsequently, a large number of studies based on these models gradually emerged. For example, Cho and Perakis (1996) reformulated the model by introducing several generalized incidence matrices, which allowed the liner fleet deployment problem to be represented in matrix form. In their 1997 study, Powell and Perkins (1997) further expanded the model proposed by Jaramillo and Perakis (1991) by considering ship lay-up costs. Motivated by the above research, Gelareh and Meng (2010) incorporated liner speed planning into the model framework. They constructed a nonlinear programming model by considering the cubic relationship between fuel consumption and liner speed. To solve the model, an approximation method was proposed, which further transformed the model into a mixed integer programming (MIP) formulation. In the subsequent Wang et al. (2011), this model was further improved. In the following years, the academic community began to consider more practical factors, such as multiple periods (Meng & Wang, 2011) and cargo transshipment activities (Meng & Wang, 2012). In addition to enriching and developing liner fleet deployment models, scholars have also begun to link liner fleet deployment problems to other problems closely related to companies daily operations, e.g., shipping network design and slot allocation (Gao et al., 2022) and liner alliance operations (Xin et al., 2023).

However, when conducting the aforementioned research, scholars invariably used the same assumption; that is, container transportation demand is known. This assumption seems ideal in the maritime industry, which is highly intertwined with the world economy. Research considering container transportation demand uncertainty began in the 2010s and first appeared in Meng and Wang (2010) as a mathematical model with several chance constraints. The authors assumed that the demands between each port pair obeyed independent normal distributions, with both the mean and standard deviation known. These individual chance constraints could then be further reformulated as several deterministic constraints. Wang et al. (2013) subsequently considered a SP model with a joint chance constraint. With normally distributed transportation demands, the model was transformed and solved by applying the SAA technique.

In practice, it is often challenging to obtain accurate distribution information on container transportation demand. This has prompted some scholars to challenge the assumption that demand distribution information is known. For example, Ng (2014) developed a distribution-free model that requires only the upper bound, mean, and variance information of the transportation demand as inputs. However, it did not consider the stochastic dependencies of demand between different shipping routes. To address this limitation, the author further proposed a model incorporating a joint chance constraint in Ng (2015). Later, Ng and Lin (2018) established a novel model in which they assumed that conditional demands were known to avoid the over-conservative problem caused by Ng (2015). For similar research questions, one can also refer to several review papers, such as Wang and Meng (2017) and Christiansen et al. (2020). Very recently, Zhao et al. (2022) discussed the liner fleet deployment problem based on distributionally robust optimization (DRO) theory, which is also the most similar study to this thesis. The authors treated the maximum transportation demand among all legs on each route as a random variable and tried to minimize the sum of voyage costs and capital costs of the liner company. Two DRO models were constructed: one model is based on a type-1 Wasserstein ambiguity set adapted to the data-driven setting, while the other considers a set with the mean and dispersion of random variables. However, these two models can still be further improved compared with the real-world situation and latest modeling technique. First, the authors used the maximum container flow volume on a route as a random variable. This means that the authors implicitly assumed that routes do not change in the long term. However, it is common practice for liner companies to implement periodic adjustments (usually 3 to 6 months) to their shipping networks (Gao et al., 2022; Liu et al., 2021; Wang et al., 2024b). In other words, routes operated by one liner company will usually be added, deleted, or adjusted at regular intervals. Once a liner company adjusts its network, the existing model framework will no longer apply because it does not have any historical data on the random variables associated with new (or adjusted) routes. This method of setting random variables affects the applicability of the model. Second, the authors simply ignored the liner operating costs in their model. Generally, liner operating costs usually account for approximately 20% of the total cost of ocean shipping. For a 10-year-old Capesize bulk carrier, the operating costs are equivalent to 60% of the voyage costs (see Fig. 6.3 in Stopford (2008)). This neglect is equivalent to eliminating the impact of 20% of the cost on the model results, making the model conclusions lack practical guidance. Third, the authors applied **Proposition 2** in Chen et al. (2024) to transform their original model into an MIP. However, according to Xie (2021), this transformation may encounter difficulties in solving certain cases even for small-scale problems due to the additional structure imposed on the support of random variables.

2.2.2. Research on slot allocation problem

SAP research commenced in the 1990s and was often combined with the freight rate pricing problem, which is regarded as a special type of revenue management problem. Maragos (1994) pioneered the joint optimization problem of slot allocation and pricing in the field of liner shipping. At the beginning of the 21st century, Ting and Tzeng (2004) attempted to optimize the container transportation volume between each port pair and proposed an mixed integer programming (MIP) model. The model established by Feng and Chang (2010) considered allocating both laden and empty containers to specific routes. Zurheide and Fischer (2012) proposed a new SAP by dividing orders into urgent and non-urgent orders and taking into account the transshipment of containers. These two authors further considered adjusting the slot allocation strategy from the booking limit to the bid price (Zurheide & Fischer, 2015). The transportation demand in the maritime shipping industry often exhibits seasonal fluctuations. In light of this, Wang et al. (2015) constructed an MIP and developed a customized branch-and-bound algorithm. Throughout the above literature, it is evident that early studies all assumed that container transportation demand is fixed and known. Based on the known demand, the authors considered various allocation strategies and the operating behavior of liner companies to allocate slots.

As with the research on LFDP, research on SAPs has also gradually shifted from deterministic problems to uncertain problems in recent years. Wang et al. (2020) distinguished shippers as contract shippers and spot shippers, and two types of slot optimization models were proposed based on different marketing psychology (i.e., loyal strategy and expansive strategy). The authors believed that a liner company only needs to meet the demands of the contract shipper among the two types of shippers, which serves as the foundation for the assumptions of this thesis (see Chapter 5). Considering the uncertainty of transportation demand and the uncertainty of liner staying time at ports, the authors constructed two SP models to optimize the slot allocation scheme and freight rate pricing scheme. Assuming that each random variable obeys a uniform distribution with known parameters, a customized SAA embedded in the reformulation linearization technique was designed to solve the model. Wang et al. (2021) subsequently established a two-stage stochastic MIP to address the SAP with freight rate pricing problem considering demand uncertainty and the empty container repositioning factor. To address uncertainty, the authors assumed that the container transportation demand between each port pair follows a known normal distribution and transformed the model into a deterministic one by applying the SAA method. To address this SAA problem, the authors performed dual decomposition on the original model and designed a Lagrangian relaxation algorithm. Very recently, Liang et al. (2023) designed several slot allocation policies considering two types of shippers (i.e., contract shippers and spot shippers). Similar to the loyal strategy proposed by Wang et al. (2020), the authors also assumed that priority should be given to ensuring that the demands of the contract shipper are met. Under the assumption that the distribution function of the transportation demand of the two types of shippers between each port pair is known (i.e., a truncated normal distribution), the authors constructed a scenario-based SP model. Several policies were also developed to allocate slots, including the first-come-first-serve policy, minimum quantity commitment policy, and threshold-based perturbation approach. Based on 5,000 scenarios generated from this known distribution, the authors conducted numerical experiments for different policies. In summary, most of the current studies that consider random factors in SAPs focus on transportation demand uncertainty. As the research progresses, additional factors (e.g., differentiating between different types of shippers, empty container repositioning, demurrage charges for stranded containers, liner staying time at the port) are incorporated into the model framework. To make the stochastic model tractable, the authors without exception assumed that the distribution function of transportation demand is known (e.g., a normal distribution or uniform distribution). However, as Ksciuk et al. (2023) noted, maritime shipping demand uncertainty is caused by changes in economic policy, and combined with the lack of historical data, it is extremely difficult to accurately estimate its true distribution.

2.2.3. Research on the joint optimization of LFDP, SNDP and SAP

As previously stated, a reasonable *liner fleet deployment scheme* is necessary for liner companies to reduce costs. However, the *liner shipping network design scheme* must be known before fleet deployment can be carried out. Moreover, once the fleet deployment scheme is determined, an excellent *slot allocation scheme* can further increase the income of the liner company. These three types of decisions are interconnected, and as a result, joint optimization studies of LFDP, SNDP and SAP have sprung up. Mourão et al. (2002) is regarded as the earliest study on collaborative optimization of LFDP and SAP, as the authors considered container transshipment operations in an LFDP. Container transshipment refers to the transportation of a container via one or more routes, with the associated cost varying according to the loading and unloading activities involved. Consequently, the liner company must allocate containers to the limited slots of the liner operating on a single route (or liners on multiple routes, in the case of transshipment). However, the authors considered a liner shipping network comprising only one pair of ports and two routes, which is a highly simplified representation of reality. Some scholars have also considered combining LFDP, SNDP and SAP (with regard to container transshipment operations). For example, Agarwal and Ergun (2008) constructed an MIP for this joint optimization problem and designed a greedy heuristic algorithm, a column generation-based algorithm, and an algorithm based on two-stage Benders decomposition. Papers that consider similar factors also include Gelareh et al. (2010), Liu et al. (2021), Gao et al. (2022), Xin et al. (2023), and Chen et al. (2023). Although the model frameworks incorporate more realistic factors, such as liner alliances, shippers' choice inertia, and carbon taxes, the authors invariably assume that container transportation demand is known in order to solve these complex models.

Chapter 3:
Berth allocation with uncertain arrival delay[2]

As mentioned in Chapter 1, the maritime logistics system is composed of two elements: nodes (i.e., ports) and shipping routes (i.e., edges). This chapter focuses on resilient maritime logistics systems design at the port level (i.e., landside). *Ports*—which function as critical nodes connecting maritime shipping and land transportation—exert a direct influence on the efficiency of global logistics networks (Liu et al., 2025a). Therefore, in recent years, the enhancement of port operations and the augmentation of supply chain efficiency have emerged as pivotal areas of concern in both the academic and industrial domains (Xiang et al., 2025). However, the stable operation of the port is easily affected by external factors. Due to the inaccurate schedules of a large number of vessels, ports must rely on resilience strengthening to cope with unstable factors during production and operation, which has greatly increased the difficulty of port production organization. Therefore, this chapter starts with enhancing the resilience of berth allocation operations by constructing models considering uncertain factor.

[2] Xin, X, Zhang, T., Pang, K.-W., & Wang, S. (2025). Berth allocation problem under uncertainty: a distributionally robust optimization model with a joint chance constraint. *Transportation Research Part B: Methodological*, Under review.

3.1. Introduction

3.1.1. Background information

In the daily operation of the port terminal, the initial step is the *berth allocation* operation, a process that exerts a significant influence on all subsequent operations (Agra & Rodrigues, 2022). Consequently, this operational procedure has prompted extensive research on the *berth allocation problem* (BAP), a pivotal decision-making challenge confronting port managers (Lim, 1998). The abovementioned BAP relates mainly to the allocation of limited port *terminal space* (i.e., wharf) and *service time* for vessels berthed at the port, with the objective of achieving management goals set by port managers (e.g., minimizing total operating costs). Despite the prevalence of research on BAPs in recent decades, the majority of existing studies have focused on the modeling of deterministic problems, with limited attention given to the influence of uncertainty factors (Agra & Rodrigues, 2022; Wang et al., 2025). In conventional research, one can see that numerous parameters, including vessel arrival times and vessel operation times (i.e., cargo handling times), are treated as deterministic entities (see Guo et al. (2022) and Yu et al. (2023) for two examples from the recent literature).

In reality, vessel berthing operations are often subject to a variety of uncertainties, such as weather conditions (Luo et al., 2024) and mechanical failures (Lv & Gao, 2023). These factors can result in delays in vessel arrival and loading/unloading operations, potentially leading to congestion and even the closure of port terminals (Wang & Meng, 2012a; Xu et al., 2012). If port managers make adjustments to the berthing schedule in response to such delays (or disruptions), significant costs are likely to be incurred (Wang et al., 2025). To mitigate the adverse consequences of such occurrences, it is imperative to incorporate uncertainty factors into the model framework (Wang & Meng, 2012b). In response to this call, the academic community initiated the incorporation of uncertainty factors into the BAP in the early 21st century (Agra & Rodrigues, 2022). For a systematic review, one may refer to Rodrigues and Agra (2022) and Li et al. (2024a). On the basis of the abovementioned two review papers, the established methodologies for coping with uncertainty in the BAP can be broadly classified into two categories: (1) the stochastic programming (SP) approach (Moorthy & Teo, 2006) and (2) the robust optimization (RO) approach (Du et al., 2010). The fundamental distinction between these two approaches lies in the knowledge of uncertainty and the optimization objective (Rodrigues & Agra, 2022). Specifically, a necessary assumption when using SP-based approaches is that the PDFs of the uncertain parameters are known. Thus, the problem with uncertainty factors can be transformed into a deterministic problem by generating scenarios based on known probability density functions (PDFs), a method known as sample average approximation (SAA; see Sheikholeslami and Ilati (2018)). Nevertheless, PDFs obtained through assumptions are often too general to capture extreme cases (Küçükyavuz & Jiang, 2022; Wang et al., 2024a). Moreover, accurate estimation of the PDFs of uncertain parameters is challenging because of the intricate interconnection of the shipping market with the global economy, which is characterized by rapid fluctuations (Meng et al., 2012, 2015). In contrast, RO-based approaches operate under the assumption that either the PDF of the uncertain parameter is either nonexistent or is not precisely known (Al-Refaie & Abedalqader, 2022). Consequently, uncertainty parameters can be characterized by constructing uncertainty sets (Beyer & Sendhoff, 2007). Furthermore, the RO approach relies on worst-case analysis, meaning that RO-based models seek improvements on the basis of the realization of the most unfavorable uncertainty (Gabrel et al., 2014). This often results in the model finding solutions that are overly conservative (Xin et al., 2025a), making the RO approaches more suitable for decision makers with a strong risk-averse attitude. Concerted efforts have been made in recent years to develop distributionally robust optimization (DRO) theory as a means to strike a balance between these two approaches. In contrast to the SP model, the DRO model does not presuppose knowledge of the PDFs of uncertain parameters. Instead, it requires only the probability distributions of uncertain parameters within a set, known as the *ambiguity set* (Xin et al., 2025a). This model seeks improvements over the most unfavorable distribution scenario (as opposed to the most unfavorable realization scenario), thereby preventing an overly conservative solution. Furthermore, the establishment of this ambiguity set necessitates only partial information associated with uncertain parameters, such as several samples, which are more readily obtainable in practice.

However, almost no decision can definitely exclude the later constraint violation caused by various uncertain factors. The reality is that there are always temporary and unexpected circumstances (e.g., mechanical failure) that disrupt the established berthing schedule, and the cost associated with maintaining an overly robust schedule is considered unacceptable (Wang et al., 2024a). Therefore, we employ the chance-constrained methodology originally proposed by Charnes and Cooper (1959) and recently extended by Wang et al. (2024a) to maintain operational compliance with port managers' predetermined service level requirements. This approach enables the realization of a trade-off between the service level and cost. Specifically, we attempt to design a joint chance constraint into the model framework, stipulating that all vessels' berthing times succeed in their respective uncertain arrival times with a collective probability of at least $1-\varepsilon$, where $\varepsilon \in [0,1]$ denotes the predefined risk tolerance (service level) threshold of the port manager. In other words, this chance constraint guarantees at least $1-\varepsilon$ probability of zero berthing schedule adjustments of all vessels under the most unfavorable distribution scenario governed by the established ambiguity set.

3.1.2. Research objective and contributions

Motivated by the aforementioned background, the research objective of this chapter is to address the inherent uncertainty of the BAP by employing distributionally robust chance-constrained (DRCC) theory. In this chapter, we consider adopting the type-1 Wasserstein ambiguity set, which is defined as a family of probability distributions centered around a reference distribution (often called an *empirical distribution*) and constrained by a type-1 Wasserstein distance. Recent years have seen the rise of the Wasserstein ambiguity set (Ho-Nguyen et al., 2023). This approach has gained prominence because of its advantageous statistical properties, including the finite sample guarantee property (see Mohajerin Esfahani and Kuhn (2018)), compared with ambiguity sets based on moments and ϕ-divergences (e.g., Kullback–Leibler divergence ambiguity sets). Specifically, when more historical data are available, models constructed with moment-based ambiguity sets usually demonstrate more conservative results than models developed with Wasserstein ambiguity sets do (Shen & Jiang, 2023). In addition, the possibility of noisy measurements is not considered when constructing ambiguity sets via ϕ-divergence in certain modeling scenarios, as the distributions are compared on a scenario-by-scenario basis (Chen et al., 2024; Gao & Kleywegt, 2023). Therefore, equipped with the latest DRO theory developments by Ho-Nguyen et al. (2023) and Jiang and Xie (2025), we construct a DRCC model with a type-1 Wasserstein ambiguity set and reformulate it as a mixed integer programming (MIP) model. In addition, we strengthen the model by introducing SAA constraints and accelerate the solution process via coefficient strengthening via the value-at-risk (VaR) outer approximation of the joint chance constraint.

The contributions of this chapter can be briefly summarized as follows: (i) We develop the first DRCC model for the BAP under ambiguous vessel arrival time distributions. (ii) We propose strategies to increase the efficacy of the solution method. To this end, several SAA constraints and a coefficient strengthening technique are proposed. (iii) Sensitivity analysis and out-of-sample analysis are conducted to verify the validity and out-of-sample performance of the DRCC model.

3.2. Problem description and model development

3.2.1. Problem description

In this section, we use the model framework proposed by Rodrigues and Agra (2022) and Zhen et al. (2011) to establish a standard mathematical model for the *continuous BAP*. From the spatial dimension, we assume that a set of heterogeneous vessels in $\mathcal{S}$ needs to berth at a wharf, whose total length is L^{Total}. The length of each vessel $i \in \mathcal{S}$ is denoted by L_i. For the convenience of modeling, the abovementioned vessel length also includes the safety margin between adjacent vessels. Owing to limited port facilities and the different drafts of different vessels, vessel $i \in \mathcal{S}$ has a lower-cost berthing position, which is denoted as p_i^{Best}, and a starting/ending position suitable for berthing vessel $i \in \mathcal{S}$, which are represented as $B_i^{\min}$ and $B_i^{\max}$, respectively. Decision makers of the port need to set an appropriate berthing location p_i for each vessel $i \in \mathcal{S}$. Any spatial deviation of vessel *i*'s assigned berth position from its optimal low-cost location incurs a marginal penalty cost C_i^1 per unit distance. From the dimension of time, each vessel $i \in \mathcal{S}$ has an arrival/departure time, recorded as α_i and β_i, respectively. The arrival delay of vessel $i \in \mathcal{S}$ is considered an uncertain parameter (i.e., random variable), denoted by ξ_i. Therefore, the uncertain arrival time of vessel $i \in \mathcal{S}$ can be represented as $(\alpha_i + \xi_i)$. Decision makers of the port need to set an appropriate berthing time t_i for each vessel $i \in \mathcal{S}$. After vessel $i \in \mathcal{S}$ berths at the wharf, it immediately starts cargo handling (i.e., cargo loading or unloading), and the above operation time is h_i. For the convenience of modeling, this handling time includes the interval between the time when a vessel finishes cargo handling and the berthing time of the next arriving vessel sharing the berthing location with it. Therefore, we can use $(t_i + h_i)$ to represent the actual departure time of vessel $i \in \mathcal{S}$. If the berthing time of vessel $i \in \mathcal{S}$ is later than the estimated arrival time α_i, a penalty cost of C_i^2 is incurred per unit time. Similarly, if the departure time of vessel $i \in \mathcal{S}$ is later than the estimated departure time β_i, a penalty cost of C_i^3 will be incurred per unit time. Moreover, to describe the temporal and spatial relationships between two vessels, we introduce two binary auxiliary variables: x_{ij}^{Space} and x_{ij}^{Time}. If vessel $i \in \mathcal{S}$ berths below vessel $j \in \mathcal{S}$ on the wharf (in position), x_{ij}^{Space} takes a value of 1. Similarly, if vessel $i \in \mathcal{S}$ berths before vessel $j \in \mathcal{S}$ (in time), x_{ij}^{Time} takes a value of 1. The optimization objective of the decision maker is to minimize the sum of all types of penalty costs. For the convenience of readers, the commonly used notations in this chapter are listed in Table 3.1.

Table 3.1 Notation table

Sets	
$\mathcal{S}$	Set of vessels, whose elements are denoted as i or j
$\mathcal{P}(\theta)$	A type-1 Wasserstein ambiguity set with radius θ
$\mathbb{R}_+$	Set of non-negative real numbers
Parameters	
C_i^1	Unit distance cost penalty when vessel $i \in \mathcal{S}$ berths away from its lowest-cost berthing position
C_i^2, C_i^3	Unit time cost penalty for berthing/departure delay of vessel $i \in \mathcal{S}$
p_i^{Best}	The lowest cost berthing position of vessel $i \in \mathcal{S}$
α_i, β_i	The estimated arrival/departure time of vessel $i \in \mathcal{S}$
h_i	The operation time (i.e., cargo handling time) of vessel $i \in \mathcal{S}$ (including the preparation time before the vessel leaves the wharf)
L_i	The length of vessel $i \in \mathcal{S}$ (including the safety margin)
L^{Total}	The total length of the wharf
$B_i^{\min}$, $B_i^{\max}$	The starting/ending position suitable for berthing vessel $i \in \mathcal{S}$
ε	The risk tolerance level (service level) set by the port manager
T	The length of the planning period
Random variable	
ξ_i	The arrival delay time of vessel $i \in \mathcal{S}$
Decision variables	
x_{ij}^{Space}	A binary auxiliary variable, that is 1 if vessel $i \in \mathcal{S}$ berths below vessel $j \in \mathcal{S}$ (in position)
x_{ij}^{Time}	A binary auxiliary variable, that is 1 if vessel $i \in \mathcal{S}$ berths before vessel $j \in \mathcal{S}$ (in time)
p_i	The berthing position of vessel $i \in \mathcal{S}$
t_i	The berthing time of vessel $i \in \mathcal{S}$

3.2.2. Model development

On the basis of our description of the BAP and the introduced notations, we can construct the following DRCC model for modeling the BAP, abbreviated as **M1**.

<u>M1:</u>

$$\min_{(\boldsymbol{p},\boldsymbol{t},\boldsymbol{x}_{\mathrm{S}},\boldsymbol{x}_{\mathrm{T}})} obj = \sum_{i\in\mathcal{S}} \left[C_i^1 \left| p_i - p_i^{\text{Best}} \right| + C_i^2 \left(t_i - \alpha_i\right)^+ + C_i^3 \left(t_i + h_i - \beta_i\right)^+ \right] \tag{3.1}$$

$$s.t.\quad p_i + L_i \le L^{\text{Total}} \qquad \forall i \in \mathcal{S} \tag{3.2}$$

$$p_i + L_i \le p_j + L^{\text{Total}}\left(1 - x_{ij}^{\text{Space}}\right) \qquad \forall i, j \in \mathcal{S}, i \ne j \tag{3.3}$$

$$B_i^{\min} \le p_i \le B_i^{\max} \qquad \forall i \in \mathcal{S} \tag{3.4}$$

$$t_i + h_i \le t_j + M\left(1 - x_{ij}^{\text{Time}}\right) \qquad \forall i, j \in \mathcal{S}, i \ne j \tag{3.5}$$

$$x_{ij}^{\text{Space}} + x_{ji}^{\text{Space}} + x_{ij}^{\text{Time}} + x_{ji}^{\text{Time}} \ge 1 \qquad \forall i, j \in \mathcal{S}, i \ne j \tag{3.6}$$

$$\inf_{\mathbb{P} \in \mathcal{P}(\theta)} \mathbb{P}\left\{t_i \ge \alpha_i + \xi_i, \forall i \in \mathcal{S}\right\} \ge 1 - \varepsilon \tag{3.7}$$

$$t_i + h_i \le T \qquad \forall i \in \mathcal{S} \tag{3.8}$$

$$\boldsymbol{p}, \boldsymbol{t} \in \mathbb{R}_+^{|\mathcal{S}|}, \boldsymbol{x}_{\text{S}}, \boldsymbol{x}_{\text{T}} \in \{0,1\}^{|\mathcal{S}| \times |\mathcal{S}|} \tag{3.9}$$

where M is a sufficiently large constant; $\boldsymbol{p} = (p_i)$; $\boldsymbol{t} = (t_i)$; $\boldsymbol{x}_{\text{S}} = \left(x_{ij}^{\text{Space}}\right)$; $\boldsymbol{x}_{\text{T}} = \left(x_{ij}^{\text{Time}}\right)$; and the function $(\cdot)^+ = \max\{\cdot, 0\}$.

In the above, Equation (3.1) is the objective function of **M1**, which minimizes the total cost of berth allocation. The first term in the brackets is the penalty cost incurred when the vessels' berthing positions deviate from their desired positions. The second term represents the penalty cost associated with initiating vessel service after its estimated time of arrival. The third term calculates the penalty cost associated with the departure of a vessel beyond the estimated departure time. The choice of this optimization objective is a combination of the results of different studies (i.e., Zhen et al. (2011), Rodrigues and Agra (2022) and Wang et al. (2024a)). We can easily adjust the above objective function by setting some penalty costs to 0. Our proposed model and solution methodology are also applicable to the case of different objective functions. Constraints (3.2)–(3.4) restrict the position of the vessel when berthing. Constraint (3.2) requires that the berthing position of any vessel must be within the wharf. Constraint (3.3) requires that any two pairs of vessels cannot overlap in space. Constraint (3.4) reflects the draft requirement for each ship. Constraint (3.5) imposes temporal non-overlapping requirements for all vessel pairs (i, j). Constraint (3.6) defines the relationship between two auxiliary variables. The joint chance constraint (3.7) requires that each vessel's berthing time after its corresponding uncertain arrival time is jointly met with a probability greater than or equal to $1-\varepsilon$. Constraint (3.8) ensures that all vessels depart within the planning period. Finally, Constraint (3.9) gives the domains of the decision variables. This model is highly extensible, and we illustrate this through the following two examples.

Example 1 (Tidal factor). Some scholars have considered tidal factors in their research. The following example shows that we can extend the model to consider this factor by simply adding a few constraints to the original model. We assume that there is a series of tidal cycles during the planning period (e.g., period $[0,T]$ where T is the length of the planning period) and use $\mathcal{C}$ to represent the set of cycles. The berthing time and actual departure time of each vessel $i \in \mathcal{S}$ within tidal cycle $c \in \mathcal{C}$ need to be within a specific time window, say $\left[\underline{t}_{i,c}^{\text{Berth}}, \overline{t}_{i,c}^{\text{Berth}}\right]$ (where $\overline{t}_{i,c}^{\text{Berth}} \leq T$, $\forall i \in \mathcal{S}$, $c \in \mathcal{C}$), to ensure navigation safety. Two binary variables, i.e., $\delta_{i,c}^{\text{Berth}}$ and $\delta_{i,c}^{\text{Depart}}$, are introduced to indicate whether vessel $i \in \mathcal{S}$ is berthing (or departing) in tidal cycle $c \in \mathcal{C}$. At this point, **M1** is transformed into **M1-R**.

M1-R1:

$$\min_{(\boldsymbol{p},\boldsymbol{t},\boldsymbol{x}_{\text{S}},\boldsymbol{x}_{\text{T}})} obj = \sum_{i\in\mathcal{S}} \left[C_i^1 \left| p_i - p_i^{\text{Best}} \right| + C_i^2 \left(t_i - \alpha_i\right)^+ + C_i^3 \left(t_i + h_i - \beta_i\right)^+ \right] \tag{3.10}$$

$s.t.$ (3.2)–(3.9),

$$t_i \geq \underline{t}_{i,c}^{\text{Berth}} - M\left(1-\delta_{i,c}^{\text{Berth}}\right) \qquad \forall i \in \mathcal{S}, c \in \mathcal{C} \tag{3.11}$$

$$t_i \leq \overline{t}_{i,c}^{\text{Berth}} + M\left(1-\delta_{i,c}^{\text{Berth}}\right) \qquad \forall i \in \mathcal{S}, c \in \mathcal{C} \tag{3.12}$$

$$t_i + h_i \geq \underline{t}_{i,c}^{\text{Berth}} - M\left(1-\delta_{i,c}^{\text{Depart}}\right) \qquad \forall i \in \mathcal{S}, c \in \mathcal{C} \tag{3.13}$$

$$t_i + h_i \leq \overline{t}_{i,c}^{\text{Berth}} + M\left(1-\delta_{i,c}^{\text{Depart}}\right) \qquad \forall i \in \mathcal{S}, c \in \mathcal{C} \tag{3.14}$$

$$\sum_{c \in \mathcal{C}} \delta_{i,c}^{\text{Berth}} = 1 \qquad \forall i \in \mathcal{S} \tag{3.15}$$

$$\sum_{c \in \mathcal{C}} \delta_{i,c}^{\text{Depart}} = 1 \qquad \forall i \in \mathcal{S} \tag{3.16}$$

$$\delta_{i,c}^{\text{Berth}}, \delta_{i,c}^{\text{Depart}} \in \{0,1\} \qquad \forall i \in \mathcal{S}, c \in \mathcal{C}\,. \tag{3.17}$$

In the above, Constraints (3.11)–(3.12) require that the berthing time of vessel $i \in \mathcal{S}$ satisfy the time window; Constraints (3.13)–(3.14) require that the actual departure time of vessel $i \in \mathcal{S}$ satisfy the time window. Constraints (3.15)–(3.16) limit each vessel $i \in \mathcal{S}$ to only one berth or departure out of tidal cycles in set $\mathcal{C}$. Finally, Constraint (3.17) gives the domain of definition of variables $\delta_{i,c}^{\text{Berth}}$ and $\delta_{i,c}^{\text{Depart}}$.

Example 2 (Discrete BAP). Owing to differences in actual port layout, scholars may model BAPs on the basis of a discrete modeling framework. In **Appendix A** of Rodrigues and Agra (2022), the authors gave a standard formulation of the discrete BAP. We borrow the notation from **Appendix A** and modify the model as follows: **M1-R2**. For the meaning of the newly introduced notation, one may refer to Rodrigues and Agra (2022). At this point, we construct a DRCC for the discrete BAP. The solution method in this chapter is also applicable to **M1-R2**.

M1-R2:

$$\min obj = \sum_{i\in\mathcal{S}}\left[C_i^2\left(t_i - a_i\right)^+ + C_i^3\left(t_i + \sum_{k\in B} c_{ki}x_{ki} - d_i\right)^+\right] \tag{3.18}$$

s.t. (24)–(30), and (32) in Rodrigues and Agra (2022),

$$\inf_{\mathbb{P}\in\mathcal{P}(\rho)} \mathbb{P}\left\{t_i \geq a_i + \xi_i, \forall i \in V\right\} \geq 1-\varepsilon . \tag{3.19}$$

Note that the objective function of model **M1** contains both an absolute value term and two terms involving the maximum function $(\cdot)^+$. For the sake of computational convenience, we further convert **M1** to the following **M2** by introducing several auxiliary variables.

M2:

$$\min_{\left(\boldsymbol{p},\boldsymbol{t},\boldsymbol{x}_{\mathrm{S}},\boldsymbol{x}_{\mathrm{T}},\boldsymbol{\varphi}^+,\boldsymbol{\varphi}^-,\boldsymbol{\delta}^+,\boldsymbol{\delta}^-,\boldsymbol{\gamma}^+,\boldsymbol{\gamma}^-\right)} obj = \sum_{i\in\mathcal{S}}\left[C_i^1\left(\varphi_i^+ + \varphi_i^-\right) + C_i^2\delta_i^+ + C_i^3\gamma_i^+\right] \tag{3.20}$$

s.t. (3.2)–(3.9),

$$p_i - p_i^{\mathrm{Best}} = \varphi_i^+ - \varphi_i^- \qquad \forall i \in \mathcal{S} \tag{3.21}$$

$$t_i - \alpha_i = \delta_i^+ - \delta_i^- \qquad \forall i \in \mathcal{S} \tag{3.22}$$

$$t_i + h_i - \beta_i = \gamma_i^+ - \gamma_i^- \qquad \forall i \in \mathcal{S} \tag{3.23}$$

$$\varphi_i^+, \varphi_i^-, \delta_i^+, \delta_i^-, \gamma_i^+, \gamma_i^- \in \mathbb{R}_+ \qquad \forall i \in \mathcal{S} \tag{3.24}$$

where $\boldsymbol{\varphi}^+ = \left(\varphi_i^+\right)$; $\boldsymbol{\varphi}^- = \left(\varphi_i^-\right)$; $\boldsymbol{\delta}^+ = \left(\delta_i^+\right)$; $\boldsymbol{\delta}^- = \left(\delta_i^-\right)$; $\boldsymbol{\gamma}^+ = \left(\gamma_i^+\right)$; and $\boldsymbol{\gamma}^- = \left(\gamma_i^-\right)$.

The introduction of these auxiliary variables allows us to eliminate the absolute value and maximum function present in the objective function. For example, Constraint (3.21) indicates that if $p_i - p_i^{\mathrm{Best}} \geq 0$, then we have $\left|p_i - p_i^{\mathrm{Best}}\right| = \lambda_i^+$; otherwise, we can obtain $\left|p_i - p_i^{\mathrm{Best}}\right| = \lambda_i^-$. Therefore, $\left|p_i - p_i^{\mathrm{Best}}\right| = \lambda_i^+ + \lambda_i^-$ when the objective function is minimized.

3.3. Model reformulation

Since DRCC is characterized by nonconvex feasible regions, solving it is challenging. The objective of this section is to convert the established DRCC model, that is, **M2**, into a computationally tractable version. To this end, we first introduce the ambiguity set we adopt in Section 3.3.1. In Section 3.3.2, we transform **M2** into an exact MIP model reformulation via an indicator function and strong conic duality. Several SAA constraints are introduced into the model framework in Section 3.3.3.1 to enhance the model. Finally, in Section 3.3.3.2, we introduce some valid inequalities into **M2** to increase its solution efficiency.

3.3.1. Type-1 Wasserstein ambiguity set

An important consideration when constructing a DRCC is the selection of the ambiguity set. In Section 3.1.2, we state the reasons for choosing the type-1 Wasserstein ambiguity set. The core idea of constructing such an ambiguity set is to use an *empirical distribution* constructed on the basis of historical data (also known as *samples*) of an uncertain parameter to approximate the true distribution of this uncertain parameter. Despite the inability of port managers to accurately ascertain the distributions of uncertain parameters, real operational data are produced daily. As we mentioned earlier, this chapter considers only the arrival time of vessel $i \in \mathcal{S}$, i.e., ξ_i, as a random variable. We set $\boldsymbol{\xi} = (\xi_i)$ to denote the random vector with a joint probability distribution $\mathbb{P}$. The support set of $\boldsymbol{\xi}$ is denoted by Ξ. Suppose that the port manager generates an empirical distribution $\mathbb{P}_{\zeta}^{N}$ by collecting *N* i.i.d. samples associated with (true) distribution $\mathbb{P}$, i.e., $\Omega = \{\boldsymbol{\zeta}^1, \boldsymbol{\zeta}^2, \boldsymbol{\zeta}^3, \cdots, \boldsymbol{\zeta}^n, \cdots, \boldsymbol{\zeta}^N\} \subseteq \Xi$, where $\boldsymbol{\zeta}^n = (\zeta_i^n)$, $n \in [N]$ represents the n^{th} sample obtained, and $\boldsymbol{\zeta} = (\zeta_i)$ denotes the random vector associated with empirical distribution $\mathbb{P}_{\zeta}^{N}$ (which is also known as an empirical random vector). Then, we can approximate $\mathbb{P}_{\zeta}^{N}$ as $\sum_{n\in[N]} dis_{\zeta_n} / N$, where $[N] := \{1, 2, 3, \cdots, N\}$ and dis_{ζ_n} denotes the *Dirac distribution* concentrating the unit mass at $\boldsymbol{\zeta}^n$. This concept shows that for all $n \in [N]$, $\mathbb{P}_{\zeta}^{N}\{\boldsymbol{\zeta} = \boldsymbol{\zeta}^n\} = 1/N$. On the basis of these concepts and notations, we can present **Definition 3.1** below to define the type-1 Wasserstein ambiguity set.

Definition 3.1 (Type-1 Wasserstein ambiguity set). Let $\mathcal{P}_{\Xi}$ be a set of distributions associated with a random vector supported on set Ξ. Given an empirical (or reference) distribution $\mathbb{P}_{\zeta}^{N}$ obtained by collecting *N* observations and the type-1 Wasserstein metric $\text{dis}_{\text{Type 1-W}}(\cdot,\cdot) : \mathcal{P}_{\Xi} \times \mathcal{P}_{\Xi} \mapsto \mathbb{R}_+$, the type-1 Wasserstein ambiguity set can be expressed as

$$\mathcal{P}(\theta) := \left\{ \mathbb{P} \,\middle|\, \begin{array}{c} \mathbb{P}(\boldsymbol{\xi} \in \Xi) = 1 \\ \text{dis}_{\text{Type 1-W}}\left(\mathbb{P}, \mathbb{P}_{\zeta}^{N}\right) \le \theta \end{array} \right\} \tag{3.25}$$

where $\theta \in \mathbb{R}_+$ is a parameter (called the radius) and $\text{dis}_{\text{Type 1-W}}(\cdot,\cdot)$ can be defined as

$$\text{dis}_{\text{Type 1-W}}\left(\mathbb{P}, \mathbb{P}_{\zeta}^{N}\right) = \inf_{\hat{\mathbb{P}}} \mathbb{E}_{\hat{\mathbb{P}}}\left[\|\boldsymbol{\xi} - \boldsymbol{\zeta}\|\right] \tag{3.26}$$

$$s.t. \quad \boldsymbol{\xi} \sim \mathbb{P}, \boldsymbol{\zeta} \sim \mathbb{P}_{\zeta}^{N} \tag{3.27}$$

$$(\boldsymbol{\xi}, \boldsymbol{\zeta}) \sim \hat{\mathbb{P}} \tag{3.28}$$

$$\hat{\mathbb{P}}\{(\boldsymbol{\xi}, \boldsymbol{\zeta}) \in \Xi \times \Xi\} = 1 \tag{3.29}$$

where $\hat{\mathbb{P}}$ denotes the joint distribution of $(\boldsymbol{\xi}, \boldsymbol{\zeta})$ and $\|\bullet\|$ represents the norm.

Remark 3.1. According to **Definition 3.1**, the type-1 Wasserstein distance of two distributions (true distribution $\mathbb{P}$ and empirical distribution $\mathbb{P}_{\zeta}^{N}$) can be intuitively viewed as the minimal cost for moving $\mathbb{P}$ to $\mathbb{P}_{\zeta}^{N}$, with the unit Dirac point mass moving cost from ξ to ζ being $\|\xi-\zeta\|$ (Chen et al., 2024). Calculating this distance is equivalent to solving an optimal transport problem (Givens & Shortt, 1984), and $\theta \in \mathbb{R}_{+}$ in $\mathcal{P}(\theta)$ can be viewed as a budget on the cost. An example model of this transport problem can be found in **Appendix D** of Zhang et al. (2023). For a more general definition of the Wasserstein distance, interested readers may refer to recent theoretical studies, such as Mohajerin Esfahani and Kuhn (2018) and Zhao and Guan (2018).

3.3.2. Exact MIP model transformation

Since a joint chance Constraint (3.7) exists in **M2**, we need to restructure the model to make it computationally tractable. This sub-section attempts to convert **M2** into an MIP model. Let decision vector $\mathbf{t}=(t_i)$; Constraint (3.7) in **M2** can be rewritten as set J_1, as shown in (3.30). We introduce **Proposition 3.1** to reformulate the set J_1.

$$J_1 := \left\{ \mathbf{t} \in \mathbb{R}_{+}^{|\mathcal{S}|} : \inf_{\mathbb{P} \in \mathcal{P}(\theta)} \mathbb{P}\left\{ \alpha_i + \xi_i \le t_i, \forall i \in \mathcal{S} \right\} \ge 1-\varepsilon \right\} \tag{3.30}$$

Proposition 3.1. Set J_1 can be equivalently reformulated as the following set by introducing a non-negative auxiliary variable, i.e., $\lambda \ge 0$.

$$J_2 := \left\{ \mathbf{t} \in \mathbb{R}_{+}^{|\mathcal{S}|} : \begin{array}{c} \theta - \varepsilon\lambda \le \dfrac{1}{N} \sum_{n \in [N]} \min\left\{0, g\left(\mathbf{t}, \zeta^{n}\right) - \lambda\right\} \\ \lambda \ge 0 \end{array} \right\} \tag{3.31}$$

where $g\left(\mathbf{t},\boldsymbol{\zeta}^n\right) := \left(\min_{i\in\mathcal{S}}\left\{t_i-\alpha_i-\zeta_i^n\right\}\right)^+$.

Proof of Proposition 3.1. Similar to the proof process in Xie (2021), we use three steps (i.e., **Step A** to **Step C**) to complete the reformulation of the set.

Step A: For chance constraint (3.7), the following relationship exists:

$$\inf_{\mathbb{P}\in\mathcal{P}(\theta)} \mathbb{P}\left\{\alpha_i+\xi_i \le t_i, \forall i\in\mathcal{S}\right\} \ge 1-\varepsilon = \sup_{\mathbb{P}\in\mathcal{P}(\theta)} \mathbb{P}\left\{\alpha_i+\xi_i > t_i, \exists i\in\mathcal{S}\right\} \le \varepsilon .$$

We set $\mathbb{I}\left(m\in\mathcal{M}\right)$ to represent the *indicator function*. When $m\in\mathcal{M}$, we have $\mathbb{I}\left(m\in\mathcal{M}\right)=1$ and $\mathbb{I}\left(m\in\mathcal{M}\right)=0$ otherwise. Using this function, we can construct the following equation:

$$\mathbb{P}\left\{\alpha_i+\xi_i \le t_i, \exists i\in\mathcal{S}\right\} = \mathbb{E}_{\mathbb{P}}\left[\mathbb{I}\left(\alpha_i+\xi_i > t_i, \exists i\in\mathcal{S}\right)\right].$$

If we regard

$$p_{\text{primal}} : \sup_{\mathbb{P}\in\mathcal{P}(\theta)} \mathbb{E}_{\mathbb{P}}\left[\mathbb{I}\left(\alpha_i+\xi_i > t_i, \exists i\in\mathcal{S}\right)\right]$$

as a primal problem, then its dual problem is as follows:

$$p_{\text{dual}} : \inf_{\tilde{\lambda}\ge 0}\left\{\tilde{\lambda}\theta - \frac{1}{N}\sum_{n\in[N]} \inf_{\boldsymbol{\xi}}\left[\tilde{\lambda}\left\|\boldsymbol{\xi}-\boldsymbol{\zeta}^n\right\| - \mathbb{I}\left(\alpha_i+\xi_i > t_i, \exists i\in\mathcal{S}\right)\right]\right\}.$$

Note that $\mathbb{I}\left(x\in A\right)$ is a bounded and upper semi-continuous function. According to the strong duality (i.e., **Corollary 2**) presented in Gao and Kleywegt (2023), we know that $p_{\text{primal}} = p_{\text{dual}}$. This property allows us to transform (3.30) into

$$\left\{\mathbf{t}\in\mathbb{R}_+^{|\mathcal{S}|} : \tilde{\lambda}\theta - \frac{1}{N}\sum_{n\in[N]} \inf_{\boldsymbol{\xi}}\left[\tilde{\lambda}\left\|\boldsymbol{\xi}-\boldsymbol{\zeta}^n\right\| - \mathbb{I}\left(\alpha_i+\xi_i > t_i, \exists i\in\mathcal{S}\right)\right] \le \varepsilon, \exists\tilde{\lambda}\ge 0\right\}.$$

Step B: After the transformation by **Step A**, function $\mathbb{I}\left(x\in\mathcal{M}\right)$ appears in the set. We consider eliminating it in this step.

First, we find that $\mathbb{I}\left(\alpha_i+\xi_i > t_i, \exists i\in\mathcal{S}\right) = \max_{i\in\mathcal{S}} \mathbb{I}\left(\alpha_i+\xi_i > t_i\right)$. Given $\tilde{\lambda}\ge 0$,

$n \in [N]$ and $\boldsymbol{\zeta}_n \in \Omega$, we know that $\inf_{\boldsymbol{\xi}} \left[\tilde{\lambda} \left\| \boldsymbol{\xi} - \boldsymbol{\zeta}^n \right\| - \mathbb{I}\left(\alpha_i + \xi_i > t_i, \exists i \in \mathcal{S} \right) \right]$ can be reformulated as

$$\min_{i \in \mathcal{S}} \inf_{\boldsymbol{\xi}} \left[\tilde{\lambda} \left\| \boldsymbol{\xi} - \boldsymbol{\zeta}^n \right\| - \mathbb{I}\left(\alpha_i + \xi_i > t_i \right) \right].$$

Therefore, we can obtain that for any $i \in \mathcal{S}$, there is

$$\inf_{\boldsymbol{\xi}} \left[\tilde{\lambda} \left\| \boldsymbol{\xi} - \boldsymbol{\zeta}^n \right\| - \mathbb{I}\left(\alpha_i + \xi_i > t_i \right) \right] = \min \left\{ \inf_{\alpha_i + \xi_i > t_i} \left[\tilde{\lambda} \left\| \boldsymbol{\xi} - \boldsymbol{\zeta}^n \right\| - 1 \right], 0 \right\}. \quad (3.32)$$

Equation (3.32) is valid and can be proven via classification discussion. To this end, we consider the following two cases: (a) and (b).

Case (a): When $\alpha_i + \zeta_i^n > t_i$, we let $\boldsymbol{\xi} = \boldsymbol{\zeta}_n$. Then, we can find that the infimum on both sides of Equation (3.32) is -1.

Case (b): When $\alpha_i + \zeta_i^n \le t_i$, for any $\boldsymbol{\xi} \in \Xi$, one of the two situations (i) $\alpha_i + \xi_i > t_i$ or (ii) $\alpha_i + \xi_i \le t_i$ is true. Hence, the left side of (3.32) can be rewritten as

$$\begin{aligned} &\inf_{\boldsymbol{\xi}} \left[\tilde{\lambda} \left\| \boldsymbol{\xi} - \boldsymbol{\zeta}^n \right\| - \mathbb{I}\left(\alpha_i + \xi_i > t_i \right) \right] \\ &= \min \left\{ \inf_{\alpha_i + \xi_i > t_i} \left[\tilde{\lambda} \left\| \boldsymbol{\xi} - \boldsymbol{\zeta}^n \right\| - 1 \right], \inf_{\alpha_i + \xi_i \le t_i} \left[\tilde{\lambda} \left\| \boldsymbol{\xi} - \boldsymbol{\zeta}^n \right\| \right] \right\} = \min \left\{ \inf_{\alpha_i + \xi_i > t_i} \left[\tilde{\lambda} \left\| \boldsymbol{\xi} - \boldsymbol{\zeta}^n \right\| - 1 \right], 0 \right\} \end{aligned}$$

where the second equality holds because we let $\boldsymbol{\xi} = \boldsymbol{\zeta}^n$.

Through the above discussion, we can finally conclude that for a given $\tilde{\lambda} \ge 0$, $n \in [N]$ and $\boldsymbol{\zeta}^n \in \Omega$,

$$\inf_{\boldsymbol{\xi}} \left[\tilde{\lambda} \left\| \boldsymbol{\xi} - \boldsymbol{\zeta}^n \right\| - \mathbb{I}\left(\alpha_i + \xi_i > t_i, \exists i \in \mathcal{S} \right) \right] = \min \left\{ \min_{i \in \mathcal{S}} \inf_{\alpha_i + \xi_i > t_i} \left[\bar{\xi} \left\| \boldsymbol{\xi} - \boldsymbol{\zeta}^n \right\| - 1 \right], 0 \right\}.$$

At this point, (3.30) is converted to

$$\left\{ \mathbf{t} \in \mathbb{R}_+^{|\mathcal{S}|} : \min_{\tilde{\lambda} \ge 0} \left\{ \theta \tilde{\lambda} - \frac{1}{N} \sum_{n \in [N]} \min \left\{ \min_{i \in \mathcal{S}} \inf_{\alpha_i + \xi_i > t_i} \left(\tilde{\lambda} \left\| \boldsymbol{\xi} - \boldsymbol{\zeta}^n \right\| - 1 \right), 0 \right\} \right\} \le \varepsilon \right\}. \quad (3.33)$$

Second, we attempt to rewrite the term $\inf_{\alpha_i + \xi_i > t_i} \left(\tilde{\lambda} \left\| \boldsymbol{\xi} - \boldsymbol{\zeta}^n \right\| - 1 \right)$ in set (3.33). Using the idea of the proof of **Lemma 2** in Chen et al. (2024), we can show that when $i=1$, for any $n\in[N]$, there exists

$$\begin{aligned}\inf_{\alpha_i+\xi_i>t_i}\left\|\boldsymbol{\xi}-\boldsymbol{\zeta}^n\right\| &= \inf_{\gamma,\boldsymbol{\xi}}\left\{\gamma \middle| \left\|\boldsymbol{\xi}-\boldsymbol{\zeta}^n\right\|\le\gamma,\xi_1>t_1-\alpha_1\right\}\\ &= \sup_{u,\boldsymbol{\upsilon},w}\left\{w(t_1-\alpha_1)-\boldsymbol{\eta}_1^{\mathrm{T}}\boldsymbol{\zeta}^n \middle| u=1,\boldsymbol{\eta}_1=\mathbf{e}_1 w,u\ge\left\|\boldsymbol{\eta}_1\right\|_*,w\ge 0\right\}\\ &= \sup_{w}\left\{\left(t_1-\alpha_1-\zeta_1^n\right)w \middle| 0\le w\le 1\right\}\\ &= \left(t_1-\alpha_1-\zeta_1^n\right)^+.\end{aligned}$$

where $\mathbf{e}_i$ denotes a vector whose i^{th} element is 1 and the rest are 0; the second equality holds because of the strong conic duality. When $i\ge 1$, for all $n\in[N]$, we have

$$\begin{aligned}\inf_{\alpha_i+\xi_i>t_i}\left\|\boldsymbol{\xi}-\boldsymbol{\zeta}^n\right\| &= \min_{i\in\mathcal{S}}\left\{\inf_{\gamma,\boldsymbol{\xi}}\left\{\gamma:\gamma\ge\left\|\boldsymbol{\xi}-\boldsymbol{\zeta}^n\right\|,\xi_i>t_i-\alpha_i\right\}\right\}\\ &= \min_{i\in\mathcal{S}}\left\{\left(t_i-\alpha_i-\zeta_i^n\right)^+\right\}=\left(\min_{i\in\mathcal{S}}\left\{t_i-\alpha_i-\zeta_i^n\right\}\right)^+.\end{aligned}$$

Finally, we define $g\left(\mathbf{t},\boldsymbol{\zeta}^n\right):=\left(\min_{i\in\mathcal{S}}\left\{t_i-\alpha_i-\zeta_i^n\right\}\right)^+$ and J_2 can be reformulated as J_2':

$$J_2':=\left\{\mathbf{t}\in\mathbb{R}_+^{|S|}\middle|\begin{array}{c}\theta\tilde{\lambda}-\varepsilon\le\frac{1}{N}\sum_{a\in[N]}\min\left\{\tilde{\lambda}g\left(\mathbf{t},\boldsymbol{\zeta}^n\right)-1,0\right\}\\ \tilde{\lambda}\ge 0\end{array}\right\}. \tag{3.34}$$

Step C: We prove that (3.34) is equivalent to J_2 in this step. The proof process is divided into the following two parts.

$\left(J_2'\subseteq J_2\right)$. When we have $\mathbf{t}\in J_2'$, we know that $\exists\tilde{\lambda}\ge 0$ such that $\left(\mathbf{t},\tilde{\lambda}\right)$ satisfies Constraint (3.34). If $\tilde{\lambda}>0$, then we set $\lambda=1/\tilde{\lambda}$. We can obtain that Constraint (3.34) holds with $(\mathbf{t},\lambda)$. Therefore, $\mathbf{t}\in J_2$. If we have $\tilde{\lambda}=0$, then $-\varepsilon\le -1$ in J_2', which contradicts the condition that $\varepsilon\in(0,1)$.

$\left(J_2\subseteq J_2'\right)$. When we have $\mathbf{t}\in J_2$, we need to explore whether there is $\lambda\ge 0$ such that $(\mathbf{t},\lambda)$ satisfies Constraint (3.34). If $\lambda>0$, then we let

$\lambda = 1/\tilde{\lambda}$. Then, vector $(\mathbf{t},\lambda)$ satisfies Constraint (3.34). Therefore, $\mathbf{t}\in J_2$. When $\lambda=0$, we find that $\min\left\{g\left(\mathbf{t},\zeta^n\right)-\lambda,0\right\}=0$ for all $n\in[N]$ in J_2, and we can conclude that $\theta\le 0$ in J_2, which is against $\theta>0$. □

Following **Proposition 3.1** proposed above, set J_2 is mixed integer representable. We illustrate this point through **Proposition 3.2** below.

Proposition 3.2. Let J_2 be a mixed integer represented as follows:

$$J_3=\left\{\mathbf{t}\in\mathbb{R}_+^{|\mathcal{S}|}:\begin{array}{l}\theta\omega-\varepsilon\lambda\le\dfrac{1}{N}\sum_{n\in[N]}\psi_n \\ \psi_n+\lambda\le\max\left\{t_i-\alpha_i-\zeta_i^n,0\right\},\forall i\in\mathcal{S},n\in[N] \\ \psi_n\le 0,\forall n\in[N] \\ \omega\ge 1,\lambda\ge 0\end{array}\right\}. \quad \begin{array}{r}(3.35a)\\(3.35b)\\(3.35c)\\(3.35d)\end{array}$$

Proof of Proposition 3.2. This proof process is equivalent to proving that $J_2=J_3$. We consider the following two cases.

$(J_3\subseteq J_2)$. If $\mathbf{t}\in J_3$, then there exists $(\lambda,\omega,\boldsymbol{\psi},\mathbf{t})^{\mathrm{T}}$ such that Constraint (3.34) holds, where $\boldsymbol{\psi}=(\psi_n)$. For any $i\in\mathcal{S}$, we can obtain

$$\begin{aligned}\frac{\psi_a}{\omega}&\le\min\left\{\frac{1}{\omega}\min_{i\in\mathcal{S}}\max\left\{t_i-\alpha_i-\zeta_i^n,0\right\}-\frac{\lambda}{\omega},0\right\}\\&\le\min\left\{\min_{i\in\mathcal{S}}\max\left\{t_i-\alpha_i-\zeta_i^n,0\right\}-\frac{\lambda}{\omega},0\right\}=\min\left\{g\left(\mathbf{t},\zeta^n\right)-\frac{\lambda}{\omega},0\right\}\end{aligned}$$

where the second inequality holds since $\omega\ge 1$. Now, we divide both sides of inequality (3.35a) by ω and obtain

$$\theta-\varepsilon\frac{\lambda}{\omega}\le\frac{1}{N}\sum_{n\in[N]}\frac{\psi_a}{\omega}\le\frac{1}{N}\sum_{n\in[N]}\min\left\{g\left(\mathbf{t},\zeta^n\right)-\frac{\lambda}{\omega},0\right\}.$$

This shows that $\left(\mathbf{t},\dfrac{\lambda}{\omega}\right)$ satisfies J_2, that is, $J_3\subseteq J_2$.

$(J_2\subseteq J_3)$. If $\mathbf{t}\in J_2$, then we know that there exists a vector $(\mathbf{t},\lambda)$ that satisfies Constraint (3.31). For any $n \in [N]$, we set $\lambda' = \lambda$, $\omega = 1$, and $\psi_n = \min_{i\in\mathcal{S}} \left\{ \max\left\{ t_i - \alpha_i - \zeta_i^n \right\} - \lambda', 0 \right\}$. Then, $\left(\hat{\xi}, \omega, \mathbf{J}, \mathbf{y}\right)$ satisfies (3.35), and $\mathbf{t} \in J_3$. This completes the proof. □

After we use **Proposition 3.2** to complete the transformation of Constraint (3.7), we find that there are still nonlinear terms in the obtained set J_3. Therefore, we introduce a new proposition to eliminate the nonlinear terms in set J_3 by adding some big-M coefficients.

Proposition 3.3 (Big-M transformation). Let $\mathbf{M} \in \mathbb{R}_+^N$ denote a vector consisting of N big-M coefficients, i.e., $\mathbf{M} = (M_n)$, and $\min_{i\in\mathcal{S}} \max_{\mathbf{t}\in J_3} \left\{ \left| t_i - \alpha_i - \zeta_i^n \right| \right\} \le M_n$ for all $n \in [N]$. Then, J_3 can be reformulated as J_4.

$$
J_4 = \left\{ \mathbf{t} \in \mathbb{R}_+^{|\mathcal{S}|} : \begin{array}{ll}
\theta\omega - \varepsilon\lambda \le \frac{1}{N}\sum_{n\in[N]} \psi_n & \text{(3.36a)} \\
\psi_n + \lambda \le \pi_n, \forall n \in [N] & \text{(3.36b)} \\
\pi_n \le t_i - \alpha_i - \zeta_i^n + M_n\sigma_n, \forall i \in \mathcal{S}, n \in [N] & \text{(3.36c)} \\
\pi_n \le M_n\left(1 - \sigma_n\right), \forall n \in [N] & \text{(3.36d)} \\
\omega \ge 1 & \text{(3.36e)} \\
\lambda \ge 0 & \text{(3.36f)} \\
\psi_n \le 0, \pi_n \ge 0, \sigma_n \in \{0,1\}, \forall n \in [N] & \text{(3.36g)}
\end{array} \right\}.
$$

Proof of Proposition 3.3. After we introduce $\sigma_n \in \{0,1\}$ and the big-M coefficient M_n, we can reformulate the constraint

$$\psi_n + \lambda \le \max\left\{ t_i - \alpha_i - \zeta_i^n, 0 \right\} \qquad \forall i \in \mathcal{S}, n \in [N]$$

as the following two constraints:

$$\psi_n + \lambda \le t_i - \alpha_i - \zeta_i^n + M_n\sigma_n \qquad \forall i \in \mathcal{S}, n \in [N] \tag{3.37}$$

$$\psi_n + \lambda \le M_n\left(1 - \sigma_n\right) \qquad \forall i \in \mathcal{S}, n \in [N]. \tag{3.38}$$

The existence of the auxiliary variable $\sigma_n \in \{0,1\}$ allows Constraints (3.37) and (3.38) to be valid and only one of them. Since $\left(t_i - \alpha_i - \zeta_i^n\right)$, ψ_n and λ are bounded, one can always find a bounded coefficient M_n. We can transform (3.37)–(3.38) into (3.36b)–(3.36d) by simply introducing a constraint $\psi_n + \lambda \le \pi_n$, where $\pi_n \ge 0$. □

Remark 3.2. The big-M coefficients in Constraints (3.36c) and (3.36d) can be further set to $M_{i,n}^1$ and $M_{i,n}^2$, respectively, and their values can be set as follows:

$$M_{i,n}^1 \ge \max_{\mathbf{t} \in \mathrm{dom}(\mathbf{t})} \left\{\zeta_i^n - t_i + \alpha_i\right\} \tag{3.39}$$

$$M_{i,n}^2 \ge \max_{\mathbf{t} \in \mathrm{dom}(\mathbf{t})} \left\{t_i - \alpha_i - \zeta_i^n\right\} \tag{3.40}$$

where $\mathrm{dom}(\mathbf{t})$ represents the domain of vector $\mathbf{t}$ defined in **M1**. After replacing M, Constraints (3.35c) and (3.35d) are rewritten as

$$\pi_n \le t_i - \alpha_i - \zeta_i^n + M_{i,n}^1 \sigma_n \qquad \forall i \in \mathcal{S}, n \in [N]$$

$$\pi_n \le M_{i,n}^2 \left(1 - \sigma_n\right) \qquad \forall i \in \mathcal{S}, n \in [N].$$

After our efforts mentioned above, the original DRCC model, i.e., **M2**, is rewritten as a computationally tractable MIP model **M3**.

M3:

$$\min_{\left(\boldsymbol{p}, \boldsymbol{t}, \boldsymbol{\pi}_{\mathrm{S}}, \boldsymbol{\pi}_{\mathrm{T}}, \boldsymbol{\varphi}^+, \boldsymbol{\varphi}^-, \boldsymbol{\delta}^+, \boldsymbol{\delta}^-, \boldsymbol{\gamma}^+, \boldsymbol{\gamma}^-\right)} obj = \sum_{i \in \mathcal{S}} \left[C_i^1 \left(\varphi_i^+ + \varphi_i^-\right) + C_i^2 \delta_i^+ + C_i^3 \gamma_i^+ \right] \tag{3.41}$$

$s.t.$ (3.2)–(3.5), (3.7)–(3.9), (3.21)–(3.24), and $\mathbf{t} \in J_5$.

3.3.3. Model strengthening

According to Ho-Nguyen et al. (2022b), **M3** can present a significant challenge in terms of its solution. In certain particular scenarios, even following a period of one hour devoted to computation employing commercial solvers (e.g., CPLEX), a substantial optimality gap remains. Therefore, in this section, we discuss several methods to strengthen the model. On the one hand, we try to reduce the values of big-M coefficients; on the other hand, we strengthen the model formulations. Specifically, Section 3.3.3.1 introduces how to integrate the SAA formulation into the DRCC to achieve model enhancement. Then, in Section 3.3.3.2 we introduce a coefficient strengthening method via the VaR outer approximation.

3.3.3.1. Model strengthening by SAA constraints

This section introduces the relationship between set J_4 and traditional SAA methods. The core of the SAA method is to introduce the following set to address chance constraints:

$$J_{\text{SAA}} = \left\{ \mathbf{t} \in \mathbb{R}_+^{|\mathcal{S}|} : \frac{1}{N} \sum_{a \in [N]} \mathbb{I}\left(t_i \geq \alpha_i + \xi_i, \forall i \in \mathcal{S}\right) \geq 1 - \varepsilon \right\}.$$

Notably, when the radius $\theta \in \mathbb{R}_+$ of our type-1 Wasserstein ambiguity set is set to 0, we have $\mathcal{P}(\theta) = \mathcal{P}(0)$ and $\text{dis}_{\text{Type 1-W}}\left(\mathbb{P}, \mathbb{P}_\zeta^N\right) = 0$. At this time, there is only one element in set $\mathcal{P}(0)$, i.e., the empirical distribution $\mathbb{P}_\zeta^N$. Currently, J_1 coincides with J_{SAA}. Correspondingly, the DRO model is also reduced to the SO model. J_{SAA} is a relaxation version of J_1 because $\mathcal{P}(0) \subseteq \mathcal{P}(\theta)$ for any $\theta \geq 0$. This feature helps us make further improvements to the MIP formulation J_4. In accordance with Ruszczyński (2002) and Luedtke et al. (2010), we establish the following MIP reformulation, also known as the big-M formulation.

$$J_{\mathrm{SAA}}=\left\{\mathbf{t}\in\mathbb{R}_{+}^{|\mathcal{S}|}:\begin{array}{ll}t_i-\alpha_i-\zeta_i^n+M_n\hat{\sigma}_n\geq 0,\forall i\in\mathcal{S},n\in[N] & \text{(3.42a)}\\ \sum_{n\in[N]}\hat{\sigma}_n\geq N-\lfloor N\varepsilon\rfloor+\mathbb{I}(\theta>0) & \text{(3.42b)}\\ \hat{\sigma}_n\in\{0,1\},\forall n\in[N] & \text{(3.42c)}\end{array}\right\}$$

where M_n are sufficiently large constants and $\hat{\sigma}_n$ is a binary indicator variable. If $t_i-\alpha_i-\zeta_i^n<0$ for some $n\in[N]$, then we have $\hat{\sigma}_n=0$. In practice, we usually call Constraint (3.42a) the big-M constraint and Constraint (3.42b) the knapsack or cardinality constraint. Since J_{SAA} is a relaxation version of J_1, we can add inequalities in (3.42) to J_1. At this point, the abovementioned set J_1 can be reconstructed into J_5.

$$J_5=\left\{\mathbf{t}\in\mathbb{R}_{+}^{|\mathcal{S}|}:\begin{array}{ll}\theta\omega-\varepsilon\lambda\leq\frac{1}{N}\sum_{n\in[N]}\psi_n & \text{(3.43a)}\\ \psi_n+\lambda\leq\pi_n,\forall a\in[N] & \text{(3.43b)}\\ \pi_n\leq t_i-\alpha_i-\zeta_i^n+M_n\sigma_n,\forall i\in\mathcal{S},n\in[N] & \text{(3.43c)}\\ \pi_n\leq M_n(1-\sigma_n),\forall a\in[N] & \text{(3.43d)}\\ t_i-\alpha_i-\zeta_i^n+M_n\hat{\sigma}_n\geq 0,\forall i\in\mathcal{S},n\in[N] & \text{(3.43e)}\\ \sum_{n\in[N]}\hat{\sigma}_n\geq N-\lfloor N\varepsilon\rfloor+\mathbb{I}(\theta>0) & \text{(3.43f)}\\ \omega\geq 1 & \text{(3.43g)}\\ \lambda\geq 0 & \text{(3.43h)}\\ \psi_n\leq 0,\pi_n\geq 0,\sigma_n\in\{0,1\},\hat{\sigma}_n\in\{0,1\},\forall n\in[N] & \text{(3.43i)}\end{array}\right\}$$

However, doing so results in two sets of binary variables (each group contains N binary variables) in J_5, i.e., $\sigma_n\in\{0,1\}$ $(\forall n\in[N])$ and $\hat{\sigma}_n\in\{0,1\}$ $(\forall n\in[N])$, which may increase the time it takes to run the solver. Therefore, we use a key proposition, i.e., **Proposition 3.4**, to prove that $\hat{\sigma}_n\in\{0,1\}$ can be *simply* replaced by $\sigma_n\in\{0,1\}$ *without* affecting the validity of J_1, thereby reducing the introduction of variables.

Proposition 3.4. We have $J_5=J_6$, where

$$J_6 = \left\{ \mathbf{t} \in \mathbb{R}_+^{|\mathcal{S}|} : \begin{array}{ll} \theta\omega - \varepsilon\lambda \le \frac{1}{N}\sum_{n\in[N]} \psi_n & \text{(3.44a)} \\ \psi_n + \lambda \le \pi_n, \forall a \in [N] & \text{(3.44b)} \\ \pi_n \le t_i - \alpha_i - \zeta_i^n + M_{i,n}^1 (1-\sigma_n), \forall i \in \mathcal{S}, n \in [N] & \text{(3.44c)} \\ \pi_n \le M_{i,n}^2 \sigma_n, \forall i \in \mathcal{S}, \forall a \in [N] & \text{(3.44d)} \\ t_i - \alpha_i - \zeta_i^n + M_n \sigma_n \ge 0, \forall i \in \mathcal{S}, n \in [N] & \text{(3.44e)} \\ \sum_{n\in[N]} \sigma_n \ge N - \lfloor N\varepsilon \rfloor + \mathbb{I}(\theta > 0) & \text{(3.44f)} \\ \omega \ge 1 & \text{(3.44g)} \\ \lambda \ge 0 & \text{(3.44h)} \\ \psi_n \le 0, \pi_n \ge 0, \sigma_n \in \{0,1\}, \forall n \in [N] & \text{(3.44i)} \end{array} \right\}.$$

Proof of Proposition 3.4. To prove that $J_5 = J_6$, we need only $J_5 \subseteq J_6$ and $J_6 \subseteq J_5$. Obviously, $J_6 \subseteq J_5$. Therefore, we need only prove that $J_5 \subseteq J_6$. To this end, we assume that $\mathbf{t} \in J_5$ with some $(\omega, \lambda, \boldsymbol{\pi}, \boldsymbol{\psi}, \boldsymbol{\sigma})$, and we can find that a vector $\boldsymbol{\sigma}^* \in \{0,1\}^N$ satisfies (3.43), i.e., for any $n \in [N]$, we have $\sigma_n^* = 1$ if $\min_{i\in\mathcal{S}} \{t_i - \alpha_i - \zeta_i^n\} < 0$ and $\sigma_n^* = 0$ if $\min_{i\in\mathcal{S}} \{t_i - \alpha_i - \zeta_i^n\} \ge 0$. For ease of notation, we let $f(\mathbf{t}, \boldsymbol{\zeta}^n) := \min_{i\in\mathcal{S}} \{t_i - \alpha_i - \zeta_i^n\}$. Since M_n is sufficiently large, we have $f(\mathbf{t}, \boldsymbol{\zeta}^n) + M_n \ge 0$; thus, $(\mathbf{t}, \boldsymbol{\sigma}^*)$ satisfies (3.43e). Moreover, for any $n \in [N]$, we can reduce Constraints (3.43c) and (3.43d) to $\min\{ f(\mathbf{t}, \boldsymbol{\zeta}^n) + M_n\sigma_n, M_n(1-\sigma_n)\} \ge \pi_n$. Owing to the properties of $\boldsymbol{\sigma}^*$ and M_n, for any $n \in [N]$, we know that $\min\{ f(\mathbf{t}, \boldsymbol{\zeta}^n) + M_n\sigma_n^*, M_n(1-\sigma_n^*)\}$ equals 0 if $f(\mathbf{t}, \boldsymbol{\zeta}^n) < 0$ and equals $f(\mathbf{t}, \boldsymbol{\zeta}^n)$ otherwise. Hence, we can obtain

$$\min\{ f(\mathbf{t}, \boldsymbol{\zeta}^n) + M_n\sigma_n^*, M_n(1-\sigma_n^*)\} \ge \min\{ f(\mathbf{t}, \boldsymbol{\zeta}^n) + M_n\sigma_n, M_n(1-\sigma_n)\} \ge \pi_n$$

for any $\sigma_n \in \{0,1\}$. Obviously, $(\omega, \lambda, \boldsymbol{\pi}, \boldsymbol{\psi}, \boldsymbol{\sigma}^*, \mathbf{t})$ satisfies (3.43c)–(3.43d) because $(\omega, \lambda, \boldsymbol{\pi}, \boldsymbol{\psi}, \boldsymbol{\sigma})$ already satisfies (3.43c)–(3.43d). Then, we have

$$\frac{1}{N}\sum_{n\in[N]} \sigma_n^* = \frac{1}{N}\sum_{n\in[N]} \mathbb{I}(t_i \ge \alpha_i + \xi_i, \forall i \in \mathcal{S}) \ge 1 - \varepsilon,$$

where the first equality holds because of the property of $\boldsymbol{\sigma}^*$; the second inequality is the result of (3.42). Hence, $(\omega,\lambda,\boldsymbol{\pi},\boldsymbol{\psi},\boldsymbol{\sigma}^*,\mathbf{t})$ satisfies (3.43f). Finally, we can conclude that $\mathbf{t}\in J_6$, which indicates that $J_5\subseteq J_6$. □

After our efforts mentioned above, the original MIP formulation **M3** can be strengthened by introducing SAA constraints, i.e., (3.42), and reconstructed into **M4**.

<u>**M4:**</u>

$$\min_{\left(p,t,x_{\mathrm{S}},x_{\mathrm{T}},\varphi^+,\varphi^-,\delta^+,\delta^-,\gamma^+,\gamma^-\right)} obj=\sum_{i\in\mathcal{S}}\left[C_i^1\left(\varphi_i^+ + \varphi_i^-\right)+C_i^2\delta_i^+ + C_i^3\gamma_i^+\right] \tag{3.45}$$

$$s.t.\ \ \text{(3.2)–(3.5), (3.7)–(3.9), (3.21)–(3.24), and } \mathbf{t}\in J_6.$$

After our efforts mentioned above, the original DRCC model, i.e., **M2**, is rewritten as MIP model **M3**.

3.3.3.2. Coefficient strengthening via the VaR outer approximation

According to **Theorem 3** in Xie (2021), we can obtain a lower bound of **M3** by performing a VaR outer approximation of chance constraint (3.7). The VaR outer approximation is shown below.

$$\min_{\left(p,t,x_{\mathrm{S}},x_{\mathrm{T}},\varphi^+,\varphi^-,\delta^+,\delta^-,\gamma^+,\gamma^-\right)} obj=\sum_{i\in\mathcal{S}}\left[C_i^1\left(\varphi_i^+ + \varphi_i^-\right)+C_i^2\delta_i^+ + C_i^3\gamma_i^+\right] \tag{3.46}$$

$$s.t.\ \ \text{(3.2)–(3.5), (3.7)–(3.9), (3.21)–(3.24), and}$$

$$\mathbf{t}\in J_{\mathrm{out}}:=\left\{\mathbf{t}\in\mathbb{R}_+^{|\mathcal{S}|}:\begin{array}{l}\theta\varepsilon^{-1}+\zeta_i^n\le t_i-\alpha_i+M_{i,n}^{\mathrm{VAR}}\left(1-\tilde{\sigma}_n\right),\forall i\in\mathcal{S},n\in[N]\\ \sum_{n\in[N]}\tilde{\sigma}_n\ge N-\lfloor N\varepsilon\rfloor\\ \tilde{\sigma}_n\in\{0,1\},\forall n\in[N]\end{array}\right\} \tag{3.47}$$

where $M_{i,n}^{\mathrm{VAR}}$ is a sufficiently large constant and $M_{i,n}^{\mathrm{VAR}}\ge \max_{t_i\in\mathrm{dom}(t_i)}\left\{\theta\varepsilon^{-1}+\zeta_i^n-t_i+\alpha_i\right\}$ for all $i\in\mathcal{S}$ and $n\in[N]$.

Using this outer approximation, we can strengthen the big-M coefficients in (3.39) and (3.40) by relaxing $\tilde{\sigma}_n \in \{0,1\}^N$ in J_{out} to $\tilde{\sigma}_n \in [0,1]^N$. At this point, Constraints (3.39) and (3.40) can be reformulated as

$$M^1_{i,n} \geq \max_{\tilde{\boldsymbol{\sigma}},\mathbf{t}\in\text{dom}(\mathbf{t})} \left\{ \zeta^n_i - t_i + \alpha_i : \begin{array}{l} \theta\varepsilon^{-1} + \zeta^n_i \leq t_i - \alpha_i + M^{\text{VAR}}_{i,n}\left(1-\tilde{\sigma}_n\right), \forall i \in \mathcal{S}, n \in [N] \\ \sum_{n\in[N]} \tilde{\sigma}_n \geq N - \lfloor N\varepsilon \rfloor \\ \tilde{\sigma}_n \in [0,1], \forall n \in [N] \end{array} \right\} \tag{3.48}$$

$$M^2_{i,n} \geq \max_{\tilde{\boldsymbol{\sigma}},\mathbf{t}\in\text{dom}(\mathbf{t})} \left\{ t_i - \alpha_i - \zeta^n_i : \begin{array}{l} \theta\varepsilon^{-1} + \zeta^n_i \leq t_i - \alpha_i + M^{\text{VAR}}_{i,n}\left(1-\tilde{\sigma}_n\right), \forall i \in \mathcal{S}, n \in [N] \\ \sum_{n\in[N]} \tilde{\sigma}_n \geq N - \lfloor N\varepsilon \rfloor \\ \tilde{\sigma}_n \in [0,1], \forall n \in [N] \end{array} \right\} \tag{3.49}$$

where $\tilde{\boldsymbol{\sigma}} = \left(\tilde{\sigma}_n\right)$.

3.4. Numerical experiments

In this section, we conduct a series of numerical experiments to verify the effectiveness of the model and algorithm. First, we introduce the data we use in Section 3.4.1. Section 3.4.2 compares different acceleration strategies and observes the implementation effects of these strategies. Several sensitivity analyses of the key parameters are carried out in Section 3.4.3. Section 3.4.4 conducts out-of-sample analysis. Finally, Section 3.4.5 provides some management insights.

3.4.1. Data description

The data used in our experiments come from a public dataset. Interested readers can visit http://sweet.ua.pt/aagra/ to obtain relevant information. For labeling convenience, we use R_S_i to represent each instance. Here, S denotes the number of vessels, where $6 \le S \le 15$ and $S \in \mathbb{Z}_+$, and i is a serial number indicating an instance. The total length of the wharf (L^{Total}) is set to 1100 m, which is similar to the actual length of Tianjin Port in China (1202 m). The length of each vessel (L_i), the estimated arrival time of each vessel (α_i), the total amount of cargo loaded on each vessel (C_i^{cap}), and the quay crane operation efficiency (Q_0) are all from the abovementioned public database. Following Agra and Rodrigues (2022), the operation time (i.e., cargo handling time) of vessel $i \in \mathcal{S}$, i.e., h_i, can be calculated via $h_i = C_i^{\text{cap}} / 1.5Q_0$. The coefficient 1.5 in the above equation is used to make the time range from 4 hours to 2 days to better fit the real-world situation. The estimated departure time of each vessel (β_i) is set to $\beta_i = \alpha_i + 1.2h_i$. The cost coefficient C_i^1 is set to $20L_i/230$ USD, and the cost coefficients C_i^2 and C_i^3 are both set to $4000L_i/230$ USD (Kim & Moon, 2003; Zeng et al., 2011b). The lowest cost berthing position of each vessel (p_i^{Best}) is generated according to the uniform distribution $U\left[0, L^{\text{Total}} - L_i\right]$. The starting/ending positions suitable for berthing each vessel ($B_i^{\min}$ and $B_i^{\max}$) are generated on the basis of $U\left[0, 0.8L^{\text{Total}}\right]$ and $U\left[0.2L^{\text{Total}}, L^{\text{Total}} - L_i\right]$, respectively. Note that we need to verify that $B_i^{\max} - B_i^{\min} \ge L_i$ holds. The samples of the arrival delay time of each vessel are generated based on the uniform distribution $U\left[0,10\right]$. In each instance, we randomly generated 1,000 samples for each vessel. In other words, we set $\Omega = \left\{\zeta^1, \zeta^2, \zeta^3, \cdots, \zeta^n, \cdots, \zeta^{1000}\right\}$ $\subseteq \Xi$ for each instance. Finally, we set the length of the planning period (T) to one week (168 hours). For the experiments, we use GAMS with the default options (https://www.gams.com/) for programming, and all programs are run on a laptop produced by *Lenovo* with an Intel® Core™ Ultra 5-125H CPU and 32 GB of RAM.

3.4.2. The effects of the acceleration strategies

This section verifies the effectiveness of several acceleration strategies we propose in Section 3.3.3. To this end, we use 10 instances to conduct comparative experiments. Specifically, we conduct experiments on instances R_S_1, where $6 \le S \le 15$ and $S \in \mathbb{Z}_+$. Three different strategies are considered:

- Basic: In this strategy scenario, we do not consider any acceleration strategies.
- SAA: In this strategy scenario, we implement model strengthening by introducing SAA constraints (see Section 3.3.3.1).
- Coe: In this strategy scenario, we implement coefficient strengthening by performing a VaR outer approximation on the model (see Section 3.3.3.2).

The running time of the program, in seconds, considering different strategy scenarios and their combinations is shown in Table 3.2. In this table, each row represents the calculation of an instance under four different strategies (or strategy combinations), and the bold numbers represent the shortest program running time. The optimality gaps when solving the model via the four strategies in different instances are also reported, all of which are zero. We can clearly see that the strategies SAA and Coe have a significant effect on reducing the program running time.

Table 3.2 Performance of different acceleration strategies

No.	Instance	Program running time (s)				Optimality gap
		Basic	SAA	Coe	SAA+Coe	(%)
1	R_6_1	3.51	1.36	**1.35**	1.36	0.00
2	R_7_1	4.84	1.26	1.99	**1.24**	0.00
3	R_8_1	3.57	**1.91**	2.78	2.01	0.00
4	R_9_1	53.38	5.33	**4.50**	4.59	0.00
5	R_10_1	36.71	4.62	**3.84**	5.37	0.00
6	R_11_1	4.08	3.09	3.36	**1.96**	0.00
7	R_12_1	549.69	246.70	**56.48**	195.05	0.00
8	R_13_1	607.35	25.45	828.81	90.23	0.00
9	R_14_1	182.26	39.99	**52.43**	33.47	0.00
10	R_15_1	571.43	116.71	**21.93**	179.39	0.00

Specifically, the Coe strategy demonstrates dominant acceleration capabilities in 60% of several instances (e.g., instances R_6_1, R_9_1, R_10_1, R_12_1, and R_15_1), exhibiting particularly profound scalability for larger instances: for example, it reduces runtime by 89.7% (from 549.69 s to 56.48 s in R_12_1) and 96.2% (from 571.43 s to 21.93 s in R_15_1) compared with the Basic strategy scenario, while it also outperforms the SAA scenario by 77% in R_12_1. Moreover, the SAA strategy delivers consistent but modest gains for smaller-scale problems (i.e., R_6_1 to R_8_1) but struggles with computational intensity in large instances such as instance R_12_1 (246.70 s). Crucially, the hybrid strategy (i.e., SAA+Coe) fails to consistently leverage synergies: it achieves the lowest runtime in only two instances (i.e., R_7_1 and R_11_1) but underperforms the standalone Coe strategy in critical cases such as R_10_1 and R_15_1. The above results are different from our conventional understanding. It is not the case that the more acceleration strategies are added during the calculation process, the better the acceleration effect. Collectively, these results position the Coe strategy as the most potent accelerator for large-scale optimization problems.

3.4.3. Results and analysis

3.4.3.1. Impact of the tolerance level

This section conducts a sensitivity analysis on the port manager's predetermined service level. In other words, we change parameter ε in (3.7) to adjust the service level set by port managers. We set 10 different values of ε with an initial value of 0.01 (corresponding to a service level of 99%) and a step size of 0.01. Therefore, as ε increases, the service level set by the port manager gradually decreases. Fig. 3.1 shows the sensitivity of objective function values to the service level parameter ε across four heterogeneous instances, revealing a consistent negative correlation. Moreover, this downward trend is fast at first and then slow. For example, the initial service level decrease from $\varepsilon = 0.01$ to $\varepsilon = 0.03$ (service level from 99% to 97%) triggers precipitous objective function value reductions, most pronounced in R_15_1, with a 45.6% decrease (from 4503.06 to 2448.79). Beyond $\varepsilon = 0.08$ (service level <92%), marginal improvements become negligible (<1.5% per step). These results are in line with our expectations. First, when port managers set higher service levels, they will inevitably set more conservative schemes for berth allocation, which will lead to an increase in the penalty costs of berthing time. As service levels gradually decrease, berth allocation schemes become less conservative. Second, as the service level decreases, the effect of reducing time penalty costs becomes less obvious. This is because, for lower service levels, regardless of how the berth allocation scheme is adjusted, it is almost impossible to further reduce various costs. Therefore, the curve shown in Fig. 3.1 is steep at first and then flat, and the result is the same for all four instances. The above results show that port managers should set the port's service level scientifically. In the four instances, a decrease in the service level from 99% ($\varepsilon = 0.01$) to 97% ($\varepsilon = 0.03$) can result in a decrease of nearly half of the objective function value. Port managers' excessive pursuit of extremely high service levels often leads to enormous cost investments, which are not conducive to the allocation of port funds.

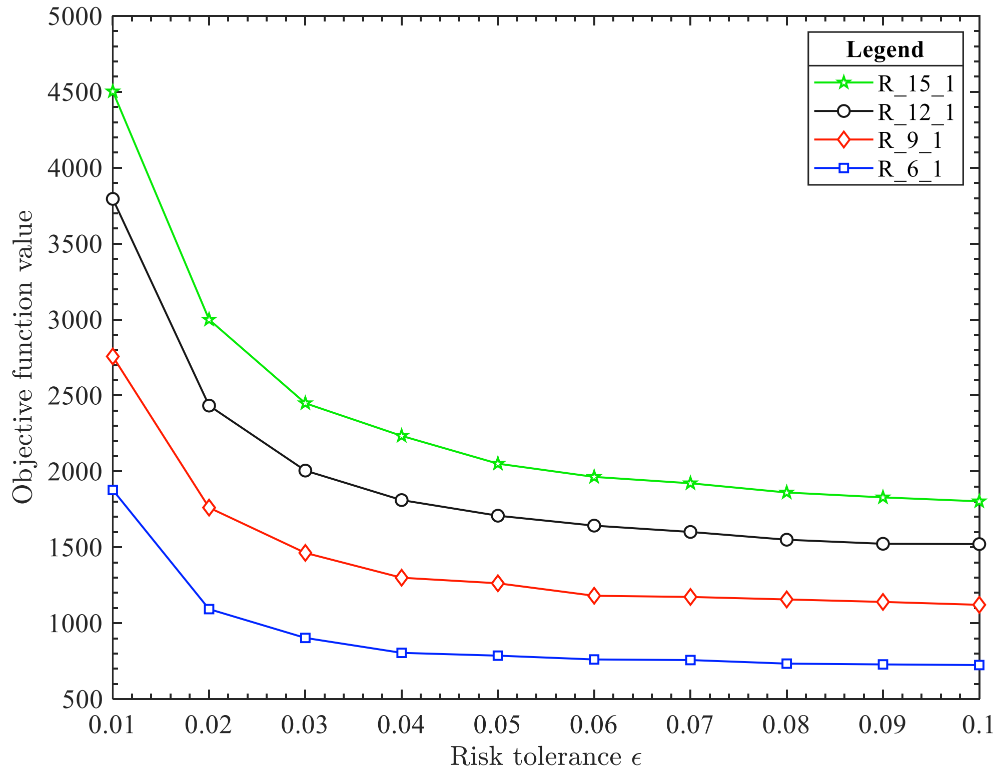

Fig. 3.1 Cost of the model solution as a function of the parameter ε $(\theta = 0.1)$

3.4.3.2. Impact of the radius of the ambiguity set

This section presents a sensitivity analysis of the radius of the type-1 Wasserstein ambiguity set. We consider four representative instances, i.e., R_6_1, R_9_1, R_12_1, and R_15_1. Specifically, we keep parameter $\varepsilon = 0.05$ (the port manager's predetermined service level is 95%) in all instances and adjust the parameter θ in ambiguity set (3.24). For each instance, we set the minimum radius θ_1 to 0.001. Then, we increase the parameter radius in each instance until the model has no feasible solution and obtain a maximum radius parameter value θ_{10}. On the basis of θ_1 and θ_{10}, we divide the interval $[\theta_1, \theta_{10}]$ into 9 equal parts and obtain 8 radius values from θ_2 to θ_9. Fig. 3.2 quantifies the sensitivity of objective function values to parameter θ variations across four representative instances. We can see that parameter θ directly affects the cost of distributionally robust solutions. All instances exhibit monotonic cost growth, with R_15_1 displaying the highest absolute costs across all θ values (starting at 1629.911 for θ_1 and reaching 6073.093 at θ_{10}), whereas R_6_1 maintains the lowest costs (626.546 at θ_1 to 2204.657 at θ_{10}). The above curve change trend is in line with our expectations. When the radius θ is equal to 0, the solution of the model is equivalent to the solution of the stochastic programming model with an empirical distribution as the distribution of uncertain parameters. When the radius θ tends to infinity, the solution of the model is equivalent to the solution of the robust optimization model (only the worst case is considered). Therefore, as the radius increases, the model becomes increasingly conservative, which incurs more cost. The above phenomenon is also called the *price of robustness* in Bertsimas and Sim (2004). To obtain a more robust solution (with better risk resistance), more costs are often needed.

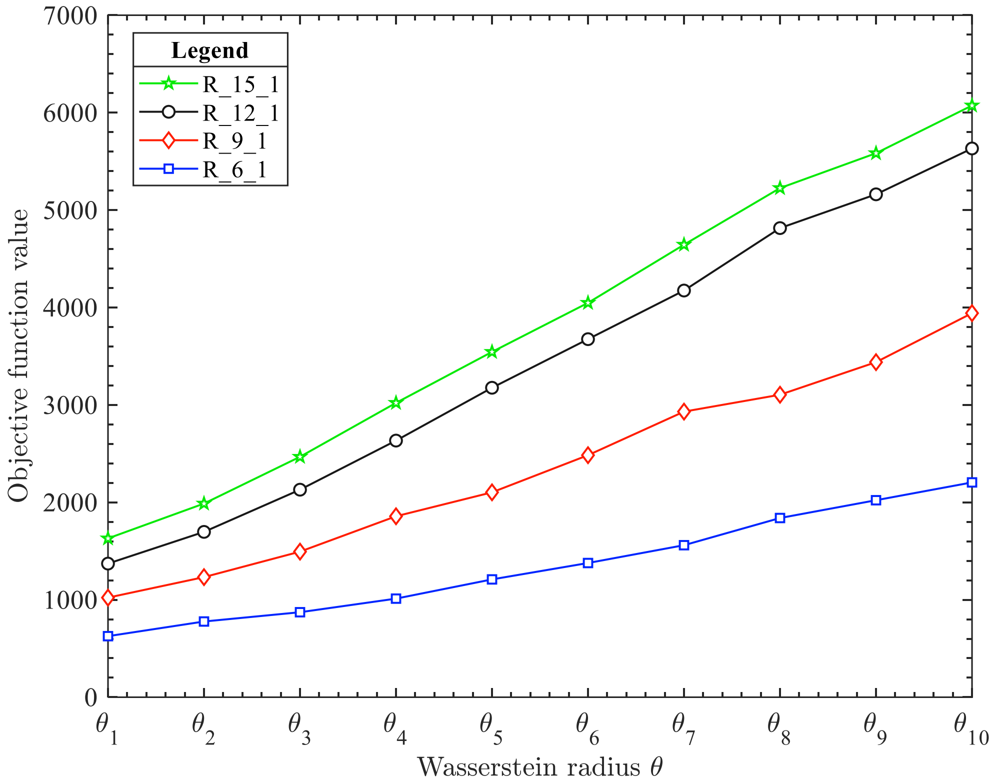

Fig. 3.2 Cost of the model solution as a function of the parameter θ

As the radius changes, the structure of the solution to the model (i.e., the berth allocation scheme) also changes. The solutions corresponding to the four instances in Fig. 3.3 are summarized in Table 3.3. Intervals $\left[t_i, t_i^{\text{end}}\right]$ and $\left[p_i, p_i^{\text{end}}\right]$ represent the time and space intervals occupied by vessel $i \in \mathcal{S}$, respectively. To visualize the berth allocation scheme, we additionally plotted Figs. 3.3 to 3.6. Fig. 3.3 contrasts spatiotemporal berth allocation solutions to instance R_6_1 at three decisive radius parameter values, i.e., θ_1, θ_6, and θ_{10}. In Fig. 3.3, the horizontal axis represents the time axis, and each unit represents 2 hours. The vertical axis represents the spatial axis, and each unit represents 50 meters.

When $\theta = \theta_1$ (see Fig. 3.3(a)), the vessel berthing time and spatial layout are relatively compact, and the time–space blocks are closely arranged without significant gaps; then, when θ increases to θ_6 (see Fig. 3.3(*b*)), it can be observed that the berthing time of some vessels is significantly delayed, but the spatial position remains essentially unchanged; then, under the high uncertainty of $\theta = \theta_{10}$ (see Fig. 3.3(*c*)), not only is the berthing time of vessels further delayed, but the spatial position is also reorganized, indicating that the response logic of berthing time adjustment takes precedence over spatial reconstruction. The changing trend shown in Figs. 3.4 to 3.6 is basically consistent with that in Fig. 3.3. The above changes in the vessel berthing location and time reflect the changes in the means by which port managers cope with uncertainty. When the uncertainty of the vessel arrival delay time is low, the port manager will prioritize appropriately delaying the berthing time of each vessel. When the uncertainty of the vessel arrival delay time increases further, simply delaying the berthing time is no longer sufficient to address the above uncertainty. At this point, the port manager will choose to systematically adjust the berthing position and time of each vessel.

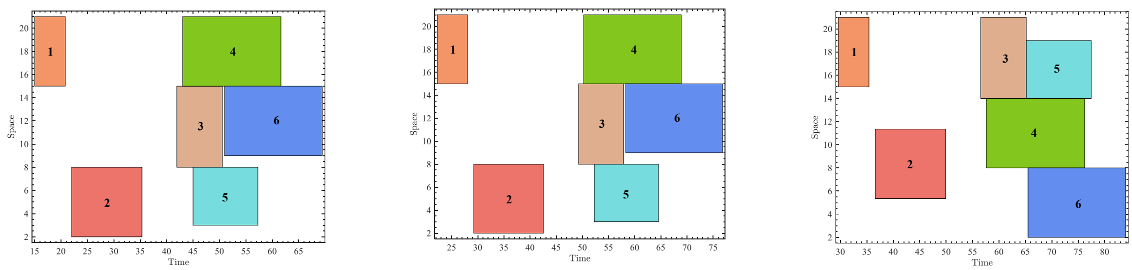

$(a)\,\theta = \theta_1$ $(b)\,\theta = \theta_6$ $(c)\,\theta = \theta_{10}$

Fig. 3.3 Solution of R_6_1 under different radii

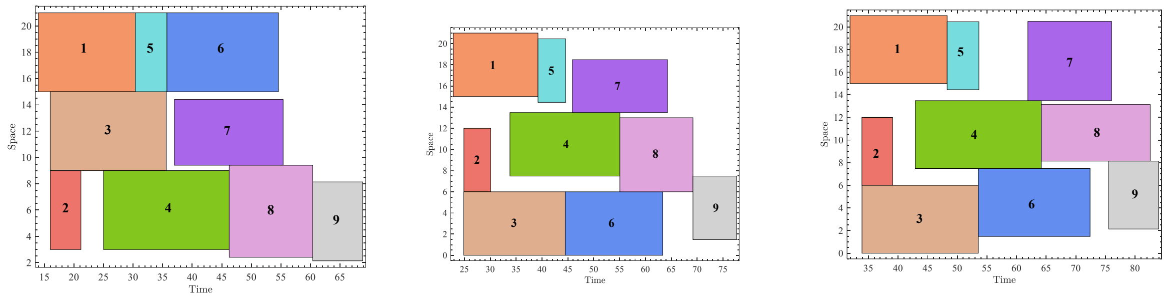

$(a)\,\theta = \theta_1$ $(b)\,\theta = \theta_6$ $(c)\,\theta = \theta_{10}$

Fig. 3.4 Solution of R_9_1 under different radii

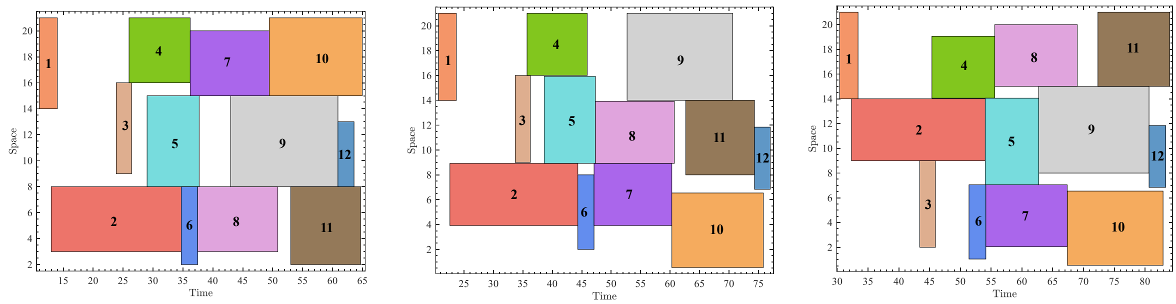

$(a)\,\theta = \theta_1$ $(b)\,\theta = \theta_6$ $(c)\,\theta = \theta_{10}$

Fig. 3.5 Solution of R_12_1 under different radii

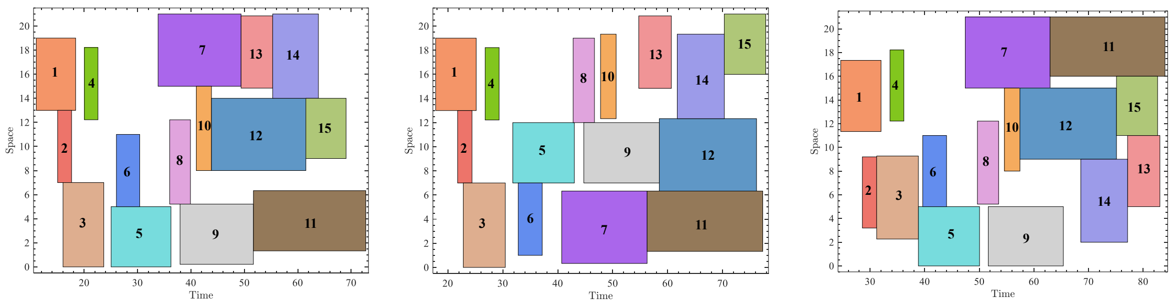

$(a)\,\theta = \theta_1$ $(b)\,\theta = \theta_6$ $(c)\,\theta = \theta_{10}$

Fig. 3.6 Solution of R_15_1 under different radii

Table 3.3 Solutions of four different instances under different radii

Instance	Vessel No.	$\theta=\theta_1$				$\theta=\theta_6$				$\theta=\theta_{10}$			
		t_i	t_i^{end}	p_i	p_i^{end}	t_i	t_i^{end}	p_i	p_i^{end}	t_i	t_i^{end}	p_i	p_i^{end}
R_6_1	1	15.00	20.79	15.00	21.00	22.25	28.04	15.00	21.00	29.60	35.39	15.00	21.00
	2	22.00	35.32	2.00	8.00	29.24	42.56	2.00	8.00	36.59	49.92	5.35	11.35
	3	41.93	50.54	8.00	15.00	49.25	57.87	8.00	15.00	56.55	65.16	14.00	21.00
	4	43.01	61.64	15.00	21.00	50.26	68.89	15.00	21.00	57.60	76.23	8.00	14.00
	5	44.99	57.27	3.00	8.00	52.27	64.55	3.00	8.00	65.17	77.45	14.00	19.00
	6	50.96	69.47	9.00	15.00	58.28	76.79	9.00	15.00	65.49	84.00	2.00	8.00
R_9_1	1	13.98	30.37	15.00	21.00	22.83	39.22	15.00	21.00	31.90	48.29	15.00	21.00
	2	16.00	21.18	3.00	9.00	24.89	30.07	6.00	12.00	33.91	39.09	6.00	12.00
	3	15.99	35.61	9.00	15.00	24.87	44.49	0.00	6.00	33.92	53.55	0.00	6.00
	4	25.00	46.26	3.00	9.00	33.80	55.06	7.48	13.48	42.92	64.18	7.48	13.48
	5	30.37	35.73	15.00	21.00	39.22	44.58	14.46	20.46	48.29	53.65	14.46	20.46
	6	35.73	54.59	15.00	21.00	44.50	63.35	0.00	6.00	53.55	72.41	1.48	7.48
	7	36.99	55.38	9.41	14.41	45.88	64.27	13.48	18.48	64.18	82.56	8.14	13.14
	8	46.26	60.39	2.41	9.41	55.06	69.19	6.00	13.00	61.91	76.04	13.48	20.48
	9	60.39	68.83	2.14	8.14	69.19	77.63	1.48	7.48	75.56	84.00	2.14	8.14
R_12_1	1	11.01	14.01	14.00	21.00	20.68	23.68	14.00	21.00	30.37	33.37	14.00	21.00
	2	12.98	34.72	3.00	8.00	22.60	44.33	3.92	8.92	32.30	54.03	9.00	14.00
	3	23.86	26.42	9.00	16.00	33.71	36.27	9.00	16.00	43.39	45.95	2.00	9.00
	4	25.99	36.21	16.00	21.00	35.70	45.92	16.00	21.00	45.37	55.58	14.05	19.05
	5	29.00	37.71	8.00	15.00	38.62	47.32	8.92	15.92	54.03	62.73	7.05	14.05
	6	34.71	37.46	2.00	8.00	44.33	47.08	2.00	8.00	51.39	54.14	1.05	7.05
	7	36.21	49.42	15.00	20.00	47.08	60.29	3.92	8.92	54.14	67.35	2.05	7.05
	8	37.46	50.85	3.00	8.00	47.32	60.71	8.92	13.92	55.59	68.98	15.00	20.00
	9	42.98	60.90	8.00	15.00	52.69	70.61	14.00	21.00	62.73	80.65	8.00	15.00
	10	49.42	64.96	15.00	21.00	60.29	75.83	0.54	6.54	67.39	82.93	0.54	6.54
	11	53.02	64.68	2.00	8.00	62.66	74.32	8.00	14.00	72.34	84.00	15.00	21.00
	12	60.90	63.59	8.00	13.00	74.32	77.01	6.84	11.84	80.65	83.34	6.84	11.84
R_15_1	1	11.02	18.40	13.00	19.00	17.78	25.16	13.00	19.00	24.62	32.00	11.34	17.34
	2	15.02	17.64	7.00	13.00	21.78	24.40	7.00	13.00	28.58	31.20	3.20	9.20
	3	16.04	23.67	0.00	7.00	22.81	30.45	0.00	7.00	31.20	38.84	2.27	9.27
	4	20.04	22.58	12.22	18.22	26.79	29.33	12.22	18.22	33.64	36.18	12.22	18.22
	5	25.04	36.25	0.00	5.00	31.82	43.02	7.00	12.00	38.84	50.04	0.00	5.00
	6	26.03	30.40	5.00	11.00	32.80	37.17	1.00	7.00	39.63	44.00	5.00	11.00
	7	33.84	49.38	15.00	21.00	40.72	56.26	0.33	6.33	47.42	62.96	15.00	21.00
	8	36.01	39.90	5.21	12.21	42.80	46.68	12.00	19.00	49.65	53.53	5.21	12.21
	9	37.96	51.69	0.21	5.21	44.74	58.48	7.00	12.00	51.64	65.38	0.00	5.00
	10	41.00	43.84	8.00	15.00	47.78	50.62	12.33	19.33	54.60	57.44	8.00	15.00
	11	51.70	72.74	1.33	6.33	56.26	77.30	1.33	6.33	62.96	84.00	16.00	21.00
	12	43.84	61.52	8.00	14.00	58.48	76.17	6.33	12.33	57.44	75.12	9.00	15.00
	13	49.38	55.31	14.84	20.84	54.74	60.67	14.84	20.84	77.15	83.07	5.00	11.00
	14	55.30	63.87	14.00	21.00	61.74	70.31	12.33	19.33	68.59	77.15	2.00	9.00
	15	61.52	69.05	9.00	14.00	70.30	77.84	16.00	21.00	75.12	82.65	11.00	16.00

3.4.3.3. Differences between independent and joint chance constraints

This section explores the differences between introducing a joint chance constraint and several independent chance constraints into the model. In some papers, e.g., Wang et al. (2025), the authors attempted to control the service level of port operations via several independent chance constraints. This motivates us to compare the effects of introducing two types of chance constraints on the solutions. To this end, we rewrite the joint chance constraint (3.7) in the model into several independent chance constraints as follows:

$$\inf_{\mathbb{P}\in\mathcal{P}(\rho)} \mathbb{P}\left\{t_i \geq a_i + \xi_i\right\} \geq 1-\varepsilon_i \qquad \forall i \in V. \tag{3.50}$$

At this time, each vessel corresponds to a risk tolerance level (service level) set by the port manager, i.e., ε_i. We then obtain a DRO model with several independent chance constraints (3.50), denoted as **M5**. Since the DRO model with independent chance constraints is a special case of the DRO model with a joint chance constraint, we can apply **Propositions 1** to **3** to transform **M5** to **M6**.

M5:

$$\min_{\left(\boldsymbol{p},\boldsymbol{t},\boldsymbol{x}_{\mathrm{S}},\boldsymbol{x}_{\mathrm{T}},\boldsymbol{\varphi}^{+},\boldsymbol{\varphi}^{-},\boldsymbol{\delta}^{+},\boldsymbol{\delta}^{-},\boldsymbol{\gamma}^{+},\boldsymbol{\gamma}^{-}\right)} obj = \sum_{i\in\mathcal{S}}\left[C_i^1\left(\varphi_i^{+}+\varphi_i^{-}\right)+C_i^2\delta_i^{+}+C_i^3\gamma_i^{+}\right] \tag{3.51}$$

$$s.t. \quad (3.2)\text{–}(3.6),\ (3.8)\text{–}(3.9),\ (3.21)\text{–}(3.24),\ (3.50).$$

M6:

$$\min_{\left(\boldsymbol{p},\boldsymbol{t},\boldsymbol{x}_{\mathrm{S}},\boldsymbol{x}_{\mathrm{T}},\boldsymbol{\varphi}^{+},\boldsymbol{\varphi}^{-},\boldsymbol{\delta}^{+},\boldsymbol{\delta}^{-},\boldsymbol{\gamma}^{+},\boldsymbol{\gamma}^{-}\right)} obj = \sum_{i\in\mathcal{S}}\left[C_i^1\left(\varphi_i^{+}+\varphi_i^{-}\right)+C_i^2\delta_i^{+}+C_i^3\gamma_i^{+}\right] \tag{3.52}$$

$$s.t. \quad (3.2)\text{–}(3.6),\ (3.8)\text{–}(3.9),\ (3.21)\text{–}(3.24),$$

$$t_i \in J_i \qquad \forall i \in \mathcal{S} \tag{3.53}$$

$$J_i = \left\{ t_i \in \mathbb{R}_+ : \begin{array}{l} \theta_i\omega_i - \varepsilon_i\lambda_i \leq \dfrac{1}{N}\sum\limits_{n\in[N]}\psi_{i,n} \\ \psi_{i,n} + \lambda_i \leq \pi_{i,n}, \forall n\in[N] \\ \pi_{i,n} \leq t_i - \alpha_i - \zeta_i^n + M_{i,n}\sigma_{i,n}, \forall n\in[N] \\ \pi_{i,n} \leq M_{i,n}\left(1-\sigma_{i,n}\right), \forall n\in[N] \\ \omega_i \geq 1 \\ \lambda_i \geq 0 \\ \psi_{i,n} \leq 0, \pi_{i,n} \geq 0, \sigma_{i,n} \in \{0,1\}, \forall n\in[N] \end{array} \right\} \qquad \forall i \in \mathcal{S}. \tag{3.54}$$

Using **M3** and **M6** above, we first compare program running times of the corresponding models for the two types of chance constraints. To this end, we set parameter $\varepsilon = \varepsilon_i = 0.05$ (the port manager's predetermined service level is 95%) in all instances and $\theta = \theta_6$. We do not add any acceleration strategies to these two models, and the program running times of four typical instances are reported in Table 3.4. We set the program running time limit to 1,000 seconds. It can be found that the existence of independent chance constraints significantly increases the number of constraints in the model, and the solution time of all instances exceeds the upper bound. Even in the smaller instance R_6_1, the solution efficiency is significantly increased by 300 times. This suggests that when port managers pursue solution efficiency, they should prioritize the use of joint chance constraints to construct models.

Next, we compare the differences between the optimal solutions of the two models. The objective function values of **M3** and **M6** are shown in Table 3.5. We also visualize the optimal solutions of four typical instances in Figs. 3.7 to 3.10. From the objective function value, for the same instance, the objective function value of **M3** is greater than that of **M6**, which indicates that the solution of **M3** is more conservative. We can also draw similar conclusions from Figs. 3.7 to 3.10. The specific solutions corresponding to these images are shown in Table 3.6. For example, Fig. 3.7(*a*) shows that the berthing times of vessels 5 and 6 are closely scheduled after the departure time of vessel 3. Fig. 3.7(*b*) shows that only the berthing time of vessel 6 is closely arranged after the departure time of vessel 3. Therefore, the solution of **M3** provides a greater time buffer for vessel 5 to berth. Overall, the **M3** solution provides more buffer for vessel berthing, but it also results in greater costs for port managers.

Table 3.4 Program running time for solving M3 and M6

No.	Instance	Program running time (s)	
		M3	M6
1	R_6_1	3.51	>1,000.00
2	R_7_1	4.84	>1,000.00
3	R_8_1	3.57	>1,000.00
4	R_9_1	53.38	>1,000.00
5	R_10_1	36.71	>1,000.00
6	R_11_1	4.08	>1,000.00
7	R_12_1	549.69	>1,000.00
8	R_13_1	607.35	>1,000.00
9	R_14_1	182.26	>1,000.00
10	R_15_1	571.43	>1,000.00

Table 3.5 Objective function values of M3 and M6

No.	Instance	Objective function value under radius $\theta = \theta_6$	
		M3	M6
1	R_6_1	1377.37	1450.51
2	R_9_1	2484.11	2450.51
3	R_12_1	3674.98	3587.74
4	R_15_1	4047.66	3953.57

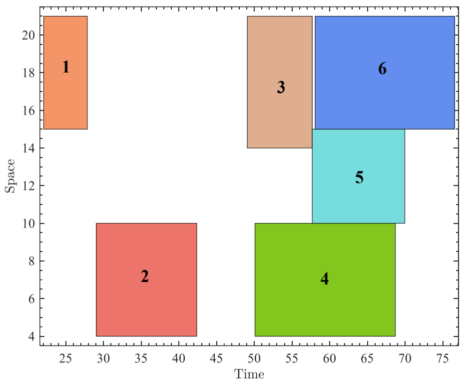

(a) Solution to M6

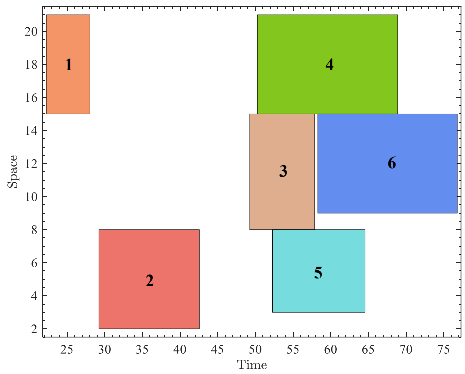

(b) Solution to M3

Fig. 3.7 Solution of R_6_1 under radius $\theta = \theta_6$

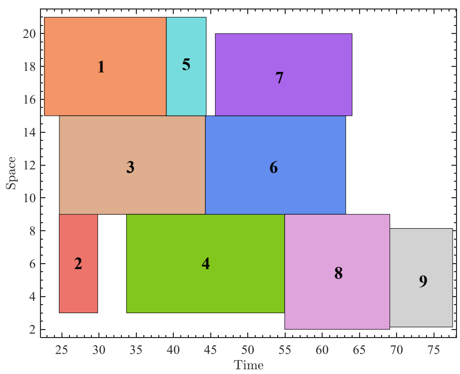

(a) Solution to M6

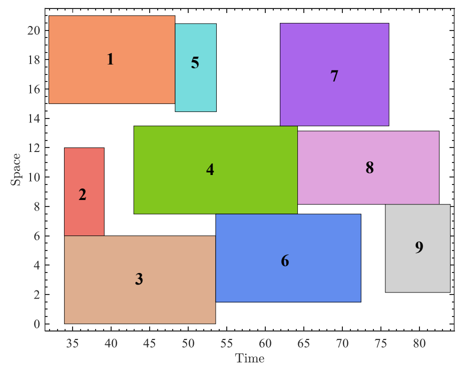

(b) Solution to M3

Fig. 3.8 Solution of R_9_1 under radius $\theta = \theta_6$

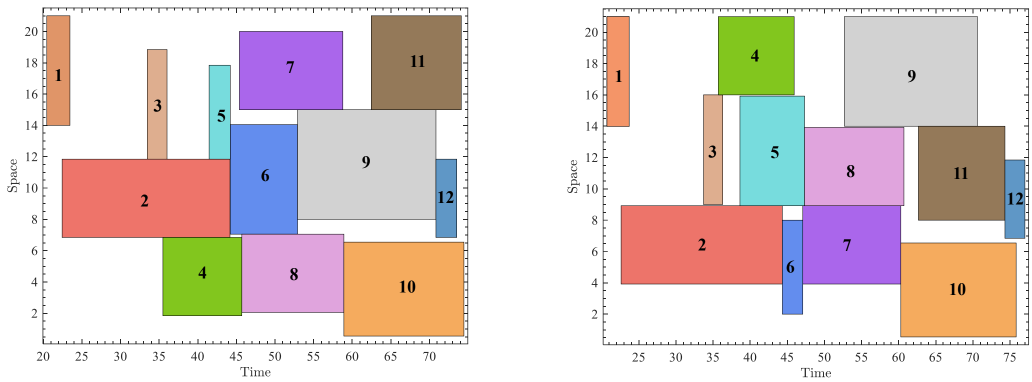

(a) Solution to M6 (b) Solution to M3

Fig. 3.9 Solution of R_12_1 under radius $\theta = \theta_6$

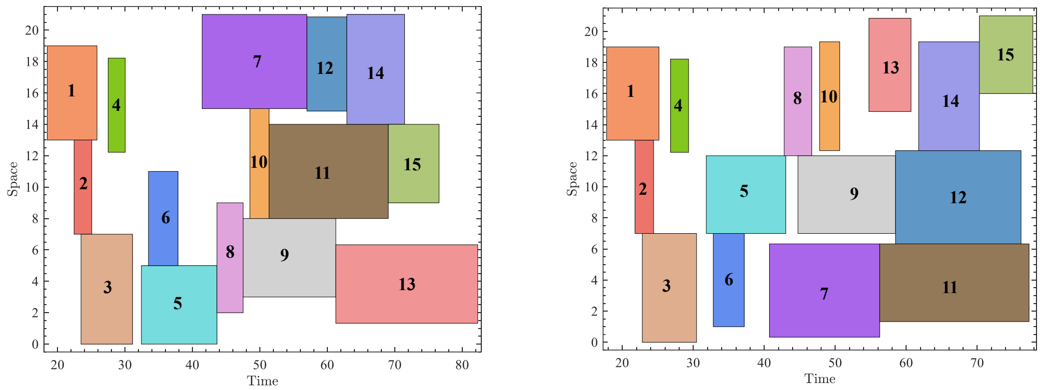

(a) Solution to M6 (b) Solution to M3

Fig. 3.10 Solution of R_15_1 under radius $\theta = \theta_6$

Table 3.6 Solutions of four different instances with M6 under different radii

Instance	Vessel No.	$\theta=\theta_1$				$\theta=\theta_6$				$\theta=\theta_{10}$			
		t_i	t_i^{end}	p_i	p_i^{end}	t_i	t_i^{end}	p_i	p_i^{end}	t_i	t_i^{end}	p_i	p_i^{end}
R_6_1	1	22.05	27.85	15.00	21.00	22.25	28.04	15.00	21.00	29.60	35.39	15.00	21.00
	2	29.04	42.37	4.00	10.00	29.24	42.56	2.00	8.00	36.59	49.92	5.35	11.35
	3	49.06	57.68	14.00	21.00	49.25	57.87	8.00	15.00	56.55	65.16	14.00	21.00
	4	50.09	68.71	4.00	10.00	50.26	68.89	15.00	21.00	57.60	76.23	8.00	14.00
	5	57.68	69.97	10.00	15.00	52.27	64.55	3.00	8.00	65.17	77.45	14.00	19.00
	6	58.07	76.57	15.00	21.00	58.28	76.79	9.00	15.00	65.49	84.00	2.00	8.00
R_9_1	1	22.65	39.04	15.00	21.00	22.83	39.22	15.00	21.00	31.90	48.29	15.00	21.00
	2	24.64	29.82	3.00	9.00	24.89	30.07	6.00	12.00	33.91	39.09	6.00	12.00
	3	24.66	44.29	9.00	15.00	24.87	44.49	0.00	6.00	33.92	53.55	0.00	6.00
	4	33.69	54.95	3.00	9.00	33.80	55.06	7.48	13.48	42.92	64.18	7.48	13.48
	5	39.04	44.40	15.00	21.00	39.22	44.58	14.46	20.46	48.29	53.65	14.46	20.46
	6	44.29	63.15	9.00	15.00	44.50	63.35	0.00	6.00	53.55	72.41	1.48	7.48
	7	45.62	64.01	15.00	20.00	45.88	64.27	13.48	18.48	64.18	82.56	8.14	13.14
	8	54.95	69.08	2.00	9.00	55.06	69.19	6.00	13.00	61.91	76.04	13.48	20.48
	9	69.08	77.52	2.14	8.14	69.19	77.63	1.48	7.48	75.56	84.00	2.14	8.14
R_12_1	1	20.45	23.45	14.00	21.00	20.68	23.68	14.00	21.00	30.37	33.37	14.00	21.00
	2	22.44	44.17	6.84	11.84	22.60	44.33	3.92	8.92	32.30	54.03	9.00	14.00
	3	33.46	36.02	11.84	18.84	33.71	36.27	9.00	16.00	43.39	45.95	2.00	9.00
	4	35.49	45.70	1.84	6.84	35.70	45.92	16.00	21.00	45.37	55.58	14.05	19.05
	5	44.22	52.92	7.05	14.05	38.62	47.32	8.92	15.92	54.03	62.73	7.05	14.05
	6	41.47	44.21	11.84	17.84	44.33	47.08	2.00	8.00	51.39	54.14	1.05	7.05
	7	45.71	58.92	2.05	7.05	47.08	60.29	3.92	8.92	54.14	67.35	2.05	7.05
	8	45.39	58.78	15.00	20.00	47.32	60.71	8.92	13.92	55.59	68.98	15.00	20.00
	9	52.92	70.84	8.00	15.00	52.69	70.61	14.00	21.00	62.73	80.65	8.00	15.00
	10	58.92	74.46	0.54	6.54	60.29	75.83	0.54	6.54	67.39	82.93	0.54	6.54
	11	62.46	74.12	15.00	21.00	62.66	74.32	8.00	14.00	72.34	84.00	15.00	21.00
	12	70.84	73.53	6.84	11.84	74.32	77.01	6.84	11.84	80.65	83.34	6.84	11.84
R_15_1	1	18.45	25.83	13.00	19.00	17.78	25.16	13.00	19.00	24.62	32.00	11.34	17.34
	2	22.44	25.06	7.00	13.00	21.78	24.40	7.00	13.00	28.58	31.20	3.20	9.20
	3	23.46	31.10	0.00	7.00	22.81	30.45	0.00	7.00	31.20	38.84	2.27	9.27
	4	27.49	30.02	12.22	18.22	26.79	29.33	12.22	18.22	33.64	36.18	12.22	18.22
	5	32.42	43.62	0.00	5.00	31.82	43.02	7.00	12.00	38.84	50.04	0.00	5.00
	6	33.47	37.84	5.00	11.00	32.80	37.17	1.00	7.00	39.63	44.00	5.00	11.00
	7	41.42	56.96	15.00	21.00	40.72	56.26	0.33	6.33	47.42	62.96	15.00	21.00
	8	43.62	47.50	2.00	9.00	42.80	46.68	12.00	19.00	49.65	53.53	5.21	12.21
	9	47.51	61.25	3.00	8.00	44.74	58.48	7.00	12.00	51.64	65.38	0.00	5.00
	10	48.51	51.35	8.00	15.00	47.78	50.62	12.33	19.33	54.60	57.44	8.00	15.00
	11	61.25	82.29	1.33	6.33	56.26	77.30	1.33	6.33	62.96	84.00	16.00	21.00
	12	51.35	69.03	8.00	14.00	58.48	76.17	6.33	12.33	57.44	75.12	9.00	15.00
	13	56.96	62.89	14.84	20.84	54.74	60.67	14.84	20.84	77.15	83.07	5.00	11.00
	14	62.88	71.45	14.00	21.00	61.74	70.31	12.33	19.33	68.59	77.15	2.00	9.00
	15	69.03	76.56	9.00	14.00	70.30	77.84	16.00	21.00	75.12	82.65	11.00	16.00

3.4.4. Out-of-sample analysis

This section presents an out-of-sample analysis of our proposed model[3]. Our optimization model performs well on the empirical distribution (in-sample) but may overfit specific scenarios (such as fixed vessel arrival patterns). Therefore,

[3] Out-of-sample analysis is the practice of evaluating the performance of a model on a dataset that was not used during parameter estimation phase.

the purpose of conducting out-of-sample analysis is to test strategy performance under unknown scenarios (e.g., emergencies, arrival time fluctuations, and new vessel scheduling patterns). To this end, we can generate stochastic test sets (e.g., randomized vessel arrival delay times) via Monte Carlo simulation. Specifically, we consider the following three different distribution functions. In each distribution function, the mean μ_i and standard deviation σ_i are generated according to Section 3.4.1.

(1) *Uniform distribution* (UN): For each vessel $i \in \mathcal{S}$, we set its arrival delay time $\xi_i \sim U\left(\mu_i - \sqrt{3}\sigma_i, \mu_i + \sqrt{3}\sigma_i\right)$.

(2) *Normal distribution* (NO): For each vessel $i \in \mathcal{S}$, we set its arrival delay time $\xi_i \sim N\left(\mu_i, (\sigma_i)^2\right)$.

(3) *Log-normal distribution* (LN): For each vessel $i \in \mathcal{S}$, we set its arrival delay time $\xi_i \sim L\left(\mu_i^{\mathrm{L}}, \left(\sigma_i^{\mathrm{L}}\right)^2\right)$, where $\mu_i^{\mathrm{L}} = \ln\left((\mu_i)^2 / \sqrt{(\mu_i)^2 + (\sigma_i)^2}\right)$ and $\sigma_i^{\mathrm{L}} = \ln\left(1 + (\sigma_i)^2 / (\mu_i)^2\right)$.

For each of the above distribution functions, we generate 10,000 samples to obtain 3 stochastic test sets. To test the out-of-sample performance of the model, we focus on two key metrics, i.e., average individual probability (AIP) and average joint probability (AJP). They can be calculated as follows:

$$AIP = \frac{1}{N'|\mathcal{S}|} \sum_{n \in [N']} \sum_{i \in \mathcal{S}} \mathbb{I}\left(t_i \geq \alpha_i + \hat{\zeta}_i^n\right) \times 100\% \tag{3.55}$$

$$AJP = \frac{1}{N'} \sum_{n \in [N']} \mathbb{I}\left(t_i \geq \alpha_i + \hat{\zeta}_i^n, \forall i \in \mathcal{S}\right) \times 100\% \tag{3.56}$$

where $|\mathcal{S}|$ denotes the cardinality of set $\mathcal{S}$; $\hat{\zeta}_i = \left(\hat{\zeta}_i^n\right)$ $\left(n \in [N']\right)$ represents randomly generated samples for out-of-sample analysis; and $N' = 10,000$.

First, we conduct out-of-sample analysis on different instances. Specifically, we solve four typical instances with different theta values (i.e., θ_1, θ_6, and θ_{10}) to obtain their optimal solutions. By doing this, we can observe the resilience of the optimal solution for different theta values. We then substitute the optimal solutions and stochastic test sets into Equations (3.55) and (3.56) to obtain the results in Table 3.7. We can see that in the calculation of each instance, as the radius parameter θ increases, the out-of-sample performance of the model gradually improves. Moreover, the objective function value of the optimal solution also increases. When $\theta = \theta_1$, the AIP and AJP metrics of each instance under different distribution functions are low. Under the UN function, some metric values are less than 30%. However, when we increase θ to θ_6, the AIP and AJP values for each instance exceed 90% under the three distribution functions. The above results confirm that the DRO model has better out-of-sample performance than the SP model does. Moreover, its performance is similar to that of the RO model, but it does not produce solutions as conservative as the RO model does. The above results also indicate that port managers should focus on choosing appropriate models when characterizing uncertainty. Different models have different degrees of conservatism, and their out-of-sample performance also varies, which in turn leads to differences in costs.

Table 3.7 AIP (in %) and AJP (in %) of solutions of different models

No.	Instance	Objective function value	Radius	AIP (%)			AJP (%)		
				UN	NO	LOG	UN	NO	LOG
1	R_6_1	626.55	θ_1	72.20	95.80	94.00	13.60	77.30	69.50
		1377.37	θ_6	100.00	100.00	99.50	100.00	100.00	97.20
		2204.66	θ_{10}	100.00	100.00	99.90	100.00	100.00	99.50
2	R_9_1	1022.02	θ_1	85.00	97.10	95.30	19.60	76.50	64.80
		2484.11	θ_6	100.00	100.00	99.80	100.00	100.00	97.80
		3941.98	θ_{10}	100.00	100.00	100.00	100.00	100.00	99.80
3	R_12_1	1371.38	θ_1	88.90	97.10	95.20	19.70	69.70	55.10
		3674.98	θ_6	100.00	100.00	99.80	100.00	100.00	97.70
		5632.14	θ_{10}	100.00	100.00	100.00	100.00	100.00	99.90
4	R_15_1	1629.91	θ_1	93.20	96.80	95.00	28.90	60.50	46.20
		4047.66	θ_6	100.00	100.00	99.50	100.00	100.00	93.20
		6073.09	θ_{10}	100.00	100.00	99.90	100.00	100.00	99.00

Second, we conduct out-of-sample analysis for different types of chance constraints (i.e., independent chance constraints and joint chance constraints). The radius of the ambiguity set is kept at θ_6 for all instances. The experimental results are shown in Table 3.8. The model corresponding to the joint chance constraint usually has higher objective function values, which is discussed in Section 3.4.3.3. In addition, in our calculation, the two types of models have comparable out-of-sample performance. This means that considering the program running time, the port manager should choose M3 for daily operational decisions. Compared with M3, M6 can customize service levels for different vessels. Considering their similar out-of-sample performance, port managers can also improve the service level of some key vessels in M6 to ensure that some key liner companies are satisfied with port services and enhance the competitiveness of ports.

Table 3.8 AIP (in %) and AJP (in %) of solutions with different chance constraints

No.	Instance	Model	Radius	Objective function value	AIP (%)			AJP (%)		
					UN	NO	LOG	UN	NO	LOG
1	R_6_1	M3	θ_6	1377.37	100.00	100.00	99.50	100.00	100.00	97.20
2		M6		1450.51	100.00	100.00	99.50	100.00	100.00	97.30
3	R_9_1	M3	θ_6	2484.11	100.00	100.00	99.80	100.00	100.00	97.80
4		M6		2450.51	100.00	100.00	99.70	100.00	100.00	97.60
5	R_12_1	M3	θ_6	3674.98	100.00	100.00	99.80	100.00	100.00	97.70
6		M6		3587.74	100.00	100.00	99.80	100.00	100.00	97.60
7	R_15_1	M3	θ_6	4047.66	100.00	100.00	99.50	100.00	100.00	93.20
8		M6		3953.57	100.00	100.00	99.60	100.00	100.00	94.20

3.4.5. Managerial insights

On the basis of the calculation results in this section, we can obtain the following managerial insights.

(1) Port service levels need to be set scientifically. According to the calculation results (see Fig. 3.1), it can be found that a slight relaxation of service levels by port managers can lead to a significant reduction in costs. When we adjust the parameter ε from 0.01 to 0.03 (corresponding to a decrease in the service level from 99% to 97%), the objective value of instance R_15_1 decreases by 45.6% (from 4503.06 to 2448.79). This phenomenon overturns the traditional perception that “the higher the service level, the better” and reveals management insight into logistics system optimization, i.e., strategic service elasticity, the core of which is to achieve a leap in operational efficiency by precisely controlling marginal adjustments to service levels. The precipitous cost reduction achievable with minor service relaxation (e.g., 99% to 97%) implies that port managers operating in ultrahigh-service regimes (≥97%) should prioritize targeted service-level adjustments over incremental efficiency gains, as this offers the most

significant absolute cost savings. To this end, port managers can identify customer sensitivity thresholds for non-core services in practice (e.g., Liner Company A has a higher tolerance for delayed arrival than Liner Company B) and build a graded service commitment system accordingly (e.g., “platinum, gold, and silver” service levels, corresponding to 97%/95%/92% on-time rates). Based on the calculation results in Section 3.4.3.3, port managers can apply the model containing several independent chance constraints to adjust the service levels of liners belonging to different liner companies.

(2) Port managers need to scientifically construct a graded response mechanism. According to the calculation results (see Fig. 3.3 and Fig. 3.4), when dealing with uncertainty, port managers adopt a step-by-step resource allocation strategy: when environmental disturbances are in the primary stage (i.e., $\theta = \theta_1$), port managers prioritize absorbing fluctuations through time elastic buffers (such as postponing vessel berthing time windows). In this stage, the original spatial layout is maintained. When the uncertainty is subsequently increased to the medium threshold (i.e., $\theta = \theta_6$), the large-scale instance (i.e., R_15_1) needs to start spatiotemporal coordination adjustment, whereas the small-scale instance (i.e., R_6_1) can still cope with it only by time delay, revealing that the scale of the problem significantly affects the triggering time of the resilience strategy. Finally, at higher levels of uncertainty (i.e., $\theta = \theta_{10}$), port managers are forced to adjust vessel berthing time and space regardless of the problem size. The above decision-making changes reveal that port managers should choose reasonable

coping methods when facing different degrees of uncertainty. In daily management practice, to address different types and degrees of uncertainty, port managers should make plans in advance and develop a layered uncertainty response system.

3.5. Conclusions

In the daily operation and management of the terminal, the berth allocation operation is the initial step, making the berth allocation problem (BAP) a fundamental problem in the field of port management. However, due to changing weather conditions and frequent mechanical failures, uncertainties need to be considered. In response to this call, a series of modeling methods for dealing with uncertainty, including the robust optimization approach and stochastic programming approach, have been widely applied in the modeling of the BAP since the early 21st century. Nonetheless, few studies have used a distributionally robust optimization approach to address the BAP. Notably, this cutting-edge theory can not only overcome the drawbacks of robust optimization approaches in generating overly conservative solutions but also avoid the assumption required by the stochastic programming approach that the distribution functions of uncertain parameters are known.

Motivated by the above background, we investigate the BAP by establishing a distributionally robust chance-constrained (DRCC) model with a type-1 Wasserstein ambiguity set. This ambiguity set has advantageous statistical properties compared with moment-based and ϕ-divergence-based ambiguity sets. On the one hand, it can avoid generating conservative solutions such as moment-based ambiguity sets when the sample size increases. On the other hand, it also avoids ignoring the possibility of noisy measurements in certain modeling scenarios, as ϕ-divergence-based sets do. In addition, the joint chance constraint is introduced to keep the vessel berthing operations in line with the service level requirements set by the port manager. This DRCC model is then converted into a mixed integer programming model, and several acceleration strategies are also designed to reduce the computation time.

During numerical experiments, we verify that the performance of our algorithm running time is enhanced by introducing several sample average approximation (SAA) constraints and coefficient strengthening techniques into the model framework. The acceleration effect of introducing coefficient strengthening technology alone is better than that of using SAA constraints alone and the superposition of the two methods. A sensitivity analysis of service levels reveals that a slight decrease in service levels can lead to a significant reduction in the objective function value. A sensitivity analysis of the radius of the ambiguity set shows that under different uncertainties, port managers adjust the BAP scheme in different ways, usually giving priority to adjusting the berthing time. Comparison experiments on models with independent chance constraints and a joint chance constraint show that the solution time of the model with independent chance constraints increases significantly. In addition, out-of-sample analysis examines the out-of-sample performance of the DRCC model. DRCC models with independent chance constraints and a joint chance constraint have comparable out-of-sample performance. Finally, several managerial insights are proposed, which can provide necessary decision-making support for daily port operation and management.

In future work, we aim to further expand the problem scenario. For example, we can investigate the classic berth allocation and quay crane assignment (BAQCA) joint optimization problem via DRCC theory. In more intelligent scenarios, such as automated container terminals, the uncertainties generated by vessels and various devices overlap and affect each other. Thus, we believe that the joint optimization of BAPs and BAQCAs in such scenarios is also an interesting research direction. Finally, we can explore other acceleration strategies to solve the model more efficiently.

Chapter 4:
Liner fleet deployment with uncertain demand[4]

In Chapter 3, we discuss how to make reasonable berth allocation to enhance the resilience of port operations. This chapter starts from another perspective. We take container transportation as the research object and examine the *liner fleet deployment problem* to achieve a resilience maritime logistics systems design at the shipping route level (i.e., seaside). Since the invention of containers in the mid-20th century, the standardization of liner shipping has led to a significant reduction in transcontinental transportation costs (Gao et al., 2022). Even during the COVID-19 pandemic, container transportation volume declined by only 1.2% (Notteboom et al., 2021). Thus, it is not surprising that scientific liner deployment has become a focus of attention in recent years in both academia and industry (Christiansen et al., 2020). However, in practice, several unpredictable factors, such as slot booking contract cancellation and delayed container arrival (Wang et al., 2013), may affect container transportation demand. Motivated by the above background, this chapter discusses a liner fleet deployment problem considering demand uncertainty to enhance the resilience of the maritime logistics system.

[4]Xin, X., Wang, S., & Zhang, T. (2025). Liner shipping fleet planning with uncertain demand: a data-driven distributionally robust chance-constrained optimization approach. *European Journal of Operational Research*, Under review.

4.1. Introduction

4.1.1. Background information

Nowadays, ocean transportation represents a significant component of the global economy, with approximately 80% of the world's cargo transported by sea on an annual basis (Chen et al., 2023; Ksciuk et al., 2023; Zhao et al., 2022). In order to achieve efficient transportation of cargos, a liner company often forms a fleet of different-class liners on its routes with a regular schedule (Meng & Wang, 2012; Wang et al., 2013). The liner company (typically its strategic management department) must reasonably plan the liner fleet in accordance with market conditions and decide (1) the composition and class of the liner fleet and (2) the deployment scheme consisting of liner-to-route decisions (Xin et al., 2023). During this process, a significant challenge faced by liner companies is coping with container transportation demand fluctuations between two ports (Liu et al., 2025b; Wang et al., 2013). For instance, during the Christmas season, the volume of container transportation from Asia to Europe tends to increase dramatically, as a large number of Chinese small commodities (e.g., toys and Christmas decorations) are exported to Europe. Thus, in 2021, Maersk added a new TP-X route during the peak season to transport e-commerce goods. Consequently, liner companies need to implement periodic adjustments to liner shipping fleets to provide stable and reliable services. The aforementioned period is usually between three and six months (Christiansen et al., 2020; Liu et al., 2021), and cargo owners can obtain the latest liner schedules and freight rate information from the liner company's official channels (e.g., official website, see https://www.oocl.com).

It can be demonstrated that *container transportation demand* is an important input parameter in the liner fleet deployment process of strategic departments. Prior to the actual demand being realized (i.e., the order being fulfilled), the class and number of liners deployed to each route are already determined and announced by the liner company. Initially, studies usually assumed that container transportation demands were known (e.g., Jaramillo and Perakis (1991)). However, in practice, there are several unpredictable factors, such as slot booking contract cancellation and delayed container arrival (Wang et al., 2013). In other words, it is nearly impossible for a liner company to estimate transportation demand according to historical data to precisely match the actual demand. Regardless of whether this transportation demand is overestimated or underestimated, the liner company will incur losses. Thus, the uncertainty of container transportation demand has emerged as a prominent research topic in recent years, particularly in the context of liner shipping fleet deployment (Christiansen et al., 2020).

In the past decade, the discussion of container transportation demand uncertainty has usually followed a stochastic programming (SP) research paradigm, which originated from (Meng & Wang, 2012). In the majority of studies, researchers usually assume that the demand between each port pair (e.g., the Port of Shanghai to the Port of Hong Kong) is a *random variable* with a known distribution function (e.g., a normal distribution; see Chua et al. (2023)) and that the transportation demands of different port pairs are *independent* of each other. Based on these known independent distribution functions, scholars are able to generate several possible scenarios (usually dozens to hundreds, see Wang et al. (2020)) and further reformulate the SP model based on scenario-based methods, such as sample average approximation (SAA). However, the realization of a random variable is usually the result of a combination of numerous factors interacting together, which makes accurate estimation of its distribution difficult. In particular, for an industry such as maritime transportation, which is deeply integrated into the world economy, transportation demands usually change dynamically in response to variations in the global economy (Zhao et al., 2022). This undoubtedly adds to the difficulty of accurately predicting the distribution function. Table 4.1 shows the China Container Freight Index (CCFI) for the first two weeks of April 2024 (see https://en.sse.net.cn/indices/ccfinew.jsp for details). During these two weeks, there are fluctuations in container freight rates on various routes, indicating that demand will also fluctuate simultaneously.

When we consider container transportation demand uncertainty, we can make the liner shipping fleet deployment problem closer to the actual operations of liner companies. However, this consideration introduces a new problem: almost no decision can definitely exclude the later constraint violation caused by various uncertain factors (e.g., changes in the political and economic landscape). In other words, once a decision is made by a liner company regarding its fleet deployment, the fleet capacity is fixed for a certain period of time (usually 3 to 6 months; see Xiang et al. (2025)). When some unforeseen events occur, the fleet is faced with not being able to fully meet the transportation demand, which could potentially result in financial losses for liner companies. Since this situation is difficult to avoid, it makes sense for liner companies to keep the probability of this situation at a low level, i.e., only a low proportion of the realization of the uncertain parameters (i.e., container transportation demand) under this known and fixed fleet deployment decision leads to constraint violations. With this in mind, we follow Wang et al. (2013) and adopt the chance constrained programming approach proposed by Charnes and Cooper (1959), incorporating a chance constraint into our model to formulate the situation where the constraint is violated.

Table 4.1 China Containerized Freight Index (CCFI) in April 2024

Composite index and service	Period 1 (2024-3-29)	Period 2 (2024-4-3)	Weekly growth (%)	Period 3 (2024-4-12)	Weekly growth (%)	Weekly growth (%)
	(1)	(2)	[(2)–(1)]/(1)	(4)	[(4)–(2)]/(2)	[(4) –(1)]/(1)
Composite index	1208.42	1191.37	-1.41%	1185.13	-0.52%	-1.93%
Japan service	767.95	742.04	-3.37%	738.45	-0.48%	-3.84%
Europe service	1781.21	1769.46	-0.66%	1725.59	-2.48%	-3.12%
W/C America service	958.83	932.29	-2.77%	953.08	2.23%	-0.60%
E/C America service	1120.53	1077.23	-3.86%	1063.41	-1.28%	-5.10%
Korea service	462.6	454.04	-1.85%	462.11	1.78%	-0.11%
Southeast Asia service	700.94	715.54	2.08%	704.79	-1.50%	0.55%
Mediterranean service	2349.48	2276.33	-3.11%	2262.61	-0.60%	-3.70%
Australia/New Zealand service	828.96	816.11	-1.55%	790.46	-3.14%	-4.64%
South Africa service	886.25	911.93	2.90%	869.1	-4.70%	-1.94%
South America service	656.42	669.70	2.02%	707.86	5.70%	7.84%
West East Africa service	586.89	590.8	0.67%	570.84	-3.38%	-2.73%
Persian Gulf/ Red Sea service	1318.08	1325.59	0.57%	1353.12	2.08%	2.66%

4.1.2. Research objective and contributions

Motivated by the abovementioned background, this chapter attempts to address the liner fleet deployment problem using the DRO technique and abstracts the above problem as a data-driven **D**istributionally **R**obust **C**hance-**C**onstrained liner shipping fleet deployment **P**roblem (DRCCP). Unlike scenario-based SP model methods, the DRO technique assumes that the distribution function of a random variable is not clear but is in an *ambiguity set* (Bertsimas et al., 2019). The DRO method offers several advantages: (1) This method does not require full information about the distribution of the demand. Therefore, the strategic management department of the liner company is able to evaluate the worst-case distribution by searching for the ambiguity set, which can avoid the difficulty of scenario recognition (Snyder, 2006). (2) DRO can use the data at hand to limit the range of random variables (Zhao et al., 2022), which can prevent overly conservative decision-making compared with scenario-based SP and robust optimization (RO) techniques (Xin et al., 2025b; Zhang et al., 2025). Due to its numerous advantages, DRO has been successfully applied in numerous fields, including location problems (Liu et al., 2019), inventory control problems (Thorsen & Yao, 2017), scheduling problems (Chang et al., 2021), signal control problems (Han et al., 2016), berth allocation problems (Agra & Rodrigues, 2022), and network design problems (Wang & Chen, 2020). Interested readers can also read Chen et al. (2024) and its references for more information on modeling techniques.

In comparison to the methodology proposed by (Zhao et al., 2022), we first redefine the random variables as the container transportation demand between port pairs, which usually does not lack historical data as the route changes. This enhances the applicability of our model. Although the proposed model is more practical, it also brings additional computational challenges because the number of random variables and the number of constraints involved are significantly increased. Second, we accurately calculate the costs faced by liner companies and improve the objective function of the model to align it more closely with real-world scenarios. Third, equipped with recent techniques in the DRO field by (Xie, 2021) and (Ho-Nguyen et al., 2022a), we develop a DRO model with a joint chance constraint and transform it into an MIP. To avoid computational challenges, we integrate our MIP model with the traditional SAA by introducing a series of SAA constraints and apply several valid inequalities to increase model-solving efficiency.

Overall, the contributions of our chapter include the following three aspects. (1) This study contributes to the literature by establishing a data-driven DRO model with a joint chance constraint to achieve mathematical modeling of the DRCCP. This model guides the day-to-day operations of liner companies, especially in light of the changing world economic and political environment. (2) The proposed DRO model is an extension of Xie (2021) and Ho-Nguyen et al. (2022a) for maritime transportation. By doing so, we reformulate the model in Wang et al. (2013), and our data-driven model can cover the traditional SAA approach proposed in Wang et al. (2013) by considering the empirical distribution of random variables as a special case. Furthermore, the Wasserstein distance-based DRO model established in Zhao et al. (2022) also appears to be a special case of the model presented in this chapter. (3) Numerical experiments are conducted to verify the solution performance between the DRO model and the RO model, SAA-based model and deterministic model (DM). The results indicate that the DRO model is more reliable than traditional approaches and it also yields several managerial insights.

4.2. Problem description

4.2.1. Definition of a liner shipping network

In this chapter, we consider a liner company that is responsible for operating a number of routes, which together form the liner shipping network of the company. We denote this shipping network by $\mathcal{V}$, where an element v is a route. On each route, liners make scheduled calls at a number of ports in a fixed sequence. We represent the set of all ports of call with element k by $\mathcal{K}$. A route is usually a closed loop, and we can define the sequence of liner port calls as follows:

$$p_v^1 \to p_v^2 \to p_v^3 \to \cdots \to p_v^{k_v} \to p_v^1$$

where p_v^i denotes the i^{th} port to be called on route $v \in \mathcal{V}$ and k_v is the number of ports to be called on route $v \in \mathcal{V}$. We say that a liner completes a *voyage* when it departs from a particular port (e.g., p_v^1 and p_v^2), calls at the remaining ports on its route in sequence and returns to that particular port. The portion of a route that connects two consecutive ports of call is referred to as a *leg*. For example, $p_v^1 \to p_v^2$ is a leg. Finally, set $\mathcal{L}$ is used to denote all the legs in the shipping network.

Fig. 4.1 shows a route that is abstracted from reality. It is noteworthy that each port may be called by a liner several times during a voyage (e.g., port 4 in Fig. 4.1). Such ports of call are also referred to as *butterfly nodes* in the literature. This characteristic distinguishes liner shipping networks from other types of shipping networks. Considering this, liner companies sometimes differentiate the direction of the route, i.e., a route is differentiated into a forward sub-route (i.e., the red solid arrow line in Fig. 4.1) and a backward sub-route (i.e., the blue dotted arrow line in Fig. 4.1). For example, Chinese liner companies often refer to the portion of the route sailing from China to abroad as the forward sub-route (out-bound trip). In Fig. 4.1, we can define the forward sub-route as $p_r^1(\text{Port 1}) \to p_r^2(\text{Port 2}) \to p_r^3(\text{Port 4}) \to p_r^4(\text{Port 5})$ and the backward sub-route (in-bound trip) as $p_r^4(\text{Port 5}) \to p_r^5(\text{Port 4}) \to p_r^6(\text{Port 3}) \to p_r^1(\text{Port 1})$. It is important to acknowledge that routes are not static; rather, liner companies generally implement periodic adjustments to their routes. For example, Maersk introduced temporary trans-Pacific routes (e.g., the TP-X route in 2021) during the fourth quarter of each year to address the surge in e-commerce cargo demand ahead of Black Friday and the Christmas season. During the COVID-19 pandemic, CMA CGM rerouted some Asia-US West Coast services to East Coast ports (e.g., New York/Savannah) to bypass severe congestion at U.S. West Coast hubs. In 2023, the Ocean Alliance restructured its Asia–Europe network by consolidating overlapping routes and launching the Asia-Med Express service to increase coverage in the Mediterranean region. Moreover, Hapag-Lloyd optimized its Asia-South America East Coast routes by adjusting port call sequences and adopting slow steaming to reduce fuel consumption, aligning with the International Maritime Organization's (IMO) low-sulfur fuel regulations. These adaptations reflect responses to fluctuating market demand, cost-efficiency objectives, external disruptions (e.g., pandemics, geopolitical conflicts), and regulatory requirements, highlighting the dynamic capacity of liner companies to align with evolving global trade conditions.

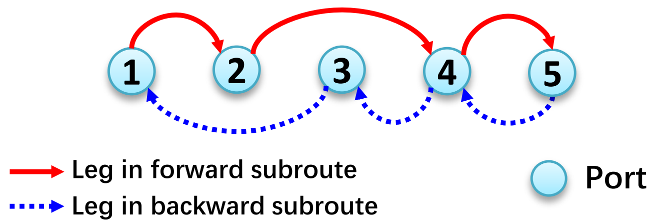

Fig. 4.1 A toy route containing seven ports of call

4.2.2. Definition of transportation demand uncertainty

We use $\mathcal{W}_v$ to denote the set of port pairs associated with a route $v \in \mathcal{V}$. The elements of set $\mathcal{W}_v$ are denoted as $\left(k_v^i, k_v^j\right)$, where k_v^i and k_v^j denote the ports of call $i \in \mathcal{K}$ and $j \in \mathcal{K}$ on route $v \in \mathcal{V}$, respectively. In fact, for different routes, there may also be the same ports of call. For example, in a liner shipping network $\mathcal{V}$, it is possible that both routes $v \in \mathcal{V}$ and $v' \in \mathcal{V}$ contain legs that allow a liner to sail from the Port of Dalian to the Port of Shanghai.

However, because of the different lengths of the routes and the different classes of liners deployed on the routes, the time to call the same port varies from route to route. It is therefore necessary to distinguish between port pairs according to route $v \in \mathcal{V}$. Given the above concept, we let random variable $\lambda^{\left(k_v^i, k_v^j\right)}$ denote the container transportation demand (i.e., the number of container transportation orders) between port pair $\left(k_v^i, k_v^j\right)$ during the planning horizon, expressed in twenty-foot equivalent units (TEUs), and let $\boldsymbol{\lambda} = (\lambda^{\left(k_v^i, k_v^j\right)})$ denote a random vector[5]. This way of constructing random variables ensures that our model structure is not affected by the periodic route adjustments made by liner companies.

Based on the above definitions, there will be container transportation demand for different port pairs on each leg. For example, consider a route v that includes the Port of Dalian, Port of Shanghai, and Port of Hong Kong, and there are two legs, i.e.,

$$p_v^1\left(\text{Dalian}\right) \to p_v^2\left(\text{Shanghai}\right) \text{ and } p_v^2\left(\text{Shanghai}\right) \to p_v^3\left(\text{Hong Kong}\right),$$

in the route.

Then, a liner sailing on leg $p_v^2\left(\text{Shanghai}\right) \to p_v^3\left(\text{Hong Kong}\right)$ loads containers associated with both the port pair (Dalian, Hong Kong) and the port pair (Shanghai, Hong Kong). In other words, the container transportation demand

[5] We take the random vector (i.e., $\boldsymbol{\lambda}$) consisting of random variables of all port pairs as the model input. By doing this, the Wasserstein ambiguity set constructed from samples implicitly captures the correlation between components (i.e., $\lambda^{(k_v^i, k_v^j)}$) within the random vector (i.e., $\boldsymbol{\lambda}$). This is a key advantage of the Wasserstein distance in distributionally robust optimization.

on leg $p_v^2(\text{Shanghai}) \to p_v^3(\text{Hong Kong})$ should be $\lambda^{\left(k_v^1,k_v^3\right)} + \lambda^{\left(k_v^2,k_v^3\right)}$. Taking this into account, we introduce a binary indicator $\delta_l^{\left(k_v^i,k_v^j\right)}$ to compute the container transportation demand on each leg. If the container transportation path associated with port pair $\left(k_v^i, k_v^j\right)$ contains leg *l*, indicator $\delta_l^{\left(k_v^i,k_v^j\right)}$ equals 1. Mathematically, we can calculate the demand that needs to pass through leg *l* as follows: $\sum_{\left(k_v^i,k_v^j\right)\in\mathcal{W}_v} \lambda^{\left(k_v^i,k_v^j\right)} \delta_l^{\left(k_v^i,k_v^j\right)}$.

4.2.3. Container liner fleet deployment

In the DRCCP, the fundamental decision facing liner companies is to deploy the optimal number and class of liners for each route, with the objective of minimizing their own costs while meeting as much of the container transportation demand (orders) as possible. We denote by $\mathcal{S}$ the set of liner classes, whose elements are denoted as *s*, and an *s*-class liner has a capacity of Q_s (in terms of TEUs). Typically, a liner company can either deploy self-owned liners to a route or charter in liners from the charter market. The liner charter market generally offers three types of models, namely, (1) time charter, (2) voyage charter and (3) bareboat charter. The third model is the simplest model. The shipowner provides only an empty liner, which is fully crewed by and under the direction of the charterer. The charterer is responsible for the operation of the liner and for any loss of time during the charter period. Without loss of generality, we assume that liner companies can only charter vessels from the market using the bareboat charter model. Moreover, NO_s^{M} and NC_s^{M} denote the number of *s*-class liners owned by the liner company and the number available in the charter market, respectively.

In general, the costs to be paid by liner companies during the planning horizon include operating costs, voyage costs, capital costs and liner maintenance costs. Operating costs represent the cost of operating a liner on a daily basis, such as crew wages, insurance, and administrative fees, but excludes fuel costs. We use c_s^{OP} (yuan/day) to denote the daily operating cost, which is related to the liner class. Voyage costs, such as fuel costs and pilotage costs, are closely related to the number of voyages. Obviously, the voyage cost is different for different routes v and different liner classes s, and we use c_{sv}^{VO} (yuan/voyage) to represent this cost. The main component of capital costs is liner rentals. We do not consider the case of liner companies purchasing new liners because even if a liner company makes a decision to purchase during a planning horizon (usually 3–6 months), it usually takes 6 months to even 2 years for the new liner to be delivered. We set the daily charter rate for a liner of class s to c_s^{IN} (yuan/day). Maintenance costs are typically incurred at fixed intervals (e.g., biennial dry docking and quadrennial special surveys). Therefore, we do not consider maintenance costs in our modeling, given that the DRCCP involves a planning period that is typically less than six months. The goal of designing a liner fleet is to create an efficient deployment scheme that minimizes total costs while satisfying certain constraints (e.g., service frequency constraints).

Before proceeding to modeling, we present several assumptions used in this chapter. (1) We do not take into account the queuing of liners for berthing at each port. (2) We do not consider empty container relocation or inland transportation; that is, we assume that there are always enough empty containers for holding cargo. (3) The planning horizon of the DRCCP is set to 6 months. These assumptions are made to ensure the computational tractability of our model. For the convenience of readers, the notations commonly used are listed below.

Sets	
$\mathcal{V}$	Set of routes in the liner shipping network, whose elements are represented as v
$\mathcal{K}$	Set of ports of call, whose elements are represented as k
$\mathcal{S}$	Set of liner classes, whose elements are denoted as s
$\mathcal{L}$	Set of legs, whose elements are denoted as l
$\mathcal{W}_v$	Set of port pairs associated with route v
$\mathbb{Z}_+$	Set of non-negative integers
$[N]$	A set containing the integers 1 to N, i.e., $[N] := \{1, 2, \cdots, N\}$
Parameters	
c_s^{OP}	The operating cost of a class s liner (Unit: yuan/day)
c_{sv}^{VO}	The voyage cost of a class s liner sailing on route v (Unit: yuan/voyage)
c_s^{IN}	The daily chartering cost of a class s (Unit: yuan/day)
NO_s^{M}	Number of class s liners owned by the liner company
NC_s^{M}	Number of class s liners can be chartered in by the liner company in the shipping market
t_{sv}	The sailing time of a class s liner on route v (Unit: day)
N_v	The minimum number of voyages should be completed on route v to maintain the established service frequency
$\left(k_v^i, k_v^j\right)$	Port pair with origin port k_v^i and destination port k_v^i
$\delta_l^{\left(k_v^i, k_v^j\right)}$	A binary indicator, which equals 1 if containers transportation path associated with port pair $\left(k_v^i, k_v^j\right)$ contains leg l
T	The length of the planning horizon (Unit: day)
Q_s	Capacity of a class s liner (Unit: TEU)
Random variable	
$\lambda^{\left(k_v^i, k_v^j\right)}$	Container transportation demand of port pair $\left(k_v^i, k_v^j\right)$ during the planning horizon
Decision variables	
x_{sv}^{TO}	Number of class s liners (both owned and chartered) deployed by the liner company to route v
x_s^{IN}	Number of class s liners chartered in by the liner company
y_{sv}	Number of voyages completed on route v by class s liners

4.3. Model development

This section constructs a data-driven DRO model with a joint chance constraint for solving the DRCCP. Before establishing the model, we first introduce the necessary notation. Let T represent the length of the planning horizon; $\mathcal{V}$ denote the set of routes, where $v \in \mathcal{V}$; $\mathcal{S}$ is the set of liner classes, whose elements are denoted as s; and c_s^{OP}, c_{sv}^{VO}, and c_s^{IN} represent the daily operating cost, voyage cost, and chartering cost of a class s liner, respectively. x_s^{IN} is the number of class s liners chartered in by the liner company; x_{sv}^{TO} denotes the number of class s liners deployed by the liner company on route v; y_{sv} represents the number of voyages completed by the class s liners on route v; NO_s^{M} is the number of class s liners owned by the liner company; NC_s^{M} denotes the maximum number of class s liners that can be chartered in by the liner company from the market; t_{sv} is the sailing time required by a class s liner to complete a single voyage on route v; N_v denotes the minimum number of voyages to be completed on route v to fulfill the established service frequency; $\mathcal{K}$ represents the set of ports of call, where $k \in \mathcal{K}$; $\mathcal{L}$ is the set of legs, where $l \in \mathcal{L}$; and $\mathcal{W}_v$ denotes the set of port pairs associated with route v. Each port pair is denoted as $\left(k_v^i, k_v^j\right)$. $\tilde{\lambda}^{\left(k_v^i, k_v^j\right)}$ represents the container transportation demand associated with port pair $\left(k_v^i, k_v^j\right)$; $\delta_l^{\left(k_v^i, k_v^j\right)}$ is a binary indicator that equals 1 when leg l is necessary to fulfill the container transportation demand $\left(k_v^i, k_v^j\right)$ and 0 otherwise; Q_s denotes the capacity of a class s liner; $\mathcal{P}(\rho)$ represents a Wasserstein ambiguity set with radius ρ;

η is a pre-determined parameter that indicates the confidence level; $\mathbb{Z}^{+}$ denotes the set of non-negative integers; and function $\lfloor a \rfloor$ represents the maximum integer not greater than a. Based on the above notation, the model for solving the DRCCP can be developed as the following [**SPM**].

SPM:

$$\min obj_1 = T\sum_{v\in\mathcal{V}}\sum_{s\in\mathcal{S}} c_s^{\mathrm{OP}} x_{sv}^{\mathrm{TO}} + \sum_{v\in\mathcal{V}}\sum_{s\in\mathcal{S}} c_{sv}^{\mathrm{VO}} y_{sv} + T\sum_{s\in\mathcal{S}} c_s^{\mathrm{IN}} x_s^{\mathrm{IN}} \tag{4.1}$$

$$s.t. \quad \sum_{v\in\mathcal{V}} x_{sv}^{\mathrm{TO}} \le NO_s^{\mathrm{M}} + x_s^{\mathrm{IN}} \qquad \forall s\in\mathcal{S} \tag{4.2}$$

$$x_s^{\mathrm{IN}} \le NC_s^{\mathrm{M}} \qquad \forall s\in\mathcal{S} \tag{4.3}$$

$$y_{sv} \le x_{sv}^{\mathrm{TO}} \times \left\lfloor \frac{T}{t_{sv}} \right\rfloor \qquad \forall v\in\mathcal{V}, s\in\mathcal{S} \tag{4.4}$$

$$\sum_{s\in\mathcal{S}} y_{sv} \ge N_v \qquad \forall v\in\mathcal{V} \tag{4.5}$$

$$\inf_{\mathbb{P}\in\mathcal{P}(\rho)} \mathbb{P}\left(\sum_{\left(k_v^i,k_v^j\right)\in\mathcal{W}_v} \lambda^{\left(k_v^i,k_v^j\right)} \delta_l^{\left(k_v^i,k_v^j\right)} \le \sum_{s\in\mathcal{S}} y_{sv} Q_s, \forall v\in\mathcal{V}, l\in\mathcal{L} \right) \ge 1-\eta \tag{4.6}$$

$$x_s^{\mathrm{IN}} \in \mathbb{Z}_+ \qquad \forall s\in\mathcal{S} \tag{4.7}$$

$$x_{sv}^{\mathrm{TO}}, y_{sv} \in \mathbb{Z}_+ \qquad \forall v\in\mathcal{V}, s\in\mathcal{S}. \tag{4.8}$$

Equation (4.1) is the objective function of the model, which aims to minimize the total operational cost of the liner company over the planning horizon. The right-hand side of Equation (4.1) is formed by three terms. The first term calculates the fleet operational cost over the planning horizon, the second term is the voyage cost of the fleet, and the third term calculates the charter cost over the planning horizon. Constraint (4.2) presents the relationships among variables x_{sv}^{TO}, x_s^{IN} and parameter NO_s^{M}. It is required that the number of liners deployed by the liner company on each route is not greater than or equal to the sum of liners owned and chartered in. Constraint (4.3) requires that the number of liners chartered in by the liner company cannot exceed NC_s^{M}, which is the maximum number of available class s liners in the market. Constraint (4.4) requires that the number of voyages completed by each class of liner on each route cannot exceed its upper bound. This upper bound is determined by both the number of liners deployed on the route and the liner sailing speed. Constraint (4.5) indicates that the number of voyages performed should be at least N_v for all route v to meet the established service frequency. Constraint (4.6) is a joint chance constraint for container transportation demand. It requires that the container transportation passing through each leg (i.e., $\sum_{(k_v^i, k_v^j) \in \mathcal{W}_v} \lambda^{(k_v^i, k_v^j)} \delta_l^{(k_v^i, k_v^j)}$) does not exceed the liner capacity (i.e., $\sum_{s \in \mathcal{S}} y_{sv} Q_s$) assigned to this leg to be met with a certain probability. In other words, it is required that for all $v \in \mathcal{V}$, $l \in \mathcal{L}$ and for all probability distributions from $\mathcal{P}(\rho)$, this constraint should be satisfied with a probability of at least $1-\eta$, where $\eta \in (0,1)$ is the confidence level, also known as the risk tolerance. The introduction of this constraint follows from our earlier research (i.e., Wang et al. (2013)). This modelling idea helps us to compare with the established method in Wang et al. (2013). In addition, doing so is consistent with the realities of liner shipping operations. Liner needs to sail continuously on a route consisting of several legs. Therefore, the transportation demands on different legs of the same route affect each other, preventing us from looking at each leg independently. **Example 1** in Zhao et al. (2022) further explains the rationality of our consideration. Given a distribution $\mathbb{P}$ that governs vector

$\boldsymbol{\lambda} = (\lambda^{(k_v^i, k_v^j)})$, the [**SPM**] can be solved by an SP approach. However, this approach faces several challenges in terms of both computational and practical considerations. On the one hand, checking the feasibility of a known liner shipping fleet design scheme involves multidimensional integration, which becomes increasingly difficult if the dimensions of the random vectors rise. On the other hand, the SAA technique may cause poor out-of-sample performance due to the well-known overfitting phenomenon (Zhao et al., 2022). Finally, Constraints (4.7)–(4.8) are non-negative integer constraints on decision variables x_s^{IN} , x_{sv}^{TO} and y_{sv} .

4.4. Model reformulation

To overcome the problems mentioned in Section 4.3, we reformulate the model proposed. Section 4.4.1 provides a brief description of the ambiguity set we considered. Section 4.4.2 transforms the [**SPM**] to an exact MIP reformulation by using an indicator function and strong conic duality. Section 4.4.3 strengthens the model reformulation by introducing several SAA constraints. Finally, several valid inequalities are introduced into the model framework in Section 4.4.4 to enhance model-solving efficiency.

4.4.1. Ambiguity set construction

Currently, historical data on random variables are becoming increasingly available. To obtain the probability distribution of random variables, a natural idea is to approximate the true distribution through the *empirical distribution* corresponding to historical data. We let $\boldsymbol{\lambda} = (\lambda^{\left(k_v^i, k_v^j\right)})$ denote a random vector supported on set Ξ with a joint probability distribution $\mathbb{P}$ from a distribution family $\mathcal{P}$. Here, $\mathcal{P}$ is also called an *ambiguity set*, and the construction of $\mathcal{P}$ varies according to the problem properties in different studies. In this chapter, we use the type-1 Wasserstein metric to characterize the distribution function of random vectors $\boldsymbol{\lambda}$, as shown in Equation (4.9). Similarly, one can see **Appendix B** proposed in Zhao et al. (2022).

$$\mathcal{P}(\rho) := \left\{ \mathbb{P} : \mathbb{P}(\boldsymbol{\lambda} \in \Xi) = 1,\ \mathrm{dis}_W\left(\mathbb{P}, \mathbb{P}_{\boldsymbol{\varphi}}\right) \le \rho \right\} \tag{4.9}$$

where $\mathbb{P}_{\boldsymbol{\varphi}}$ is an *empirical distribution* of $\boldsymbol{\varphi}$.

In the above equation, $\boldsymbol{\varphi}$ is called the *empirical random vector* corresponding to the random vector $\boldsymbol{\lambda}$, generated from N i.i.d. samples $\Omega = \{\boldsymbol{\varphi}^a\}_{a \in [N]} \subseteq \Xi$ from the true distribution $\mathbb{P}$ of the random vector $\boldsymbol{\lambda}$, where $[N] := \{1, 2, \cdots, N\}$. The point mass function (PMF) of $\boldsymbol{\varphi}$ is $\mathbb{P}_{\boldsymbol{\varphi}}\left(\boldsymbol{\varphi} = \boldsymbol{\varphi}^a\right) = 1/N$. In other words, the empirical distribution $\mathbb{P}_{\boldsymbol{\varphi}}$ is a discrete uniform distribution over N historical data points of random vector $\boldsymbol{\lambda}$. Parameter $\rho > 0$ denotes the radius of the Wasserstein ball, and $\mathrm{dis}_W\left(\mathbb{P}, \mathbb{P}_{\boldsymbol{\varphi}}\right)$ represents the 1-Wasserstein distance between distributions $\mathbb{P}$ and $\mathbb{P}_{\boldsymbol{\varphi}}$ based on a norm $\|\bullet\|$, which is defined as:

$$\mathrm{dis}_W\left(\mathbb{P}, \mathbb{P}_{\boldsymbol{\varphi}}\right) = \inf_{\hat{\mathbb{P}}} \mathbb{E}_{(\boldsymbol{\lambda}, \boldsymbol{\varphi}) \sim \hat{\mathbb{P}}}\left[\|\boldsymbol{\lambda} - \boldsymbol{\varphi}\| : \hat{\mathbb{P}} \text{ has marginal distributions } \mathbb{P},\ \mathbb{P}_{\boldsymbol{\varphi}}\right] \tag{4.10}$$

where $\hat{\mathbb{P}}$ is the joint probability distribution of $\boldsymbol{\lambda}$ and $\boldsymbol{\varphi}$; and $\hat{\mathbb{P}}\left[(\boldsymbol{\lambda}, \boldsymbol{\varphi}) \in \Xi \times \Xi\right] = 1$.

4.4.2. Exact MIP reformulation

In this section, the joint chance constraint (4.6) in [**SPM**] given in Section 4 is reformulated as an exact MIP based on the definition of the *indicator function* and *strong conic duality* and theories proposed by Xie (2021) and Ho-Nguyen et al. (2022a). For ease of presentation, we rewrite the random variables and decision variables in matrix form. Let $\boldsymbol{\lambda}^v = (\lambda^{(k_v^i, k_v^j)})$, $\mathbf{y} = (y_{sv})$. In this way, the decision variables and parameters in joint chance constraint (4.6) can be re-expressed as set (4.11). Then, we introduce **Proposition 4.1** to reformulate set (4.11).

$$\mathcal{JCC} := \left\{ \mathbf{y} \in \mathbb{Z}_+^{s \times v} : \inf_{\mathbb{P} \in \mathcal{P}(\rho)} \mathbb{P}\left\{ \left(\boldsymbol{\delta}_l^v\right)^T \boldsymbol{\lambda}^v \leq \mathbf{Q}^T \mathbf{y}_v, \forall (v,l) \in \mathcal{V} \times \mathcal{L} \right\} \geq 1 - \eta \right\} \quad (4.11)$$

Proposition 4.1. Equation (4.11) can be equivalently transformed into Equation (4.12) by introducing a non-negative auxiliary variable $\xi \geq 0$.

$$\mathcal{JCC} := \left\{ \mathbf{y} \in \mathbb{Z}_+^{s \times v} : \begin{array}{c} \rho - \eta\xi \leq \dfrac{1}{N} \sum\limits_{a \in [N]} \min\left\{ f\left(\mathbf{y}, \boldsymbol{\varphi}_a\right) - \xi, 0 \right\}, \\ \xi \geq 0, \end{array} \right\} \quad (4.12)$$

where the function $f\left(\mathbf{y}, \boldsymbol{\varphi}_a\right) := \left[\min\limits_{v \in \mathcal{V}, l \in \mathcal{L}} \dfrac{\left(\mathbf{Q}^T \mathbf{y}_v - \left(\boldsymbol{\delta}_l^v\right)^T \boldsymbol{\varphi}_a^v \right)}{\left\| \boldsymbol{\delta} \right\|_*} \right]^+$; $\|\bullet\|_*$ denotes the dual norm; and $(\bullet)^+ := \max\{\bullet, 0\}$.

Proof. Following Xie (2021), our proof process is divided into 3 stages (i.e., **Stages 1** to **3**). In each stage, we reformulate Equation (4.11) to convert it to Equation (4.12).

Stage 1: Obviously, the inf part, i.e.,

$$\inf_{\mathbb{P}\in\mathcal{P}(\rho)} \mathbb{P}\left\{\left(\boldsymbol{\delta}_l^v\right)^T \boldsymbol{\lambda}^v \le \mathbf{Q}^T\mathbf{y}_v, \forall(v,l)\in\mathcal{V}\times\mathcal{L}\right\} \ge 1-\eta,$$

is equivalent to

$$\sup_{\mathbb{P}\in\mathcal{P}(\rho)} \mathbb{P}\left\{\left(\boldsymbol{\delta}_l^v\right)^T \boldsymbol{\lambda}^v > \mathbf{Q}^T\mathbf{y}_v, \exists(v,l)\in\mathcal{V}\times\mathcal{L}\right\} \le \eta.$$

It is well known that the indicator function is a bounded and upper semi-continuous function. Let $\mathbb{I}(x\in A)$ denote the indicator function, which equals 1 when $x\in A$ and 0 otherwise. Based on this definition, we have

$$\mathbb{P}\left\{\left(\boldsymbol{\delta}_l^v\right)^T \boldsymbol{\lambda}^v > \mathbf{Q}^T\mathbf{y}_v, \exists(v,l)\in\mathcal{V}\times\mathcal{L}\right\} = \mathbb{E}_{\mathbb{P}}\left[\mathbb{I}\left(\left(\boldsymbol{\delta}_l^v\right)^T \boldsymbol{\lambda}^v > \mathbf{Q}^T\mathbf{y}_v, \exists(v,l)\in\mathcal{V}\times\mathcal{L}\right)\right].$$

We set function $f_{\text{primal}} := \sup_{\mathbb{P}\in\mathcal{P}(\rho)} \mathbb{E}_{\mathbb{P}}\left[\mathbb{I}\left(\left(\boldsymbol{\delta}_l^v\right)^T \boldsymbol{\lambda}^v > \mathbf{Q}^T\mathbf{y}_v, \exists(v,l)\in\mathcal{V}\times\mathcal{L}\right)\right]$, and its dual can be written as

$$f_{\text{dual}} := \inf_{\bar{\xi}\ge 0}\left\{\bar{\xi}\rho - \frac{1}{N}\sum_{a\in[N]}\inf_{\boldsymbol{\lambda}}\left[\bar{\xi}\left\|\boldsymbol{\lambda}-\boldsymbol{\varphi}_a\right\| - \mathbb{I}\left(\left(\boldsymbol{\delta}_l^v\right)^T \boldsymbol{\lambda}^v > \mathbf{Q}^T\mathbf{y}_v, \exists(v,l)\in\mathcal{V}\times\mathcal{L}\right)\right]\right\}.$$

Based on strong duality from **Corollary 2** in Gao and Kleywegt (2023), we have $f_{\text{primal}} = f_{\text{dual}}$. Thus far, set $\mathcal{JCC}$ becomes

$$\mathcal{JCC} := \left\{\mathbf{y}\in\mathbb{Z}_+^{s\times v} : \rho\bar{\xi} - \frac{1}{N}\sum_{a\in[N]}\inf_{\boldsymbol{\lambda}}\begin{bmatrix}\bar{\xi}\left\|\boldsymbol{\lambda}-\boldsymbol{\varphi}_a\right\| \\ -\mathbb{I}\begin{pmatrix}\left(\boldsymbol{\delta}_l^v\right)^T \boldsymbol{\lambda}^v > \mathbf{Q}^T\mathbf{y}_v, \\ \exists(v,l)\in\mathcal{V}\times\mathcal{L}\end{pmatrix}\end{bmatrix} \le \eta, \exists\bar{\xi}\ge 0\right\}.$$

Stage 2: After **Stage 1** ends, an additional indicator function appears in set $\mathcal{JCC}$. The goal of this stage is to eliminate it.

First, we notice that

$$\mathbb{I}\left(\left(\boldsymbol{\delta}_l^v\right)^T \boldsymbol{\lambda}^v > \mathbf{Q}^T\mathbf{y}_v, \exists(v,l)\in\mathcal{V}\times\mathcal{L}\right) = \max_{(v,l)\in\mathcal{V}\times\mathcal{L}} \mathbb{I}\left(\left(\boldsymbol{\delta}_l^v\right)^T \boldsymbol{\lambda}^v > \mathbf{Q}^T\mathbf{y}_v\right).$$

Therefore, for a group of known $\bar{\xi}\ge 0$ and $\boldsymbol{\varphi}_a\in\Omega$,

$$\inf_{\boldsymbol{\lambda}}\left[\bar{\xi}\left\|\boldsymbol{\lambda}-\boldsymbol{\varphi}_a\right\| - \mathbb{I}\left(\left(\boldsymbol{\delta}_l^v\right)^T \boldsymbol{\lambda}^v > \mathbf{Q}^T\mathbf{y}_v, \exists(v,l)\in\mathcal{V}\times\mathcal{L}\right)\right]$$

is equivalent to

$$\min_{(v,l)\in\mathcal{V}\times\mathcal{L}} \inf_{\boldsymbol{\lambda}} \left[\bar{\xi} \left\| \boldsymbol{\lambda} - \boldsymbol{\varphi}_a \right\| - \mathbb{I}\left(\left(\boldsymbol{\delta}_l^v \right)^T \boldsymbol{\lambda}^v > \mathbf{Q}^T \mathbf{y}_v \right) \right].$$

Hence, for all $(v,l)\in\mathcal{V}\times\mathcal{L}$, we can obtain

$$\inf_{\boldsymbol{\lambda}} \left[\bar{\xi} \left\| \boldsymbol{\lambda} - \boldsymbol{\varphi}_a \right\| - \mathbb{I}\left(\left(\boldsymbol{\delta}_l^v \right)^T \boldsymbol{\lambda}^v > \mathbf{Q}^T \mathbf{y}_v \right) \right] = \min \left\{ \inf_{\left(\boldsymbol{\delta}_l^v\right)^T \boldsymbol{\lambda}^v > \mathbf{Q}^T \mathbf{y}_v} \left[\bar{\xi} \left\| \boldsymbol{\lambda} - \boldsymbol{\varphi}_a \right\| - 1 \right], 0 \right\}. \tag{4.13}$$

We can prove that Equation (4.13) holds according to the following categorical discussion.

Case (a): If $\left(\boldsymbol{\delta}_l^v\right)^T \boldsymbol{\varphi}_a^v > \mathbf{Q}^T \mathbf{y}_v$, then we only need to set $\boldsymbol{\lambda} = \boldsymbol{\varphi}_a$. At this time, both sides of Equation (4.13) take an optimal value.

Case (b): If $\left(\boldsymbol{\delta}_l^v\right)^T \boldsymbol{\varphi}_a^v \le \mathbf{Q}^T \mathbf{y}_v$, then either $\left(\boldsymbol{\delta}_l^v\right)^T \boldsymbol{\lambda}^v > \mathbf{Q}^T \mathbf{y}_v$ or $\left(\boldsymbol{\delta}_l^v\right)^T \boldsymbol{\lambda}^v \le \mathbf{Q}^T \mathbf{y}_v$ holds for any $\boldsymbol{\lambda}^v \in \Xi$. Considering the above two cases, for all $(v,l)\in\mathcal{V}\times\mathcal{L}$, the left side of Equation (4.13) can be transformed as

$$\begin{aligned}
&\inf_{\boldsymbol{\lambda}} \left[\bar{\xi} \left\| \boldsymbol{\lambda} - \boldsymbol{\varphi}_a \right\| - \mathbb{I}\left(\left(\boldsymbol{\delta}_l^v \right)^T \tilde{\boldsymbol{\lambda}}^v > \mathbf{Q}^T \mathbf{y}_v \right) \right] \\
&= \min \left\{ \inf_{\left(\boldsymbol{\delta}_l^v\right)^T \tilde{\boldsymbol{\lambda}}^v > \mathbf{Q}^T \mathbf{y}_v} \left[\bar{\xi} \left\| \boldsymbol{\lambda} - \boldsymbol{\varphi}_a \right\| - 1 \right], \inf_{\left(\boldsymbol{\delta}_l^v\right)^T \tilde{\boldsymbol{\lambda}}^v \le \mathbf{Q}^T \mathbf{y}_v} \left[\bar{\xi} \left\| \boldsymbol{\lambda} - \boldsymbol{\varphi}_a \right\| \right] \right\} \\
&= \min \left\{ \inf_{\left(\boldsymbol{\delta}_l^v\right)^T \tilde{\boldsymbol{\lambda}}^v > \mathbf{Q}^T \mathbf{y}_v} \left[\bar{\xi} \left\| \boldsymbol{\lambda} - \boldsymbol{\varphi}_a \right\| - 1 \right], 0 \right\}
\end{aligned}$$

where the second equality holds because we set $\boldsymbol{\lambda} = \boldsymbol{\varphi}_a$.

Based on the above equations, we have

$$\begin{aligned}
&\inf_{\boldsymbol{\lambda}} \left[\bar{\xi} \left\| \boldsymbol{\lambda} - \boldsymbol{\varphi}_a \right\| - \mathbb{I}\left(\left(\boldsymbol{\delta}_l^v \right)^T \tilde{\boldsymbol{\lambda}}^v > \mathbf{Q}^T \mathbf{y}_v, \exists (v,l)\in\mathcal{V}\times\mathcal{L} \right) \right] \\
&= \min \left\{ \min_{(v,l)\in\mathcal{V}\times\mathcal{L}} \inf_{\left(\boldsymbol{\delta}_l^v\right)^T \tilde{\boldsymbol{\lambda}}^v > \mathbf{Q}^T \mathbf{y}_v} \left[\bar{\xi} \left\| \boldsymbol{\lambda} - \boldsymbol{\varphi}_a \right\| - 1 \right], 0 \right\}.
\end{aligned}$$

Hence, the indicator function in set $\mathcal{JCC}$ can be eliminated, and $\mathcal{JCC}$ can be further reformulated as

$$\mathcal{JCC} := \left\{ \mathbf{y} \in \mathbb{Z}_+^{s\times v} : \min_{\overline{\xi}\geq 0} \left\{ \rho\overline{\xi} - \frac{1}{N}\sum_{a\in[N]} \min\left\{ \min_{(v,l)\in\mathcal{V}\times\mathcal{L}} \inf_{\left(\boldsymbol{\delta}_l^v\right)^T \boldsymbol{\lambda}^v > \mathbf{Q}^T\mathbf{y}_v} \left[\overline{\xi}\left\|\boldsymbol{\lambda}-\boldsymbol{\varphi}_a\right\| - 1\right], 0 \right\} \right\} \leq \eta \right\}.$$

However, the presence of $\inf_{\left(\boldsymbol{\delta}_l^v\right)^T \boldsymbol{\lambda}^v > \mathbf{Q}^T\mathbf{y}_v} \left\|\boldsymbol{\lambda}-\boldsymbol{\varphi}_a\right\|$ in set $\mathcal{JCC}$ still makes the expression complicated, and we attempt to simplify it further. First, we consider the case where $l=1$ and $v=1$. Currently, for all $a\in[N]$, we have

$$\begin{aligned}
\inf_{\boldsymbol{\delta}_1^T\boldsymbol{\lambda}>\mathbf{Q}^T\mathbf{y}_1} \left\|\boldsymbol{\lambda}-\boldsymbol{\varphi}_a\right\| &= \inf_{\varsigma,\boldsymbol{\lambda}} \left\{ \varsigma \middle| \varsigma \geq \left\|\boldsymbol{\lambda}-\boldsymbol{\varphi}_a\right\|, \boldsymbol{\delta}_1^T\boldsymbol{\lambda} > \mathbf{Q}^T\mathbf{y}_1 \right\} \\
&= \sup_{\boldsymbol{\upsilon},\vartheta} \left\{ \vartheta\mathbf{Q}^T\mathbf{y}_1 - \boldsymbol{\upsilon}^T\boldsymbol{\varphi}_a \middle| \varpi = 1, \boldsymbol{\upsilon} = \boldsymbol{\delta}_1\vartheta, \varpi \geq \left\|\boldsymbol{\upsilon}\right\|_*, \vartheta \geq 0 \right\} \\
&= \sup_{\vartheta} \left\{ \left(\mathbf{Q}^T\mathbf{y}_1 - \boldsymbol{\delta}_1^T\boldsymbol{\varphi}_a\right)\vartheta \middle| \vartheta \leq \frac{1}{\left\|\boldsymbol{\delta}_1\right\|_*}, \vartheta \geq 0 \right\} = \frac{\left(\mathbf{Q}^T\mathbf{y}_1 - \boldsymbol{\delta}_1^T\boldsymbol{\varphi}_a\right)^+}{\left\|\boldsymbol{\delta}_1\right\|_*}
\end{aligned}$$

where the second equality holds due to the strong conic duality in Hota et al. (2019) and the third equality holds as a consequence of finding the supremum for ϖ and $\boldsymbol{\upsilon}$.

Then, we consider the case where $l\geq 1$ and $v\geq 1$. For all $a\in[N]$, we have

$$\begin{aligned}
&\inf_{\left(\boldsymbol{\delta}_l^v\right)^T \boldsymbol{\lambda}^v > \mathbf{Q}^T\mathbf{y}_v} \left\|\boldsymbol{\lambda}-\boldsymbol{\varphi}_a\right\| \\
&= \min_{v\in\mathcal{V},l\in\mathcal{L}} \left\{ \inf_{\varsigma,\boldsymbol{\lambda}} \left\{ \varsigma : \varsigma \geq \left\|\boldsymbol{\lambda}-\boldsymbol{\varphi}_a\right\|, \left(\boldsymbol{\delta}_l^v\right)^T \boldsymbol{\lambda}^v > \mathbf{Q}^T\mathbf{y}_v \right\} \right\} \qquad (4.14) \\
&= \min_{v\in\mathcal{V},l\in\mathcal{L}} \left\{ \frac{\left(\mathbf{Q}^T\mathbf{y}_v - \left(\boldsymbol{\delta}_l^v\right)^T\boldsymbol{\varphi}_a^v\right)^+}{\left\|\boldsymbol{\delta}\right\|_*} \right\} = \left(\min_{v\in\mathcal{V},l\in\mathcal{L}} \left\{ \frac{\mathbf{Q}^T\mathbf{y}_v - \left(\boldsymbol{\delta}_l^v\right)^T\boldsymbol{\varphi}_a^v}{\left\|\boldsymbol{\delta}\right\|_*} \right\} \right)^+.
\end{aligned}$$

Finally, we define function $f\left(\mathbf{y},\boldsymbol{\varphi}_a\right) := \left(\min_{v\in\mathcal{V},l\in\mathcal{L}} \left\{ \left(\mathbf{Q}^T\mathbf{y}_v - \left(\boldsymbol{\delta}_l^v\right)^T\boldsymbol{\varphi}_a^v\right) \big/ \left\|\boldsymbol{\delta}\right\|_* \right\} \right)^+$.

Thus far, (4.6) can be reformulated as

$$\mathcal{JCC} := \left\{ \mathbf{y} \in \mathbb{Z}_+^{s\times v} : \begin{array}{c} \rho\overline{\xi} - \eta \leq \dfrac{1}{N}\sum_{a\in[N]} \min\left\{ \overline{\xi} f\left(\mathbf{y},\boldsymbol{\varphi}_a\right) - 1, 0 \right\}, \\ \overline{\xi} \geq 0, \end{array} \right\}. \qquad (4.15)$$

Stage 3: In this stage, we prove that Equation (4.15) is equivalent to Equation

(4.12), i.e.,

$$\mathcal{JCC}' := \left\{ \mathbf{y} \in \mathbb{Z}_+^{s\times v} : \begin{array}{c} \rho - \eta\xi \le \frac{1}{N} \sum_{a\in[N]} \min\left\{ f\left(\mathbf{y}, \boldsymbol{\varphi}_a\right) - \xi, 0 \right\}, \\ \xi \ge 0, \end{array} \right\}. \quad (4.16)$$

To this end, we only need to prove that $\mathcal{JCC} \subseteq \mathcal{JCC}'$ and that $\mathcal{JCC}' \subseteq \mathcal{JCC}$.

$(\mathcal{JCC} \subseteq \mathcal{JCC}')$ If $\mathbf{y} \in \mathcal{JCC}$ is given, then $\exists \bar{\xi} \ge 0$ such that $(\mathbf{y}, \bar{\xi})$ satisfies Equation (4.16). Specifically, if $\bar{\xi} > 0$, we can set $\xi = \bar{\xi}^{-1}$; thus, $(\mathbf{y}, \xi)$ satisfies Equation (4.16). Consequently, we have $\mathbf{y} \in \mathcal{JCC}'$. If $\bar{\xi} = 0$, then there exists $-\eta \le -1$ in Equation (4.15), which contradicts $\eta \in (0,1)$.

$(\mathcal{JCC}' \subseteq \mathcal{JCC})$ If $\mathbf{y} \in \mathcal{JCC}'$ is given, then it is necessary to verify that $\exists \xi \ge 0$ such that $(\mathbf{y}, \xi)$ satisfies Equation (4.15). Specifically, if $\xi > 0$, then we can set $\bar{\xi} = \xi^{-1}$. At this time, we can observe that $(\mathbf{y}, \xi)$ also satisfies Equation (4.15). Therefore, we have $\mathbf{y} \in \mathcal{JCC}$. If $\xi = 0$, then we have $\min\left\{ f\left(\mathbf{y}, \boldsymbol{\varphi}_a\right) - \xi, 0 \right\} = 0$, $\forall a \in [N]$ in Equation (4.16), and this equation reduces to $\rho \le 0$, which is against $\rho > 0$. (Q.E.D.)

Given the conclusion of **Proposition 4.1**, we can represent set $\mathcal{JCC}$ is mixed integer representable using **Proposition 4.2** as follows.

Proposition 4.2. Set $\mathcal{JCC}$ can be mixed integer representable as Eq. (4.17).

$$\mathcal{JCC}_{\text{MIP}} = \left\{ \mathbf{y} \in \mathbb{Z}_+^{s\times v} : \begin{array}{ll} \rho\omega - \eta\xi \le \frac{1}{N} \sum_{a\in[N]} J_a & (4.17\text{a}) \\ J_a + \xi \le \max\left\{ \mathbf{Q}^T \mathbf{y}_v - \left(\boldsymbol{\delta}_l^v\right)^T \boldsymbol{\varphi}_a^v, 0 \right\}, \forall (v,l) \in \mathcal{V}\times\mathcal{L}, a \in [N] & (4.17\text{b}) \\ J_a \le 0, \forall a \in [N] & (4.17\text{c}) \\ \|\boldsymbol{\delta}\|_* \le \omega & (4.17\text{d}) \\ \omega > 0, \xi \ge 0 & (4.17\text{e}) \end{array} \right\}.$$

Proof. Proving **Proposition 4.2** is equivalent to proving $\mathcal{JCC} \subseteq \mathcal{JCC}_{\text{MIP}}$ and

$\mathcal{JCC}_{\text{MIP}} \subseteq \mathcal{JCC}$.

$(\mathcal{JCC}_{\text{MIP}} \subseteq \mathcal{JCC})$. Given $\mathbf{y} \in \mathcal{JCC}_{\text{MIP}}$, then there exist $(\xi, \omega, \mathbf{J}, \mathbf{y})$ such that all constraints in Equation (4.17) are satisfied. For all $(v,l) \in \mathcal{V} \times \mathcal{L}$, we have

$$\frac{J_a}{\omega} \le \min\left\{\frac{1}{\omega}\min_{(v,l)\in\mathcal{V}\times\mathcal{L}} \max\left\{\mathbf{Q}^T\mathbf{y}_v - \left(\boldsymbol{\delta}_l^v\right)^T \boldsymbol{\varphi}_a^v, 0\right\} - \frac{\xi}{\omega}, 0\right\}$$

$$\le \min\left\{\min_{(v,l)\in\mathcal{V}\times\mathcal{L}} \max\left\{\frac{\mathbf{Q}^T\mathbf{y}_v - \left(\boldsymbol{\delta}_l^v\right)^T \boldsymbol{\varphi}_a^v}{\|\boldsymbol{\delta}\|_*}, 0\right\} - \frac{\xi}{\omega}, 0\right\} = \min\left\{f\left(\mathbf{y}, \boldsymbol{\varphi}^a\right) - \frac{\xi}{\omega}, 0\right\}$$

where the second inequality holds since $\|\boldsymbol{\delta}\|_* \le \omega$. Then, we can obtain

$$\rho - \eta\frac{\xi}{\omega} \le \frac{1}{N}\sum_{a\in[N]} \frac{J_a}{\omega} \le \frac{1}{N}\sum_{a\in[N]} \min\left\{f\left(\mathbf{y}, \boldsymbol{\varphi}_a\right) - \frac{\xi}{\omega}, 0\right\}.$$

The above inequalities show that $(\xi/\omega, \mathbf{y})$ satisfies all constraints of $\mathcal{JCC}$, i.e., $\mathbf{y} \in \mathcal{JCC}$. Therefore, we have $\mathcal{JCC}_{\text{MIP}} \subseteq \mathcal{JCC}$.

$(\mathcal{JCC} \subseteq \mathcal{JCC}_{\text{MIP}})$. Given $\mathbf{y} \in \mathcal{JCC}$, then there exists $(\xi, \mathbf{y})$ satisfying the constraints listed in Equation (4.12). For all $a \in [N]$, we set $\hat{\xi} = \xi\|\boldsymbol{\delta}\|_*$, $\omega = \|\boldsymbol{\delta}\|_*$, and $J_a = \min_{(v,l)\in\mathcal{V}\times\mathcal{L}}\left\{\max\left\{\mathbf{Q}^T\mathbf{y} - \boldsymbol{\delta}^T\boldsymbol{\varphi}_a, 0\right\} - \hat{\xi}, 0\right\}$. Obviously, $\left(\hat{\xi}, \omega, \mathbf{J}, \mathbf{y}\right)$ also satisfies constraints in (4.17). Thus, we can obtain $\mathbf{y} \in \mathcal{JCC}_{\text{MIP}}$. (Q.E.D.)

In Equation (4.16), $\mathcal{JCC}'$ is a closed set since it is induced by a chance constraint. However, we introduce $\omega > 0$ in $\mathcal{JCC}_{\text{MIP}}$, making it not guaranteed to be closed. In practice, we can find a $\underline{\omega} > 0$ during the computation process such that $\underline{\omega} \le \inf\left\{\|\boldsymbol{\delta}\|_* : \|\boldsymbol{\delta}\|_* \ne 0\right\}$. In addition, we can also set $\underline{\omega}$ a sufficiently small positive number and replace $\omega > 0$ in $\mathcal{JCC}_{\text{MIP}}$ with $\omega \ge \underline{\omega}$.

Considering that nonlinear constraints still exist in $\mathcal{JCC}_{\text{MIP}}$, we use **Proposition 4.3** to transform them into linear constraints.

Proposition 4.3. Assume that there exists a vector $\mathbf{M} \in \mathbb{R}_{+}^{N}$ consisting of big-M coefficients M_a satisfying

$$\min_{(v,l)\in\mathcal{V}\times\mathcal{L}} \max_{\mathbf{y}\in\mathcal{JCC}_{\mathrm{MIP}}} \left\{\left|\mathbf{Q}^T\mathbf{y} - \boldsymbol{\delta}^T\boldsymbol{\varphi}_a\right|\right\} \le M_a$$

for all $a \in [N]$. Then, set $\mathcal{JCC}_{\mathrm{MIP}}$ can be mixed integer represented as set $\mathcal{JCC}_{\mathrm{M}}$, where

$$\mathcal{JCC}_{\mathrm{M}} = \left\{ \mathbf{y} \in \mathbb{Z}_{+}^{s\times v} : \begin{array}{ll} \rho\omega - \eta\xi \le \frac{1}{N}\sum_{a\in[N]} J_a & \text{(4.18a)} \\ J_a + \xi \le p_a, \forall a \in [N], & \text{(4.18b)} \\ p_a \le \mathbf{Q}^T\mathbf{y}_v - \left(\boldsymbol{\delta}_l^v\right)^T \boldsymbol{\varphi}_a^v + M_a d_a, \forall (v,l) \in \mathcal{V}\times\mathcal{L}, a \in [N] & \text{(4.18c)} \\ p_a \le M_a\left(1-d_a\right), \forall a \in [N] & \text{(4.18d)} \\ \left\|\boldsymbol{\delta}\right\|_* \le \omega & \text{(4.18e)} \\ \omega > 0, \xi \ge 0 & \text{(4.18f)} \\ p_a \ge 0, J_a \le 0, d_a \in \{0,1\}, \forall a \in [N] & \text{(4.18g)} \end{array} \right\}.$$

Proof. We first introduce a binary auxiliary variable, say d_a, and a continuous bounded auxiliary variable, say p_a, and a big-M coefficient vector, say $\mathbf{M} = (M_a) \in \mathbb{R}_{+}^{N}$. Thus, in set $\mathcal{JCC}_{\mathrm{MIP}}$, the constraint

$$J_a + \xi \le \max\left\{\mathbf{Q}^T\mathbf{y}_v - \left(\boldsymbol{\delta}_l^v\right)^T \boldsymbol{\varphi}_a^v, 0\right\} \qquad \forall (v,l) \in \mathcal{V}\times\mathcal{L}, a \in [N] \quad (4.19)$$

is equivalent to

$$J_a + \xi \le \mathbf{Q}^T\mathbf{y}_v - \left(\boldsymbol{\delta}_l^v\right)^T \boldsymbol{\varphi}_a^v + M_a d_a \qquad \forall (v,l) \in \mathcal{V}\times\mathcal{L}, a \in [N] \quad (4.20)$$

$$J_a + \xi \le M_a\left(1-d_a\right) \qquad \forall a \in [N]. \quad (4.21)$$

The inclusion of d_a in Constraints (4.20) and (4.21) ensures that one and only one of the two constraints holds. When the model achieves an optimal solution, $d_a = 0$ if $\mathbf{Q}^T\mathbf{y}_v - \left(\boldsymbol{\delta}_l^v\right)^T \boldsymbol{\varphi}_a^v > 0$, and $d_a = 1$ if $\mathbf{Q}^T\mathbf{y}_v - \left(\boldsymbol{\delta}_l^v\right)^T \boldsymbol{\varphi}_a^v < 0$. Since $\mathbf{Q}^T\mathbf{y}_v - \left(\boldsymbol{\delta}_l^v\right)^T \boldsymbol{\varphi}_a^v$, J_a and ξ are all bounded, a finite M_a must be found. Therefore, we let $J_a + \xi \le p_a$ and Constraints (4.20)–(4.21) be equivalent to Constraints (4.18c)–(4.18d). (Q.E.D.)

In practice, we can straightforwardly take M_a to be a finite value, e.g., we can set

$$M_a = \max_{\mathbf{y}\in\mathbb{Z}_+^{s\times v}, v\in\mathcal{V}, l\in\mathcal{L}} \left|\mathbf{Q}^T\mathbf{y}_v - \left(\boldsymbol{\delta}_l^v\right)^T \boldsymbol{\varphi}_a^v\right|. \tag{4.22}$$

Based on the above transformation, the data-driven distributionally robust chance-constrained model [**SPM**] is converted into an MIP, denoted as the following [**SPM-MIP**].

SPM-MIP:

$$\min obj_1 = T\sum_{v\in\mathcal{V}}\sum_{s\in\mathcal{S}} c_s^{\mathrm{OP}} x_{sv}^{\mathrm{TO}} + \sum_{v\in\mathcal{V}}\sum_{s\in\mathcal{S}} c_{sv}^{\mathrm{VO}} y_{sv} + T\sum_{s\in\mathcal{S}} c_s^{\mathrm{IN}} x_s^{\mathrm{IN}}$$

s.t. (4.2), (4.3), (4.4), (4.5), (4.7), (4.8), (4.22), and $\mathbf{y}\in\mathcal{JCC}_{\mathrm{M}}$.

4.4.3. Strengthened model using the SAA constraint

In this section, we first review the chance-constrained reformulation method based on SAA and then propose a strengthened MIP reformulation of chance constraint (4.6) using the SAA constraint in **Proposition 4.4**. Based on the basic concept of SAA, we transform (4.6) into

$$\mathcal{SAA}_{\text{basic}} := \left\{\mathbf{y}\in\mathbb{Z}_+^{s\times v} : \frac{1}{N}\sum_{a\in[N]}\mathbb{I}\left(\left(\boldsymbol{\delta}_l^v\right)^T \boldsymbol{\varphi}_a^v \le \mathbf{Q}^T\mathbf{y}_v, \forall (v,l)\in\mathcal{V}\times\mathcal{L}\right) \ge 1-\eta\right\}.$$

At this time, the original [**SPM**] can be rewritten as the following model [**SAA**] and solved using the SAA approach.

SAA:

$$\min obj_1 = T\sum_{v\in\mathcal{V}}\sum_{s\in\mathcal{S}} c_s^{\mathrm{OP}} x_{sv}^{\mathrm{TO}} + \sum_{v\in\mathcal{V}}\sum_{s\in\mathcal{S}} c_{sv}^{\mathrm{VO}} y_{sv} + T\sum_{s\in\mathcal{S}} c_s^{\mathrm{IN}} x_s^{\mathrm{IN}} \tag{4.23}$$

s.t. (4.2), (4.3), (4.4), (4.5), (4.7), (4.8), and $\mathbf{y}\in\mathcal{SAA}_{\text{basic}}$.

Proposition 4.4. Set $\mathcal{SAA}_{\text{basic}}$ can be equivalently represented as a mixed integer formulation (4.24) by introducing a binary auxiliary variable d_a.

$$\mathcal{SAA}_{\text{MIP}} := \left\{ \mathbf{y} \in \mathbb{Z}_+^{s \times v} : \begin{array}{ll} \left(\boldsymbol{\delta}_l^v\right)^T \boldsymbol{\varphi}_a^v \le \mathbf{Q}^T \mathbf{y}_v + d_a \left(\boldsymbol{\delta}_l^v\right)^T \boldsymbol{\varphi}_a^v, \forall (v,l) \in \mathcal{V} \times \mathcal{L}, a \in [N] & \text{(4.24a)} \\ \sum_{a \in [N]} d_a \le N\eta & \text{(4.24b)} \\ d_a \in \{0,1\}, \forall a \in [N] & \text{(4.24c)} \end{array} \right\}$$

Proof. We only need to prove that $\mathcal{SAA}_{\text{basic}} \subseteq \mathcal{SAA}_{\text{MIP}}$ and that $\mathcal{SAA}_{\text{MIP}} \subseteq \mathcal{SAA}_{\text{basic}}$.

$\left(\mathcal{SAA}_{\text{basic}} \subseteq \mathcal{SAA}_{\text{MIP}}\right)$ We assume that there exists $\mathbf{y}$ that satisfies $\mathcal{SAA}_{\text{basic}}$. Let $d_a = \mathbb{I}\left\{\left(\boldsymbol{\delta}_l^v\right)^T \boldsymbol{\varphi}_a^v > \mathbf{Q}^T \mathbf{y}_v, \forall (v,l) \in \mathcal{V} \times \mathcal{L}\right\}$. In other words, $d_a = 1$ when $\left(\boldsymbol{\delta}_l^v\right)^T \boldsymbol{\varphi}_a^v > \mathbf{Q}^T \mathbf{y}_v$; $d_a = 0$ when $\left(\boldsymbol{\delta}_l^v\right)^T \boldsymbol{\varphi}_a^v \le \mathbf{Q}^T \mathbf{y}_v$. Moreover, $\sum_{a \in [N]} d_a = \sum_{a \in [N]} \mathbb{I}\left\{\left(\boldsymbol{\delta}_l^v\right)^T \boldsymbol{\varphi}_a^v > \mathbf{Q}^T \mathbf{y}_v, \forall (v,l) \in \mathcal{V} \times \mathcal{L}\right\} \le N\eta$ holds. Hence, vector $\mathbf{y}$ also satisfies $\mathcal{SAA}_{\text{MIP}}$.

$\left(\mathcal{SAA}_{\text{MIP}} \subseteq \mathcal{SAA}_{\text{basic}}\right)$ Similarly, we assume that $\mathbf{y}$ satisfies $\mathcal{SAA}_{\text{MIP}}$. For all $a \in [N]$ and $(v,l) \in \mathcal{V} \times \mathcal{L}$, if $\left(\boldsymbol{\delta}_l^v\right)^T \boldsymbol{\varphi}_a^v \le \mathbf{Q}^T \mathbf{y}_v$, then d_a is free, i.e., either $d_a = 1$ or $d_a = 0$ holds, and $\mathbb{I}\left\{\left(\boldsymbol{\delta}_l^v\right)^T \boldsymbol{\varphi}_a^v > \mathbf{Q}^T \mathbf{y}_v\right\} = 0$. In contrast, if $\left(\boldsymbol{\delta}_l^v\right)^T \boldsymbol{\varphi}_a^v > \mathbf{Q}^T \mathbf{y}_v$, then we have $d_a = 1$ and $\mathbb{I}\left\{\left(\boldsymbol{\delta}_l^v\right)^T \boldsymbol{\varphi}_a^v > \mathbf{Q}^T \mathbf{y}_v\right\} = 1$. Hence, $d_a \ge \mathbb{I}\left\{\left(\boldsymbol{\delta}_l^v\right)^T \boldsymbol{\varphi}_a^v > \mathbf{Q}^T \mathbf{y}_v\right\}$ always holds for all $a \in [N]$ and $(v,l) \in \mathcal{V} \times \mathcal{L}$. Finally, we can observe that $\sum_{a \in [N]} \mathbb{I}\left\{\left(\boldsymbol{\delta}_l^v\right)^T \boldsymbol{\varphi}_a^v > \mathbf{Q}^T \mathbf{y}_v\right\} \le \sum_{a \in [N]} d_a \le N\eta$ holds for all $(v,l) \in \mathcal{V} \times \mathcal{L}$, which indicates that $\mathbf{y}$ also satisfies $\mathcal{SAA}_{\text{basic}}$. (Q.E.D.)

Proposition 4.5. The joint chance constraint (4.6) can be strengthened as the following exact reformulation by introducing set $\mathcal{SAA}_{\text{MIP}}$ in set $\mathcal{JCC}_{\text{M}}$.

$$
\mathcal{JCC}_{\text{M-SAA}} = \left\{ \mathbf{y} \in \mathbb{Z}_{+}^{s \times v} : \begin{array}{ll} \rho\omega - \eta\xi \le \frac{1}{N}\sum_{a \in [N]} J_a & \text{(4.25a)} \\ J_a + \xi \le p_a, \forall a \in [N] & \text{(4.25b)} \\ p_a \le \mathbf{Q}^T \mathbf{y}_v - \left(\boldsymbol{\delta}_l^v\right)^T \boldsymbol{\varphi}_a^v + M_a d_a, \forall (v,l) \in \mathcal{V} \times \mathcal{L}, a \in [N] & \text{(4.25c)} \\ p_a \le M_a\left(1 - d_a\right), \forall a \in [N] & \text{(4.25d)} \\ \|\boldsymbol{\delta}\|_* \le \omega & \text{(4.25e)} \\ \left(\boldsymbol{\delta}_l^v\right)^T \boldsymbol{\varphi}_a^v \le \mathbf{Q}^T \mathbf{y}_v + M_a d_a, \forall a \in [N], (v,l) \in \mathcal{V} \times \mathcal{L} & \text{(4.25f)} \\ \sum_{a \in [N]} d_a \le N\eta & \text{(4.25g)} \\ \omega > 0, \xi \ge 0 & \text{(4.25h)} \\ p_a \ge 0, J_a \le 0, d_a \in \{0,1\}, \forall a \in [N] & \text{(4.25i)} \end{array} \right\}
$$

Proof. We only need to prove $\mathcal{JCC}_{\text{M-SAA}} = \mathcal{JCC}_{\text{M}}$. Obviously, $\mathcal{JCC}_{\text{M-SAA}} \subseteq \mathcal{JCC}_{\text{M}}$. Thus, we just need to prove that $\mathcal{JCC}_{\text{M}} \subseteq \mathcal{JCC}_{\text{M-SAA}}$.

Suppose that $\mathbf{y} \in \mathcal{JCC}_{\text{M}}$ with some $(\omega, \xi, \mathbf{p}, \mathbf{J}, \mathbf{d})$. We can choose a proper vector $\mathbf{d}$, say $\mathbf{d}' \in \{0,1\}^N$; then, for all $a \in [N]$, $d'_a = 1$ if $\mathbf{Q}^T \mathbf{y}_v - \left(\boldsymbol{\delta}_l^v\right)^T \boldsymbol{\varphi}_a^v < 0$, and $d'_a = 0$ if $\mathbf{Q}^T \mathbf{y}_v - \left(\boldsymbol{\delta}_l^v\right)^T \boldsymbol{\varphi}_a^v \ge 0$. Thus, $(\mathbf{y}, \mathbf{d}')$ satisfies (4.25f). Note that (4.25c) and (4.25d) can be reformulated as

$$
\min\left\{\mathbf{Q}^T \mathbf{y}_v - \left(\boldsymbol{\delta}_l^v\right)^T \boldsymbol{\varphi}_a^v + M_a d_a, M_a\left(1 - d_a\right)\right\} \ge p_a \qquad \forall (v,l) \in \mathcal{V} \times \mathcal{L}, a \in [N].
$$

Due to the property of $\mathbf{d}'$, we have

$$
\min\left\{\mathbf{Q}^T \mathbf{y}_v - \left(\boldsymbol{\delta}_l^v\right)^T \boldsymbol{\varphi}_a^v + M_a d'_a, M_a\left(1 - d'_a\right)\right\} = 0
$$

if $\mathbf{Q}^T \mathbf{y}_v - \left(\boldsymbol{\delta}_l^v\right)^T \boldsymbol{\varphi}_a^v < 0$, and it equals $\mathbf{Q}^T \mathbf{y}_v - \left(\boldsymbol{\delta}_l^v\right)^T \boldsymbol{\varphi}_a^v$ if $\mathbf{Q}^T \mathbf{y}_v - \left(\boldsymbol{\delta}_l^v\right)^T \boldsymbol{\varphi}_a^v \ge 0$ for all $a \in [N]$. Hence, we can derive:

$$
\begin{aligned}
&\min\left\{\mathbf{Q}^T \mathbf{y}_v - \left(\boldsymbol{\delta}_l^v\right)^T \boldsymbol{\varphi}_a^v + M_a d'_a, M_a\left(1 - d'_a\right)\right\} \\
&\ge \min\left\{\mathbf{Q}^T \mathbf{y}_v - \left(\boldsymbol{\delta}_l^v\right)^T \boldsymbol{\varphi}_a^v + M_a d_a, M_a\left(1 - d_a\right)\right\} \ge p_a.
\end{aligned}
$$

Obviously, $(\mathbf{y}, \omega, \xi, \mathbf{p}, \mathbf{J}, \mathbf{d}')$ satisfies (4.25a)–(4.25e). Then, we have

$$
\frac{1}{N}\sum_{a \in [N]} d_a = \frac{1}{N}\sum_{a \in [N]} \mathbb{I}\left\{\left(\boldsymbol{\delta}_l^v\right)^T \tilde{\boldsymbol{\lambda}}_a^v > \mathbf{Q}^T \mathbf{y}_v, \forall (v,l) \in \mathcal{V} \times \mathcal{L}\right\} \le \eta
$$

where the first equality holds due to the property of $\mathbf{d}'$; the second inequality is the result of set $\mathcal{SAA}_{\text{MIP}}$. Hence, $(\mathbf{y}, \omega, \xi, \mathbf{p}, \mathbf{J}, \mathbf{d}')$ satisfies (4.25g). Finally, we can observe that $\mathbf{y} \in \mathcal{JCC}_{\text{M-SAA}}$ also holds, which indicates that $\mathcal{JCC}_{\text{M}} \subseteq \mathcal{JCC}_{\text{M-SAA}}$. (Q.E.D.)

Since SAA constraints are part of the ambiguity set, [**SPM-MIP**] can be further strengthened into the following model [**SPM-MIP-SAA**] by introducing SAA constraints.

SPM-MIP-SAA:

$$\min obj_1 = T \sum_{v \in \mathcal{V}} \sum_{s \in \mathcal{S}} c_s^{\text{OP}} x_{sv}^{\text{TO}} + \sum_{v \in \mathcal{V}} \sum_{s \in \mathcal{S}} c_{sv}^{\text{VO}} y_{sv} + T \sum_{s \in \mathcal{S}} c_s^{\text{IN}} x_s^{\text{IN}}$$

$s.t.$ (4.2), (4.3), (4.4), (4.5), (4.7), (4.8), (4.22) and $\mathbf{y} \in \mathcal{JCC}_{\text{M-SAA}}$.

4.4.4. Several valid inequalities

Although reformulation (4.18) is improved to (4.25) by adding additional SAA constraints, we can further reduce the unnecessary constraints and shorten the computation time of the model by introducing several *valid inequalities* associated with (4.25f) and (4.25g). An inequality of the form $\boldsymbol{\mu}^T \mathbf{y} + \boldsymbol{\pi}^T \mathbf{d} \ge \beta$ is called a valid inequality for the SAA constraints. We define

$$\bar{h}_a(\boldsymbol{\mu}) := \min\left\{ \boldsymbol{\mu}^T \mathbf{y} : \mathbf{Q}^T \mathbf{y}_v - \left(\boldsymbol{\delta}_l^v\right)^T \boldsymbol{\varphi}_a^v \ge 0, \mathbf{y} \in \mathbb{Z}_+^{s \times v} \right\}.$$

By examining Equation (4.25f), we can observe that when $d_a = 0$, $\boldsymbol{\mu}^T \mathbf{y} \ge \bar{h}_a(\boldsymbol{\mu})$ holds. For all $a \in [N]$, we put $\bar{h}_a(\boldsymbol{\mu})$ in non-decreasing order, i.e., we set $k = \lfloor N\eta \rfloor$ and $\bar{h}_N(\boldsymbol{\mu}) \ge \cdots \ge \bar{h}_{N-k}(\boldsymbol{\mu}) \ge \cdots \ge \bar{h}_1(\boldsymbol{\mu})$. For all $a \in \{N-k, N-k+1, \cdots, N\}$, we have $d_a = 0$ due to $\sum_{a \in [N]} d_a \le k$. Without loss of generality, we assume that $d_{a'} = 0$; then, $\boldsymbol{\mu}^T \mathbf{y} \ge \bar{h}_{a'}(\boldsymbol{\mu}) \ge \bar{h}_{N-k}(\boldsymbol{\mu})$. Note that

$\boldsymbol{\mu}^T \mathbf{y} \geq \overline{h}_{N-k}(\boldsymbol{\mu})$ always holds regardless of whether $d_a = 0$ or $d_a = 1$. Therefore, we can construct a valid inequality as

$$\boldsymbol{\mu}^T \mathbf{y} + \left(\overline{h}_a(\boldsymbol{\mu}) - \overline{h}_{N-k}(\boldsymbol{\mu}) \right) d_a \geq \overline{h}_a(\boldsymbol{\mu}).$$

Observe formulation (4.25), we can straightforwardly define $\boldsymbol{\mu} := \mathbf{Q}$. Correspondingly, the value of $\overline{h}_a(\boldsymbol{\mu})$ is

$$\min\left\{ \mathbf{Q}^T \mathbf{y}_v : \mathbf{Q}^T \mathbf{y}_v - \left(\boldsymbol{\delta}_l^v\right)^T \boldsymbol{\varphi}_a^v \geq 0, \mathbf{y} \in \mathbb{Z}_+^{s \times v} \right\} = \left(\boldsymbol{\delta}_l^v\right)^T \boldsymbol{\varphi}_v^a.$$

We suppose that $\left(\boldsymbol{\delta}_l^v\right)^T \boldsymbol{\varphi}_v^N \geq \cdots \geq \left(\boldsymbol{\delta}_l^v\right)^T \boldsymbol{\varphi}_v^1$, and we can define q_l^v as the $k+1$ largest value of $\left(\boldsymbol{\delta}_l^v\right)^T \boldsymbol{\varphi}_v^a$ among all $a \in [N]$, i.e., we let $q_l^v = \left(\boldsymbol{\delta}_l^v\right)^T \boldsymbol{\varphi}_v^{N-k}$.

At this time, we have $\boldsymbol{\mu}^T \mathbf{y} \geq \overline{h}_{N-k}(\boldsymbol{\mu})$, and two valid inequalities can be developed:

$$\mathbf{Q}^T \mathbf{y}_v - q_l^v \geq 0 \tag{4.26a}$$

$$\mathbf{Q}^T \mathbf{y}_v - \left(\boldsymbol{\delta}_l^v\right)^T \boldsymbol{\varphi}_a^v + \left(\left(\boldsymbol{\delta}_l^v\right)^T \boldsymbol{\varphi}_a^v - q_l^v \right) d_a \geq 0 \tag{4.26b}$$

Comparing $\left(\boldsymbol{\delta}_l^v\right)^T \boldsymbol{\varphi}_a^v \leq \mathbf{Q}^T \mathbf{y}_v + M_a d_a$ in the SAA constraints, one may find that the valid inequalities are obtained by taking the value of M_a to be $\left(\boldsymbol{\delta}_l^v\right)^T \boldsymbol{\varphi}_a^v - q_l^v$. Thus, a new exact reformulation can be introduced, as shown in **Proposition 4.6**.

Proposition 4.6. With the help of the above valid inequalities, an improved exact reformulation can be derived as

$$\mathcal{JCC}_{\text{IM}} = \left\{ \mathbf{y} \in \mathbb{Z}_+^{s\times v} : \begin{array}{ll} \rho\omega - \eta\xi \le \dfrac{1}{N}\sum_{a\in[N]} J_a & \text{(4.27a)} \\ J_a + \xi \le p_a, \forall a \in [N] & \text{(4.27b)} \\ p_a \le M_a(1-d_a), \forall a \in [N] & \text{(4.27c)} \\ \|\boldsymbol{\delta}\|_* \le \omega & \text{(4.27d)} \\ \sum_{a\in[N]} d_a \le N\eta & \text{(4.27e)} \\ p_a \le \mathbf{Q}^T\mathbf{y}_v - \left(\boldsymbol{\delta}_l^v\right)^T \boldsymbol{\varphi}_a^v + \left(\left(\boldsymbol{\delta}_l^v\right)^T \boldsymbol{\varphi}_a^v - q_l^v\right) d_a, \forall (v,l) \in \mathcal{V}\times\mathcal{L}, a \in [N] & \text{(4.27f)} \\ \omega > 0, \xi \ge 0, p_a \ge 0, J_a \le 0, d_a \in \{0,1\}, \forall a \in [N] & \text{(4.27g)} \end{array} \right\}.$$

Proof. Comparing (4.17) and (4.27), we can observe that the main difference between them is Constraint (4.17c) in $\mathcal{JCC}_{\text{MIP}}$ and Constraints (4.27c) and (4.27f) in $\mathcal{JCC}_{\text{IM}}$. Thus, it is only necessary to show that for all $(v,l) \in \mathcal{V}\times\mathcal{L}$ and $a \in [N]$, (4.27c) and (4.27f) can represent $J_a + \xi \le \max\left\{\mathbf{Q}^T\mathbf{y}_v - \left(\boldsymbol{\delta}_l^v\right)^T \boldsymbol{\varphi}_a^v, 0\right\}$.

If $\mathbf{Q}^T\mathbf{y}_v - \left(\boldsymbol{\delta}_l^v\right)^T \boldsymbol{\varphi}^v < 0$, then $\max\left\{\mathbf{Q}^T\mathbf{y}_v - \left(\boldsymbol{\delta}_l^v\right)^T \boldsymbol{\varphi}_a^v, 0\right\} = 0$, and $d_a = 1$ holds due to $\mathbf{Q}^T\mathbf{y}_v - \left(\boldsymbol{\delta}_l^v\right)^T \boldsymbol{\varphi}_a^v + \left(\left(\boldsymbol{\delta}_l^v\right)^T \boldsymbol{\varphi}_a^v - q_l^v\right) d_a \ge 0$. Hence, (4.27c) and (4.27f) can be reformulated as

$$p_a \le 0 \text{ and } p_a \le \mathbf{Q}^T\mathbf{y}_v - \left(\boldsymbol{\delta}_l^v\right)^T \boldsymbol{\varphi}_a^v + \left(\left(\boldsymbol{\delta}_l^v\right)^T \boldsymbol{\varphi}_a^v - q_l^v\right) d_a = \mathbf{Q}^T\mathbf{y}_v - q_l^v.$$

Since $\mathbf{Q}^T\mathbf{y}_v - q_l^v \ge 0$, the first inequality is stronger than the second one, and (4.27f) becomes redundant.

When $\mathbf{Q}^T\mathbf{y}_v - \left(\boldsymbol{\delta}_l^v\right)^T \boldsymbol{\varphi}^v \ge 0$, there exists $\max\left\{\mathbf{Q}^T\mathbf{y}_v - \left(\boldsymbol{\delta}_l^v\right)^T \boldsymbol{\varphi}_a^v, 0\right\} = \mathbf{Q}^T\mathbf{y}_v - \left(\boldsymbol{\delta}_l^v\right)^T \boldsymbol{\varphi}_a^v$. If we set $d_a = 0$, then (4.27c) is redundant and (4.27f) is equivalent to $J_a + \xi \le \max\left\{\mathbf{Q}^T\mathbf{y}_v - \left(\boldsymbol{\delta}_l^v\right)^T \boldsymbol{\varphi}_a^v, 0\right\}$. Conversely, if we set $d_a = 1$, then (4.27f) becomes redundant, and (4.27c) becomes $J_a + \xi \le 0$. Therefore, $J_a + \xi \le 0$ is stronger than $J_a + \xi \le \max\left\{\mathbf{Q}^T\mathbf{y}_v - \left(\boldsymbol{\delta}_l^v\right)^T \boldsymbol{\varphi}_a^v, 0\right\}$. In conclusion,

$J_a + \xi \leq \max\left\{\mathbf{Q}^T \mathbf{y}_v - \left(\boldsymbol{\delta}_l^v\right)^T \boldsymbol{\varphi}_a^v, 0\right\}$ can be fully represented by (4.27c) and (4.27f). (Q.E.D.)

Proposition 4.7. For all $\mathcal{JCC}_{\text{IM}}$, there exists a vector $\left(\xi, J_a, d_a\right)$ such that $\left(\mathbf{y}, \xi, J_a, d_a\right)$ satisfies $\mathcal{JCC}_{\text{IM}}$, and for all $\left(v, l\right) \in \mathcal{V} \times \mathcal{L}$, we can obtain

$$u_l^v = \mathbf{Q}^T \mathbf{y}_v - q_l^v - \xi \geq 0 . \tag{4.28}$$

Proof. Recall that $f\left(\mathbf{y}, \boldsymbol{\varphi}_a\right) := \left[\min\limits_{v \in \mathcal{V}, l \in \mathcal{L}} \frac{\left(\mathbf{Q}^T \mathbf{y}_v - \left(\boldsymbol{\delta}_l^v\right)^T \boldsymbol{\varphi}_a^v\right)}{\left\|\boldsymbol{\delta}\right\|_*}\right]^+$ in **Proposition 4.1**. Without loss of generality, we suppose that $f\left(\mathbf{y}, \boldsymbol{\varphi}_1\right) \leq \cdots \leq f\left(\mathbf{y}, \boldsymbol{\varphi}_N\right)$ and denote $f\left(\mathbf{y}, \boldsymbol{\varphi}_{k+1}\right)$ as the $\left(k+1\right)^{\text{st}}$ smallest value in the above inequalities.

According to **Lemma 1** in Ho-Nguyen et al. (2022a), for all $\mathbf{y} \in \mathcal{JCC}_{\text{IM}}$, when ξ takes the $\left(k+1\right)^{\text{st}}$ smallest value of $f\left(\mathbf{y}, \boldsymbol{\varphi}_a\right)$, there exists a vector, i.e., $\left(\mathbf{y}, \xi, J_a, d_a\right)$, that satisfies Constraints (4.27a)–(4.27e). Considering this, we let $\left(J_a, \xi\right)$ be $J_a = \left[f\left(\mathbf{y}, \boldsymbol{\varphi}_a\right) - \xi\right]^+$, $\xi = f\left(\mathbf{y}, \boldsymbol{\varphi}_{k+1}\right)$, and $d_a = 1$ when $\min\limits_{v \in \mathcal{V}, l \in \mathcal{L}} \frac{\left(\mathbf{Q}^T \mathbf{y}_v - \left(\boldsymbol{\delta}_l^v\right)^T \boldsymbol{\varphi}_a^v\right)}{\left\|\boldsymbol{\delta}\right\|_*} < 0$ and $d_a = 0$ otherwise. Thus, $\left(\mathbf{y}, \xi, J_a, d_a\right)$ satisfies all the constraints in $\mathcal{JCC}_{IM}$ except (4.27f). Then, we show that $\left(\mathbf{y}, \xi, J_a, d_a\right)$ also satisfies (4.27f). When $d_a = 0$, recall (4.12) and the definition of $\left(\mathbf{y}, \xi, J_a, d_a\right)$, we derive $f\left(\mathbf{y}, \boldsymbol{\varphi}\right) \geq J_a + \xi$ and $\left[\min\limits_{v \in \mathcal{V}, l \in \mathcal{L}} \frac{\left(\mathbf{Q}^T \mathbf{y}_v - \left(\boldsymbol{\delta}_l^v\right)^T \boldsymbol{\varphi}_a^v\right)}{\left\|\boldsymbol{\delta}\right\|_*}\right]^+ = \min\limits_{v \in \mathcal{V}, l \in \mathcal{L}} \frac{\left(\mathbf{Q}^T \mathbf{y}_v - \left(\boldsymbol{\delta}_l^v\right)^T \boldsymbol{\varphi}_a^v\right)}{\left\|\boldsymbol{\delta}\right\|_*}$; then, (4.27f) holds. When $d_a = 1$, we have

$\left[\min_{v\in\mathcal{V},l\in\mathcal{L}} \frac{\left(\mathbf{Q}^T\mathbf{y}_v - \left(\boldsymbol{\delta}_l^v\right)^T \boldsymbol{\varphi}_a^v\right)}{\|\boldsymbol{\delta}\|_*}\right]^+ = 0$ and $J_a = -\xi$, which indicates that $J_a + \xi = 0$.

Hence, (4.27f) reduces to $\mathbf{Q}_l^T\mathbf{y}_v - q_l^v \geq 0$, which is obviously satisfied by $(\mathbf{y},\xi,J_a,d_a)$. Note that for all $(v,l)\in\mathcal{V}\times\mathcal{L}$, we have $\frac{\mathbf{Q}^T\mathbf{y}_v - q_l^v}{\|\boldsymbol{\delta}\|_*} - \xi =$ $\frac{\mathbf{Q}^T\mathbf{y}_v - q_l^v}{\|\boldsymbol{\delta}\|_*} - f\left(\mathbf{y},\boldsymbol{\varphi}_{k+1}\right) \geq 0$.

According to the definition of q_l^v, $\frac{\mathbf{Q}^T\mathbf{y}_v - q_l^v}{\|\boldsymbol{\delta}\|_*}$ represents the $(k+1)$th smallest value of $\frac{\left(\mathbf{Q}^T\mathbf{y}_v - \left(\boldsymbol{\delta}_l^v\right)^T \boldsymbol{\varphi}_a^v\right)}{\|\boldsymbol{\delta}\|_*}$ among all $a\in[N]$. Then, we consider two cases. If $\min_{v\in\mathcal{V},l\in\mathcal{L}} \frac{\mathbf{Q}^T\mathbf{y}_v - q_l^v}{\|\boldsymbol{\delta}\|_*} \leq 0$, then $f\left(\mathbf{y},\boldsymbol{\varphi}_{k+1}\right) = \xi = \left[\min_{v\in\mathcal{V},l\in\mathcal{L}} \frac{\left(\mathbf{Q}^T\mathbf{y}_v - q_l^v\right)}{\|\boldsymbol{\delta}\|_*}\right]^+ = 0$; thus, $\rho\varpi - \eta\xi \leq \frac{1}{N}\sum_{a\in[N]} J_a$ cannot be satisfied because the left hand is non-negative and the right hand is non-positive, so we cannot derive $\min_{v\in\mathcal{V},l\in\mathcal{L}} \frac{\mathbf{Q}^T\mathbf{y}_v - q_l^v}{\|\boldsymbol{\delta}\|_*} \leq 0$. If $\min_{v\in\mathcal{V},l\in\mathcal{L}} \frac{\mathbf{Q}^T\mathbf{y}_v - q_l^v}{\|\boldsymbol{\delta}\|_*} > 0$, then we derive $\min_{v\in\mathcal{V},l\in\mathcal{L}} \frac{\mathbf{Q}^T\mathbf{y}_v - q_l^v}{\|\boldsymbol{\delta}\|_*} = f\left(\mathbf{y},\boldsymbol{\varphi}_{k+1}\right) \leq \frac{\mathbf{Q}^T\mathbf{y}_v - q_l^v}{\|\boldsymbol{\delta}\|_*}$ for all $(v,l)\in\mathcal{V}\times\mathcal{L}$. Based on the above relationship, we have $\mathbf{Q}^T\mathbf{y}_v - q_l^v - \xi \geq 0$. (Q.E.D.)

Following **Proposition 4.7**, we can add $u_l^v \geq 0$ explicitly to (4.27). Note that (4.27f) can be equivalently represented as $u_l^v - J_a \geq \left(\left(\boldsymbol{\delta}_l^v\right)^T \boldsymbol{\varphi}_a^v - q_l^v\right)\left(1-d_a\right)$. Therefore, $\left(\boldsymbol{\delta}_l^v\right)^T \boldsymbol{\varphi}_a^v - q_l^v \leq 0$ is redundant because the left side is non-negative, and the right side is non-positive. Hence, we construct $\left[N_l^v\right]:=$

$\left\{a \in [N] : \left(\boldsymbol{\delta}_l^v\right)^T \boldsymbol{\varphi}_a^v - q_l^v > 0\right\}, \forall v, l \in \mathcal{V} \times \mathcal{L}$ to eliminate the case of $\left(\boldsymbol{\delta}_l^v\right)^T \boldsymbol{\varphi}_a^v - q_l^v \leq 0$, and the improved formulation, i.e., $\mathcal{JCC}_{\text{IM2}}$, is derived as follows.

$$\mathcal{JCC}_{\text{IM2}} = \left\{ \mathbf{y} \in \mathbb{Z}_+^{s \times v} : \begin{array}{ll} \rho\omega - \eta\xi \leq \dfrac{1}{N} \sum_{a \in [N]} J_a & \text{(4.29a)} \\ J_a + \xi \leq p_a, \forall a \in [N] & \text{(4.29b)} \\ p_a \leq M_a \left(1 - d_a\right), \forall a \in [N] & \text{(4.29c)} \\ \|\boldsymbol{\delta}\|_* \leq \omega & \text{(4.29d)} \\ \sum_{a \in [N]} d_a \leq N\eta & \text{(4.29e)} \\ p_a \leq \mathbf{Q}^T \mathbf{y}_v - \left(\boldsymbol{\delta}_l^v\right)^T \boldsymbol{\varphi}_a^v + \left(\left(\boldsymbol{\delta}_l^v\right)^T \boldsymbol{\varphi}_a^v - q_l^v\right) d_a, \forall v, l \in \mathcal{V} \times \mathcal{L}, a \in \left[N_l^v\right] & \text{(4.29f)} \\ \mathbf{Q}^T \mathbf{y}_v - q_l^v - \xi \geq 0, \forall v, l \in \mathcal{V} \times \mathcal{L} & \text{(4.29g)} \\ \omega > 0, \xi \geq 0, & \text{(4.29h)} \\ p_a \geq 0, J_a \leq 0, d_a \in \{0,1\}, \forall a \in [N] & \text{(4.29i)} \end{array} \right\}$$

Remark 4.1. The cardinality of set N_l^v is not greater than $k = \lfloor N\eta \rfloor$; thus, the formulation of $\mathcal{JCC}_{\text{IM2}}$ reduces at least $\left(\left(1-\eta\right)N - 1\right)|\mathcal{V}||\mathcal{L}|$ constraints, where $|\bullet|$ represents the cardinality of the set. The effect is extremely obvious when η is sufficiently small and N, $\mathcal{V}$, and $\mathcal{L}$ are sufficiently large.

Finally, the proposed [**SPM-MIP-SAA**] can be improved as model [**DRCC**].

<u>**DRCC**</u>**:**

$$\min obj_1 = T \sum_{v \in \mathcal{V}} \sum_{s \in \mathcal{S}} c_s^{\text{OP}} x_{sv}^{\text{TO}} + \sum_{v \in \mathcal{V}} \sum_{s \in \mathcal{S}} c_{sv}^{\text{VO}} y_{sv} + T \sum_{s \in \mathcal{S}} c_s^{\text{IN}} x_s^{\text{IN}} \tag{4.30}$$

s.t. (4.2), (4.3), (4.4), (4.5), (4.7), (4.8) and

$$\mathbf{y} \in \mathcal{JCC}_{\text{IM2}}. \tag{4.31}$$

4.5. Numerical experiments

4.5.1. Data description

The example consists of several routes operated by a liner company based in Hong Kong called the *Orient Overseas Container Line* (OOCL; see http://www.oocl.com for details). The total number of routes is set to 10, which contains 346 port pairs, and the distance of each route is calculated according to the data proposed by Meng et al. (2012), as shown in Table 4.2. The setting of liner-related parameters used are listed in Table 4.3 (Meng et al., 2012). Similar to Meng et al. (2012), we set the time horizon to 180 days. The samples of container demand $\lambda^{\left(k_v^i,k_v^j\right)}$ in each port pair $\left(k_v^i,k_v^j\right)$ are generated through the normal distribution $N(\mu^{\left(k_v^i,k_v^j\right)},\sigma^{\left(k_v^i,k_v^j\right)})$, and the ratio $\mu^{\left(k_v^i,k_v^j\right)}/\sigma^{\left(k_v^i,k_v^j\right)}$ is assumed to be the same for all port pairs. The weekly CCFI changes shown in Table 4.1 indicate that the freight rate index may change by more than 7% within a week. This shows that the container transportation demand also reveals sufficient fluctuations, which cannot be easily captured by simply taking the sample mean. However, information associated with transportation demand is often difficult to obtain because liner companies consider this type of data to be commercially confidential. Therefore, existing studies usually randomly generate demand data (e.g., in Zhao et al. (2022)), the expected container transportation demand on different routes is assumed to vary from 26,000 TEUs to 130,000 TEUs). To improve this chapter's practical impact on the liner shipping fleet deployment problem, we collect demand data based on the publicly available dataset LINER-LIB[6] released by Brouer et al. (2014) as the parameter $\mu^{\left(k_v^i,k_v^j\right)}$. If the dataset does not contain the port pair we consider, we infer the demand on the basis of the port

[6] See https://www.linerlib.org/ and https://github.com/blof/LINERLIB/ for details.

throughput. Moreover, the ratio $\mu^{\left(k_v^i,k_v^j\right)} / \sigma^{\left(k_v^i,k_v^j\right)}$ is determined based on the CCFI. We set $\sigma^{\left(k_v^i,k_v^j\right)} / \mu^{\left(k_v^i,k_v^j\right)}$ to the maximum percentage fluctuation between two consecutive weeks when observing the CCFI in April 2024. This ensures that the parameters reflect the true fluctuations of real-world data. Unless otherwise stated, we use 30 samples generated from the distribution $N(\mu^{\left(k_v^i,k_v^j\right)},\sigma^{\left(k_v^i,k_v^j\right)})$ in our calculations. The model is solved in GAMS using the CPLEX solver. All the codes are run on a computer with an Intel i7-1260P CPU and 32 GB of RAM.

Table 4.2 Voyage distance and ports of call for different routes

Route No.	Voyage distance (n mile)	Ports of call
1	3440	Yokohama → Tokyo → Nagoya → Kobe → Shanghai → Hong Kong → Yokohama
2	2361	Ho Chi Minh → Laem Chabang → Singapore → Port Klang → Ho Chi Minh
3	8591	Brisbane → Sydney → Melbourne → Adelaide → Fremantle → Jakarta → Singapore → Brisbane
4	1622	Manila → Kaohsiung → Xiamen → Hong Kong → Yantian → Chiwan → Manila
5	1997	Dalian → Xingang → Qingdao → Shanghai → Ningbo → Kwangyang → Busan → Dalian
6	4948	Chittagong → Chennai → Colombo → Cochin → Nhava Sheva → Chittagong
7	6400	Sokhna → Aqabah → Jeddah → Salalah → Karachi → Jebel Ali → Sokhna
8	1193	Southampton → Thamesport → Hamburg → Bremerhaven → Rotterdam → Antwerp → Zeebrugge → Le Havre → Southampton
9	6009	Port Klang → Singapore → Jakarta → Kaohsiung → Busan → Hong Kong → Chiwan → Port Klang
10	20478	Yantian → Hamburg → Sokhna → Jeddah → Port Klang → Singapore → Manila → Yantian

Table 4.3 Liner performance parameters of different classes

Item	Liner class				
	1	2	3	4	5
Size (TEUs)	2808	3218	4500	5714	8063
Economic speed (knots)	21.00	22.00	24.20	24.60	25.20
Operation cost (10^3 \$/day)	19.80	22.50	30.90	38.80	54.20
Chartering in rate (million \$)	2.00	2.60	3.50	4.70	6.00
NO_s^{MAX}	2	2	9	2	12
NC_s^{MAX}	5	5	5	3	3

4.5.2. Performance of the basic and improved models

In this subsection, we implement several groups of numerical experiments to investigate the performance of the models we established, especially the impact of the number of samples on the experimental results and calculation time. Therefore, we conduct several experiments to obtain the results of the [**DRCC**]. We set the radius of the Wasserstein set ρ equal to 0.1 and the confidence level (i.e., risk tolerance) η equal to 0.05. Similar to Ho-Nguyen et al. (2022a), the number of samples is set to $\{100, 1000, 3000\}$. Tables 4.4 and 4.5 present the optimal solutions to the [**DRCC**] with different sample sizes. They illustrate the liner deployment scheme on each route and how many voyages are performed on each route. The results show that the liner company deploys 20 liners on the liner shipping network. This number exceeds the current liners owned by the company. Therefore, the company decides to charter in an additional 4 liners from the liner charting market. Among all the classes of liners, class 3 liners are the most popular, while class 5 liners are rarely used. We can also observe that at least 26 voyages are required for each route due to the limited service frequency. In addition, there are 4 routes that require additional voyages, which indicates that in more than half of the routes, transportation demand can be met by the current minimum number of voyages. From the solutions under different sample sizes, we can observe that our model performs well among all the scenarios. The changes in liner classes and voyages indicate that more sample information facilitates model improvements to existing solutions, which is one of the core benefits of the Wasserstein ambiguity set. In today's ever-changing political and economic landscape, liner companies should improve their digitalization level, accurately and effectively capture changes in their own operations.

Table 4.4 Liner fleet deployment scheme

N	Liner fleet deployment scheme	Route 1	2	3	4	5	6	7	8	9	10
100	Liner class 1				1		1	1		1	
	Liner class 2	1	1				1				
	Liner class 3			3		1		1			5
	Liner class 4									1	1
	Liner class 5								1		
1000	Liner class 1		1		1		2	1		1	1
	Liner class 2	1		1							
	Liner class 3			2	1			1			5
	Liner class 4					1				1	
	Liner class 5			1					1		1
3000	Liner class 1						1	1			2
	Liner class 2	1					1				
	Liner class 3			3	1					2	3
	Liner class 4					1			1		
	Liner class 5	1	1					1			1

Table 4.5 Number of voyages

N	Number of voyages	Route 1	2	3	4	5	6	7	8	9	10
100	Liner class 1				32		13	14		10	
	Liner class 2	27	26				13				
	Liner class 3			27		27		12			24
	Liner class 4									16	2
	Liner class 5								26		
1000	Liner class 1		26		10		26	14		10	1
	Liner class 2	27		3							
	Liner class 3			21	16			12			24
	Liner class 4					26				16	
	Liner class 5			2					26		1
3000	Liner class 1						18	14			7
	Liner class 2	24					8				
	Liner class 3			27	26					27	15
	Liner class 4					26			28		
	Liner class 5	2	26					12			4

To better compare the performances of different DRCCP formulations, we conduct experiments to analyze the solving times of [**SPM-MIP**], [**SPM-MIP-SAA**], [**DRCC**] and [**SAA**]. According to the route and liner information proposed in Section 4.5.1, we then randomly generate 10 groups of transportation demand data and report the solving times in the following figures. Following the default settings of the GAMS software, we set the upper limit of the solution time for each model to 1,000 seconds. The program running time under three sample sizes is plotted as a boxplot in Fig. 4.2. It does not show the program running time of [**SPM-MIP**] because the running time exceeds the specified upper limit when we set the number of samples to $\{1000, 3000\}$. The average time of solving various models is also recorded in Table 4.6. Overall, the solving time can be summarized as follows: [**SPM-MIP**]>[**SPM-MIP-SAA**]>[**SAA**]$\geq$[**DRCC**], and the model [**SPM-MIP-SAA**] requires much more time to obtain an optimal solution. This is reasonable because complicated structures are introduced in the model reformulation process. The boxplot also illustrates the advantages of the proposed [**DRCC**], and the model is approximately four times faster than the original [**SPM-MIP-SAA**]. As we mentioned in **Remark 4.1**, the improvement of formulation (4.31) is more obvious when N increases, which is proven in the experiments with 3000 samples.

Table 4.6 Program average running time of different models

Model	Program average running time (s)		
	Sample size N=10	Sample size N=1000	Sample size N=3000
[**SPM-MIP**]	0.039	>1000	>1000
[**SPM-MIP-SAA**]	0.442	4.316	11.214
[**DRCC**]	0.139	0.975	2.880
[**SAA**]	0.156	1.341	3.528

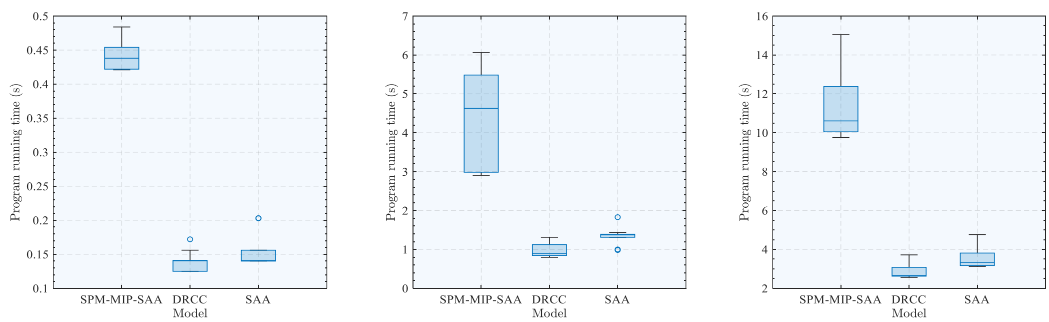

(*a*) N=10 (*b*) N=1000 (*c*) N=3000

Fig. 4.2 Program running time of different models under three sample sizes

4.5.3. Sensitivity analysis

4.5.3.1. Sensitivity analysis of the Wasserstein ball radius ρ

The radius ρ of the type-1 Wasserstein set is a crucial parameter in the model since it represents the level of uncertainty. The sample size is set to 100, and the risk tolerance η is set to 0.1. Then, we set 10 different values of ρ, following the order of $\rho_1 < ... < \rho_{10}$, and the value of ρ_1 is set to 0.001. Then, we set the maximum value $\rho_{\max}$ such that the model is still feasible and the other radius is set as $\rho_i = 0.1(i-1)\rho_{\max}$ for $i = 2,...,10$. Fig. 4.3 shows the objective function value ('OBJ' for short) when different Wasserstein radii are adopted. The OBJ of the [**DRCC**] increases rapidly as the radius increases, from approximately 2 billion yuan when $\rho = \rho_1$ to over 8 billion yuan when $\rho = \rho_{10}$. This relationship indicates that the liner company spends more money on deploying liners. This phenomenon is expected because the purpose of a liner company is to hedge against increased uncertainty. Fig. 4.4 shows the optimal solution of the [**DRCC**] with different Wasserstein radii ρ. Note that the number of ships in the legend of Fig. 4.4 represents the number of ships deployed in all routes under the solution. The total number of liners deployed remains similar (i.e., approximately 21), while the number of voyages increases as the Wasserstein radius increases. This finding indicates that liner companies tend to arrange more voyages to address higher levels of uncertainty.

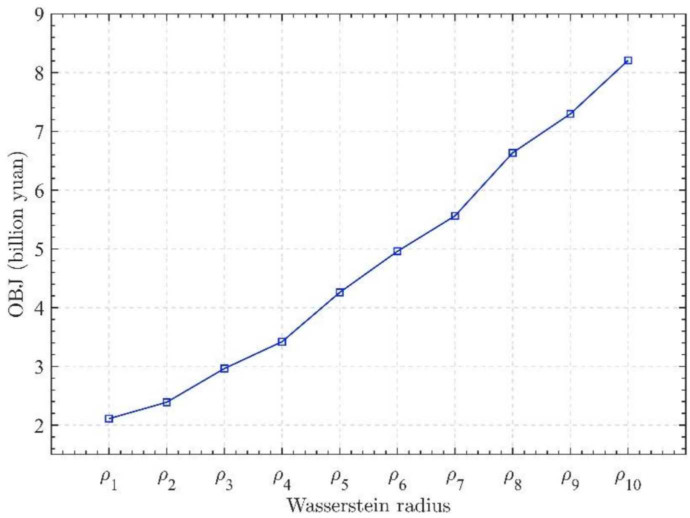

Fig. 4.3 OBJs of [**DRCC**] with different Wasserstein radii

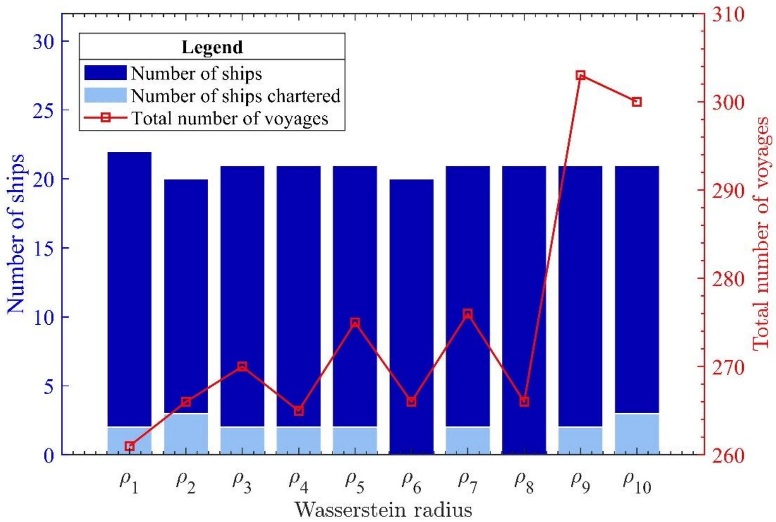

Fig. 4.4 [**DRCC**] solutions with different Wasserstein radii

From Figs. 4.3 and 4.4, one can see that tuning the Wasserstein ball radius is crucial. Now, we show how we use the cross-validation method to choose a proper radius. First, we assume that the possible Wasserstein radii are from $\rho \in \{\rho_i | i = 1,2,...,10\}$ and set the confidence level (i.e., risk tolerance) η equal to 0.05. For each possible radius ρ in set $\{\rho_i | i = 1,2,...,10\}$, we solve the model [**DRCC**] to obtain an optimal solution. Second, we generate $N = 10^4$ i.i.d. samples $\hat{\boldsymbol{\lambda}}^{(k_v^i, k_v^j)} = (\hat{\lambda}_a^{(k_v^i, k_v^j)})$ $(a \in [N])$ from a normal distribution with sample mean $\boldsymbol{\mu} = (\mu^{(k_v^i, k_v^j)})$ and standard deviation information $\boldsymbol{\sigma} = (\kappa\sigma^{(k_v^i, k_v^j)})$

generated in Section 4.5.1, where κ is a positive integer parameter. Third, for each $\rho \in \{\rho_i | i = 1, 2, ..., 10\}$, we set $\kappa = 1$ and substitute these sample values and the corresponding optimal solution solved into the joint chance constraint (4.6) to test the violation probability of this constraint. If the violation probability of the constraint is less than 0.05 (i.e., target violation), we continue to increase κ until it is above 0.05. The smallest κ value for which the constraint violation probability exceeds the target violation probability is recorded. We summarize the optimal objective and the smallest κ under different ρ values in Table 4.7 below. The larger the κ value in the table is, the stronger the ability of the optimal solution to resist risk, but the corresponding cost (i.e., objective value) also increases. From the data in the table, we can see that in order to balance the ability to cope with demand uncertainty and the operation costs incurred, the liner company should choose $\rho = \rho_3$ in the computation. On the one hand, the optimal solution under ρ_3 still has a 95% probability of not violating the constraints when $\kappa = 5$. On the other hand, its corresponding operation cost is not much greater than that of the solution with $\rho = \rho_2$.

Table 4.7 Choosing a Wasserstein ball radius via the cross-validation method

ρ_i	OBJ (Billion yuan)	κ	Target violation
1	2.07	1	0.05
2	2.49	2	0.05
3	2.96	6	0.05
4	3.58	7	0.05
5	4.26	8	0.05
6	4.67	10	0.05
7	5.74	>10	0.05
8	6.51	>10	0.05
9	7.49	>10	0.05
10	8.23	>10	0.05

4.5.3.2. Sensitivity analysis of the risk tolerance η

To verify the influence of risk tolerance η, we conduct several experiments to explore the relationship between η and OBJ. The conclusions in this section are beneficial for liner companies to determine the parameters η when actually applying our model. For this purpose, the number of samples N is set to 100, the radius of the type-1 Wasserstein set is set to 0.1, and the range of risk tolerance η is set to $[0.001,1]$. In order to verify the generality of the model and provide insights, four different datasets are set up following Wang et al. (2024a): dataset 1, dataset 2, dataset 3, and dataset 4. Each dataset possesses an equal sample size, yet they are generated with distinct sample means and standard deviations. Specifically, the standard deviation of dataset 2 and the mean of dataset 3 are twice those of dataset 1. The mean and standard deviation of dataset 4 are both twice those of dataset 1. The OBJs of [**DRCC**] with different η values and datasets are shown in Fig. 4.5. It can be seen that OBJ decreases as the risk tolerance increases. In particular, there is a large decrease when η is slightly greater than 0. Then, the OBJ remains similar when η increases within the range of $[0.03,1]$. Similar to other studies, we find that the change curve of the OBJ has nothing to do with the dataset. Typically, it is related to the construction of ambiguity sets. The above result indicates that the strategic management department of a liner company should cover additional expenditures if the risk tolerance is not allowed to be greater than 0.03. Furthermore, the details of the solutions under $\eta = 0.001$ and 1 with dataset 1 are illustrated in Tables 4.8 and

4.9. The total number of liners remains stable under different settings of risk tolerance, increasing by only one liner when η decreases from 1 to 0.001. However, the classes of liners change dramatically under different η values, class 5 liners are deployed most frequently, and the numbers of class 1 and class 2 liners are all equal to 0. This indicates that the stress of risk tolerance leads to a difference in liner classes, which also shows the significance of various liner classes. Another way for liner companies to cope with low risk tolerance is to deploy more voyages on almost all routes.

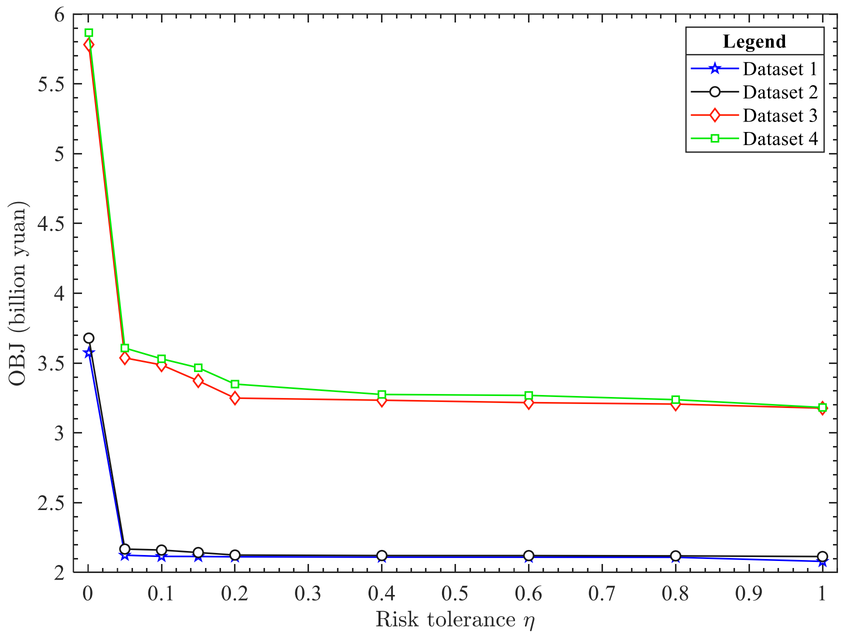

Fig. 4.5 OBJs of the DRCC under different risk tolerance values and datasets

Table 4.8 Liner planning scheme under $\eta = 0.001$ and 1 with dataset 1

Liner planning		Route 1	2	3	4	5	6	7	8	9	10
$\eta = 0.001$ (OBJ = 3.837 billion yuan)	Liner class 1										
	Liner class 2										
	Liner class 3			2			1	3			
	Liner class 4	2	1		1				1		
	Liner class 5			2		1	1			2	6
$\eta = 1$ (OBJ = 2.155 billion yuan)	Liner class 1	2						1		1	
	Liner class 2		1				1	1			
	Liner class 3			3		1					5
	Liner class 4				1						1
	Liner class 5						1	1	1	1	

Table 4.9 Number of voyages under $\eta = 0.001$ and 1 with dataset 1

Number of voyages		Route									
		1	2	3	4	5	6	7	8	9	10
$\eta = 0.001$ (OBJ = 3.837 billion yuan)	Liner class 1										
	Liner class 2										
	Liner class 3			20			10	45			
	Liner class 4	35	27		36				48		
	Liner class 5			18		29	16			29	29
$\eta = 1$ (OBJ = 2.155 billion yuan)	Liner class 1	30						14		15	
	Liner class 2		26				19	12			
	Liner class 3			26		26					25
	Liner class 4				26						1
	Liner class 5						7	1	26	11	

4.5.4. Comparative analysis of related models

4.5.4.1. Objective function values and solution times of related models

In this section, we compare related models and our proposed [**DRCC**]. For this purpose, we develop an RO model (abbreviated as [**RO**]), an SP model (abbreviated as [**SAA**]) and a deterministic model (abbreviated as [**DM**]). The formulations of the above [**RO**] and [**DM**] are presented in **Appendix A**. The numbers of samples in models [**SAA**] and [**DRCC**] are both set to 100. The Wasserstein radius ρ is set to 0.1, and the risk tolerance level η is set to $[0.001, 1]$.

First, we focus on the impact of demand uncertainty by solving related models with different risk tolerances. From Fig. 4.6, we can observe that the OBJ of the [**DM**] model is always lower. Fig. 4.7 shows that the main cause for the different costs is attributed to the number of voyages performed, while the number of liners deployed both in total and chartered is similar. These results indicate that liner companies tend to arrange more voyages to cope with the impact of uncertainty rather than deploying more liners on routes. As illustrated in Fig. 4.6, the differences among all related models are obvious. The relationships of their OBJs can be summarized as follows: [**RO**] ≥ [**DRCC**] ≥ [**SAA**] ≥ [**DM**]. To gain a certain level of robustness, in models focusing on the worst-case scenario (distribution), i.e., [**RO**] and [**DRCC**], the liner company should pay for higher costs. Moreover, introducing the distributionally robust chance-constraint prevents our proposed [**DRCC**] from being as conservative as [**RO**], and only a slight increase in the total cost is needed. Second, we use Fig. 4.7 to show the solutions of related models. In Fig. 4.7, the number of ships represents the number of liners deployed in all routes under different solutions. Notably, the liner company does not need to charter in any liners according to the results of [**RO**], but its OBJ is the highest. The reason for this phenomenon is that the optimal solution is to deploy more liners with larger capacity and higher daily operational cost.

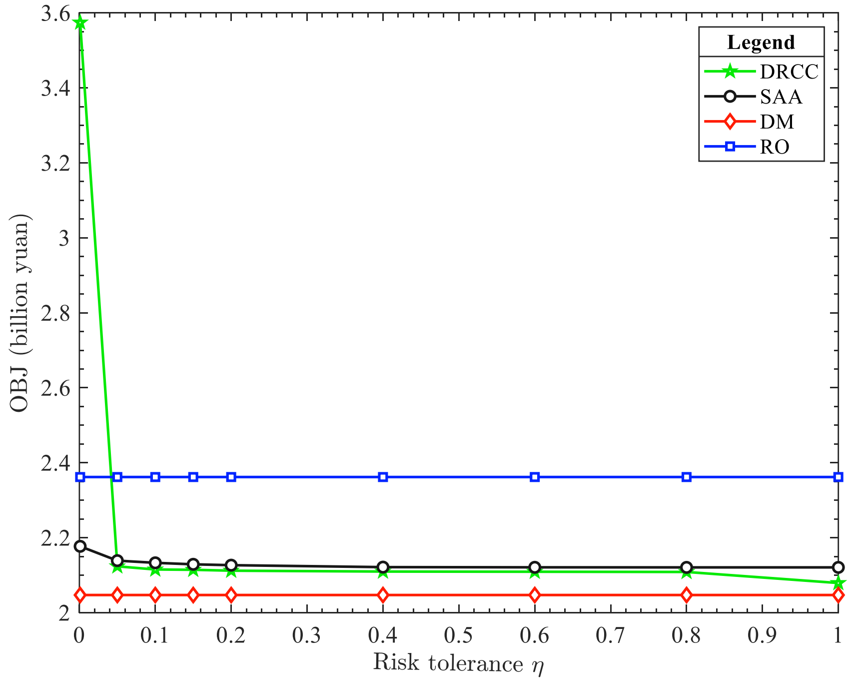

Fig. 4.6 OBJ of related models with different risk tolerances

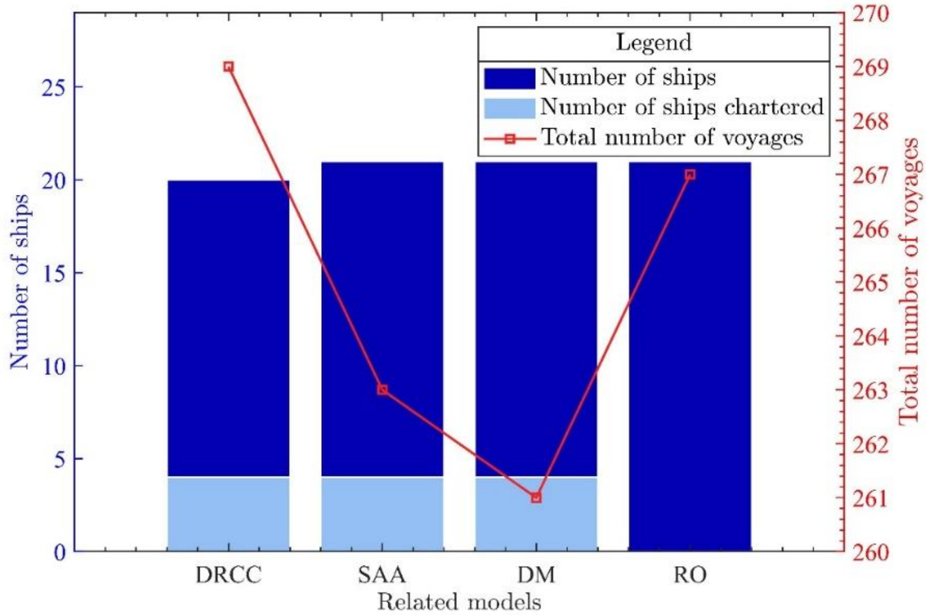

Fig. 4.7 Solutions of related models ($\rho = 0.1$ and $\eta = 0.1$)

Second, we also compare the computation times of related models. This is because, in practical applications, computation time is also a metric to consider when selecting a model. Table 4.10 presents a comparative analysis of computational efficiency among the four optimization models under varying sample sizes. As seen from the data in Table 4.10, the relationship between model solution times can be summarized as follows: [**DM**] $\approx$ [**RO**] $<$ [**DRCC**] $<$ [**SAA**]. The above-mentioned results are in line with our expectations. [**DM**] and [**RO**] are the most efficient to solve because they do not require samples as parameters. As the sample size increases, the time required to solve [**DRCC**] and [**SAA**] increases significantly. However, due to the introduction of SAA constraints and valid inequalities, our efficiency in solving [**DRCC**] is higher than that in solving [**SAA**]. These findings imply that liner companies can reasonably select models on the basis of the amount of data they have, thereby achieving a trade-off between solution quality and calculation time.

Table 4.10 Program average running time of different models

Model	Program average running time (s)		
	Sample size *N*=10	Sample size *N*=1000	Sample size *N*=3000
[**DM**]		0.032	
[**RO**]		0.031	
[**SAA**]	0.156	1.341	3.528
[**DRCC**]	0.139	0.975	2.880

4.5.4.2. Out-of-sample test of solutions to related models

This subsection conducts several out-of-sample analyses with the different models we constructed. We use the sample mean $\boldsymbol{\mu} = (\mu^{\left(k_v^i, k_v^j\right)})$ and standard deviation information $\boldsymbol{\sigma} = (\sigma^{\left(k_v^i, k_v^j\right)})$ generated in Section 4.5.1 as the baseline and consider the following common random variable distribution types.

(1) *Uniform distribution* (UN): For each port pair $\left(k_v^i, k_v^j\right)$, we set the container transportation demand $\lambda^{\left(k_v^i, k_v^j\right)} \sim U(\mu^{\left(k_v^i, k_v^j\right)} - \kappa\sqrt{3}\sigma^{\left(k_v^i, k_v^j\right)}, \mu^{\left(k_v^i, k_v^j\right)} + \kappa\sqrt{3}\sigma^{\left(k_v^i, k_v^j\right)})$.

(2) *Normal distribution* (NO): For each port pair $\left(k_v^i, k_v^j\right)$, we set demand $\lambda^{\left(k_v^i, k_v^j\right)} \sim N(\mu^{\left(k_v^i, k_v^j\right)}, (\kappa\sigma^{\left(k_v^i, k_v^j\right)})^2)$.

(3) *Log-normal distribution* (LN): For each port pair $\left(k_v^i, k_v^j\right)$, we set demand $\lambda^{\left(k_v^i, k_v^j\right)} \sim L(\mu_{\mathrm{L}}^{\left(k_v^i, k_v^j\right)}, (\kappa\sigma_{\mathrm{L}}^{\left(k_v^i, k_v^j\right)})^2)$, where $\mu_{\mathrm{L}}^{\left(k_v^i, k_v^j\right)} = \ln((\mu^{\left(k_v^i, k_v^j\right)})^2 / \sqrt{(\mu^{\left(k_v^i, k_v^j\right)})^2 + (\sigma^{\left(k_v^i, k_v^j\right)})^2})$ and $\sigma_{\mathrm{L}}^{\left(k_v^i, k_v^j\right)} = \ln(1 + (\sigma^{\left(k_v^i, k_v^j\right)})^2 / (\mu^{\left(k_v^i, k_v^j\right)})^2)$.

In the out-of-sample tests, we mainly focus on two key metrics, i.e., average individual probability (AIP) and average joint probability (AJP). They can be calculated as follows:

$$AIP = \frac{1}{N|\mathcal{V}||\mathcal{L}|} \sum_{n \in [N]} \sum_{v \in \mathcal{V}} \sum_{l \in \mathcal{L}} \mathbb{I}\left(\sum_{\left(k_v^i, k_v^j\right) \in \mathcal{W}_v} \hat{\lambda}_n^{\left(k_v^i, k_v^j\right)} \delta_l^{\left(k_v^i, k_v^j\right)} < \sum_{s \in \mathcal{S}} y_{sv} Q_s \right) \times 100\% \quad (4.32)$$

$$AJP = \frac{1}{N}\sum_{n\in[N]}\mathbb{I}\left(\sum_{\left(k_v^i,k_v^j\right)\in\mathcal{W}_v}\hat{\lambda}_n^{\left(k_v^i,k_v^j\right)}\delta_l^{\left(k_v^i,k_v^j\right)} < \sum_{s\in\mathcal{S}} y_{sv}Q_s, \forall v\in\mathcal{V}, l\in\mathcal{L}\right)\times 100\% \quad (4.33)$$

where $\hat{\boldsymbol{\lambda}}^{\left(k_v^i,k_v^j\right)} = (\hat{\lambda}_n^{\left(k_v^i,k_v^j\right)})$ $\left(n\in[N]\right)$ represents randomly generated test samples.

We use the solutions of [**DRCC**] shown in Fig. 4.7 to test the out-the-sample performance with 10,000 randomly generated transportation demand samples under different distribution functions. The optimal solutions of the other models are obtained under the same parameter settings. As illustrated in Tables 4.11 to 4.12, all the models except [**DM**] perform well when the parameter κ is not very large. This trend is expected and indicates that our [**DRCC**] is able to effectively cope with uncertainty. We then focus on common situations when $\kappa = 1$. All the models except [**DM**] performed well on both AIP and AJP. The AIP and AJP of the proposed [**DRCC**] remain 100% for almost all distributions, while those of the [**SAA**] are less than 100%. Notably, the AJP of the [**SAA**] under a log-normal distribution is less than 95%, indicating that the solution of [**SAA**] breaks the risk tolerance of the joint chance constraint. In other words, under the out-of-sample test, the solution of the [**SAA**] cannot ensure that the capacity requirement holds, with a probability of 95%.

To further investigate the ability of all related models to hedge against uncertainty when facing unreasonable situations, we propose additional stress tests with great value κ. Notably, some scenarios may not be possible in practical liner fleet operations. The results of our out-of-sample analysis are also affected by the ratio of the mean to the standard deviation. Therefore, the trend among different models is more meaningful when discussing the out-of-sample performance compared with the results. To depict the trend of the changes in the two metrics, we construct Fig. 4.8. In Fig. 4.8(*b*), Fig. 4.8(*d*) and Fig. 4.8(*f*), the AIP and AJP metrics of [**RO**] and [**DM**] are both 100% and 0%, respectively; therefore, we omit them. It is obvious that all the models exhibit better performance in the AIP tests than in the AJP tests. This is reasonable due to the high difficulty of jointly satisfying constraints. Among all the scenarios, [**RO**] always has better performance than any other model does, whereas [**DM**] is the worst approach when facing stressful situations. However, [**RO**] cannot be considered a more advanced model than the proposed [**DRCC**], although it performs better in out-of-sample analysis. As discussed earlier, the high additional cost of [**RO**] is one of its drawbacks. The performance of our [**DRCC**] is also similar to that of the [**RO**] under low-stress conditions.

Table 4.11 Average individual probability (in %) of solutions of different models

κ	Uniform distribution				Normal distribution				Log-normal distribution			
	DRCC	SAA	DM	RO	DRCC	SAA	DM	RO	DRCC	SAA	DM	RO
1	100.0	99.9	99.9	100.0	100.0	99.9	99.9	100.0	100.0	99.9	99.9	100.0
2	99.4	96.6	87.3	100.0	99.4	96.5	87.5	100.0	98.3	93.3	81.3	100.0
3	96.4	91.5	81.4	99.9	96.4	91.6	81.4	99.9	88.9	81.5	65.9	99.0
4	92.4	87.6	76.7	99.3	92.4	87.7	77.0	99.3	76.0	70.6	52.2	94.5
5	88.7	84.7	73.5	98.1	88.8	84.8	73.6	98.1	63.7	61.4	41.5	87.2
6	85.6	82.4	71.0	96.7	85.6	82.4	71.1	96.7	53.0	53.3	33.4	78.7
7	83.0	80.5	68.9	95.2	83.0	80.5	69.0	95.2	43.5	45.7	27.0	69.6
8	80.8	78.9	67.3	93.7	80.9	79.0	67.5	93.8	35.3	38.5	22.0	60.0
9	78.9	77.6	66.1	92.4	79.0	77.6	66.2	92.4	28.3	31.9	18.1	50.8
10	77.3	76.4	65.0	91.1	77.3	76.4	65.0	91.1	22.8	26.3	15.1	42.6
11	75.9	75.3	64.0	89.8	76.0	75.4	64.1	89.9	18.5	21.6	12.7	35.4
12	74.6	74.3	63.2	88.7	74.6	74.4	63.2	88.6	15.1	17.7	10.8	29.5
13	73.4	73.5	62.6	87.6	73.5	73.5	62.6	87.6	12.6	14.7	9.3	24.4
14	72.4	72.7	61.8	86.4	72.5	72.7	61.9	86.5	10.6	12.3	8.0	20.4
15	71.4	71.9	61.3	85.4	71.5	72.0	61.4	85.5	9.1	10.4	7.0	17.2

Table 4.12 Average joint probability (in %) of solutions of different models

κ	Uniform distribution				Normal distribution				Log-normal distribution			
	DRCC	SAA	DM	RO	DRCC	SAA	DM	RO	DRCC	SAA	DM	RO
1.0	100.0	96.3	0.6	100.0	100.0	95.4	0.6	100.0	100.0	94.1	0.8	100.0
1.1	100.0	91.0	0.3	100.0	99.9	90.1	0.4	100.0	99.8	86.3	0.4	100.0
1.2	99.7	82.5	0.3	100.0	99.7	82.0	0.3	100.0	99.3	73.4	0.1	100.0
1.3	99.4	72.3	0.1	100.0	99.1	71.7	0.1	100.0	97.7	57.8	0.1	100.0
1.4	98.5	60.1	0.1	100.0	97.8	58.9	0.1	100.0	94.2	40.9	0.0	100.0
1.5	96.6	48.8	0.1	100.0	96.1	46.8	0.0	100.0	89.2	26.8	0.0	100.0
1.6	94.1	37.6	0.0	100.0	92.9	37.0	0.1	100.0	81.4	16.6	0.0	100.0
1.7	89.2	27.7	0.1	100.0	87.7	27.2	0.0	100.0	70.9	9.6	0.0	100.0
1.8	83.5	20.4	0.0	100.0	82.9	21.1	0.0	100.0	58.6	5.0	0.0	100.0
1.9	77.0	14.0	0.0	100.0	76.1	14.7	0.0	100.0	45.2	2.5	0.0	100.0
2.0	69.7	10.7	0.0	100.0	67.8	10.5	0.0	100.0	33.4	1.0	0.0	100.0
2.1	61.1	7.1	0.0	100.0	60.5	7.5	0.0	100.0	22.5	0.5	0.0	100.0
2.2	52.5	5.1	0.0	100.0	52.8	5.0	0.0	100.0	14.5	0.2	0.0	100.0
2.3	45.0	3.3	0.0	100.0	44.9	3.5	0.0	100.0	8.5	0.1	0.0	100.0
2.4	38.2	2.5	0.0	100.0	36.3	2.5	0.0	100.0	5.0	0.1	0.0	100.0

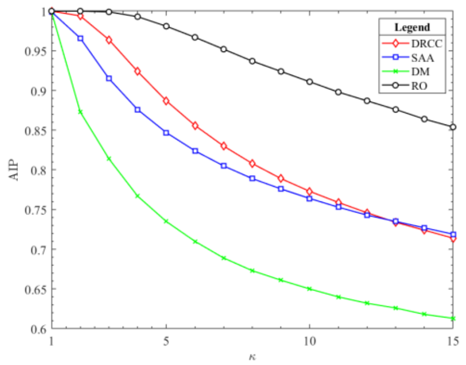

(*a*) AIP under uniform distribution

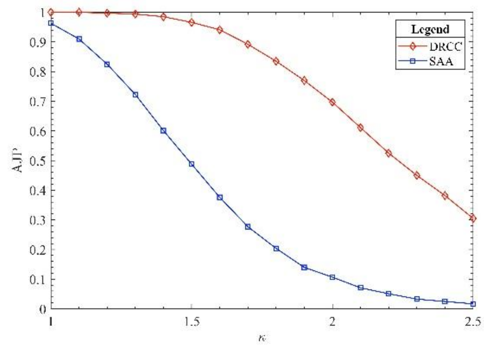

(*b*) AJP under uniform distribution

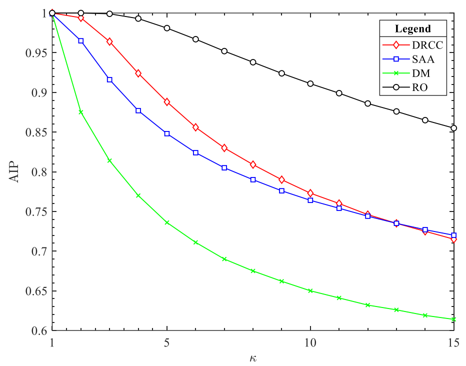

(*c*) AIP under normal distribution

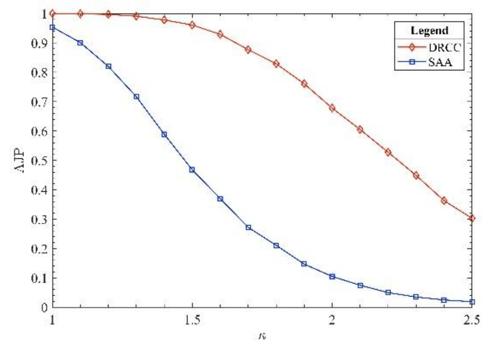

(*d*) AJP under normal distribution

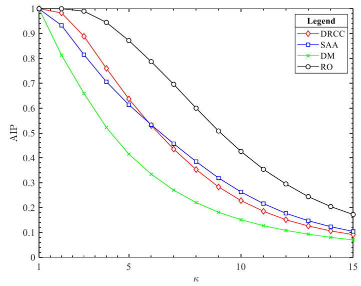

(*e*) AIP under log-normal distribution

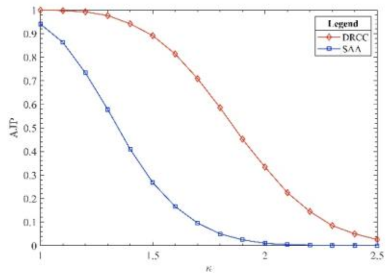

(*f*) AJP under log-normal distribution

Fig. 4.8 Results of the out-of-sample tests

The results of our sample analysis also revealed the advantages of [**DRCC**] over previously used SAA methods in related areas. First, from the performance of the AIP metric, it is noticeable that the proposed [**DRCC**] has obviously better performance when $\kappa \leq 10$, while the SAA approach performs similarly when κ increases. The results of the AJP metric further support the advances of the [**DRCC**] model. We can observe that the performance of the SAA approach decreases sharply when facing stressful tests, which means that solutions under the SAA approach lose the ability to cope with uncertain contract demand when facing slight stress. For all the models, AJP decreases quickly as κ increases. However, this drop does not indicate that the out-of-sample performance is poor because the standard deviation setting is large.

It is evident that the model exhibits disparate performance metrics under varying conditions. Consequently, on the basis of the comparative experiments outlined in Sections 4.5.4.1 and 4.5.4.2, we summarize the advantages and disadvantages of the relevant models in terms of different metrics in Table 4.13 to perform a comprehensive evaluation by combining these metrics. Specifically, three types of metrics are considered: model solution time, objective function value, and out-of-sample performance (i.e., AIP and AJP). The results highlight critical decision trade-offs: while [**RO**] achieves the highest OBJ, reflecting conservative solutions that prioritize robustness at elevated operational costs, it maintains the fastest computational speed and superior out-of-sample performance, making it suitable for high-reliability scenarios. Especially when liner companies have a strong sense of risk aversion, the [**RO**] can become the liner companies' preferred choice. Conversely, [**DM**] has the lowest OBJ value, indicating less conservative solutions that reduce immediate costs but risk inadequacy in extreme cases, compounded by its poor out-of-sample performance despite fast execution. This model can be used by liner companies when historical data (information) are difficult to obtain effectively. [**DRCC**] and [**SAA**] both demonstrate medium OBJ conservatism and comparable AIP performance but diverge in AJP: [**DRCC**] achieves better performance. Moreover, [**DRCC**] operates at a medium runtime, while [**SAA**] is the slowest. These findings suggest that when liner companies have more historical information, they should prioritize the [**DRCC**] rather than the [**SAA**]. [**DRCC**] not only has a faster solution speed but also has better out-of-sample performance. In summary, liner companies should target their choice of model for solving the problem to different historical data holdings and different risk preferences.

Table 4.13 Performance of different models

Model	Performance in different metrics			
	Program running time	OBJ	Out-of-sample performance	
			AIP	AJP
[**DM**]	Fast	Low	Bad	Bad
[**RO**]	Fast	High	Good	Good
[**DRCC**]	Medium	Medium	Medium	Medium
[**SAA**]	Slow	Medium	Medium	Bad

4.5.5. Managerial insights

To comprehensively understand the effect of the uncertainty of container transportation demand, we conduct further discussion and provide several managerial insights into liner shipping fleet deployment.

(1) *The impact of demand uncertainty and model selection*: The impact of uncertain container transportation demand on the entire liner shipping network is significant, as evidenced by the sensitivity analysis results presented in Section 4.5.3. As the uncertainty increases, the liner company must pay four times as much, even if uncertainty is incorporated into the analytical framework before decisions are made. Liner companies may suffer enormous losses if measures are not proposed in advance to address uncertainty, especially in the current situation where supply chain disruptions frequently occur. Therefore, as discussed in Section 4.5.4, liner companies should make rational choices in the optimization model to achieve successful business. When selecting an optimization model, the main considerations are the amount of historical information the liner company has and its own risk preference. For instance, in scenarios where historical data are scarce or non-existent, liner companies are constrained to utilize deterministic models. In circumstances where liner companies exhibit a high degree of risk aversion, the [**RO**] emerges as a viable option. When liner companies have limited historical information, the [**DRCC**] we propose is an effective tool for addressing fluctuations in container demand. Compared with establishing an

SP model and using the SAA method, our DRO method shows better performance in out-of-sample analysis without increasing the computational time. This advantage is due to the SAA constraints and effective inequalities we introduced in the model. It should be noted that when using the [**DRCC**], liner companies need to use the cross-validation method to choose a proper Wasserstein ball radius, as shown in Table 4.7. In summary, no single optimization model can be universally applied to all situations. Liner companies are advised to judiciously select a model that aligns with their preferences and the richness of information.

(2) *Risk tolerance of the liner company*: The risk tolerance parameter in the proposed [**DRCC**] reflects the risk aversion preference of liner companies. The smaller its value is, the less tolerant the liner company is of constraint violations; conversely, the more tolerant the liner company is of violations. In our model, the liner deployment scheme that matches the preferences of the strategic management department can be obtained by adjusting the tolerance level. In practice, the strategic management department is able to adjust the setting of the risk tolerance parameter to obtain a proper solution that satisfies its own risk preference. For example, the department can determine the liner fleet deployment scheme with a differentiated risk tolerance level by comparing optimal solutions under different tolerances, considering its own preferences and the financial objectives of the company. As demonstrated in Section 4.5.4.2, the OBJ for liner deployment remains stable when the risk

tolerance is greater than 0.03. Conversely, a slight reduction in risk tolerance, to below 0.03, has the potential to markedly enhance the actual service level. This suggests that strategic management does not need to set this risk tolerance parameter too large. When the risk tolerance decreases from 1.00 to 0.03, the OBJ does not change significantly. This finding can offer valuable insights for liner companies' strategic management to determine appropriate target risk tolerance. Furthermore, in Fig. 4.5, we conduct a series of experiments using four different datasets and find that the OBJs all show the same turning point. This finding aligns with the conclusions of existing studies (e.g., Wang et al., 2024a), suggesting that the actual service levels of different datasets are consistent.

4.6. Conclusions

Motivated by the complex global situation and the fluctuating shipping market, we improve the traditional stochastic programming model to a data-driven distributionally robust optimization model with a joint chance constraint (abbreviated as [**DRCC**]) to solve the liner shipping fleet deployment problem using historical samples. Our model aims to minimize the liner company's total operational cost during the planning horizon, including the fleet operational cost, voyage cost and capital cost (i.e., charter cost). The demand between each port pair is considered a random variable, and its distribution function is defined within a type-1 Wasserstein ambiguity set. To ensure the reliability of the liner shipping fleet deployment scheme, a joint chance constraint is introduced to ensure that the container flow does not exceed the capacity provided on the route with a probability of $1-\eta$, where η is the risk tolerance of the strategic management department of the liner company. Under the type-1 Wasserstein ambiguity set, our proposed [**DRCC**] is reformulated into a mixed integer programming (MIP) model. Furthermore, we adopt several sample average approximation (SAA) constraints to strengthen our model. High-quality solutions that can be solved via two types of valid inequalities are introduced into the exact MIP reformulation to reduce the computational complexity.

To investigate the performance of our basic model (without valid inequalities) and improved (with valid inequalities) model, we conduct numerical experiments using a dataset from a real-world liner shipping network. The results indicate that our proposed model is able to generate optimal solutions with high reliability and low operational cost. Meanwhile, the introduction of valid inequalities can significantly enhance the solving effectiveness, requiring only close to a quarter of the solving time. Extensive sensitivity analysis is conducted to explore the impact of the Wasserstein radius and risk tolerance on the results. The results show the influence of the degree of uncertainty and the preference of the strategic management department of the liner company and provide management insights for liner deployment and liner shipping network design in practical operation progress. The out-of-sample test results indicate that if the strategic management department of the liner company only uses the deterministic method and the SAA-based stochastic programming method with historical data, although the liner fleet operating cost obtained may be lower than that of methods based on robust optimization, many actual transportation demands may not be met. The robust optimization method is overly conservative, resulting in higher liner shipping fleet operating costs. Finally, we conduct out-of-sample analyses on a moment-based ambiguity set. The experimental results confirm the superiority of the type-1 Wasserstein ambiguity set.

By and large, there are also several flaws in model construction, and future research could improve in these directions. First, this chapter considers only a single kind of uncertain parameter. However, multiple uncertainties affect liner operations. Considering multiple uncertainties in an integrated way and finding an appropriate model and reformulation approach is a direction for expansion. Moreover, we do not differentiate between types of container transportation demand. Incorporating the different uncertainties faced by spot market transportation demand and contract market transportation demand into the framework is also an interesting idea. Second, we use the Wasserstein distance-based ambiguity set to portray uncertainty. It may also inspire the construction of ambiguity sets based on moment information or the analysis of container transportation demand data. Finally, this chapter focuses on overall reliability through joint chance constraints. A sub-regional discussion of realistic route networks, focusing on the balance of reliability between different routes and additional reliability constraints in key routes and key port pairs, is also a topic that can be expanded.

Chapter 5: Liner fleet deployment and slot allocation with uncertain demand[7]

In Chapter 4, we consider the liner fleet deployment problem to enhance the resilience of shipping route operations. This chapter continues the ideas of the previous chapter and considers further expanding the problem involved in the previous chapter. Specifically, we try to investigate the *liner fleet deployment and slot allocation joint optimization problem*. This is because after the liner fleet deployment is completed, the liner company also needs to decide how to allocate the cargo owners' transportation demand (i.e. orders) to liners in the fleet with limited transportation capacity in to seek maximum benefits. Liner fleet deployment is the basis for providing transportation services; allocating cargo owners' orders to liners is the key to achieving profitability of liner companies. These two decisions are interconnected and influence each other, forming an organic whole.

[7]Zhang, T., Wang, S., & Xin, X (Corresponding author). (2025). Liner fleet deployment and slot allocation problem: A distributionally robust optimization model with joint chance constraints. *Transportation Research Part B: Methodological*, 197, 103236.

5.1. Introduction

5.1.1. Background information

Recall that in Chapter 4, we argue that liner companies provide container transportation services by establishing a liner fleet comprising different classes of liners and deploying the appropriate number and class of liners to operate on the liner shipping network (i.e., various routes) according to potential transportation demand (Wang et al., 2013). Subsequently, liners make port calls at regular intervals (e.g., once a week or twice a week) on these routes according to pre-designed service frequencies (Meng et al., 2012). This decision-making problem is also referred to as the **L**iner **F**leet **D**eployment **P**roblem (LFDP) in the field of maritime shipping, which is generally carried out once every 3 to 6 months in order to ensure the stability of the service (Wang et al., 2013; Xin et al., 2023). Once the deployment is completed, cargo owners can access the information on the routes operated by liner companies, including service frequency, freight rates, and liner information, through the official channels provided by liner companies (e.g., the official website; see https://www.oocl.com for an example). Should cargo owners require the purchase of maritime shipping services, they must contact the relevant liner company (typically via a freight forwarder). At this point, the liner company must make another decision.

Specifically, the liner company needs to determine whether to accept the order based on the number of available slots (i.e., space on board a liner occupied by a container) (Meng et al., 2012), a process also known as *slot allocation*. As liner companies operate multiple routes simultaneously in their networks, the key decision for liner companies is to assign containers (orders) to the limited number of slots available on the liner on the optimal route. This decision problem is also called **S**lot **A**llocation **P**roblem (SAP). There are times when a liner company may choose to utilize different routes to fulfill an order, and this may be accomplished by utilizing slots on liners sailing on multiple routes. In the freight market, some cargo owners may sign long-term contracts with liner companies, also known as *contract shippers*, owing to their stable and large demand for container transportation. Other cargo owners, known as *spot shippers*, only have temporary transportation demands and can only passively accept quotes from liner companies (Wang et al., 2020). In light of this, the strategic management departments of liner companies typically prioritize meeting the transportation demands of contract shippers when making SAP decisions, which is considered a *loyal strategy* (Liu & Yang, 2015).

One can notice that in the process of addressing both LFDP and SAP for liner companies, container transportation demand is still a critical parameter. However, in contrast to other types of transportation, container liner transportation activities are deeply coupled with the global political and economic environment and are frequently influenced by a number of uncontrollable factors, such as delayed container arrivals at ports due to bad weather (Wang et al., 2013). In practice, fluctuations in container transportation demand are sometimes so dramatic that it is almost impossible for liner companies to estimate them accurately (Meng et al., 2012). Consequently, since the beginning of the 2010s, scholars have gradually reached a consensus that the uncertain factor of container transportation demand needs to be taken into consideration when handling LFDP, SAP, or both, and a significant number of models considering demand uncertainty have been constructed via stochastic programming (SP) theory, including Wang et al. (2013) and Wang et al. (2020). However, the majority of established studies that consider uncertain demand assume that transportation demand is a random variable with a known distribution function (typically assumed to be a normal distribution function). On the basis of this assumption, several scenarios can be generated, and effective methods, such as sample sampling approximation (SAA), can be used to approximate the SP model by a deterministic problem with a limited number of scenarios. In practice, it is challenging to obtain the true distribution of container transportation demand in the context of complex political and economic circumstances (Zhao et al., 2022). This leads to the possibility that the traditional method of using prior knowledge to estimate the parameter distribution and solve a scenario-based SP may have large deviations (Xin et al., 2025a).

5.1.2. Research objective and contributions

Motivated by the abovementioned background, we attempt to develop a two-stage distribution-free robust chance-constrained model to address the joint optimization of LFDP and SAP under demand uncertainty as an extension of Meng et al. (2012) in this chapter. In the first stage (also referred to *here-and-now* stage), the liner company is responsible for determining the liner fleet deployment scheme. Once the decision-making in the first stage is known and the random variables are realized, the liner company optimizes the slot allocation scheme in the second stage (*wait-and-see* stage). In contrast to previous studies, we do not assume that we have the distribution information of demand. Distributionally robust optimization (DRO) theory, which is a tool for effectively addressing uncertainty, allows us to identify the optimal liner deployment scheme and slot allocation scheme that perform the best in the worst-case distribution. This is achieved by requiring that the true distribution function be within an *ambiguity set* that contains possible distribution functions with similar characteristics, such as moment conditions. Although obtaining a precise description of container transportation demand distribution functions can be challenging, liner companies can collect partial statistical information or empirical data. Equipped with recent theories and techniques in the DRO field (e.g., theories in Delage and Ye (2010) and Chen et al. (2010)), this chapter establishes a data-driven distributionally robust joint chance-constrained model, where the ambiguity sets rely only on mean and covariance information obtained from historical data. Although ambiguity sets are introduced to the model to characterize transportation demand uncertainty, solving such a model is still computationally intractable. Thus, we use the characteristics of the *conditional value at risk* (CVaR) to convert the original model into another model called the *second-order cone programming model* (SOCPM) and utilize an outer approximation algorithm (OAA) to solve this SOCPM exactly.

Overall, the contributions of this chapter are as follows. (1) This chapter contributes to the current literature by addressing a distributionally robust joint chance-constrained model for solving the joint optimization of LFDP and SAP. To our knowledge, this is the first study to extend data-driven DRO theory to the joint optimization of two sub-problems in container liner shipping. (2) Based on the moment and covariance information of historical data, we transform the original distribution-free model into a standard SOCPM to make it computationally tractable by taking advantage of the properties of CVaR. (3) We design an OAA for the SOCPM that can be solved in a targeted manner to achieve an efficient and obtain the global optimal solution in a reasonable time.

5.2. Problem description

5.2.1. Liner shipping network

We consider that a liner company operates a liner shipping network that includes several pre-determined routes, and the set composed of them is denoted as $\mathcal{R}$. Each route calls several ports in sequence. We let $\mathcal{P}$ denote the set composed of ports of call and use r and p to represent the elements in $\mathcal{R}$ and $\mathcal{P}$, respectively. A route is usually a loop structure, which we can define on the basis of the calling sequence of the liner. For example, we can set:

$$p_r^1 \to p_r^2 \to p_r^3 \to \cdots \to p_r^{k_r} \to p_r^1$$

where $p_r^i \in \mathcal{P}$ represents the i^{th} port of call on route $r \in \mathcal{R}$ and k_r is the number of ports of call on route $r \in \mathcal{R}$. When a liner departs from a certain port (e.g., p_r^1), sails around the loop route and returns to this port, we say that the liner has completed a *voyage*. The part of the route from port p_r^i to port p_r^{i+1} is also called *leg i* of route $r \in \mathcal{R}$. The set composed of legs on route *r* is denoted as $\mathcal{L}_r$.

Fig. 5.1 shows the shape of a route in the real world. The liner company first selects 5 ports (i.e., Port 1 to Port 4 and Port 6) from 6 candidate ports to form a route. One thing worth noting is that some ports may be called more than once in a route (e.g., port 2 in Fig. 5.1), which are usually called *butterfly nodes*. This is a significant difference between container liner shipping and land transportation, such as bus transportation. In view of this, further distinctions between different parts of a route are usually made. Typically, a portion of a route is called a forward sub-route and backward sub-route. For example, Chinese liner companies usually split their routes according to sailing from China to foreign countries and returning from foreign countries to China. The routes operated in the real world are very similar to those in Fig. 5.1.

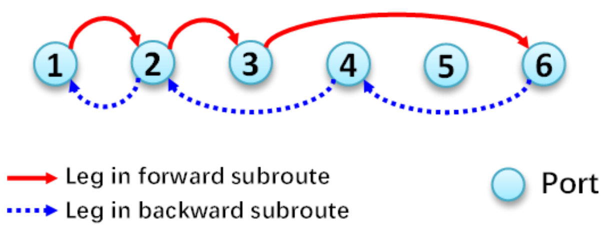

Fig. 5.1 A toy shipping route containing 6 ports

To facilitate readers' understanding, we obtain Fig. 5.2 from the official website of the Orient Overseas Container Line (OOCL; see https://www.oocl.com for details). The sub-route formed by the blue arrow is a forward sub-route, and the sub-route formed by the yellow arrow is a backward sub-route. It takes 77 days for a liner to complete a voyage. For each port, the liner company guarantees a liner call every week.

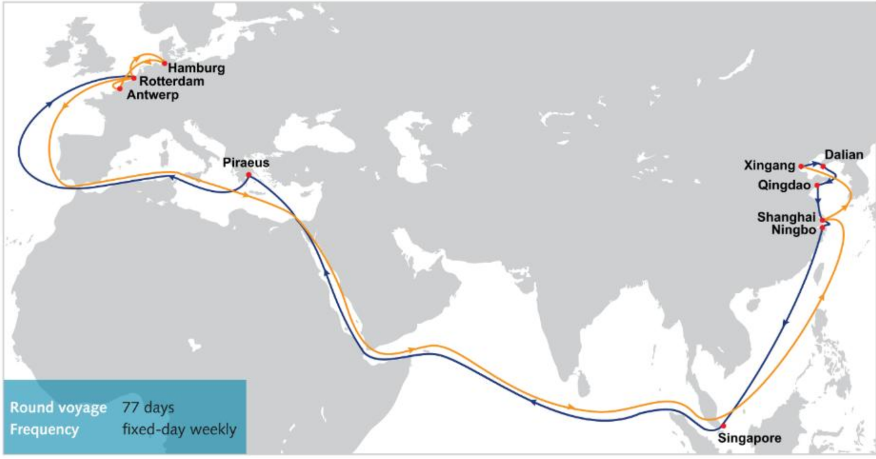

Fig. 5.2 A real-world route operating by OOCL

5.2.2. Definition of container transportation demand uncertainty

We use $\mathcal{W} = \{(o,d) | o,d \in \mathcal{P}\}$ to represent the set of origin-destination (O-D) pairs of transportation demand whose elements are denoted by $w = (o,d)$. In practice, transportation demand is generated by two types of shippers (Liang et al., 2023; Wang et al., 2020). One type of shipper is called a *contract shipper*. He/she typically has regular and substantial transportation demands. Therefore, liner companies often aim to secure the transportation demands of these shippers (referred to as 'contract demand' therein), as they can generate stable income (Liang et al., 2023). We consider that the contract demand is often generated on a weekly basis, so we let random variable ϑ_w be the weekly contract demand expressed in twenty-foot equivalent units (TEUs) between O-D pair w, i.e., the number of containers generated by the contract shippers to transport between O-D pair w each week.

Another type of shipper is called a *spot shipper*. The transportation demands of such shippers (known as 'spot demand' therein) are usually urgent, and they have no right to bargain with liner companies. Therefore, liner companies usually make order acceptance–rejection decisions on the basis of slot utilization, without the need to guarantee that the transportation demands of each shipper are met. To account for this type of transportation demand, we use a random variable θ_w to represent the total transportation demand (including both contract demand and spot demand) for O-D pair w during the planning period. Note that in this chapter, we need to collect only historical information on the total transportation demand θ_w during the entire planning period instead of the weekly spot demand. This is because we do not impose constraints on weekly spot demand.

5.2.3. Definition of container transportation paths

In the daily operation of a liner company, it needs to choose a container transportation path for container delivery on the O-D pair w. We use set $\mathcal{H}^w$ to represent the set of container transportation paths between the O-D pair w. In other words, for each O-D pair, there are several corresponding transportation paths. Here, one container transportation path can be part of a route or a combination of several parts of multiple routes. Fig. 5.3 illustrates this definition in detail. To transport one container from Port 2 to Port 4 in Fig. 5.3, the liner company can choose from two transportation paths:

$$h_1^{\text{Port 2–Port 4}} = p_3^1\left(\text{Port 2}\right) \xrightarrow{\text{Ship route 3}} p_3^2\left(\text{Port 4}\right) \text{, and}$$

$$h_2^{\text{Port 2–Port 4}} = p_1^1\left(\text{Port 2}\right) \xrightarrow{\text{Ship route 1}} p_1^2\left(\text{Port 3}\right) \mapsto p_2^2\left(\text{Port 3}\right) \xrightarrow{\text{Ship route 2}} p_2^3\left(\text{Port 4}\right).$$

If the liner company chooses the first transportation path $h_1^{\text{Port 2–Port 4}}$, this container will be loaded on a liner at port 2 and will be unloaded after the liner sails to port 4. In contrast, when the liner company selects $h_2^{\text{Port 2–Port 4}}$, this container is loaded at port 2 onto a liner deployed on route 1 and unloaded at port 3, and later, this container is reloaded (also referred to as *transshipped*) at port 3 onto a liner deployed on route 3 and finally unloaded at port 4. We can observe that the container handling costs incurred in transporting this container are different when the liner company chooses different paths due to the presence of container transshipment. In this chapter, we use c_{h^w} to denote the handling cost ($/TEU) incurred for transporting one container on path $h^w \in \mathcal{H}^w$.

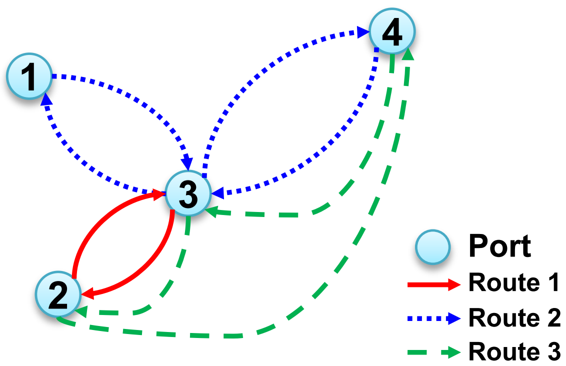

Fig. 5.3 A toy liner shipping network with 4 ports and 3 routes

5.2.4. LFDP and SAP

In our joint optimization problem, one of the decisions that the liner company needs to make is liner fleet deployment (to solve the LFDP). We let $\mathcal{S}$ be the set of liner classes and let CAP_s represent the capacity of an s-class liner (in terms of TEUs). The liner company must make decisions regarding the class and number of liners to deploy to each route, but not all liners it own need to be used. In practice, the liner company may use either its own liners or charters in liners on the charter market. Meanwhile, the liner company also has the option of charting out liners to other companies. The charter market usually offers chartering options, including time charters, voyage charters and bareboat charters. The last type of charter is the simplest. The reason is that in this type of charter, the charterer is responsible for the full management of the liner, bearing all associated costs (with the exception of capital costs, taxes, and depreciation). Consequently, the shipowner is relieved of any financial obligation and is solely responsible for collecting the agreed-upon rent. For the sake of simplicity, we assume that the liner company is only able to charter liners through a bareboat charter. The number of class $s \in \mathcal{S}$ liners chartered in and out are denoted as n_s^{IN} and n_s^{OUT}, respectively. The charter rate (including maintenance costs and insurance) for a liner of class $s \in \mathcal{S}$ during the entire planning horizon is c_s^{IN} (\$). The income that can be earned from chartering out a class $s \in \mathcal{S}$ liner is c_s^{OUT} (\$). Because the charter rate also includes maintenance costs and insurance, we have $c_s^{\mathrm{OUT}} < c_s^{\mathrm{IN}}$. We let NO_s^{MAX} and NC_s^{MAX} represent the number of class $s \in \mathcal{S}$ liners owned by the liner company and available in the market, respectively. Given these candidate liners, the company can arrange the appropriate class (number) of liners on the appropriate route. Unlike tramp shipping, liner shipping needs to provide regular service (e.g., weekly service) to add consistency for customers and usually has fixed timetables (i.e., arrival/departure times at each port of call). Therefore, months before the actual journey begins, shippers can browse timetables and freight rates published by liner companies on the internet. Considering this operational characteristic, we assume that the liner company assigns the same class liners to one route and that different classes of liners can be deployed on different routes. Each route must maintain a calling frequency of at least once a week. The optimization objective of LFDP is to establish a liner deployment scheme that minimizes costs and is subject to certain constraints (e.g., service frequency constraints).

After completing the assignment of the fleet on each route, the slots (capacity) available per week for each route are known. At this time, the liner company must carefully split the container transportation demands between each O-D pair to each container transportation path to solve the SAP. We let q_{h^w} denote the proportion of containers transported on container transportation path $h^w \in \mathcal{H}^w$ to total demand between $w \in \mathcal{W}$. The optimization objective of the SAP is to create a container transportation scheme, say q_{h^w}, which assigns both ϑ_w and θ_w to each container transportation path. This scheme is able to satisfy the uncertain transportation demand ϑ_w with a pre-determined probability and maximize the expected profit of the liner company (associated with uncertain transportation demand θ_w) over the planning horizon.

Before concluding this section, we list the assumptions used in this chapter. (1) The liner company endeavors to meet the weekly container transportation demands of contract shippers. (2) We consider only bareboat chartering as one type of charter. (3) The queuing of liners for berthing at each port is not considered. (4) The relocation of empty containers and inland transportation are not considered; it is assumed that there are always sufficient empty containers for cargo. (5) For all O-D pairs, all corresponding container transportation paths can meet the time limit requirements of the cargo owner. Moreover, the notations frequently used in this chapter are listed below.

Sets	
$\mathcal{R}$	Set of routes, where $r \in \mathcal{R}$
$\mathcal{P}$	Set of ports of call, where $p \in \mathcal{P}$
$\mathcal{L}_r$	Set of legs on route $r \in \mathcal{R}$, where $l \in \mathcal{L}_r$
$\mathcal{S}$	Set of liner classes, where $s \in \mathcal{S}$
$\mathcal{W}$	Set of original-destination (O-D) pairs with container transportation demand, where $w = (o, d) \in \mathcal{W}$
$\mathcal{H}^w$	Set of container transportation paths associated with O-D pair $w \in \mathcal{W}$, whose elements are denoted as h^w
$\mathcal{F}$	The ambiguity set (also known as distributional set) used to describe the distribution function F
$\mathcal{G}$	The ambiguity set used to describe the distribution function G
$\mathbb{Z}_+$	Set of non-negative integers
Parameters	
T	The planning horizon (Unit: day) of the liner company
c_s^{OP}	The operating cost (Unit: 10^4 \$/day) of a class s liner
c_{sr}^{VOL}	The voyage cost (Unit: 10^4 \$/voyage) of a class s liner on route $r \in \mathcal{R}$
c_s^{IN}	The charter cost paid (Unit: 10^4 \$/day) for chartering in a class s liner
c_s^{OUT}	The revenue received (Unit: 10^4 \$/day) for chartering out a class s liner
NO_s^{MAX}	Number of class s liner company owned
NC_s^{MAX}	Number of class s liner in the market
t_{sr}	The voyage time (Unit: day) of a class s liner on route $r \in \mathcal{R}$
CAP_s	The capacity (Unit: 10^2 TEU) of a class s liner
$\delta_{h^w}^{lr}$	A binary parameter, which equals 1 if path $h^w \in \mathcal{H}^w$ contains leg $l \in \mathcal{L}_r$ in the shipping network, and 0 otherwise
r_w	The freight rate (Unit: 10^4 \$/TEU) for transporting one container between O-D pair $w \in \mathcal{W}$
c_{h^w}	The handling cost (Unit: 10^4 \$/TEU) incurred for transporting one container on path $h^w \in \mathcal{H}^w$
f_r^{MIN}	The minimum calling frequency required on route $r \in \mathcal{R}$ (Unit: times/week)

Random variables	
θ_w	Random container transportation demand (Unit: 10^2 TEU) from both contract shippers and spot shippers of the planning horizon between O-D pair $w \in \mathcal{W}$, where $\boldsymbol{\theta} = (\theta_w)$
ϑ_w	Random container transportation demand (Unit: 10^2 TEU) from contract shippers of each week between O-D pair $w \in \mathcal{W}$, where $\boldsymbol{\vartheta} = (\vartheta_w)$
Decision variables	
n_{sr}^{TOTAL}	Number of class $s \in \mathcal{S}$ liners deployed on route $r \in \mathcal{R}$
n_s^{IN}	Number of class $s \in \mathcal{S}$ liners chartered in
n_s^{OUT}	Number of class $s \in \mathcal{S}$ liners chartered out
n_{sr}^{VOL}	Number of voyages completed by class $s \in \mathcal{S}$ liner deployed on route $r \in \mathcal{R}$
f_r^{call}	The service frequency on route $r \in \mathcal{R}$ (Unit: times/week)
$\mathbf{n}$	A vector representing the decision variables involved in the first stage model, where $\mathbf{n} = \left(x_{sr}, n_{sr}^{\text{TOTAL}}, n_s^{\text{IN}}, n_s^{\text{OUT}}, n_{sr}^{\text{VOL}}, f_r^{\text{call}}\right)^{\text{T}}$
x_{sr}	A binary variable, which equals 1 if class $s \in \mathcal{S}$ liner is deployed on route $r \in \mathcal{R}$, and 0 otherwise
q_{h^w}	The proportion of total transportation demand between O-D pair w transported on path $h^w \in \mathcal{H}^w$

5.3. Model establishment

Our original model **P** is a two-stage distributionally robust optimization model (2-DRO). In model **P**, each stage involves one type of decision. In other words, two types of decisions are made in a sequential fashion. In the first-stage (also referred to *here-and-now* stage), a decision related to liner fleet deployment, i.e., $\mathbf{n} = \left(x_{sr}, f_r^{\text{call}}, n_{sr}^{\text{TOTAL}}, n_s^{\text{IN}}, n_s^{\text{OUT}}, n_{sr}^{\text{VOL}}\right)^{\text{T}}$, is made before the uncertainty $\boldsymbol{\theta}$, an $|\mathcal{W}|$-dimensional random vector, is realized. After $\boldsymbol{\theta}$ realizes as a fixed value, the decision maker moves to the second-stage (also referred to as the *wait-and-see* stage) and determines q_{h^w} (related to slot allocation) by solving an optimization problem. In the following, we denote the second-stage cost by the function $g(\mathbf{n}, \boldsymbol{\theta})$.

First-stage of P:

$$\max obj = \left\{ \begin{aligned} & -T\sum_{r\in\mathcal{R}}\sum_{s\in\mathcal{S}} c_s^{\text{OP}} n_{sr}^{\text{Total}} - \sum_{r\in\mathcal{R}}\sum_{s\in\mathcal{S}} c_{sr}^{\text{VOL}} n_{sr}^{\text{VOL}} - T\sum_{s\in\mathcal{S}} c_s^{\text{IN}} n_s^{\text{IN}} \\ & +T\sum_{s\in\mathcal{S}} c_s^{\text{OUT}} n_s^{\text{OUT}} + \inf_{F\in\mathcal{F},G\in\mathcal{G}} \mathbb{E}_{F,G}\left[g\left(\mathbf{n},\boldsymbol{\theta}\right)\right] \end{aligned} \right\} \tag{5.1}$$

$$s.t. \quad \sum_{s\in\mathcal{S}} x_{sr} = 1 \qquad \forall r\in\mathcal{R} \tag{5.2}$$

$$n_{sr}^{\text{TOTAL}} \le \left(NO_s^{\text{MAX}} + NC_s^{\text{MAX}}\right) x_{sr} \qquad \forall s\in\mathcal{S}, r\in\mathcal{R} \tag{5.3}$$

$$n_s^{\text{IN}} \le NC_s^{\text{MAX}} \qquad \forall s\in\mathcal{S} \tag{5.4}$$

$$\sum_{r\in\mathcal{R}} n_{sr}^{\text{TOTAL}} = NO_s^{\text{MAX}} + n_s^{\text{IN}} - n_s^{\text{OUT}} \qquad \forall s\in\mathcal{S} \tag{5.5}$$

$$n_{sr}^{\text{VOL}} \le n_{sr}^{\text{TOTAL}} \times \left\lfloor \frac{T}{t_{sr}} \right\rfloor \qquad \forall s\in\mathcal{S}, r\in\mathcal{R} \tag{5.6}$$

$$f_r^{\text{call}} = \sum_{s\in\mathcal{S}} n_{sr}^{\text{VOL}} \Big/ \left\lceil \frac{T}{7} \right\rceil \qquad \forall r\in\mathcal{R} \tag{5.7}$$

$$f_r^{\text{call}} \ge f_r^{\text{MIN}} \qquad \forall r\in\mathcal{R} \tag{5.8}$$

$$f_r^{\text{call}} \in \mathbb{Z}_+ \qquad \forall r\in\mathcal{R} \tag{5.9}$$

$$n_s^{\text{IN}}, n_s^{\text{OUT}} \in \mathbb{Z}_+ \qquad \forall s\in\mathcal{S} \tag{5.10}$$

$$n_{sr}^{\text{TOTAL}}, n_{sr}^{\text{VOL}} \in \mathbb{Z}_+ \qquad \forall s\in\mathcal{S}, r\in\mathcal{R} \tag{5.11}$$

$$x_{sr} \in \{0,1\} \qquad \forall s\in\mathcal{S}, r\in\mathcal{R} \tag{5.12}$$

where vector $\mathbf{n} = \left(x_{sr}, f_r^{\text{call}}, n_{sr}^{\text{TOTAL}}, n_s^{\text{IN}}, n_s^{\text{OUT}}, n_{sr}^{\text{VOL}}\right)^{\text{T}}$ contains all the decision variables associated with the liner deployment scheme; $\mathbb{Z}_+$ denotes the set of non-negative integers; $\lfloor a \rfloor$ represents the maximum integer not greater than a; and $\lceil a \rceil$ is the minimum integer greater than or equal to a.

Objective function (5.1) calculates the net profit of the liner company during the planning period, which is obtained by subtracting its revenue from its cost. Here, $\sup_{F\in\mathcal{F},G\in\mathcal{G}} \mathbb{E}_{F,G}\left[g\left(\mathbf{n},\boldsymbol{\theta}\right)\right]$ is the worst-case expected wait-and-see cost.

Constraint (5.2) requires that one class of liners can be deployed on each route. Constraint (5.3) gives the relationship between decision variables n_{sr}^{TOTAL} and x_{sr}. This constraint requires that the number of liners deployed cannot exceed the sum of the number of company-owned liners and the number of liners available in the market. Constraint (5.4) requires that the number of liner ships chartered by the company in the market cannot exceed the prescribed upper limit. Constraint (5.5) gives the relationship between n_{sr}^{TOTAL}, n_{s}^{IN} and n_{s}^{OUT}. Constraint (5.6) imposes that the number of voyages completed by s class liners on route r cannot exceed the maximum number of voyages they can complete. Constraint (5.7) gives the relationship between the number of completed voyages and the calling frequency for each route. Constraint (5.8) imposes that the actual calling frequency of each route meets the established frequency lower limit. Constraints (5.9) to (5.11) are integer constraints on the decision variables. Finally, Constraint (5.12) requires x_{sr} is a binary decision variable.

Given a first-stage decision, i.e., $\mathbf{n}=\left(x_{sr}, f_r^{\text{call}}, n_{sr}^{\text{TOTAL}}, n_s^{\text{IN}}, n_s^{\text{OUT}}, n_{sr}^{\text{VOL}}\right)^{\text{T}}$, and realization of $\boldsymbol{\theta}$, the second-stage cost function $g(\mathbf{n},\boldsymbol{\theta})$ can be established as:

Second-stage of P:

$$g(\mathbf{n},\boldsymbol{\theta}) = \max \sum_{w\in\mathcal{W}} \theta_w \sum_{h^w\in\mathcal{H}^w} \left(r_w - c_{h^w}\right) q_{h^w} \tag{5.13}$$

$$s.t. \quad \sum_{h^w\in\mathcal{H}^w} q_{h^w} = 1 \qquad \forall w\in\mathcal{W} \tag{5.14}$$

$$\mathbb{P}_G\left(\begin{array}{l}\sum_{s\in\mathcal{S}} n_{sr}^{\text{VOL}} CAP_s \Big/ \left\lceil \dfrac{T}{7} \right\rceil \geq \\ \sum_{w\in\mathcal{W}} \vartheta_w \sum_{h^w\in\mathcal{H}^w} q_{h^w}\delta_{h^w}^{lr}, \forall l\in\mathcal{L}_r, r\in\mathcal{R}\end{array}\right) \geq \alpha \qquad \forall G\in\mathcal{G} \tag{5.15}$$

$$q_{h^w} \geq 0 \qquad \forall h^w\in\mathcal{H}^w, w\in\mathcal{W}. \tag{5.16}$$

Function (5.13) calculates the *profit* earned by the liner company from transporting containers during the planning period. Constraint (5.14) requires that for all O-D pairs, all container transportation demands generated (both contract demand and spot demand) need to be allocated to each transportation route every week. Constraint (5.15) is a joint chance constraint. This constraint means that the liner company's deployed capacity (i.e., slots) on all legs can meet the weekly contract demand is the probability not less than α, where α represents the service level set by the liner company. Constraint (5.16) is a non-negative constraint on q_{h^w}.

5.4. Model reformation

5.4.1. Objective function reformulation

Function (5.13) indicates that the objective function obj is linear in vector $\boldsymbol{\theta}$ and that the optimal solution of the second-stage model is influenced solely by vector $\boldsymbol{\theta}$ and two parameters (i.e., freight rate r_w and container handling cost c_{h^w}) when the vector $\mathbf{n}$ is known. Therefore, $\mathbb{E}_{F,G}\left[g\left(\mathbf{n},\boldsymbol{\theta}\right)\right]$ is determined only by the random vector $\boldsymbol{\theta}$. To describe the distribution function F of $\boldsymbol{\theta}$, we use the first moment information to establish the ambiguity set $\mathcal{F}$. In this chapter, we construct $\mathcal{F}$ based on an ellipsoid set with estimated mean-covariance information (i.e., $\boldsymbol{\mu}$ and $\boldsymbol{\Sigma} \succeq 0$). Specifically, we set

$$\mathcal{F} := \left\{F : \left(\mathbb{E}_F\left[\boldsymbol{\theta}\right]-\boldsymbol{\mu}\right)^T \boldsymbol{\Sigma}^{-1}\left(\mathbb{E}_F\left[\boldsymbol{\theta}\right]-\boldsymbol{\mu}\right) \le \epsilon^2\right\} \tag{5.17}$$

where ϵ is a pre-determined positive parameter that can reflect the size of set

$\mathcal{F}$.

The observation of set $\mathcal{F}$ reveals that the value of parameter ϵ is crucial. Its determination requires an accurate estimation of the first moment of $\boldsymbol{\theta}$. To this end, we apply the data-driven approach proposed in Section 3 of Delage and Ye (2010), which allows for a reasonable estimation of ϵ based on several independent samples. We set the mean of the random vector $\boldsymbol{\theta}$ to be $\hat{\boldsymbol{\mu}}$, and the covariance matrix to be $\hat{\boldsymbol{\Sigma}}$, respectively, and the known M samples are denoted as $\left\{\boldsymbol{\theta}^i\right\}_{i=1}^{M}$. If there are two parameters, say $R \geq 0$ and $\beta > 0$, such that $\mathbb{P}\left\{\left(\boldsymbol{\theta}-\hat{\boldsymbol{\mu}}\right)^{\mathrm{T}} \hat{\boldsymbol{\Sigma}}^{-1}\left(\boldsymbol{\theta}-\hat{\boldsymbol{\mu}}\right) \leq R^2\right\} = 1$, then the following inequality holds with a probability greater than $1-\beta$:

$$\left(\boldsymbol{\mu}_0-\hat{\boldsymbol{\mu}}\right)^{T} \hat{\boldsymbol{\Sigma}}^{-1}\left(\boldsymbol{\mu}_0-\hat{\boldsymbol{\mu}}\right) \leq \eta(\beta) \tag{5.18}$$

where $\boldsymbol{\mu}_0 = 1/M\sum_{i=1}^{M}\boldsymbol{\theta}^i$, $\eta(\beta) = \left(R^2/M\right)\left[2+\sqrt{2\ln\left(1/\beta\right)}\right]^2$.

When the above sample information is known, we use the following **Proposition 5.1** to reformulate the two-stage model **P**.

Proposition 5.1. Model **P** can be reformulated as:

$$\max obj_1' = \left\{\begin{array}{l} -T\sum_{r\in\mathcal{R}}\sum_{s\in\mathcal{S}} c_s^{\mathrm{OP}} n_{sr}^{\mathrm{Total}} - \sum_{r\in\mathcal{R}}\sum_{s\in\mathcal{S}} c_{sr}^{\mathrm{VOL}} n_{sr}^{\mathrm{VOL}} - T\sum_{s\in\mathcal{S}} c_s^{\mathrm{IN}} n_s^{\mathrm{IN}} \\ +T\sum_{s\in\mathcal{S}} c_s^{\mathrm{OUT}} n_s^{\mathrm{OUT}} + \boldsymbol{\mu}^{\mathrm{T}}\mathbf{q} - \epsilon\sqrt{\mathbf{q}^{\mathrm{T}}\boldsymbol{\Sigma}\mathbf{q}} \end{array}\right\} \tag{5.19}$$

s.t. (5.2), (5.3), (5.4), (5.5), (5.6), (5.7), (5.8), (5.9), (5.10), (5.11), (5.12), (5.14), (5.15), (5.16),

$$q_w = \sum_{h^w \in \mathcal{H}^w} \left(r_w - c_{h^w}\right) q_{h^w} \qquad \forall w \in \mathcal{W} \tag{5.20}$$

$$q_w \geq 0 \qquad \forall w \in \mathcal{W} \tag{5.21}$$

where $\|\bullet\|_n$ denotes the n-norm and $\mathbf{q} = \left(q_w\right)$ is a non-negative auxiliary vector.

Proof. To begin with, we reformulate the sup part of (5.1). As the random vector $\boldsymbol{\vartheta}=(\vartheta_w)$ does not affect the objective function (5.1), we omit the subscript G, which denotes the distribution function of $\boldsymbol{\vartheta}$ for clarity. Moreover, we introduce an auxiliary variable, i.e., $q_w=\sum_{h^w\in\mathcal{H}^w}\left(r_w-c_{h^w}\right)q_{h^w}$. With this simplification, we have

$$g(\mathbf{n},\boldsymbol{\theta})=\max\sum_{w\in\mathcal{W}}\theta_w\sum_{h^w\in\mathcal{H}^w}\left(r_w-c_{h^w}\right)q_{h^w}=\max\mathbf{q}^{\mathrm{T}}\boldsymbol{\theta},$$

and we can reformulate $\mathbb{E}_F\left[g(\mathbf{n},\boldsymbol{\theta})\right]$ in objective function (5.1) as

$$\mathbb{E}_F\left[g(\mathbf{n},\boldsymbol{\theta})\right]=\left(\mathbf{q}^*\right)^{\mathrm{T}}\mathbb{E}_F(\boldsymbol{\theta})=\max_{\mathbf{q}\in\Omega(\mathbf{n})}\mathbf{q}^{\mathrm{T}}\mathbb{E}_F(\boldsymbol{\theta})\tag{5.22}$$

where set $\Omega(\mathbf{n})$ denotes the feasible region of the second-stage model, and vector $\mathbf{q}^*$ represents an optimal solution of the second-stage model. From the minimax inequality, we have

$$\begin{aligned}\inf_{F\in\mathcal{F}}\mathbb{E}_F\left[g(\mathbf{n},\mathbf{q})\right]&=\inf_{F\in\mathcal{F}}\max_{\mathbf{q}\in\Omega(\mathbf{n})}\mathbf{q}^{\mathrm{T}}\mathbb{E}_F(\boldsymbol{\theta})\\&=\min_{\mathbb{E}_F(\boldsymbol{\theta})\in\Pi}\max_{\mathbf{q}\in\Omega(\mathbf{n})}\mathbf{q}^{\mathrm{T}}\mathbb{E}_F(\boldsymbol{\theta})\\&\geq\max_{\mathbf{q}\in\Omega(\mathbf{n})}\min_{\mathbb{E}_F(\boldsymbol{\theta})\in\Pi}\mathbf{q}^{\mathrm{T}}\mathbb{E}_F(\boldsymbol{\theta})\end{aligned}$$

where $\Pi=\left\{\boldsymbol{\chi}:(\boldsymbol{\chi}-\boldsymbol{\mu})^T\boldsymbol{\Sigma}^{-1}(\boldsymbol{\chi}-\boldsymbol{\mu})\leq\epsilon^2\right\}$. At the same time, we can obtain

$$\min_{\mathbb{E}_F(\boldsymbol{\theta})\in\Pi}\max_{\mathbf{q}\in\Omega(\mathbf{n})}\mathbf{q}^{\mathrm{T}}\mathbb{E}_F(\boldsymbol{\theta})=\min_{\mathbb{E}_F(\boldsymbol{\theta})\in\Pi}\left(\mathbf{q}^*\right)^{\mathrm{T}}\mathbb{E}_F(\boldsymbol{\theta})\leq\max_{\mathbf{q}\in\Omega(\mathbf{n})}\min_{\mathbb{E}_F(\boldsymbol{\theta})\in\Pi}\mathbf{q}^{\mathrm{T}}\mathbb{E}_F(\boldsymbol{\theta}).$$

The first equality holds because $\mathbf{q}^*$ is an optimal solution. Meanwhile, since $\mathbf{q}^*\in\Omega(\mathbf{n})$, the second inequality is straightforward. Considering the mean-covariance information of the random vector $\boldsymbol{\theta}$ as well as the ambiguity set $\mathcal{F}$ defined as (5.17), we can conclude that

$$\min_{\mathbb{E}_F[\boldsymbol{\theta}]:(\mathbb{E}_F[\boldsymbol{\theta}]-\boldsymbol{\mu})^T\boldsymbol{\Sigma}^{-1}(\mathbb{E}_F[\boldsymbol{\theta}]-\boldsymbol{\mu})\leq\epsilon^2}\mathbf{q}^{\mathrm{T}}\mathbb{E}_F(\boldsymbol{\theta})=\boldsymbol{\mu}^{\mathrm{T}}\mathbf{q}-\epsilon\sqrt{\mathbf{q}^{\mathrm{T}}\boldsymbol{\Sigma}\mathbf{q}}.$$

At this time, objective function (5.1) can be reformulated as:

$$\max obj_1' = \left\{ \begin{array}{l} -T\sum_{r\in\mathcal{R}}\sum_{s\in\mathcal{S}} c_s^{\mathrm{OP}} n_{sr}^{\mathrm{Total}} - \sum_{r\in\mathcal{R}}\sum_{s\in\mathcal{S}} c_{sr}^{\mathrm{VOL}} n_{sr}^{\mathrm{VOL}} - T\sum_{s\in\mathcal{S}} c_s^{\mathrm{IN}} n_s^{\mathrm{IN}} \\ +T\sum_{s\in\mathcal{S}} c_s^{\mathrm{OUT}} n_s^{\mathrm{OUT}} + \boldsymbol{\mu}^{\mathrm{T}}\mathbf{q} - \epsilon\sqrt{\mathbf{q}^{\mathrm{T}}\boldsymbol{\Sigma}\mathbf{q}} \end{array} \right\}. \tag{5.23}$$

Therefore, we prove **Proposition 5.1** by introducing the vector $\mathbf{q}$. (Q.E.D.)

5.4.2. Constraints reformulation

The general idea of dealing with a joint chance constraint is to first decompose it into several individual chance constraints (ICCs). We follow the same idea as above in this section. To characterize the distribution function G of random vector $\boldsymbol{\vartheta}$, we first construct the ambiguity set $\mathcal{G}$, which contains the possible distributions of $\boldsymbol{\vartheta}$, on the basis of the estimated mean $\mathbf{u}$ and covariance matrix $\boldsymbol{\Gamma}$ of $\boldsymbol{\vartheta}$. To avoid excessive conservatism, an ellipsoidal set is used. The specific expression of $\mathcal{G}$ is provided below:

$$\mathcal{G} := \left\{ \begin{array}{c} G : (\boldsymbol{\vartheta}-\mathbf{u})^{\mathrm{T}} \boldsymbol{\Gamma}^{-1} (\boldsymbol{\vartheta}-\mathbf{u}) \le \tilde{\epsilon}^2 \\ \mathbb{E}_G[\boldsymbol{\vartheta}] = \mathbf{u} \\ \mathbb{E}_G\left[\boldsymbol{\vartheta}^2\right] = \mathbf{u}^{\mathrm{T}}\mathbf{u} + \boldsymbol{\Gamma} \end{array} \right\} \tag{5.24}$$

where the pre-determined parameter $\tilde{\epsilon} > 0$ is used to control the size of the ambiguity set $\mathcal{G}$.

First, based on $\mathcal{G}$, we decompose the joint chance constraints to obtain several ICCs and perform conic transformation. For convenience of subsequent description, we set $v(\tilde{\mathbf{q}}_{lr}, \tilde{x}_r) = \sum_{w\in\mathcal{W}} \vartheta_w \sum_{h^w\in\mathcal{H}^w} q_{h^w}\delta_{h^w}^{lr} - \sum_{s\in\mathcal{S}} n_{sr}^{\mathrm{VOL}} CAP_s \Big/ \left\lceil \frac{T}{7} \right\rceil = \boldsymbol{\vartheta}^{\mathrm{T}}\tilde{\mathbf{q}}_{lr}$ $-\tilde{n}_r$, where $\tilde{n}_r = \sum_{s\in\mathcal{S}} n_{sr}^{\mathrm{VOL}} CAP_s \Big/ \left\lceil \frac{T}{7} \right\rceil$ and $\tilde{\mathbf{q}}_{lr} = \left(q_{h^w}\delta_{h^w}^{lr}\right)$. The conic reformulation for the ICC is inextricably linked to the upper bound of

$\mathbb{E}\left[v\left(\tilde{\mathbf{q}}_{lr},\tilde{n}_r\right)^{+}\right]$, where $(\bullet)^{+}:=\max\{\bullet,0\}$. Therefore, we present the expression of the above upper bound in **Lemma 5.1** and then prove the sub-additive property associated with this bound in **Lemma 5.2**.

Lemma 5.1. Let $\mathbf{u}$ and $\mathbf{\Gamma}$ denote the mean and covariance matrix of vector $\boldsymbol{\vartheta}$, respectively. An upper bound of $\mathbb{E}\left[v\left(\tilde{\mathbf{q}}_{lr},\tilde{n}_r\right)^{+}\right]$ can be written as the following function $\pi\left(\tilde{\mathbf{q}}_{lr},\tilde{n}_r\right)=\frac{1}{2}\left(\tilde{\mathbf{q}}_{lr}^{\mathrm{T}}\mathbf{u}-\tilde{n}_r\right)+\frac{1}{2}\sqrt{\left(\tilde{\mathbf{q}}_{lr}^{\mathrm{T}}\mathbf{u}-\tilde{n}_r\right)^2+\tilde{\mathbf{q}}_{lr}^{\mathrm{T}}\mathbf{\Gamma}\tilde{\mathbf{q}}_{lr}}$.

Proof. Given that $a^{+}=1/2\left(a+|a|\right)$, we obtain

$$\mathbb{E}\left[v\left(\tilde{\mathbf{q}}_{lr},\tilde{n}_r\right)^{+}\right]=\frac{1}{2}\mathbb{E}\left[v\left(\tilde{\mathbf{q}}_{lr},\tilde{n}_r\right)+\left|v\left(\tilde{\mathbf{q}}_{lr},\tilde{n}_r\right)\right|\right]. \tag{5.25}$$

Applying Jensen's inequality to the convex function $\Theta(x)=x^2$ yields

$$\begin{aligned}\left(\mathbb{E}\left[\left|v\left(\tilde{\mathbf{q}}_{lr},\tilde{n}_r\right)\right|\right]\right)^2 &\le \mathbb{E}\left[\left|v\left(\tilde{\mathbf{q}}_{lr},\tilde{n}_r\right)\right|^2\right]=\mathbb{E}\left[\left|\boldsymbol{\vartheta}^{\mathrm{T}}\tilde{\mathbf{q}}_{lr}-\tilde{n}_r\right|^2\right]\\ &=\mathbb{E}\left[\left(\boldsymbol{\vartheta}^{\mathrm{T}}\tilde{\mathbf{q}}_{lr}\right)^2+\tilde{n}_r^2-2\tilde{n}_r\boldsymbol{\vartheta}^{\mathrm{T}}\tilde{\mathbf{q}}_{lr}\right]\\ &=\mathbb{E}\left[\left(\boldsymbol{\vartheta}^{\mathrm{T}}\tilde{\mathbf{q}}_{lr}\right)^2\right]+\tilde{n}_r^2-2\tilde{n}_r\tilde{\mathbf{q}}_{lr}^{\mathrm{T}}\mathbb{E}\left[\boldsymbol{\vartheta}\right]\\ &=\left(\tilde{\mathbf{q}}_{lr}^{\mathrm{T}}\mathbf{u}\right)^2+\tilde{\mathbf{q}}_{lr}^{\mathrm{T}}\mathbf{\Gamma}\tilde{\mathbf{q}}_{lr}+\tilde{n}_r^2-2\tilde{n}_r^2\tilde{\mathbf{q}}_{lr}^{\mathrm{T}}\mathbf{u}\\ &=\left(\tilde{\mathbf{q}}_{lr}^{\mathrm{T}}\mathbf{u}-\tilde{n}_r\right)^2+\tilde{\mathbf{q}}_{lr}^{\mathrm{T}}\mathbf{\Gamma}\tilde{\mathbf{q}}_{lr}.\end{aligned} \tag{5.26}$$

Now, we have $\mathbb{E}\left[v\left(\tilde{\mathbf{q}}_{lr},\tilde{n}_r\right)^{+}\right]\le\frac{1}{2}\left(\tilde{\mathbf{q}}_{lr}^{\mathrm{T}}\mathbf{u}-\tilde{n}_r\right)+\frac{1}{2}\sqrt{\left(\tilde{\mathbf{q}}_{lr}^{\mathrm{T}}\mathbf{u}-\tilde{n}_r\right)^2+\tilde{\mathbf{q}}_{lr}^{\mathrm{T}}\mathbf{\Gamma}\tilde{\mathbf{q}}_{lr}}$. (Q.E.D.)

Lemma 5.2. $\pi\left(\tilde{\mathbf{q}}_{lr},\tilde{n}_r\right)$ is a sub-additive function. This means that for $\left(\tilde{\mathbf{q}}_{11},\tilde{n}_1\right)$ and $\left(\tilde{\mathbf{q}}_{22},\tilde{n}_2\right)$, we have $\pi\left(\tilde{\mathbf{q}}_{11},\tilde{n}_1\right)+\pi\left(\tilde{\mathbf{q}}_{22},\tilde{n}_2\right)\ge\pi\left(\tilde{\mathbf{q}}_{11}+\tilde{\mathbf{q}}_{22},\tilde{n}_1+\tilde{n}_2\right)$.

Proof. We set $A=\tilde{\mathbf{q}}^{\mathrm{T}}\mathbf{u}-\tilde{n}$, the matrix $\mathbf{B}=\left(A,\tilde{\mathbf{q}}\right)$, and the matrix $\mathbf{\Gamma}'=\begin{pmatrix}1 & \mathbf{0}\\ \mathbf{0} & \mathbf{\Gamma}\end{pmatrix}$. Then, we have $\sqrt{\left(\tilde{\mathbf{q}}^{\mathrm{T}}\mathbf{u}-\tilde{n}\right)^2+\tilde{\mathbf{q}}^{\mathrm{T}}\mathbf{\Gamma}\tilde{\mathbf{q}}}=\sqrt{A^2+\tilde{\mathbf{q}}^{\mathrm{T}}\mathbf{\Gamma}\tilde{\mathbf{q}}}=\sqrt{\mathbf{B}^{\mathrm{T}}\mathbf{\Gamma}'\mathbf{B}}$ $=\left\|\left(\mathbf{\Gamma}'\right)^{\frac{1}{2}}\mathbf{B}\right\|_1$. Therefore, function $\pi\left(\tilde{\mathbf{q}}_{lr},\tilde{n}_r\right)$ is sub-additive because the norm is a sub-additive function. (Q.E.D.)

Following **Lemma 5.1**, we can apply **Proposition 5.2** to perform a conic reformulation of the ICC decomposed by (5.15).

Proposition 5.2. The ICC

$$\mathbb{P}\left\{\sum_{s\in\mathcal{S}} n_{sr}^{\text{VOL}} CAP_s \Big/ \left\lceil \frac{T}{7} \right\rceil - \sum_{w\in\mathcal{W}} \vartheta_w \sum_{h^w\in\mathcal{H}^w} q_{h^w}\delta_{h^w}^{lr} \geq 0\right\} \geq 1-\alpha, \ \ \forall l\in\mathcal{L}_r, r\in\mathcal{R}, \quad (5.27)$$

can be conic transformed as

$$\tilde{\mathbf{q}}_{lr}^{\mathrm{T}}\mathbf{u} - \tilde{n}_r + \sqrt{\frac{(1-\varphi)\tilde{\mathbf{q}}_{lr}^{\mathrm{T}}\boldsymbol{\Gamma}\tilde{\mathbf{q}}_{lr}}{\varphi}} \leq 0, \ \ \forall l\in\mathcal{L}_r, r\in\mathcal{R}, \quad (5.28)$$

where $\varphi = 1-\alpha$.

Proof. We utilize the convex approximation method based on the CVaR measure to address the ICC to make it computationally tractable (Ben-Tal & Nemirovski, 1998; Ben-Tal & Teboulle, 1986). This approach was extended by Rockafellar and Uryasev (2000). The CVaR of $\boldsymbol{\vartheta}$ at a confidence level $1-\varphi$ is formulated as $\tau_{1-\varphi}(\boldsymbol{\vartheta}) := \min_{\partial\in\mathbb{R}}\left\{\partial + \frac{1}{\varphi}\mathbb{E}\left[(\boldsymbol{\vartheta}-\partial)^+\right]\right\}$. Moreover, it is well known that $\mathbb{P}\{y(\boldsymbol{\vartheta})\} \geq 1-\varphi$ can be convex tightest approximated by $\tau_{1-\varphi}\left[y(\boldsymbol{\vartheta})\right] \leq 0$, where $y(\boldsymbol{\vartheta})$ is affinely dependent on $\boldsymbol{\vartheta}$. Extending the above theory to our problem, the constraints specified in **Proposition 5.2** can be reformulated as:

$$\begin{aligned}&\min_{\partial\in\mathbb{R}}\left\{\partial + \frac{1}{\varphi}\mathbb{E}\left[\left(\sum_{w\in\mathcal{W}} \vartheta_w \sum_{h^w\in\mathcal{H}^w} q_{h^w}\delta_{h^w}^{lr} - \sum_{s\in\mathcal{S}} n_{sr}^{\text{VOL}} CAP_s \Big/ \left\lceil \frac{T}{7} \right\rceil - \partial\right)^+\right]\right\} \\ &= \min_{\partial\in\mathbb{R}}\left\{\partial + \frac{1}{\varphi}\mathbb{E}\left[\left(\boldsymbol{\vartheta}^{\mathrm{T}}\tilde{\mathbf{q}}_{lr} - \tilde{n}_r - \partial\right)^+\right]\right\} \leq 0.\end{aligned}$$

The closed-form solution $\mathbb{E}\left[\left(\boldsymbol{\vartheta}^{\mathrm{T}}\tilde{\mathbf{q}}_{lr} - \tilde{n}_r - \partial\right)^+\right]$ obtained remains computationally intractable. Therefore, we transform it further via **Lemma 5.1**. Applying the bound suggested in **Lemma 5.1**, we have

$$\begin{aligned}\tau_{1-\varepsilon}\left[v\left(\tilde{\mathbf{q}}_{lr},\tilde{n}_r\right)\right] &\le \min_{\partial}\left[\partial+\frac{1}{\varphi}\pi\left(\tilde{\mathbf{q}}_{lr}^{\mathrm{T}},\tilde{n}_r+\partial\right)\right]\\ &= \min_{\partial}\left[\partial+\frac{\tilde{\mathbf{q}}_{lr}^{\mathrm{T}}\mathbf{u}-\tilde{n}_r-\partial}{2\varphi}+\frac{\sqrt{\left(\tilde{\mathbf{q}}_{lr}^{\mathrm{T}}\mathbf{u}-\tilde{n}_r-\partial\right)^2+\tilde{\mathbf{q}}_{lr}^{\mathrm{T}}\mathbf{\Gamma}\tilde{\mathbf{q}}_{lr}}}{2\varphi}\right] \\ &= \tilde{\mathbf{q}}_{lr}^{\mathrm{T}}\mathbf{u}-\tilde{n}_r+\sqrt{\frac{(1-\varphi)\tilde{\mathbf{q}}_{lr}^{\mathrm{T}}\mathbf{\Gamma}\tilde{\mathbf{q}}_{lr}}{\varphi}}.\end{aligned} \tag{5.29}$$

Constraint (5.29) represents a valid conic transformation of Constraint (5.27) because the last equation is satisfied when $\partial=\partial^*=\frac{(1-2\varphi)}{2\sqrt{\varphi(1-\varphi)}}\sqrt{\tilde{\mathbf{q}}_{lr}^{\mathrm{T}}\mathbf{\Gamma}\tilde{\mathbf{q}}_{lr}}$. For clarity, hereafter, we use

$$\varrho_{1-\varphi}\left[v\left(\tilde{\mathbf{q}}_{lr},\tilde{n}_r\right)\right]=\min_{\partial}\left[\partial+\frac{1}{\varphi}\pi\left(\tilde{\mathbf{q}}_{lr}^{\mathrm{T}}\mathbf{u},\tilde{n}_r+\partial\right)\right]=\tilde{\mathbf{q}}_{lr}^{\mathrm{T}}\mathbf{u}-\tilde{n}_r+\sqrt{\frac{(1-\varphi)\tilde{\mathbf{q}}_{lr}^{\mathrm{T}}\mathbf{\Gamma}\tilde{\mathbf{q}}_{lr}}{\varphi}} \tag{5.30}$$

to denote an upper bound of $\tau_{1-\varepsilon}\left[v\left(\tilde{\mathbf{q}}_{lr},\tilde{n}_r\right)\right]$. (Q.E.D.)

Now, we extend the above method to obtain the conic transformation of (5.15). Note that (5.15) is equivalent to

$$\mathbb{P}\left(\bigcup_{l\in\mathcal{L}_r,r\in\mathcal{R}}\left(\sum_{s\in\mathcal{S}}n_{sr}^{\mathrm{VOL}}CAP_s\Big/\left\lceil\frac{T}{7}\right\rceil-\sum_{w\in\mathcal{W}}\vartheta_w\sum_{h^w\in\mathcal{H}^w}q_{h^w}\delta_{h^w}^{lr}>0\right)\right)\le\varphi \tag{5.31}$$

where $\varphi=1-\alpha$. Based on Galambos (1977), which proposed Bonferroni inequality, (5.31) can be further decomposed as

$$\begin{aligned}&\mathbb{P}\left\{\bigcup_{l\in\mathcal{L}_r,r\in\mathcal{R}}\left(\sum_{s\in\mathcal{S}}n_{sr}^{\mathrm{VOL}}CAP_s\Big/\left\lceil\frac{T}{7}\right\rceil-\sum_{w\in\mathcal{W}}\vartheta_w\sum_{h^w\in\mathcal{H}^w}q_{h^w}\delta_{h^w}^{lr}>0\right)\right\}\\ &\le\sum_{l\in\mathcal{L}_r}\sum_{r\in\mathcal{R}}\mathbb{P}\left(\sum_{s\in\mathcal{S}}n_{sr}^{\mathrm{VOL}}CAP_s\Big/\left\lceil\frac{T}{7}\right\rceil-\sum_{w\in\mathcal{W}}\vartheta_w\sum_{h^w\in\mathcal{H}^w}q_{h^w}\delta_{h^w}^{lr}>0\right)\le\varphi.\end{aligned}$$

Therefore, we obtain

$$\mathbb{P}\left(\sum_{s\in\mathcal{S}} n_{sr}^{\mathrm{VOL}} CAP_s \Big/ \left\lceil \frac{T}{7} \right\rceil - \sum_{w\in\mathcal{W}} \vartheta_w \sum_{h^w\in\mathcal{H}^w} q_{h^w}\delta_{h^w}^{lr} > 0 > 0\right) \le \varphi_{lr}, \forall l\in\mathcal{L}_r, r\in\mathcal{R}$$
$$\Rightarrow \mathbb{P}\left(\sum_{s\in\mathcal{S}} n_{sr}^{\mathrm{VOL}} CAP_s \Big/ \left\lceil \frac{T}{7} \right\rceil - \sum_{w\in\mathcal{W}} \vartheta_w \sum_{h^w\in\mathcal{H}^w} q_{h^w}\delta_{h^w}^{lr} > 0 \le 0\right) \ge 1-\varphi_{lr}, \forall l\in\mathcal{L}_r, r\in\mathcal{R} \tag{5.32}$$

where $\sum_{l\in\mathcal{L}_r}\sum_{r\in\mathcal{R}}\varphi_{lr} = \varphi$.

It is evident that the only differences between the chance constraints presented in (5.31) and (5.32) are found in φ_{lr} and φ. Therefore, if we use (5.32) directly to approximate (5.31), the challenge arises in identifying an adequately sized risk budget φ_{lr}. The techniques proposed in some papers suggests that we can set φ_{lr} to $\varphi/|\mathcal{L}|$ (where $|\mathcal{L}|$ denotes number of elements in set $\mathcal{L} := \bigcup_{r\in\mathcal{R}}\mathcal{L}_r$). Nevertheless, according to Zymler et al. (2013), this approach tends to yield overly conservative results.

To address this issue, we utilize the approach in Chen et al. (2010). This approach involves creating an optimization model with a set, say $\mathcal{D}$, and a vector (including a number of positive scaling parameters), say $\boldsymbol{\Upsilon}$, to reformulate (5.15). Here, we define set $\mathcal{D} := \left\{(l,r) \middle| l\in\mathcal{L}_r, r\in\mathcal{R}\right\}$, index set $\mathcal{Q}\subseteq\mathcal{D}$ and $\boldsymbol{\Upsilon} = (\Upsilon_{lr}) > \mathbf{0}$ $(\forall l\in\mathcal{L}_r, r\in\mathcal{R})$. Following Zymler et al. (2013), the inclusion of Υ_{lr} has no effect on the feasible region of (5.15), and furthermore, serves to enhance its approximation. In the following **Proposition 5.3**, we establish this optimization model.

Proposition 5.3. Assume that $\mathcal{J}$ is the smallest closed convex set containing the support of $\boldsymbol{\vartheta}$. The function $\psi(\mathbf{n}, \tilde{\mathbf{q}}, \boldsymbol{\Upsilon}, \mathcal{Q})$ is shown as

$$\psi\left(\mathbf{n},\tilde{\mathbf{q}},\Upsilon,\mathcal{Q}\right):=\min_{\mathbf{a}_{lr},b_r}\left\{\min_{\partial}\left[\partial+\frac{\pi\left(\mathbf{a}_{lr},b_r+\partial\right)}{\varphi}\right]+\frac{1}{\varphi}\left[\sum_{(l,r)\in\mathcal{Q}}\pi\left(\Upsilon_{lr}\tilde{\mathbf{q}}_{lr}-\mathbf{a}_{lr},\Upsilon_{lr}\tilde{n}_r-b_r\right)\right]\right\}.$$

If $\psi\left(\mathbf{n},\tilde{\mathbf{q}},\Upsilon,\mathcal{Q}\right)\le 0$ and $\max_{\vartheta\in\mathcal{J}}\left(\vartheta^{\mathrm{T}}\tilde{\mathbf{q}}_{lr}-\tilde{n}_r\right)\le 0$ $\left(\forall\left(l,r\right)\in\mathcal{D}\backslash\mathcal{Q}\right)$, then the joint chance constraint (5.15) holds.

Proof. Since the robust counterpart $\max_{\vartheta\in\mathcal{J}}\left(\vartheta^{\mathrm{T}}\tilde{\mathbf{q}}_{lr}-\tilde{n}_r\right)\le 0$ $\left(\forall\left(l,r\right)\in\mathcal{D}\backslash\mathcal{Q}\right)$ implies $\mathbb{P}\left(\vartheta^{\mathrm{T}}\tilde{\mathbf{q}}_{lr}-\tilde{n}_r>0\right)=0$ $\left(\forall\left(l,r\right)\in\mathcal{D}\backslash\mathcal{Q}\right)$ and with parameter $\Upsilon=\left(\Upsilon_{lr}\right)>0$, we have

$$\begin{aligned}\mathbb{P}\left(\vartheta^{\mathrm{T}}\tilde{\mathbf{q}}_{lr}-\tilde{n}_r\le 0,\forall\left(l,r\right)\in\mathcal{D}\right)&=\mathbb{P}\left(\vartheta^{\mathrm{T}}\tilde{\mathbf{q}}_{lr}-\tilde{n}_r\le 0,\forall\left(l,r\right)\in\mathcal{Q}\right)\\&=\mathbb{P}\left(\max_{(l,r)\in\mathcal{Q}}\left\{\Upsilon_{lr}\left[\vartheta^{\mathrm{T}}\tilde{\mathbf{q}}_{lr}-\tilde{n}_r\right]\right\}\le 0\right).\end{aligned}$$

In addition, in light of **Proposition 5.2**, it is evident that (5.28) represents the most precise convex approximation of the ICC. When $\left(\tilde{\mathbf{q}},\tilde{\mathbf{n}}\right)^{\mathrm{T}}$ is feasible, we can obtain $\tau_{1-\varphi}\left[\max_{(l,r)\in\mathcal{Q}}\left\{\Upsilon_{lr}\left[\vartheta^{\mathrm{T}}\tilde{\mathbf{q}}_{lr}-\tilde{n}_r\right]\right\}\right]\le 0$. In Meilijson and Nádas (1979), the authors proposed Equation (5.33). If we further define $K=\mathbf{a}_{lr}^{\mathrm{T}}\vartheta-b_r$, Equation (5.34) is obtained.

$$\mathbb{E}\left[\max_{i=1,\cdots,n}\left\{A_i\right\}-\iota\right]^{+}\le\mathbb{E}\left[K-\iota\right]^{+}+\sum_{i=1}^{n}\mathbb{E}\left[A_i-K\right]^{+},\ \text{for any r.v. } K \tag{5.33}$$

$$\begin{aligned}&\tau_{1-\varphi}\left[\max_{(l,r)\in\mathcal{Q}}\left[\Upsilon_{lr}\left(\vartheta^{\mathrm{T}}\tilde{\mathbf{q}}_{lr}-\tilde{n}_r\right)\right]\right]\\&=\min_{\partial}\left\{\partial+\frac{1}{\varphi}\mathbb{E}\left[\left(\max_{(l,r)\in\mathcal{Q}}\left[\Upsilon_{lr}\left(\vartheta^{\mathrm{T}}\tilde{\mathbf{q}}_{lr}-\tilde{n}_r\right)\right]-\partial\right)^{+}\right]\right\}\\&\le\min_{\partial,\mathbf{a}_{lr},b_r}\left\{\partial+\frac{1}{\varphi}\left[\mathbb{E}\left[\left(\mathbf{a}_{lr}^{\mathrm{T}}\vartheta-b_r-\partial\right)^{+}\right]+\sum_{(l,r)\in\mathcal{Q}}\mathbb{E}\left[\left(\left[\Upsilon_{lr}\tilde{\mathbf{q}}_{lr}-\mathbf{a}_{lr}\right]^{\mathrm{T}}\mathbf{q}-\Upsilon_{lr}\tilde{n}_r+b_r\right)^{+}\right]\right]\right\}\\&\le\min_{\partial,\mathbf{a}_{lr},b_r}\left\{\partial+\frac{1}{\varphi}\left[\pi\left(\mathbf{a}_{lr},b_r+\partial\right)+\sum_{(l,r)\in\mathcal{Q}}\pi\left(\Upsilon_{lr}\tilde{\mathbf{q}}_{lr}-\mathbf{a}_{lr},\Upsilon_{lr}\tilde{n}_r-b_r\right)\right]\right\}\\&=\min_{\mathbf{a}_{lr},b_r}\left\{\min_{\partial}\left[\partial+\frac{\pi\left(\mathbf{a}_{lr},b_r+\partial\right)}{\varphi}\right]+\frac{1}{\varphi}\left[\sum_{(l,r)\in\mathcal{Q}}\pi\left(\Upsilon_{lr}\tilde{\mathbf{q}}_{lr}-\mathbf{a}_{lr},\Upsilon_{lr}\tilde{n}_r-b_r\right)\right]\right\}\\&=\psi\left(\mathbf{n},\tilde{\mathbf{q}},\Upsilon,\mathcal{Q}\right)\le 0\end{aligned}\tag{5.34}$$

Therefore, if $\psi\left(\mathbf{n},\tilde{\mathbf{q}},\Upsilon,\mathcal{Q}\right)\leq 0$, then $\tau_{1-\varphi}\left[\max_{(l,r)\in\mathcal{Q}}\left\{\Upsilon_{lr}\left[\boldsymbol{\vartheta}^{\mathrm{T}}\tilde{\mathbf{q}}_{lr}-\tilde{n}_r\right]\right\}\right]\leq 0$.

(Q.E.D.)

Lemma 5.3. $\psi\left(\mathbf{n},\tilde{\mathbf{q}},\Upsilon,\mathcal{Q}\right)\leq 0$ dominates constraint (5.28).

Proof. We have

$$
\begin{aligned}
0 &\geq \min_{\partial,\mathbf{a}_{lr},b_r}\left\{\partial+\frac{1}{\varphi}\left[\pi\left(\mathbf{a}_{lr},b_r+\partial\right)+\sum_{(l,r)\in\mathcal{Q}}\pi\left(\Upsilon_{lr}\tilde{\mathbf{q}}_{lr}-\mathbf{a}_{lr},\Upsilon_{lr}\tilde{n}_r-b_r\right)\right]\right\}\\
&\geq \min_{\partial,\mathbf{a}_{lr},b_r}\left\{\partial+\frac{1}{\varphi}\left[\pi\left(\mathbf{a}_{lr},b_r+\partial\right)+\pi\left(\Upsilon_{lr}\tilde{\mathbf{q}}_{lr}-\mathbf{a}_{lr},\Upsilon_{lr}\tilde{n}_r-b_r\right)\right]\right\}\\
&\geq \min_{\partial}\left\{\partial+\frac{1}{\varphi}\left[\pi\left(\Upsilon_{lr}\tilde{\mathbf{q}}_{lr},\Upsilon_{lr}\tilde{n}_r+\partial\right)\right]\right\}\\
&\overset{\Upsilon_{lr}=1}{=} \min_{\partial}\left\{\partial+\frac{1}{\varphi}\left[\pi\left(\tilde{\mathbf{q}}_{lr},\tilde{n}_r+\partial\right)\right]\right\}\\
&= \tilde{\mathbf{q}}_{lr}^{\mathrm{T}}\mathbf{u}-\tilde{n}_r+\sqrt{\frac{(1-\varphi)\tilde{\mathbf{q}}_{lr}^{\mathrm{T}}\boldsymbol{\Gamma}\tilde{\mathbf{q}}_{lr}}{\varphi}}.
\end{aligned}
$$

According to **Proposition 5.3**, the first inequality holds, and the second inequality is a result of the fact that we select only one element from $\mathcal{Q}$. The third one is derived based on **Lemma 5.2** proposed in this section. Finally, the two equations at the end are a consequence of $\Upsilon_{lr}=1$ and Equation (5.29). (Q.E.D.)

Now, we introduce two auxiliary variables (i.e., t_0 and t_{lr}), and $\psi\left(\mathbf{n},\tilde{\mathbf{q}},\Upsilon,\mathcal{Q}\right)\leq 0$ is equivalent to $\exists b_r,t_0,t_{lr}\in\mathbb{R}$ such that constraints (5.35)–(5.37) hold.

$$t_0+\frac{1}{\varphi}\sum_{(l,r)\in\mathcal{Q}}t_{lr}\leq 0 \tag{5.35}$$

$$\varrho_{1-\varphi}\left[v\left(\mathbf{a}_{lr},b_r+\partial\right)\right]\leq t_0 \qquad \forall(l,r)\in\mathcal{Q} \tag{5.36}$$

$$\pi\left(\Upsilon_{lr}\tilde{\mathbf{q}}_{lr}-\mathbf{a}_{lr},\Upsilon_{lr}\tilde{n}_r-b_r\right)\leq t_{lr} \qquad \forall(l,r)\in\mathcal{Q} \tag{5.37}$$

The robust counterpart, i.e., $\max_{\boldsymbol{\vartheta}\in\mathcal{J}}\left(\boldsymbol{\vartheta}^{\mathrm{T}}\tilde{\mathbf{q}}_{lr}-\tilde{n}_r\right)\leq 0$ $\left(\forall(l,r)\in\mathcal{D}\setminus\mathcal{Q}\right)$, can be converted to Equation (5.38) according to **Theorem 3(c)** in Chen and Sim (2009).

$$\tilde{\mathbf{q}}_{lr}^{\mathrm{T}}\mathbf{u} - \tilde{n}_r + \tilde{\epsilon}\sqrt{\tilde{\mathbf{q}}_{lr}^{\mathrm{T}}\boldsymbol{\Gamma}\tilde{\mathbf{q}}_{lr}} \le 0 \qquad \forall (l,r) \in \mathcal{D} \backslash \mathcal{Q} \tag{5.38}$$

At this point, constraints (5.35)–(5.37) can dominate function $\psi(\mathbf{n}, \tilde{\mathbf{q}}, \Upsilon, \mathcal{Q}) \le 0$, and with Constraint (5.38), we can reformulate the original problem **P** in its deterministic equivalent form, i.e., **R-P**.

R-P:

$$\max obj_1' = \begin{Bmatrix} -T\sum_{r\in\mathcal{R}}\sum_{s\in\mathcal{S}} c_s^{\mathrm{OP}} n_{sr}^{\mathrm{Total}} - \sum_{r\in\mathcal{R}}\sum_{s\in\mathcal{S}} c_{sr}^{\mathrm{VOL}} n_{sr}^{\mathrm{VOL}} - T\sum_{s\in\mathcal{S}} c_s^{\mathrm{IN}} n_s^{\mathrm{IN}} \\ +T\sum_{s\in\mathcal{S}} c_s^{\mathrm{OUT}} n_s^{\mathrm{OUT}} + \boldsymbol{\mu}^{\mathrm{T}}\mathbf{q} - \epsilon\sqrt{\mathbf{q}^{\mathrm{T}}\boldsymbol{\Sigma}\mathbf{q}} \end{Bmatrix} \tag{5.39}$$

s.t. (5.2)–(5.12), (5.14), (5.16), (5.20), (5.21), (5.35)–(5.38).

where $\tilde{n}_r = \sum_{s\in\mathcal{S}} n_{sr}^{\mathrm{VOL}} CAP_s \Big/ \left\lceil \frac{T}{7} \right\rceil$.

Proposition 5.4. When $\tilde{\epsilon} \le \sqrt{(1-\varphi)/\varphi}$, Constraints (5.35)–(5.37) in **R-P** are redundant.

Proof. We realize the proof of this proposition by means of a counterfactual. To prove **Proposition 5.4**, we can equivalently prove that we can obtain an optimal solution of **R-P** with $\mathcal{Q} = \varnothing$ when $\tilde{\epsilon} \le \sqrt{(1-\varphi)/\varphi}$. Let us posit the existence of a counterexample. We assume that (l°, r°) enables the **R-P** to achieve an optimal solution with $(l^\circ, r^\circ) \in \mathcal{Q}$. Given that all elements within the set $\mathcal{Q}$ are required to satisfy $\psi(\mathbf{n}, \tilde{\mathbf{q}}, \Upsilon, \mathcal{Q}) \le 0$, it follows that there must be

$$\begin{aligned} &\tilde{\mathbf{q}}_{l^\circ r^\circ}^{\mathrm{T}}\mathbf{u} - \tilde{n}_{r^\circ} + \tilde{\epsilon}\sqrt{\tilde{\mathbf{q}}_{l^\circ r^\circ}^{\mathrm{T}}\boldsymbol{\Gamma}\tilde{\mathbf{q}}_{l^\circ r^\circ}} \\ &\le \tilde{\mathbf{q}}_{l^\circ r^\circ}^{\mathrm{T}}\mathbf{u} - \tilde{n}_{r^\circ} + \sqrt{(1-\varphi)\tilde{\mathbf{q}}_{l^\circ r^\circ}^{\mathrm{T}}\boldsymbol{\Gamma}\tilde{\mathbf{q}}_{l^\circ r^\circ}/\varphi}. \\ &\le \psi\left(\mathbf{n}, \tilde{\mathbf{q}}, \Upsilon, (l^\circ, r^\circ)\right) \le 0 \end{aligned}$$

We then note that, according to $\tilde{\epsilon} \le \sqrt{(1-\varphi)/\varphi}$, the first inequality holds. The second inequality is a consequence of the results presented in **Lemma 5.3**. The above series of inequalities shows that inequality $\tilde{\mathbf{q}}_{l^\circ r^\circ}^{\mathrm{T}} \mathbf{u} - \tilde{n}_{r^\circ} + \tilde{\epsilon}\sqrt{\tilde{\mathbf{q}}_{l^\circ r^\circ}^{\mathrm{T}} \boldsymbol{\Gamma} \tilde{\mathbf{q}}_{l^\circ r^\circ}} \le 0$ is less conservative than inequality $\psi\left(\mathbf{n}, \tilde{\mathbf{q}}, \boldsymbol{\Upsilon}, \left(l^\circ, r^\circ\right)\right) \le 0$. It can thus be concluded that when $\left(l^\circ, r^\circ\right) \in \mathcal{D} \setminus \mathcal{Q}$, a superior solution can be obtained in comparison to when $\left(l^\circ, r^\circ\right) \in \mathcal{Q}$. This is inconsistent with the assumption. (Q.E.D.)

Remark 5.1. It can be observed that the aforementioned proposition renders the **R-P** equivalent to a standard parametric SOCPM (Zhang & Li, 2015). Following **Proposition 5.4**, it is evident that the **R-P** is independent of $\mathcal{Q}$ and $\Upsilon_{lr} > 0 \quad \left(\forall (l,r) \in \mathcal{Q}\right)$ when $\tilde{\epsilon} \le \sqrt{(1-\varphi)/\varphi}$. Meanwhile, we introduce an auxiliary variable $\varpi \ge 0$ to eliminate the nonlinear term (i.e., $\epsilon\sqrt{\mathbf{q}^{\mathrm{T}}\boldsymbol{\Sigma}\mathbf{q}}$) in the objective function. Consequently, **R-P** can be subjected to a further conversion process to yield **R-P-1**. The OAA framework can then be employed.

R-P-1:

$$\max obj_1' = \begin{Bmatrix} -T\sum_{r\in\mathcal{R}}\sum_{s\in\mathcal{S}} c_s^{\mathrm{OP}} n_{sr}^{\mathrm{Total}} - \sum_{r\in\mathcal{R}}\sum_{s\in\mathcal{S}} c_{sr}^{\mathrm{VOL}} n_{sr}^{\mathrm{VOL}} - T\sum_{s\in\mathcal{S}} c_s^{\mathrm{IN}} n_s^{\mathrm{IN}} \\ +T\sum_{s\in\mathcal{S}} c_s^{\mathrm{OUT}} n_s^{\mathrm{OUT}} + \boldsymbol{\mu}^{\mathrm{T}}\mathbf{q} - \epsilon\varpi \end{Bmatrix} \tag{5.40}$$

$$s.t. \quad \tilde{\epsilon} \le \sqrt{(1-\varphi)/\varphi} \tag{5.41}$$

$$\left\|\boldsymbol{\Sigma}^{\frac{1}{2}}\mathbf{q}\right\| \le \varpi \tag{5.42}$$

$$\varpi \ge 0 \tag{5.43}$$

(5.2), (5.3), (5.4), (5.5), (5.6), (5.7), (5.8), (5.9), (5.10), (5.11), (5.12), (5.14), (5.16), (5.20), (5.21), (5.38).

5.5. Solution methodology

In this subsection, we present a customized algorithm to solve **P** via the OAA framework. The **R-P-1** model we reformulate at the end of Section 5.4 is a special type of MINLP. Bonami et al. (2008) demonstrated that OAA can be used to explore the global optimal solution when the problem can be formulated as a *convex MINLP model*. An MINLP is considered *convex* if the continuous relaxation of this model is convex (Shahabi et al., 2014). This reinforces the need to verify that our **R-P-1** model satisfies the stated requirements prior to implementing the OAA. This is necessary to ensure the global optimality of the solution. In the following **Proposition 5.5**, we provides the proof.

Proposition 5.5. Functions

$$F_1\left(\tilde{\mathbf{q}}_{lr}^{\mathrm{T}},\tilde{n}_r\right)=\tilde{\mathbf{q}}_{lr}^{\mathrm{T}}\mathbf{u}-\tilde{n}_r+\tilde{\epsilon}\sqrt{\tilde{\mathbf{q}}_{lr}^{\mathrm{T}}\boldsymbol{\Gamma}\tilde{\mathbf{q}}_{lr}}$$

$$F_2\left(\mathbf{q},\varpi\right)=\sqrt{\mathbf{q}^{\mathrm{T}}\boldsymbol{\Sigma}\mathbf{q}}-\varpi$$

are convex.

Proof. We know that the 1-norm is a convex function. In function $F_1\left(\tilde{\mathbf{q}}_{lr}^{\mathrm{T}},\tilde{n}_r\right)$, we have $F_1\left(\tilde{\mathbf{q}}_{lr}^{\mathrm{T}},\tilde{n}_r\right)=\tilde{\mathbf{q}}_{lr}^{\mathrm{T}}\mathbf{u}-\tilde{n}_r+\tilde{\epsilon}\sqrt{\tilde{\mathbf{q}}_{lr}^{\mathrm{T}}\boldsymbol{\Gamma}\tilde{\mathbf{q}}_{lr}}=\tilde{\mathbf{q}}_{lr}^{\mathrm{T}}\mathbf{u}-\tilde{n}_r+\tilde{\epsilon}\left\|\boldsymbol{\Gamma}^{\frac{1}{2}}\tilde{\mathbf{q}}_{lr}\right\|_1$. Moreover, in function $F_2\left(\mathbf{q},\varpi\right)$, we know that $\sqrt{\mathbf{q}^{\mathrm{T}}\boldsymbol{\Sigma}\mathbf{q}}=\left\|\boldsymbol{\Sigma}^{\frac{1}{2}}\mathbf{q}\right\|_1$. Thus, we can conclude that they are both convex functions. (Q.E.D.)

5.5.1. Algorithm initialization

We should first define a feasible $\left(\tilde{x}_{sr,0},\tilde{n}_{sr,0}^{\mathrm{Total}},\tilde{n}_{sr,0}^{\mathrm{VOL}},\tilde{n}_{s,0}^{\mathrm{IN}},\tilde{n}_{s,0}^{\mathrm{OUT}}\right)^{\mathrm{T}}$ to initialize our algorithm. To this end, it seems reasonable to posit that the liner company does not charter out liners, i.e., we set $\tilde{n}_{s,0}^{\mathrm{OUT}}=0$. The liner company deploys the liner with the highest capacity for each route, i.e., $\tilde{x}_{s^*r,0}=1$, $s^*=\{s\,|\max_{s\in\mathcal{S}} CAP_s\}$. On each route, the number of voyages completed by the liner is $\tilde{n}_{s^*r,0}^{\mathrm{VOL}}=\left\lceil \frac{T}{7}\right\rceil$ and $\tilde{n}_{s^*r,0}^{\mathrm{Total}}=\tilde{n}_{s^*r,0}^{\mathrm{VOL}}\Big/\left\lfloor \frac{T}{t_{sr}}\right\rfloor$. The liner company prioritizes the use of owned liners, and after all owned liners have been deployed, it begins to seek to charter liners in the market. Note that if the number of s^* class liners deployed in the shipping network exceeds $NO_{s^*}^{\mathrm{MAX}}+NC_{s^*}^{\mathrm{MAX}}$ according to the above rule, the introduction of liners with lower capacity begins. According to the size of the route index, we prioritize the liner with a higher capacity for routes with a smaller route index.

5.5.2. Subproblem

The subproblem is concerned with determining the optimal solution for continuous variables in **R-P**. To solve this nonlinear subproblem, integer variables are fixed. The subproblem of **R-P** is written as **R-P-SP**. In this model, we introduce wavy lines and superscripts (i.e., *i*) to all integer decision variables, i.e., $\left(\tilde{x}_{sr,0},\tilde{n}_{sr,0}^{\mathrm{Total}},\tilde{n}_{sr,0}^{\mathrm{VOL}},\tilde{n}_{s,0}^{\mathrm{IN}},\tilde{n}_{s,0}^{\mathrm{OUT}}\right)$, thereby indicating that these variables are incorporated into the subproblem at the i^{th} iteration.

R-P-SP:

$$\max sp=\left\{\begin{array}{l}-T\sum_{r\in\mathcal{R}}\sum_{s\in\mathcal{S}}c_s^{\mathrm{OP}}\tilde{n}_{sr,i}^{\mathrm{Total}}-\sum_{r\in\mathcal{R}}\sum_{s\in\mathcal{S}}c_{sr}^{\mathrm{VOL}}\tilde{n}_{sr,i}^{\mathrm{VOL}}-T\sum_{s\in\mathcal{S}}c_s^{\mathrm{IN}}\tilde{n}_{s,i}^{\mathrm{IN}}\\ +T\sum_{s\in\mathcal{S}}c_s^{\mathrm{OUT}}\tilde{n}_{s,i}^{\mathrm{OUT}}+\boldsymbol{\mu}^{\mathrm{T}}\mathbf{q}-\epsilon\varpi\end{array}\right\} \tag{5.44}$$

$$s.t.\quad \tilde{n}_r=\sum_{s\in\mathcal{S}}\tilde{n}_{sr,i}^{\mathrm{VOL}}CAP_s\Big/\left\lceil\frac{T}{7}\right\rceil \qquad \forall r\in\mathcal{R} \tag{5.45}$$

(5.14), (5.16), (5.20), (5.21), (5.38), (5.42), (5.43).

5.5.3. Master problem

The master problem is an MIP model that optimizes integer decision variables on the basis of the continuous variables obtained. Given the presence of nonlinear constraints in **P**, we use **Proposition 5.6** to perform linear approximations (also known as OA cuts) for Constraints (5.38) and (5.42).

Proposition 5.6. Let $\hat{\mathbf{q}}^i$, $\hat{\mathbf{q}}^i_{lr}$ and $\hat{\varpi}^i$ denote the optimal solutions of **R-P-SP** at the i^{th} iteration and $\mathcal{I}$ represents the maximum number of iterations. The valid linear OA cut associated with Constraints (5.38) and (5.42) can be specified as follows:

$$\left(\tilde{\mathbf{q}}_{lr}^{\mathrm{T}}\mathbf{u}-\tilde{n}_r\right)\sqrt{\left(\hat{\mathbf{q}}^i_{lr}\right)^{\mathrm{T}}\boldsymbol{\Gamma}\hat{\mathbf{q}}^i_{lr}}+\tilde{\epsilon}\tilde{\mathbf{q}}_{lr}^{\mathrm{T}}\boldsymbol{\Gamma}\hat{\mathbf{q}}^i_{lr}\le 0 \quad \forall l\in\mathcal{L}_r, r\in\mathcal{R}, i=1,2,\cdots,\mathcal{I} \tag{5.46}$$

$$\sqrt{\mathbf{q}^{\mathrm{T}}\boldsymbol{\Sigma}\hat{\mathbf{q}}^i}-\varpi\hat{\varpi}^i\le 0 \quad \forall i=1,2,\cdots,\mathcal{I}. \tag{5.47}$$

Proof. From the convexity of these two functions shown in **Proposition 5.6**, we further perform a Taylor expansion of Constraints (5.45) and (5.46), which yields

$$F_1\left(\hat{\mathbf{q}}^i_{lr},\hat{n}^i_r\right)+\nabla F_1\left(\hat{\mathbf{q}}^i_{lr},\hat{n}^i_r\right)^{\mathrm{T}}\begin{bmatrix}\mathbf{q}_{lr}-\hat{\mathbf{q}}^i_{lr}\\ \tilde{n}_r-\hat{n}^i_r\end{bmatrix}\le F_1\left(\mathbf{q}_{lr},\tilde{n}_r\right)\le 0, \text{ and}$$

$$F_2\left(\hat{\mathbf{q}}^i,\hat{\varpi}^i\right)+\nabla F_2\left(\hat{\mathbf{q}}^i,\hat{\varpi}^i\right)^{\mathrm{T}}\begin{bmatrix}\mathbf{q}-\hat{\mathbf{q}}^i\\ \varpi-\hat{\varpi}^i\end{bmatrix}\le F_2\left(\hat{\mathbf{q}}^i,\hat{\varpi}^i\right)\le 0,$$

where $\nabla F_1\left(\hat{\mathbf{q}}^i_{lr},\hat{n}^i_r\right)=\left[\mathbf{u}+\dfrac{\tilde{\epsilon}\left(\hat{\mathbf{q}}^i_{lr}\right)^{\mathrm{T}}\boldsymbol{\Gamma}}{\sqrt{\left(\hat{\mathbf{q}}^i_{lr}\right)^{\mathrm{T}}\boldsymbol{\Gamma}\hat{\mathbf{q}}^i_{lr}}},-1\right]$ and $\nabla F_2\left(\hat{\mathbf{q}}^i,\hat{\varpi}^i\right)=$

$\left[\frac{\left(\hat{\mathbf{q}}^i\right)^{\mathrm{T}}\boldsymbol{\Sigma}}{\sqrt{\left(\hat{\mathbf{q}}^i\right)^{\mathrm{T}}\boldsymbol{\Sigma}\hat{\mathbf{q}}^i}},-1\right]$. Then, we can obtain the closed-form solutions of (5.46) and (5.47) through simple algebra. (Q.E.D.)

Now, we introduce an auxiliary variable ξ and use BU^i (BL^i) to represent the upper (lower) bound of the model at the i^{th} iteration of the algorithm, respectively. On the basis of **Proposition 5.6**, we can propose **R-P-MP**, i.e., the master problem of **R-P**, as follows.

<u>R-P-MP:</u>

$$\min mp = \xi \tag{5.48}$$

s.t. (5.2), (5.3), (5.4), (5.5), (5.6), (5.7), (5.8), (5.9), (5.10), (5.11), (5.12), (5.14), (5.16), (5.20), (5.22), (5.23), (5.43), (5.46), (5.47).

$$\begin{aligned}\xi \geq\ & T\sum_{r\in\mathcal{R}}\sum_{s\in\mathcal{S}} c_s^{\mathrm{OP}} n_{sr}^{\mathrm{Total}} + \sum_{r\in\mathcal{R}}\sum_{s\in\mathcal{S}} c_{sr}^{\mathrm{VOL}} n_{sr}^{\mathrm{VOL}} \\ & + T\sum_{s\in\mathcal{S}} c_s^{\mathrm{IN}} n_s^{\mathrm{IN}} - T\sum_{s\in\mathcal{S}} c_s^{\mathrm{OUT}} n_s^{\mathrm{OUT}} - \boldsymbol{\mu}^{\mathrm{T}}\mathbf{q} + \epsilon\varpi\end{aligned} \tag{5.49}$$

$$\xi \leq BU^i - \nu \qquad \forall i \in \{1,2,\cdots,\mathcal{I}\} \tag{5.50}$$

$$\xi \geq BL^i \qquad \forall i \in \{1,2,\cdots,\mathcal{I}\} \tag{5.51}$$

where ν is a small positive number and $\tilde{n}_r = \sum_{s\in\mathcal{S}} n_{sr}^{\mathrm{VOL}} CAP_s \Big/ \left\lceil \frac{T}{7} \right\rceil$.

In the aforementioned equations, Equation (5.46) represents the objective function of **R-P-MP**. In accordance with the methodology proposed by Fletcher and Leyffer (1994), we introduce (5.50) to ensure the solution of **R-P-MP** is less than the upper bound. The termination condition is that the **R-P-MP** is infeasible. Note that it is not necessary for the **R-P-MP** to be solved optimally during the iteration of the algorithm, provided that a new feasible integer solution is produced. The solution is designated as ν-optimal. The pseudocode is shown in **Algorithm 5.1**.

Algorithm 5.1:

Input: $\tilde{x}_{sr,0}$, $\tilde{n}^{\text{Total}}_{sr,0}$, $\tilde{n}^{\text{VOL}}_{sr,0}$, $\tilde{n}^{\text{IN}}_{s,0}$, $\tilde{n}^{\text{OUT}}_{s,0}$: initial value;

BU^0 : upper bound, equals to ∞;

BL^0 : lower bound, equals to $-\infty$;

$\mathcal{I}$: maximum number of iterations.

Procedure:

For $i = 1{:}\ \mathcal{I}$ **do**

Solve **R-P-SP**. Obtain optimal solution of continuous decision variable. Denote the value of objective function as BU^i.

Add OA cuts (5.45) and (5.46) with fixed $\hat{\mathbf{q}}^i$, $\hat{\mathbf{q}}^i_{lr}$ and $\hat{\varpi}^i$. Solve **R-P-MP**, get new feasible integer decision variables. Denote the value of objective function as BL^i.

If R-P-MP is infeasible **then**

Break and return the incumbent value, report: $\left(\tilde{x}_{sr,i}, \tilde{n}^{\text{Total}}_{sr,i}, \tilde{n}^{\text{VOL}}_{sr,i}, \tilde{n}^{\text{IN}}_{s,i}, \tilde{n}^{\text{OUT}}_{s,i}\right)$, $\hat{\mathbf{q}}^i$, $\hat{\mathbf{q}}^i_{lr}$ and $\hat{\varpi}^i$;

End if

End for

5.6. Numerical experiments

In this section, numerical experiments are carried out to verify the validity of the models and algorithms. By carrying out several sensitivity analyses in Section 5.6.2, we also attempt to gain managerial insights. Finally, in Section 5.6.3, out-of-sample analysis of the robust optimization model, the SP model, and 2-DRO empirically validates the out-of-sample performance of our model.

5.6.1. Case study description

We consider an Asia–Europe liner shipping network in this chapter. The example consists of 10 routes, 46 ports, 63 legs, and 331 O-D pairs. Freight rate data are sourced from actual businesses. These routes were also chosen for the numerical experiments carried out by Meng et al. (2012) and Wang et al. (2013).

For each route, the ports of call included and the voyage distances are reported in Table 5.1.

Table 5.1 Voyage distance and ports of call for different routes

Route No.	Voyage distance (n mile)	Ports of call
R1	3440	Yokohama → Tokyo → Nagoya → Kobe → Shanghai → Hong Kong → Yokohama
R2	2361	Ho Chi Minh → Laem Chabang → Singapore → Port Klang → Ho Chi Minh
R3	8591	Brisbane → Sydney → Melbourne → Adelaide → Fremantle → Jakarta → Singapore → Brisbane
R4	1622	Manila → Kaohsiung → Xiamen → Hong Kong → Yantian → Chiwan → Manila
R5	1997	Dalian → Xingang → Qingdao → Shanghai → Ningbo → Kwangyang → Busan → Dalian
R6	4948	Chittagong → Chennai → Colombo → Cochin → Nhava Sheva → Chittagong
R7	6400	Sokhna → Aqabah → Jeddah → Salalah → Karachi → Jebel Ali → Sokhna
R8	1193	Southampton → Thamesport → Hamburg → Bremerhaven → Rotterdam → Antwerp → Zeebrugge → Le Havre → Southampton
R9	6009	Port Klang → Singapore → Jakarta → Kaohsiung → Busan → Hong Kong → Chiwan → Port Klang
R10	20478	Yantian → Hamburg → Sokhna → Jeddah → Port Klang → Singapore → Manila → Yantian

We consider that the liner company has five classes of liners, and their performance data (e.g., capacity, speed, and daily operation cost) are shown in Table 5.2. We apply the technique proposed in Delage and Ye (2010) to estimate ϵ in the ambiguity set $\mathcal{F}$. To this end, on the basis of a multivariate normal distribution, we collect $\bar{M}$ independent scenarios (i.e., samples) for random vector $\boldsymbol{\theta}$, i.e., $\left\{\boldsymbol{\theta}^i\right\}_{i=1}^{\bar{M}}$. After these samples are obtained, we calculate the mean ($\hat{\boldsymbol{\mu}}$) and covariance matrix ($\hat{\boldsymbol{\Sigma}}$) of these samples. Then, on the basis of (5.17), β is set to 0.05 and $R^2 = \max_{i=1,2,\cdots,\bar{M}} \left(\boldsymbol{\theta}^i - \hat{\boldsymbol{\mu}}\right)^{\mathrm{T}} \hat{\boldsymbol{\Sigma}}^{-1} \left(\boldsymbol{\theta}^i - \hat{\boldsymbol{\mu}}\right)$, and we estimate parameter ϵ by calculating $\epsilon = R/\sqrt{\bar{M}}\left(2+\sqrt{2\ln\left(1/\beta\right)}\right)$. In reality, the operational data (e.g., transportation demand data) of liner companies are often difficult to obtain because they involve their commercial secrets. Numerical experiments based on randomly generated transportation demand data are usually conducted. Therefore, we randomly generate 1,000 sample data, i.e., $\bar{M} = 1000$ and $\left\{\boldsymbol{\theta}^i\right\}_{i=1}^{1000}$. The mean of each component in $\boldsymbol{\theta}$ is uniformly drawn from $[10, 60]$, and the standard deviation is uniformly drawn from $[0.1, 1]$. In addition, we set the radius $\tilde{\epsilon}$ of set $\mathcal{G}$ as $\tilde{\epsilon} \in [0.001, 4]$, the mean of each component in $\boldsymbol{\vartheta}$ is uniformly drawn from $[0.1, 12]$, and the standard deviation is uniformly drawn from $[0.1, 2]$.

Table 5.2 Liner performance parameters of different classes

Item	Liner class				
	1	2	3	4	5
Liner capacity (TEUs)	2808	3218	4500	5714	8063
Sailing speed of the liner (knots)	21.00	22.00	24.20	24.60	25.20
Daily operation cost (10^3 \$)	19.80	22.50	30.90	38.80	54.20
Chartering in rate (million \$)	2.02	2.63	3.51	4.76	6.09
Chartering out rate (million \$)	1.82	2.34	3.21	4.32	5.12
NO_s^{MAX}	2	2	9	2	12
NC_s^{MAX}	5	5	6	5	10

Before the formal case study begins, we first conduct experiments on computing time to ensure that the case size involved in the case is appropriate and that our method is suitable for larger shipping networks. To this end, the number of routes is set to 5, 10, and 20, and the number of ports is set to 20, 25, 30, 40, 50, 60, 80, 100, and 120. The number of legs is set to vary from 20 to 200. The number of O-D pairs is set to 20% of the maximum possibility, considering that some O-D pairs may always have no transportation demand (e.g., two ports that are very close to each other). After combination, we obtain the 27 computing scenarios shown in Table 5.3.

Table 5.3 Computational time for different scale examples

No.	Number of routes	Number of ports	Number of legs	Average calculation time (s)	Optimality gap (%)
1	5	20	20	24	0.00
2	5	20	25	33	0.00
3	5	20	30	37	0.00
4	5	25	25	32	0.00
5	5	25	30	35	0.00
6	5	25	35	42	0.00
7	5	30	30	37	0.00
8	5	30	40	41	0.00
9	5	30	50	48	0.00
10	10	40	40	62	0.00
11	10	40	50	94	0.00
12	10	40	60	115	0.00
13	10	50	50	108	0.00
14	10	50	70	156	0.00
15	10	50	90	191	0.00
16	10	60	60	188	0.00
17	10	60	80	202	0.00
18	10	60	100	224	0.00
19	20	80	80	631	0.00
20	20	80	110	678	0.00
21	20	80	140	712	0.00
22	20	100	100	721	0.00
23	20	100	140	835	0.00
24	20	100	180	957	0.00
25	20	120	120	924	0.00
26	20	120	160	1104	0.00
27	20	120	200	1346	0.00

For each computing scenario, we randomly generate 15 groups of calculation cases and obtain the average calculation time. In all the computing scenarios, the optimal solution of the model is explored within a limited computing time (which we set as 3,600 s), so the optimality gap is 0. The experimental results are in line with our expectations. As the problem size increases, the computation time of each computational scenario gradually increases. For larger-scale problems, our algorithm can still obtain the optimal solution to the problem in a reasonable amount of time. Notably, in reality, liner companies do not combine too many routes for unified deployment. This is because if routes involving different continents (e.g., the Asia–Europe route and the Europe–America route) are unified for liner deployment, the liner company may need to pay more costs and time to liners located in Europe to Asia.

5.6.2. Sensitivity analysis of parameters in the ambiguity set

5.6.2.1. Sensitivity analysis of the radius $\tilde{\epsilon}$

The radius $\tilde{\epsilon}$ of the ambiguity set $\mathcal{G}$ indicates the size of the uncertainty of the weekly contract demand, and the uncertain model reduces to the deterministic model when the radius $\tilde{\epsilon}$ equals 0. Under different political and economic environments, the degree of uncertainty in the shipping industry's container transportation demand also varies. To explore the impact of changes in $\tilde{\epsilon}$ (degree of uncertainty) on the optimal solution and objective function value, the radius $\tilde{\epsilon}$ is set to be in the range of $\tilde{\epsilon} \in [0.001, 4]$. We set the mean and covariance of contract demand to be the same as those of the benchmark. The computation time for each scenario is approximately 100 seconds. From Fig. 5.4, with an increase in the ambiguity set radius, the profit of the liner company decreases significantly from approximately 9400 million HK dollars to over 2000 million HK dollars. Here, a large change in the profit of the liner company indicates that the liner company must cover a much greater additional cost when facing a high level of uncertainty. In contrast to the deterministic scenario where the radius $\tilde{\epsilon}$ is approximately 0, the profit of the liner company falls to approximately one-fifth of its original value when uncertainty is considered. As illustrated in Fig. 5.4, we also find that the trend is different when $\tilde{\epsilon} \leq 1$ and

$\tilde{\epsilon} > 1$. The profit of the liner company decreases more quickly when the radius is lower than 1, with a total decrease of nearly 6000 million HK dollars when $\tilde{\epsilon} \in [0,1]$. This is mainly because of the destruction resulting from the emergence of uncertainty, which makes the current scheme unable to adapt to random contract demand. The total number of voyages completed by the fleet has also undergone similar changes; that is, when $\tilde{\epsilon} \in [0,1]$, the number of voyages fluctuates, and after $\tilde{\epsilon} > 1$, it tends to stabilize. Table 5.4 shows the liner fleet deployment scheme, the average capacity of the liner in the fleet and the profit that can be earned by the liner company in three typical scenarios. As $\tilde{\epsilon}$ increases, the liner company gradually begins to use more large liners to cope with uncertainty, causing the average liner capacity in the fleet to increase.

Table 5.4 Liner fleet deployment scheme under different radii $\tilde{\epsilon}$ in the ambiguity set $\mathcal{G}$

$\tilde{\epsilon}$	Liner class	Number of liners										Average capacity (TEU)	Total profit (million $)
		R1	R2	R3	R4	R5	R6	R7	R8	R9	R10		
	1												
	2										7		
0.01	3					2		5				6218.51	8819
	4	3											
	5		2	7	2		4		1	5			
	1		1								7		
	2												
0.10	3						4					6351.13	8213
	4	3											
	5			7	2	2		5	1	5			
	1										7		
	2												
2.00	3								1			6599.94	2015
	4		2			2							
	5	3		3	2		4	5		5			

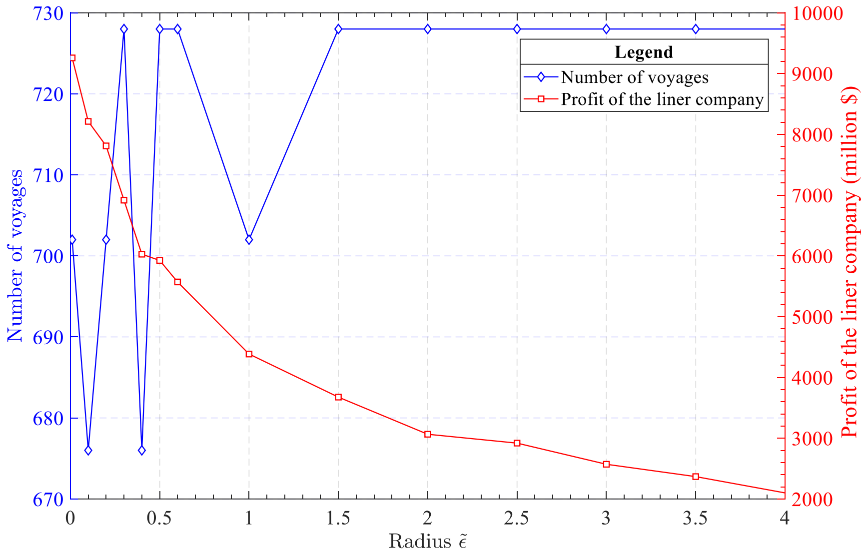

Fig. 5.4 Sensitivity analysis of the radius $\tilde{\epsilon}$ in the ambiguity set $\mathcal{G}$

5.6.2.2. Sensitivity analysis of mean contract demand $\mathbf{u}$

The mean of contract demand $\mathbf{u}$ also varies according to the different shipping seasons. To gain further insight into the impact of contract demand on the profitability of the liner company and model solution, we conduct several groups of numerical experiments on parameters in the ambiguity set $\mathcal{G}$. In this subsection, we adjust $\mathbf{u}$ to 60% to 150% of the benchmark value, and the interval is set to 10%. The coefficient of variation of $\mathbf{u}$ is between 66.67% and 166.67% because the covariance of contract demand is unchanged. The radius $\tilde{\epsilon}$ of the ambiguity set $\mathcal{G}$ is set to 2, and the risk tolerance φ is set to 0.05. Fig. 5.5 shows the results of the **R-P-1** model with different means of contract demand. As $\mathbf{u}$ increases, the profit of the liner company decreases, and this decrease is more obvious when the mean of the contract demand is lower than the benchmark value. Table 5.5 presents the specific liner fleet deployment plans of three typical scenarios and the corresponding average liner capacity of the fleet and the profit of the liner company. Similar to the situation in the previous subsection, as $\mathbf{u}$

increases, the liner company prefers to use larger liners, so the average fleet liner capacity increases. The number of voyages completed by the liner fleet remains relatively stable across scenarios, which shows that adjusting the liner class is the priority method for addressing transportation demand uncertainty.

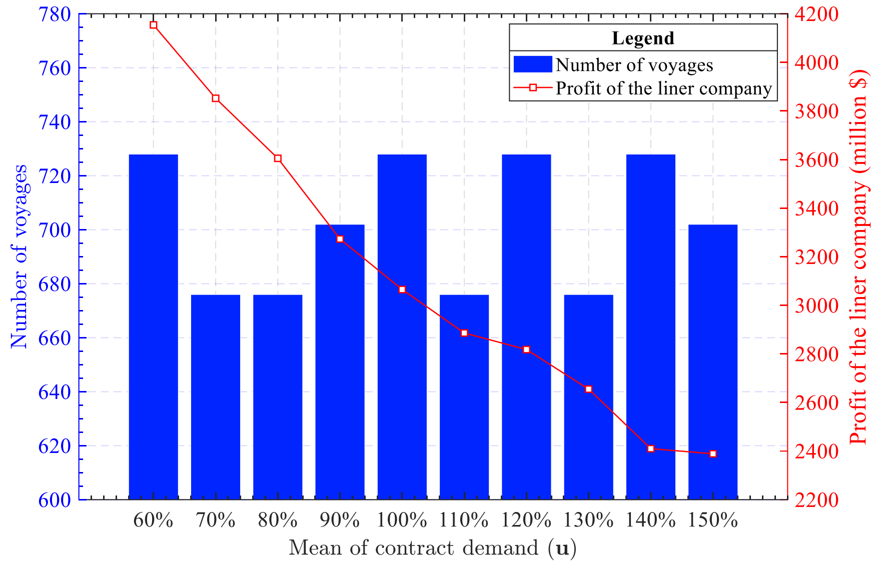

Fig. 5.5 Sensitivity analysis of mean contract demand **u**

Table 5.5 Liner fleet deployment scheme under different mean contract demands **u**

u	Liner class	Number of liners R1	R2	R3	R4	R5	R6	R7	R8	R9	R10	Average capacity (TEU)	Total profit (million $)
60%	1										7	6315.00	4430
	2												
	3			7									
	4		2										
	5	3			2	2	4	5	1	5			
70%	1										7	6517.00	3852
	2												
	3		2										
	4							5					
	5	3		6	2	2	3		1	5			
110%	1						3					6666.20	2886
	2												
	3										6		
	4	3	2										
	5			6	2	2		5	1	5			

5.6.2.3. Sensitivity analysis of covariance of contract demand **Γ**

As the world economic situation changes, sometimes the demand for container transportation is relatively stable, and sometimes the fluctuations in demand are more obvious. In this subsection, we focus on the impact of changes in contract demand covariance on the optimal solution of our model. To this end, we adjust the value of $\boldsymbol{\Gamma}$ to 60% to 150% of the benchmark, and the radius $\tilde{\epsilon}$ of the ambiguity set $\mathcal{G}$ is set to 0.5. Similarly, the coefficient of variation of $\boldsymbol{\Gamma}$ also changes from 60% to 150% because the mean of contract demand is unchanged. Fig. 5.6 shows the relationship between the profit of the liner company and the covariance of contract demand. Similarly, the profit decreases slightly when the covariance of contract demand is greater than that in the benchmark scenario. Overall, the trends shown in Fig. 5.6 are basically the same as those in the previous subsection, which reflects the changes in the decision-making of the liner company under different levels of uncertainty. However, unlike in the previous subsection, the number of voyages that the liner fleet needs to complete in different scenarios is essentially the same. This shows that when parameter $\boldsymbol{\Gamma}$ fluctuates, the main way for liner companies to deal with uncertainty is to adjust the size of the liner. We also use Table 5.6 to show three typical scenarios. As seen in the first two scenarios in Table 5.6, as uncertainty increases, the liner company responds by adjusting the class of the liners. However, the average capacity of each liner has not changed much. When $\boldsymbol{\Gamma}$ becomes the benchmark value, the liner company instead chooses to introduce more liners to cope. It can be seen that when liner companies face uncertainty, a reasonable choice is to use a variety of tools to strategically adjust their fleets to adapt to unpredictable market conditions.

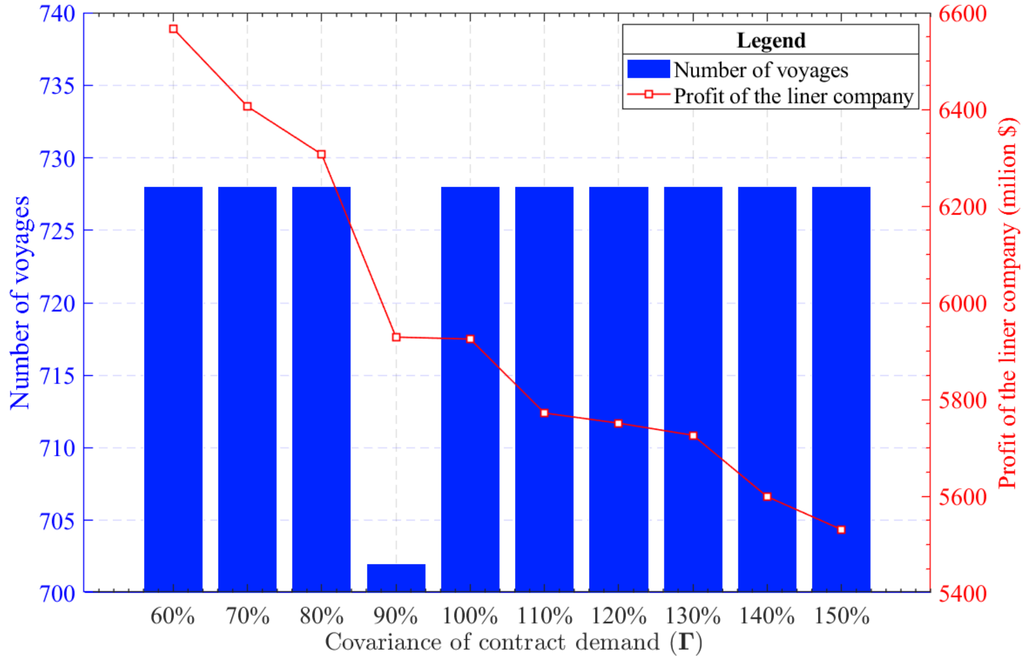

Fig. 5.6 Sensitivity analysis of the covariance of contract demand $\boldsymbol{\Gamma}$

Table 5.6 Liner fleet deployment scheme under different covariances of contract demand $\boldsymbol{\Gamma}$

$\boldsymbol{\Gamma}$	Liner class	Number of liners R1	R2	R3	R4	R5	R6	R7	R8	R9	R10	Average capacity (TEU)	Total profit (million $)
	1										7		
	2												
60%	3						4					6410.84	6567
	4							5					
	5	3	2	7	2	2			1	5			
	1												
	2										7		
70%	3						4					6486.37	6406
	4							5					
	5	3	2	7	2	2			1	5			
	1										7		
	2						5						
100%	3		2									6014.77	5925
	4							5					
	5	3		7	2	2			1	5			

5.6.2.4. Sensitivity analysis of liner capacity CAP_s

In recent years, there has been a discernible trend toward larger liners. To increase the economies of scale in freight transportation, the capacity of liners will be further expanded in the future. Therefore, in this subsection, experiments are conducted to analyze the influence of the liner capacity on the calculation results. The means and covariances of both total demand and contract demand are set to be the same as those in the benchmark scenario, the radius ϵ is calculated through the method in Section 5.6.1, and the radius $\tilde{\epsilon}$ is set to 0.6. The liner capacity is set to be in the range of 30% to 120% of the benchmark value with 10% as the interval. Fig. 5.7 shows the results of the **R-P-1** model with different liner capacity settings. The profit of the liner company increases when the liner capacity increases, while the number of voyages remains basically unchanged, but there are certain fluctuations. The aforementioned changes are consistent with our original predictions. Increasing parameter CAP_s is equivalent to reducing the operating cost of each liner. Therefore, Table 5.7 shows that liner companies are increasingly willing to use larger liners. Doing so can help the company cope with uncertainty without incurring excessive costs. In Table 5.7, when parameter CAP_s doubles, the average size of the liner in the fleet also doubles. This also reflects the impact of technological innovation on liner companies. As liner operating costs decline, the cost of liner companies responding to uncertainty gradually decreases.

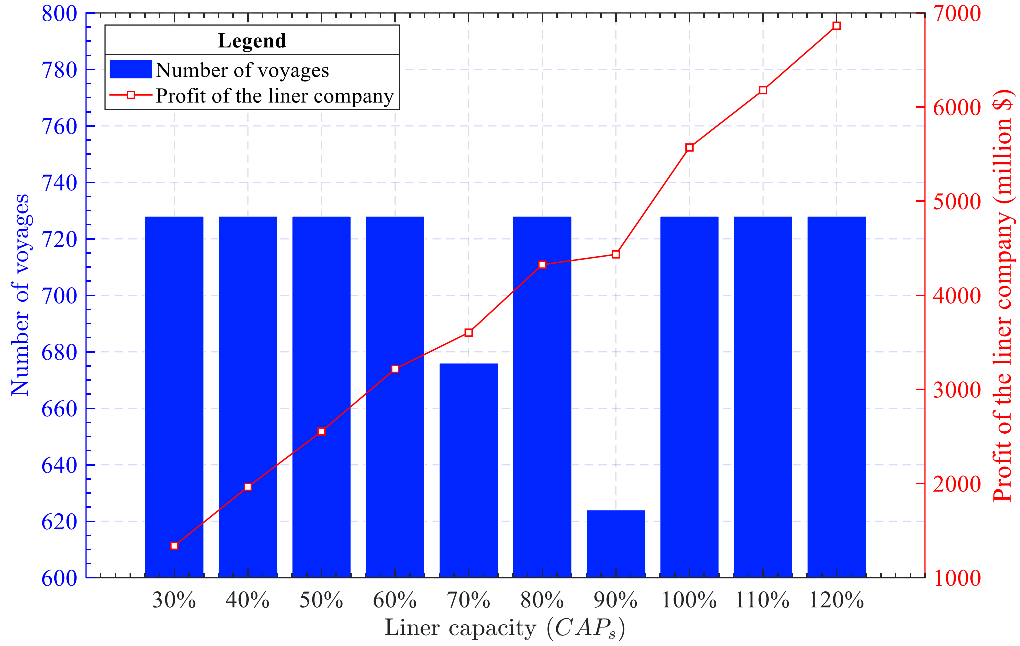

Fig. 5.7 Sensitivity analysis of liner capacity CAP_s

Table 5.7 Liner fleet deployment scheme under different liner capacities CAP_s

CAP_s	Liner class	Number of liners										Average capacity (TEU)	Total profit (million $)
		R1	R2	R3	R4	R5	R6	R7	R8	R9	R10		
60%	1										7	3846.51	3218
	2												
	3						4						
	4							5					
	5	3	2	7	2	2			1	5			
100%	1										7	6014.77	5571
	2						5						
	3		2										
	4							5					
	5	3		7	2	2			1	5			
120%	1										7	7467.98	6864
	2												
	3		2				4						
	4							5					
	5	3		7	2	2			1	5			

5.6.3. Out-of-sample analysis

As mentioned in Sections 5.1 and 5.2, the joint optimization of LFDP and SAP is usually solved via robust optimization or SP methods in existing studies. However, the results of robust optimization are often overly conservative because they optimize the worst case determined by the range of uncertain parameter values. When the worst case is poorly chosen (e.g., an extreme case is chosen as a sample), it often leads to a significant waste of resources. In addition, solving the SP model usually involves approximating this model via a deterministic problem with a limited number of scenarios (i.e., the SAA approach) on the basis of the assumption that the distribution function of uncertain parameters is known. However, the uncertain parameters we need to address (i.e., transportation demand) are highly coupled with the political and economic forms of the world. This prevents us from accurately identifying distribution functions with uncertain parameters. If the liner deployment decision is made under the wrong probability distribution function, the performance of this decision under the true probability distribution may be disappointing. This leads to the *optimization bias* phenomenon, where optimization on the basis of imperfectly distributed estimates leads to biased decisions. The abovementioned defects exposed by SP and robust optimization models (i.e., over-conservatism and optimization bias) can be empirically explored through out-of-sample analysis. Therefore, in this section, we empirically validate the benefits of the DRO approach by conducting out-of-sample analysis.

The steps of out-of-sample analysis can be summarized as follows. First, we solve the robust optimization model and the SP model to realize the joint optimization of the LFDP and SAP. Specifically, the method for solving the SP model is based on Meng et al. (2012). We generated 20 scenarios via the normal distribution function and the parameter setting scheme in Section 5.6.1. To handle the joint chance constraint (5.15) in the model, we apply the technique proposed in Section 4.1 of Wang et al. (2013). The parameters of the robust optimization model are derived from the abovementioned 20 scenarios. Secondly, two distribution functions are considered, and 10,000 test samples are randomly generated according to each distribution function. The reason for choosing these two distribution functions is that they are distribution functions that the uncertain parameters are usually assumed to obey in existing studies. Finally, we substitute each test sample into the joint chance constraint (5.15), where the values of the decision variables in this constraint are obtained by solving different models (i.e., robust optimization model, SP model and DRO model) to test the out-of-sample performance of different models. We use κ (a non-negative parameter) to control the degree of out-of-sample uncertainty and the distribution can be written as follows.

(1) *Truncated normal distribution* (TNO): For each O-D pair $w \in \mathcal{W}$, we set the random container transportation demand from the contract shippers of each week $\vartheta_w \sim N(\mu_w, (\kappa\sigma_w)^2)$ with non-negative marginal.

(2) *Truncated uniform distribution* (TUN): For each O-D pair $w \in \mathcal{W}$, we set the random container transportation demand from contract shippers of each week $\vartheta_w \sim U(\mu_w - \kappa\sqrt{3}\sigma_w, \mu_w + \kappa\sqrt{3}\sigma_w)$ with non-negative marginal.

In the out-of-sample analysis, two indicators are employed for the evaluation of the out-of-sample performance of different models: average individual probability (AIP) and average joint probability (AJP). For a test sample, the former counts each constraint in the joint chance constraint (5.15) and takes a value of 1 if one constraint is not violated. In contrast, for each test sample, the latter takes a value of 1 if all the constraints within the joint chance constraint (5.15) are not violated. The calculation results of these two indicators are within the interval $[0,1]$. The larger the value of the indicator is, the better the out-of-sample performance of the model. The calculation methods of AIP and AJP are as follows:

$$AIP = \frac{1}{N\sum_{r\in\mathcal{R}}\left(|\mathcal{L}_r||\mathcal{R}|\right)} \sum_{n\in[N]} \sum_{l\in\mathcal{L}_r, r\in\mathcal{R}} \mathbb{I}\left(\sum_{s\in\mathcal{S}} n_{sr}^{\mathrm{VOL},*} CAP_s \Big/ \left\lceil \frac{T}{7} \right\rceil \geq \sum_{w\in\mathcal{W}} \hat{\vartheta}_w^n \sum_{h^w\in\mathcal{H}^w} q_{h^w}^* \delta_{h^w}^{lr} \right) \tag{5.52}$$

$$AJP = \frac{1}{N} \sum_{n\in[N]} \mathbb{I}\left(\sum_{s\in\mathcal{S}} n_{sr}^{\mathrm{VOL},*} CAP_s \Big/ \left\lceil \frac{T}{7} \right\rceil \geq \sum_{w\in\mathcal{W}} \hat{\vartheta}_w^n \sum_{h^w\in\mathcal{H}^w} q_{h^w}^* \delta_{h^w}^{lr}, \forall l\in\mathcal{L}_r, r\in\mathcal{R} \right). \tag{5.53}$$

where $\hat{\boldsymbol{\vartheta}} = \left(\hat{\vartheta}_w^n\right)$ $\left(n\in[N]\right)$ represents N test samples; $\mathbb{I}(\bullet)$ denotes the indicator function; and $n_{sr}^{\mathrm{VOL},*}$ and $q_{h^w}^*$ are optimal solutions obtained by solving different models (e.g., robust optimization model, SP model and 2-DRO).

We set the parameter κ to range from 1 to 3 with an interval of 0.2. The results of the out-of-sample performance are shown in Fig. 5.8 and Table 5.8. In Fig. 5.8, the combination of two distribution functions and two indicators resulted in four scenarios (i.e., Figs. 5.8(a) to 5.8(d)). The three lines DRO, RO and SP represent the out-of-sample performance of the 2-DRO, the robust optimization model and the SP model under different κ values, respectively. We find that in all the scenarios, the values of the two indicators under the robust optimization model are 1. This shows that regardless of how the parameter κ changes, the robust optimization solution does not violate the constraints under out-of-sample data. Although this shows that the solution obtained by solving the robust optimization model can adapt to changes in the external environment (i.e., uncertain parameters), it also shows that the solution obtained is relatively conservative. The SP model performs the worst, and many constraints begin to be violated as κ increases. When κ increases to 3, the AJP of the SP model is less than 55% under the truncated normal distribution and 30% under the truncated uniform distribution, respectively. This shows that when there is a gap between the true distribution and the estimated distribution, the SP model exhibits obvious *Optimization Bias* phenomenon. Finally, we can observe that the out-of-sample performance of 2-DRO is between that of the robust optimization model and the SP model. When κ equals 3, the AJP indicators under the truncated normal distribution and the truncated uniform distribution still exceed 70% and 50%, respectively. The above experimental results empirically verify that the 2-DRO we proposed is robust. It can avoid the production of overly conservative solutions and the *optimization bias* caused by the SP model. Table 5.8 presents the values of each point in Fig. 5.8.

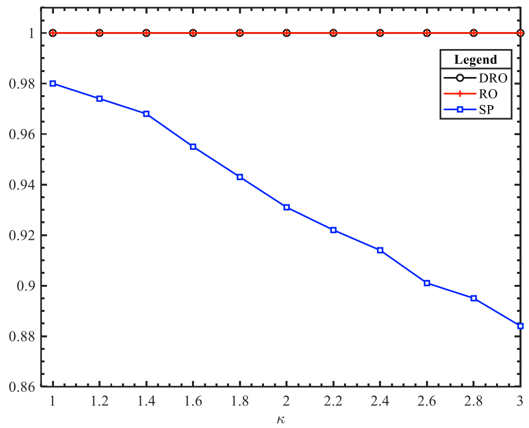

(a) AIP under truncated normal distribution

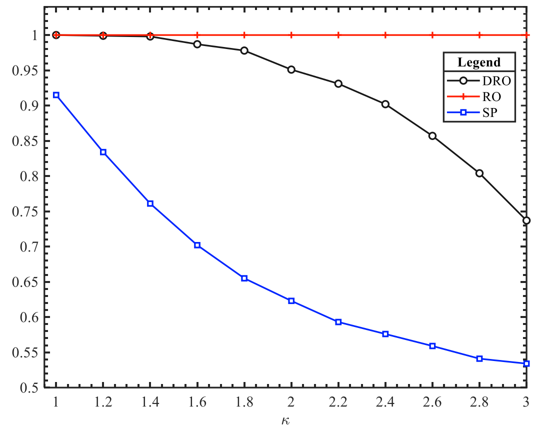

(b) AJP under truncated normal distribution

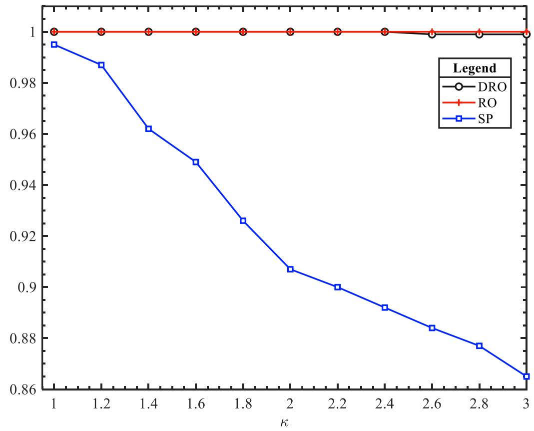

(c) AIP under truncated uniform distribution

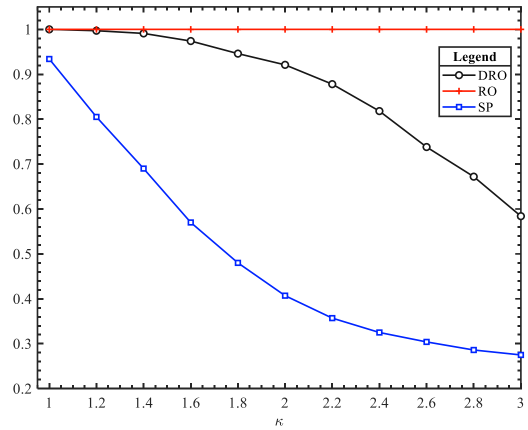

(d) AJP under truncated uniform distribution

Fig. 5.8 Out-of-sample performance of different models with two distribution functions

Table 5.8 AIP and AJP values under two distribution functions

κ	DRO				RO				SP			
	TNO		TUN		TNO		TUN		TNO		TUN	
	AIP	AJP	AIP	AJP	AIP	AJP	AIP	AJP	AIP	AJP	AIP	AJP
1.0	1.000	1.000	1.000	1.000	1.000	1.000	1.000	1.000	0.980	0.915	0.995	0.934
1.2	1.000	0.999	1.000	0.997	1.000	1.000	1.000	1.000	0.974	0.834	0.987	0.805
1.4	1.000	0.998	1.000	0.991	1.000	1.000	1.000	1.000	0.968	0.761	0.962	0.690
1.6	1.000	0.987	1.000	0.974	1.000	1.000	1.000	1.000	0.955	0.702	0.949	0.570
1.8	1.000	0.978	1.000	0.946	1.000	1.000	1.000	1.000	0.943	0.655	0.926	0.480
2.0	1.000	0.951	1.000	0.921	1.000	1.000	1.000	1.000	0.931	0.623	0.907	0.407
2.2	1.000	0.931	1.000	0.878	1.000	1.000	1.000	1.000	0.922	0.593	0.900	0.357
2.4	1.000	0.902	1.000	0.818	1.000	1.000	1.000	1.000	0.914	0.576	0.892	0.325
2.6	1.000	0.857	0.999	0.738	1.000	1.000	1.000	1.000	0.901	0.559	0.884	0.304
2.8	1.000	0.804	0.999	0.672	1.000	1.000	1.000	1.000	0.895	0.541	0.877	0.286
3.0	1.000	0.737	0.999	0.584	1.000	1.000	1.000	1.000	0.884	0.534	0.865	0.275

5.6.4. Managerial insights

According to the results of the above numerical experiments, several managerial insights into the deployment of liners and slot allocation can be provided to the operations managers of liner companies.

(1) *Multiple liner classes can help increase profit and realize adequate reliability*. As discussed in Section 5.6.2, when various uncertain parameters change, the liner company fleet liner class also changes simultaneously. Multiple liner classes mean that the liner company has more choices to adapt to the different scenarios in practical operations, which means that more strategies are available when facing uncertainty. Furthermore, more investment in the research and development of new maritime shipping technologies may be an essential tool for liner companies to cope with the shock of uncertainty in the future.

(2) *The adjustment of the existing scheme is the key to addressing various demand scenarios*. We find that a change in the number of liners is not necessary under different parameter settings, while the adjustment of existing deployment and slot allocation schemes is the core measure for coping with the uncertainty of container demand. Consequently, liner companies should not expect to solve the problems resulting from uncertainty by purchasing more liners. Today, as liners become larger, liner companies should pay attention to the management of current resources and be confident in solving uncertain problems through limited liners and voyages. The liner alliance currently popular in the shipping

industry is an example. A liner company forms partnerships with other companies to share resources and liner capacity and improve operational efficiency. This allows for better adaptation to market fluctuations and changes in demand.

(3) *Advance preparatory actions against uncertainty are meaningful for liner companies.* From the trend of the variation in the profit with the ambiguity set radius shown in Section 5.6.2, decisions that do not take uncertainty into account will lead to higher unforeseen costs when uncertainty occurs. It is obvious that there is a larger shock when unaware of uncertainty, whereas the additional cost caused by increasing uncertainty is lower when pre-considering uncertainty is considered. This reveals the value of decision-making with respect to preparedness for various uncertain scenarios in liner operations. Therefore, to reduce unexpected costs, a meaningful measure for liner companies is to address uncertainty in advance. For example, liner companies can establish a sound risk management mechanism to identify and assess risks in a timely manner and take corresponding measures to cope with them.

5.7. Conclusions

Scientific and reasonable liner fleet design and slot allocation schemes are the keys to improving the profitability of liner companies. However, the severe demand fluctuations in the maritime shipping industry make existing optimization methods (e.g., robust optimization and stochastic optimization) based on known demand distribution functions flawed. In this chapter, we abandon the current mainstream modeling ideas and develop a two-stage distributionally robust optimization model (2-DRO) for liner fleet deployment and slot allocation joint optimization problems while considering the uncertainty of container transportation demand. To ensure a certain reliability of the liner fleet, a joint chance constraint ensuring demand satisfaction is introduced into this distribution-free model. Two ellipsoid ambiguity sets are constructed with first- and second-moment data to describe the distribution functions of contract demand and total demand. This 2-DRO is then reformulated as a second-order cone programming model. We also extend this formulation into a special case considering the connection between the ambiguity set radius and risk tolerance, and a customized outer approximation algorithm (OAA) is further proposed to explore the global solution to our 2-DRO. Numerical experiments are comprehensively conducted to investigate the performance of the 2-DRO. To further analyze the impact of various parameters in the model, sensitivity analysis experiments are carried out. The effect of uncertainty is shown to be significant for the liner deployment and allocation scheme. An out-of-sample analysis of three types of models (i.e., the robust optimization model, stochastic programming model, and 2-DRO) empirically verifies that our model avoids generating overly conservative solutions while circumventing the optimization bias phenomenon caused by the stochastic programming approach.

Finally, we summarize several possible extensions for future research on the basis of previous research and this chapter. First, we consider a short-term planning horizon in our modeling framework. The dynamic properties of the long-term horizon present new challenges to our model. The combination of dynamic modeling and uncertainty may require new approaches to ensure computability. The construction of an ambiguity set in combination with dynamic features is also a challenge in this direction. Second, more factors related to liner shipping can be introduced into our model. For example, considering liner alliances may be an interesting direction. Third, other ambiguity sets, such as scenario-wise ambiguity sets, may lead to more insights into the operations and management of liners. There are distinct peak and low seasons in maritime transport, as well as temporal and spatial differences in the transportation demands of different commodities. Clustering uncertain transportation demand first via machine learning and other methods and then constructing ambiguity sets based on the clustering results is certainly a valuable direction for future research.

Chapter 6:
Conclusions and future research

6.1. Conclusions

The maritime industry is highly coupled to the world's political and economic situation, making its inherent uncertainty a focus of attention in academia and industry. Especially in recent years, various emergencies (e.g., the COVID-19 pandemic) have occurred frequently, causing stakeholders to often suffer from port congestion, fluctuating container transportation demand, and shipment delays. Against the abovementioned background, establishing a resilient maritime logistics system has become a key measure to achieve resilience of the global supply chain. This thesis addresses the critical challenge of enhancing the resilience of maritime logistics systems under two uncertainties, namely, uncertain vessel delay times and uncertain container transportation demand. In order to take into account the improvement of the resilience of multiple elements (i.e., ports and shipping routes) in the maritime logistics system, we examined three types of problems: berth allocation on the landside (focusing on improving the resilience of port operations), liner fleet deployment on the seaside (focusing on improving the resilience of shipping routes), and coordinated optimization of liner fleet deployment and slot allocation (focusing on improving the resilience of shipping routes). Through three interconnected studies (see

Chapters 3 to 5), we develop novel distributionally robust optimization (DRO) frameworks that effectively mitigate the limitations of traditional stochastic programming (SP) and robust optimization (RO) approaches. Moreover, we also design customized algorithms (or acceleration strategies) to efficiently solve larger-scale problems.

In Chapter 3, we develop a distributionally robust chance-constrained (DRCC) model with a Type-1 Wasserstein ambiguity set to address the classic landside berth allocation problem under vessel arrival time uncertainty. The model overcame the conservatism of robust optimization and avoided the distributional assumption requirement of stochastic programming. Numerical experiments validated that introducing acceleration strategies, i.e., sample average approximation constraints and coefficient strengthening techniques, can significantly reduce program running time. Several sensitivity analyses are also conducted, revealing how service levels pre-defined in the chance constraint and ambiguity set radii impact operational decisions. We also compare the effects of introducing a joint chance constraint and several independent chance constraints in the model on the solution. The solution demonstrates the out-of-sample performance of our DRCC model while meeting port service requirements.

In Chapter 4, for seaside liner fleet deployment problem under container transportation demand uncertainty, we propose a data-driven DRCC model with a type-1 Wasserstein ambiguity set. This approach minimized the total operational costs of the liner company while ensuring shipping route capacity reliability through a joint chance constraint. We reformulate the DRCC model into a mixed integer programming model, and the model is accelerated by sample average approximation constraints and valid inequalities. Sensitivity analysis on ambiguity set radius and service level pre-defined in the chance constraint is conducted. We also compared the optimal solutions obtained by stochastic programming and robust optimization with the optimal solution of our model. Out-of-sample tests confirm that the liner company can achieve high transportation demand fulfillment, and the model outperforms robust optimization (avoiding excessive conservatism) and stochastic programming (preventing optimization bias). Sensitivity analyses provided insights into Wasserstein radius and risk tolerance trade-offs.

In Chapter 5, to jointly optimize liner fleet deployment and slot allocation problem under container transportation demand uncertainty, we establish a two-stage distributionally robust model with ellipsoidal ambiguity sets. Similar to the model established in Chapter 4, this distribution-free framework also incorporates a joint chance constraint to ensure that the container transportation demands of contract shippers are met to a given service level. We reformulate the original model to a second-order cone model (SOCM) and this SOCM is solved efficiently via a customized outer approximation algorithm. Sensitivity analyses are performed on several key parameters, including the ambiguity set radius, the mean and covariance of contract demand, and liner capacity. Out-of-sample comparisons empirically verified the superiority of our DRO model: it avoided the over-conservatism of robust optimization while circumventing the optimization bias inherent in stochastic programming. Sensitivity analysis highlighted uncertainty's significant impact on operational schemes.

6.2. Future research

While this thesis has made substantial strides in optimizing under uncertainty, several avenues remain for future exploration. First, future studies should investigate integrated modeling of multiple interacting uncertainties (e.g., combining vessel delays, container transportation demand fluctuations, and mechanical failures), and moving beyond single-uncertainty frameworks. Additionally, exploring ambiguity set constructions that incorporate dynamic features or temporal patterns (e.g., peak/off-season fluctuations) is critical for long-term planning applications. The risk preferences of decision makers and choice inertia (i.e., loyalty to a specific liner company) of shippers can also be incorporated into the model framework.

Then, methodologically, developing accelerated algorithms for complex joint optimization problems—such as integrated berth allocation and quay crane assignment in automated terminals—remains essential. Research could also design scenario-wise ambiguity sets tailored to spatiotemporal demand variations or investigate alternative set constructions (e.g., moment-based sets). Testing these extensions in practical contexts like liner alliance cooperation mechanisms would further validate their utility. In addition, a deeper exploration into the optimal balance between computational tractability and customized service level offerings for different customer tiers (e.g., different service levels) would be highly valuable for practical port management.

Finally, clustering uncertain demand via machine learning techniques before constructing ambiguity sets offers promise for capturing commodity-specific and route-dependent variations. Future work should also examine reliability balancing strategies across critical routes and port pairs, addressing the current focus on system-wide reliability at the expense of sub-regional robustness.

Appendices

Appendix A.

Formulations of related models in Chapter 4

In this appendix, we first present a deterministic model. We define $\tilde{\lambda}^{\left(k_v^i,k_v^j\right)}$ as an estimate of $\lambda^{\left(k_v^i,k_v^j\right)}$. It can be an expectation based on historical data or an empirical value determined by the strategic management department of the liner company.

DM:

$$\min obj_1 = T\sum_{v\in\mathcal{V}}\sum_{s\in\mathcal{S}} c_s^{\mathrm{OP}} x_{sv}^{\mathrm{TO}} + \sum_{v\in\mathcal{V}}\sum_{s\in\mathcal{S}} c_{sv}^{\mathrm{VO}} y_{sv} + T\sum_{s\in\mathcal{S}} c_s^{\mathrm{IN}} x_s^{\mathrm{IN}} \tag{A.1}$$

s.t. (4.2), (4.3), (4.4), (4.5), (4.7), (4.8)

$$\sum_{\left(k_v^i,k_v^j\right)\in\mathcal{W}_v} \tilde{\lambda}^{\left(k_v^i,k_v^j\right)} \delta_l^{\left(k_v^i,k_v^j\right)} \le \sum_{s\in\mathcal{S}} y_{sv} Q_s, \forall v\in\mathcal{V}, l\in\mathcal{L}. \tag{A.2}$$

Then, we present a robust optimization model. This model requires that Constraint (4.8) is satisfied with a probability of 100%. Moreover, an upper bound of uncertain parameters is necessary to make the model trackable. Therefore, we assume that $\bar{\lambda}^{\left(k_v^i,k_v^j\right)}$ is the upper bound of $\lambda^{\left(k_v^i,k_v^j\right)}$. This upper bound can be the maximum value observed in historical data, or it can be an empirical value given by the strategic management department of the liner company. Thus, the corresponding model can be formulated as follows:

RO:

$$\min obj_1 = T\sum_{v\in\mathcal{V}}\sum_{s\in\mathcal{S}} c_s^{\mathrm{OP}} x_{sv}^{\mathrm{TO}} + \sum_{v\in\mathcal{V}}\sum_{s\in\mathcal{S}} c_{sv}^{\mathrm{VO}} y_{sv} + T\sum_{s\in\mathcal{S}} c_s^{\mathrm{IN}} x_s^{\mathrm{IN}} \tag{A.3}$$

$$s.t.\ (4.2), (4.3), (4.4), (4.5), (4.7), (4.8),$$

$$\sum_{\left(k_v^i,k_v^j\right)\in\mathcal{W}_v} \lambda^{\left(k_v^i,k_v^j\right)} \delta_l^{\left(k_v^i,k_v^j\right)} \le \sum_{s\in\mathcal{S}} y_{sv} Q_s \qquad \forall v\in\mathcal{V}, l\in\mathcal{L}, \lambda^{\left(k_v^i,k_v^j\right)} \in\mathcal{U} \tag{A.4}$$

where the uncertainty set $\mathcal{U} := \left[0, \overline{\lambda}^{\left(k_v^i,k_v^j\right)}\right]$.

Appendix B.

Comparison of type-1 Wasserstein ambiguity set developed in Chapter 4 with moment-based ambiguity set

Some may argue that it is not clear whether the Wasserstein distance-based DRO formulation is the best for solving the proposed liner shipping fleet deployment problem since other types of DRO frameworks exist for chance-constrained programming. Therefore, in this Appendix, we compare different ambiguity set formulations with the Wasserstein-based formulation proposed in Chapter 4. Depending on the type of information used to describe the distribution function, the current manifold ambiguity sets can be classified into two categories: (1) ambiguity sets based on generalized moment information and (2) ambiguity sets based on statistical distance.

Specifically, early studies often assumed that the distribution of uncertain parameters (e.g., the container transportation demand we consider) cannot be accurately obtained, but some of its generalized moment information (and support set) can be obtained (or estimated). The construction of ambiguity sets, which is based on generalized moment information, is possible if the liner company possesses generalized moment information associated with the uncertain parameters. Here, moments characterize the distribution of uncertain parameters. The first-order moment of an uncertain parameter is defined as the mean, which characterizes its location, whereas the second-order moment is related to the variance, which characterizes its dispersion. In addition to the aforementioned approach, the utilization of statistical distance-based ambiguity sets has emerged as a prevalent concept in recent years. The advent of digitalization in the industrial sector has facilitated the acquisition of historical information on uncertain parameters. Consequently, a rational approach to describing the distribution of uncertain parameters is to approximate the true distribution through the empirical distribution constructed from historical data. Typically, scholars operating within this paradigm assume that the statistical distance between the true probability distribution and the empirical distribution in the probability space does not exceed a certain threshold. Based on this idea, it is important to define the statistical distance between two distributions. Typical ambiguity sets based on statistical distance include (i) ambiguity sets based on ϕ-divergence and (ii) ambiguity sets based on Wasserstein distance.

Given that we construct an ambiguity set on the basis of statistical distance to describe demand $\boldsymbol{\lambda}$ in Chapter 4, we further develop an ambiguity set on the basis of generalized moment information for comparison. This ambiguity set has been widely adopted in the shipping industry, particularly in the context of optimization problems involving berth allocation and berth allocation and quay crane joint scheduling. For a more thorough exposition of this ambiguity set and its applications, readers are directed to consult the works of Agra and Rodrigues (2022) and Wang et al. (2024a). In this appendix, the ambiguity set is constructed based on the first two moments of the container transportation demand vector $\boldsymbol{\lambda}$, i.e., the empirical mean vector $\hat{\mathbf{u}} = (u^{\left(k_v^i, k_v^j\right)})$ and the centered second-moment matrix $\hat{\mathbf{\Gamma}}$. The moment-based ambiguity set is denoted as $\mathcal{F}_{\text{Moment}}$, as illustrated in Equation (B.1).

$$\mathcal{F}_{\text{Moment}} = \left\{ \mathbb{P} \in \mathcal{M} \middle| \begin{array}{l} \mathbb{P}(\boldsymbol{\lambda} \in \Omega) = 1 \\ \mathbb{E}_{\mathbb{P}}(\boldsymbol{\lambda}) = \hat{\mathbf{u}} \\ \mathbb{E}_{\mathbb{P}}\left[(\boldsymbol{\lambda} - \hat{\mathbf{u}})(\boldsymbol{\lambda} - \hat{\mathbf{u}})^{\mathrm{T}}\right] = \hat{\mathbf{\Gamma}} \end{array} \right\} \tag{B.1}$$

where $\mathcal{M}$ is the set of all probability measures on the measurable space; and Ω is the support set of vector $\boldsymbol{\lambda}$.

Based on the ambiguity set shown in Equation (B.1), a model is formulated to address the data-driven **D**istributionally **R**obust **C**hance-**C**onstrained liner shipping fleet deployment **P**roblem (DRCCP), as depicted below. Notably, to maintain the completeness of the model in this appendix, we have repeated some constraints here.

$$\min obj_1 = T\sum_{v\in\mathcal{V}}\sum_{s\in\mathcal{S}} c_s^{\mathrm{OP}} x_{sv}^{\mathrm{TO}} + \sum_{v\in\mathcal{V}}\sum_{s\in\mathcal{S}} c_{sv}^{\mathrm{VO}} y_{sv} + T\sum_{s\in\mathcal{S}} c_s^{\mathrm{IN}} x_s^{\mathrm{IN}} \tag{B.2}$$

$$s.t. \quad \sum_{v\in\mathcal{V}} x_{sv}^{\mathrm{TO}} \le NO_s^{\mathrm{M}} + x_s^{\mathrm{IN}} \qquad \forall s \in \mathcal{S} \tag{B.3}$$

$$x_s^{\mathrm{IN}} \le NC_s^{\mathrm{M}} \qquad \forall s \in \mathcal{S} \tag{B.4}$$

$$y_{sv} \le x_{sv}^{\mathrm{TO}} \times \left\lfloor \frac{T}{t_{sv}} \right\rfloor \qquad \forall v \in \mathcal{V}, s \in \mathcal{S} \tag{B.5}$$

$$\sum_{s\in\mathcal{S}} y_{sv} \ge N_v \qquad \forall v \in \mathcal{V} \tag{B.6}$$

$$\inf_{\mathbb{P}\in\mathcal{F}_{\text{Moment}}} \mathbb{P}\left(\sum_{(k_v^i, k_v^j)\in\mathcal{W}_v} \lambda^{(k_v^i, k_v^j)} \delta_l^{(k_v^i, k_v^j)} \le \sum_{s\in\mathcal{S}} y_{sv} Q_s, \forall v \in \mathcal{V}, l \in \mathcal{L} \right) \ge 1 - \eta \tag{B.7}$$

$$x_s^{\mathrm{IN}} \in \mathbb{Z}_+ \qquad \forall s \in \mathcal{S} \tag{B.8}$$

$$x_{sv}^{\mathrm{TO}}, y_{sv} \in \mathbb{Z}_+ \qquad \forall v \in \mathcal{V}, s \in \mathcal{S}. \tag{B.9}$$

In the above model, the existence of Equation (B.7) makes the model computationally intractable. To address this issue, we implement an *optimized*

Bonferroni approximation on the joint chance constraint (B.7) in accordance with the methodology proposed by Xie et al. (2022). The Constraint (B.11) is introduced to replace Equation (B.7) based on the idea proposed by **Lemma 1** in Xie et al. (2022) and technique proposed by Chen et al. (2007) and Natarajan et al. (2009). The proof of this lemma can also be found in Ghaoui et al. (2003) and Wagner (2008), and we do not describe it in detail here. At this point, we reconstruct the above model into a computationally tractable model, namely, [**DRCC-M**], as illustrated below.

DRCC-M:

$$\min obj_1 = T\sum_{v\in\mathcal{V}}\sum_{s\in\mathcal{S}} c_s^{\mathrm{OP}} x_{sv}^{\mathrm{TO}} + \sum_{v\in\mathcal{V}}\sum_{s\in\mathcal{S}} c_{sv}^{\mathrm{VO}} y_{sv} + T\sum_{s\in\mathcal{S}} c_s^{\mathrm{IN}} x_s^{\mathrm{IN}} \tag{B.10}$$

$s.t.$ (B.3), (B.4), (B.5), (B.6), (B.8) and

$$\sum_{\left(k_v^i,k_v^j\right)\in\mathcal{W}_v} \hat{u}^{\left(k_v^i,k_v^j\right)} \delta_l^{\left(k_v^i,k_v^j\right)} + \sqrt{\frac{1-s_{lv}}{s_{lv}}}\sqrt{\left(\boldsymbol{\delta}_l^{\left(k_v^i,k_v^j\right)}\right)^{\mathrm{T}} \hat{\boldsymbol{\Gamma}}_v \boldsymbol{\delta}_l^{\left(k_v^i,k_v^j\right)}} \le \sum_{s\in\mathcal{S}} y_{sv} Q_s \quad \forall v\in\mathcal{V}, l\in\mathcal{L} \tag{B.11}$$

where $\hat{\boldsymbol{\Gamma}}_v$ denotes the covariance matrix of random variables associated with route $v\in\mathcal{V}$; $\boldsymbol{\delta}_l^{\left(k_v^i,k_v^j\right)}$ represents the mean matrix of random variables associated with route $v\in\mathcal{V}$ and leg $l\in\mathcal{L}$; $s_{lv} = \eta/|\mathcal{V}||\mathcal{L}|$ is a safety factor.

For the model proposed in this appendix, the same numerical experiments are conducted as in Section 4.6, with a focus on comparing it with [**DRCC**]. Unless otherwise indicated, the parameter settings in this appendix are consistent with those in Section 4.6. The program average running time for executing the two models is presented in Table B1. A comparative analysis of computational time reveals that the solution efficiency of [**DRCC-M**] is superior to that of [**DRCC**]. This result is consistent with our expectation, as [**DRCC-M**] is developed based on a moment-based ambiguity set, thereby eliminating the necessity for historical data to be input into the model. However, for the practical case discussed in Section 5.6.2, the solution efficiency of both [**DRCC**] and [**DRCC-M**] meets the requirements of the linear company. The OBJs of the two models under different risk tolerances are shown in Fig. B1, and a discernible disparity emerges between the OBJs of the two models. When the risk tolerance is small (i.e., $\eta \le 0.1$), the difference in OBJs becomes more obvious. This shows that although [**DRCC**] and [**DRCC-M**] are both DRO models, their conservativeness is different. The solution obtained by [**DRCC-M**], which is constructed on the basis of a moment-based ambiguity set, is more conservative. This finding indicates that the DRO model, which is developed on the basis of the type-1 Wasserstein distance, can attain more comprehensive distributional robustness through a more direct data-driven construction, thereby reducing the reliance on specific moment assumptions. Furthermore, we also conduct an out-of-sample analysis on [**DRCC-M**], and the values of its AIP and AJP metrics are presented in Tables B2 and B3 and Figs. B2 and B3. As in the setting in Section 5.6, we set the confidence level (i.e., risk tolerance) η equal to 0.05. The values of the AIP and AJP metrics demonstrate that [**DRCC-M**] exhibits superior out-of-sample performance. However, when the parameter κ assumes small values, both models exhibit comparable out-of-sample performance. Specifically, when $\kappa \le 3$, the AIP metric of the two models does not differ by more than 10%. When $\kappa \le 1.6$, the AJP metric of the two models differs by no more than 20%. Notably, this excellent out-of-sample performance comes at a significant increase in cost. As illustrated in Fig. B1, when η is set to 0.05, the OBJ of [**DRCC**] is 2.12 billion yuan, and the OBJ of [**DRCC-M**] is 3.21 billion yuan. This outcome indicates superior out-of-sample performance at the cost of a 51.4% escalation in the liner company's operational expenses, and this OBJ even exceeds the OBJ of [**RO**]. When the aforementioned results are considered in conjunction with Fig. 4.8, it can be concluded that the out-of-sample performance of our [**DRCC**] meets the decision-making needs of liner companies and does not cause a significant increase in operating costs.

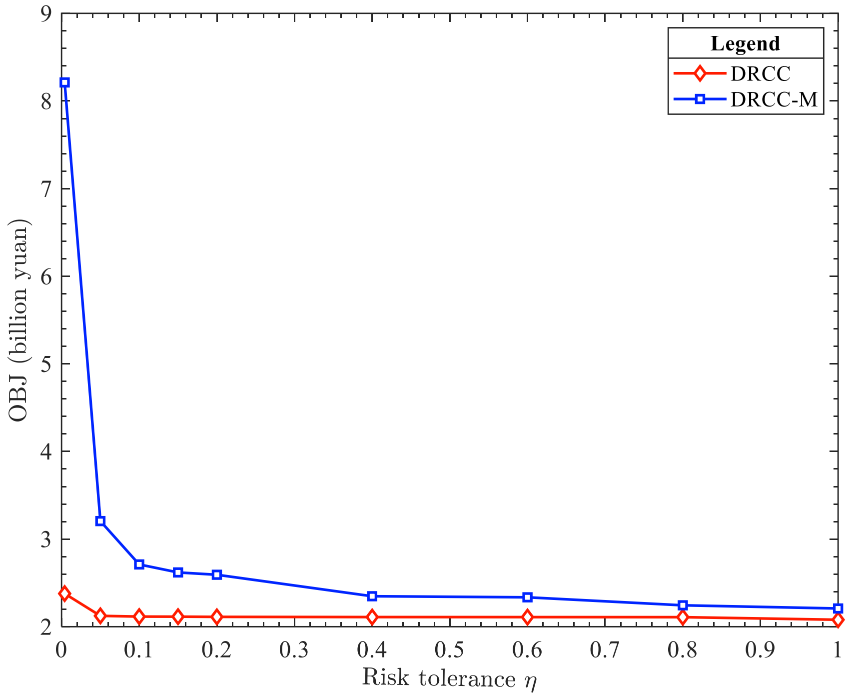

Fig. B1 OBJ of related models with different risk tolerances

Table B1 Program average running time of different models

Model	Program average running time (s)		
	Sample size N=10	Sample size N=1000	Sample size N=3000
[**DRCC**]	0.139	0.975	2.880
[**DRCC-M**]		0.014	

Table B2 AIP (in %) of solutions of different models

κ	Uniform distribution		Normal distribution		Log-normal distribution	
	DRCC	DRCC-M	DRCC	DRCC-M	DRCC	DRCC-M

1	100.0	100.0	100.0	100.0	100.0	100.0
2	99.4	100.0	99.4	100.0	98.3	100.0
3	96.4	100.0	96.4	100.0	88.9	100.0
4	92.4	100.0	92.4	100.0	76.0	100.0
5	88.7	100.0	88.8	100.0	63.7	100.0
6	85.6	100.0	85.6	100.0	53.0	99.9
7	83.0	99.7	83.0	100.0	43.5	99.2
8	80.8	95.9	80.9	100.0	35.3	96.3
9	78.9	85.8	79.0	100.0	28.3	90.0
10	77.3	73.8	77.3	100.0	22.8	80.7
11	75.9	61.6	76.0	100.0	18.5	69.9
12	74.6	48.7	74.6	100.0	15.1	59.0
13	73.4	37.1	73.5	99.9	12.6	48.9
14	72.4	28.1	72.5	99.8	10.6	40.2
15	71.4	21.8	71.5	99.7	9.1	33.0

Table B3 AJP (in %) of solutions of different models

κ	Uniform distribution		Normal distribution		Log-normal distribution	
	DRCC	DRCC-M	DRCC	DRCC-M	DRCC	DRCC-M
1.0	100.0	100.0	100.0	100.0	100.0	100.0
1.1	100.0	100.0	99.9	100.0	99.8	100.0
1.2	99.7	100.0	99.7	100.0	99.3	100.0
1.3	99.4	100.0	99.1	100.0	97.7	100.0
1.4	98.5	100.0	97.8	100.0	94.2	100.0
1.5	96.6	100.0	96.1	100.0	89.2	100.0
1.6	94.1	100.0	92.9	100.0	81.4	100.0
1.7	89.2	100.0	87.7	100.0	70.9	100.0
1.8	83.5	100.0	82.9	100.0	58.6	100.0
1.9	77.0	100.0	76.1	100.0	45.2	100.0
2.0	69.7	100.0	67.8	100.0	33.4	100.0
2.1	61.1	100.0	60.5	100.0	22.5	100.0
2.2	52.5	100.0	52.8	100.0	14.5	100.0
2.3	45.0	100.0	44.9	100.0	8.5	100.0
2.4	38.2	100.0	36.3	100.0	5.0	100.0

The results of the analysis presented in this appendix indicate that the ambiguity set based on the type-1 Wasserstein distance is more suitable for shipping problems than the moment-based ambiguity set is. The out-of-sample performance of our [**DRCC**] is sufficient to meet decision needs and does not result in overly conservative solutions, as obtained by solving [**DRCC-M**]. Theoretically, these conclusions can be verified. The type-1 Wasserstein ambiguity sets directly regulate the distribution through distance, potentially closer to the variation of the actual distribution, thus providing robustness without being too conservative. Furthermore, it is particularly well suited for scenarios where data scarcity necessitates the circumvention of excessive reliance on moment estimates. The aforementioned characteristics suggest the potential for extensive application of type-1 Wasserstein ambiguity sets in the maritime shipping industry, which is significantly influenced by the global political and economic landscape.

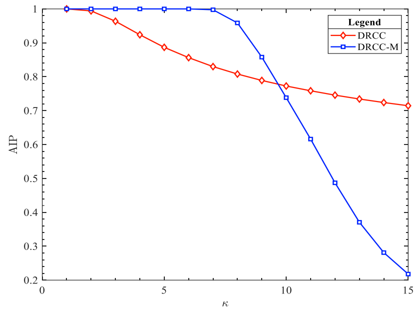

(*a*) AIP under uniform distribution

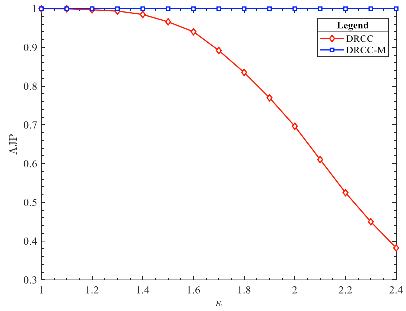

(*b*) AJP under uniform distribution

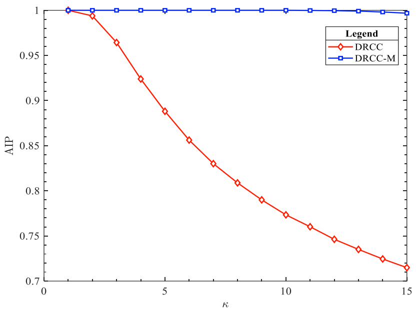

(*c*) AIP under normal distribution

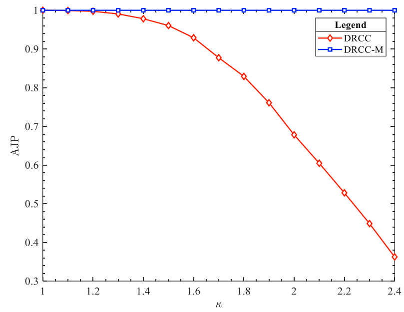

(*d*) AJP under normal distribution

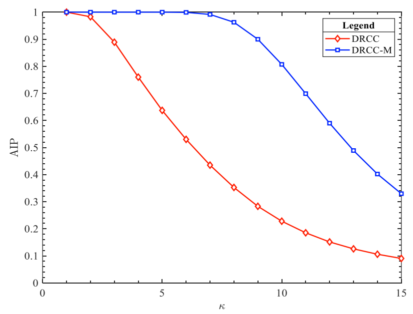

(*e*) AIP under log-normal distribution

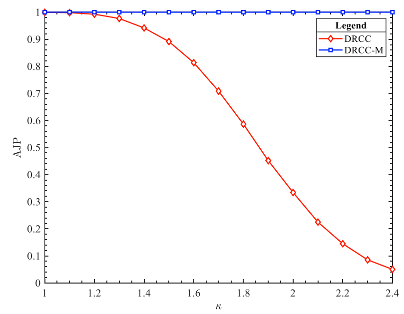

(*f*) AJP under log-normal distribution

Fig. B2 Results of the out-of-sample tests

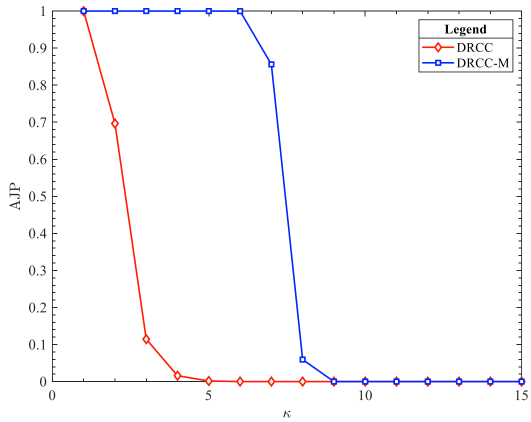

(a) AJP under uniform distribution

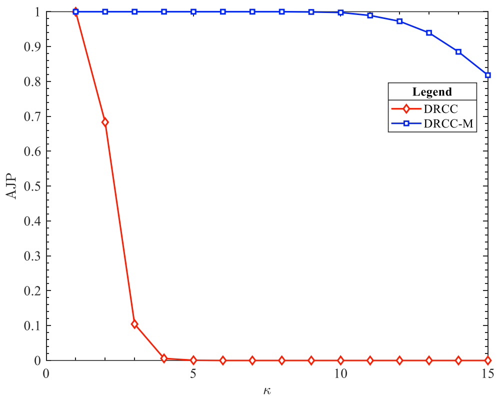

(b) AJP under normal distribution

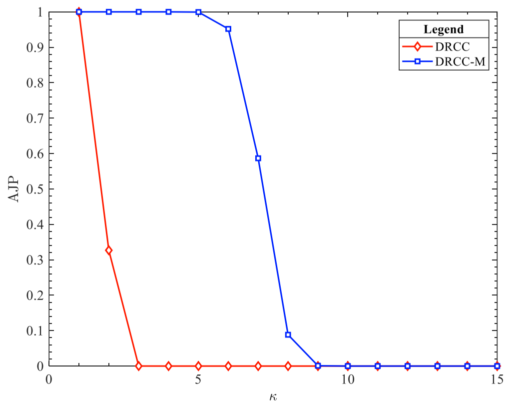

(c) AJP under log-normal distribution

Fig. B3 Results of the out-of-sample tests

References

Agarwal, R., & Ergun, Ö. (2008). Ship scheduling and network design for cargo routing in liner shipping. *Transportation Science*, *42*(2), 175–196.

Agra, A., & Oliveira, M. (2018). MIP approaches for the integrated berth allocation and quay crane assignment and scheduling problem. *European Journal of Operational Research*, *264*(1), 138–148.

Agra, A., & Rodrigues, F. (2022). Distributionally robust optimization for the berth allocation problem under uncertainty. *Transportation Research Part B: Methodological*, *164*, 1–24.

Al-Refaie, A., & Abedalqader, H. (2022). Optimal berth scheduling and sequencing under unexpected events. *Journal of the Operational Research Society*, *73*(2), 430–444.

Ben-Tal, A., & Nemirovski, A. (1998). Robust convex optimization. *Mathematics of Operations Research*, *23*(4), 769–805.

Ben-Tal, A., & Teboulle, M. (1986). Expected utility, penalty functions, and duality in stochastic nonlinear programming. *Management Science*, *32*(11), 1445–1466.

Bertsimas, D., & Sim, M. (2004). The price of robustness. *Operations Research*, *52*(1), 35–53.

Bertsimas, D., Sim, M., & Zhang, M. (2019). Adaptive distributionally robust optimization. *Management Science*, *65*(2), 604–618.

Beyer, H.-G., & Sendhoff, B. (2007). Robust optimization–a comprehensive survey. *Computer Methods in Applied Mechanics and Engineering*, *196*(33–34), 3190–3218.

Bierwirth, C., & Meisel, F. (2010). A survey of berth allocation and quay crane scheduling problems in container terminals. *European Journal of Operational Research*, *202*(3), 615–627.

Bonami, P., Biegler, L. T., Conn, A. R., Cornuéjols, G., Grossmann, I. E., Laird, C. D., Lee, J., Lodi, A., Margot, F., & Sawaya, N. (2008). An algorithmic framework for convex mixed integer nonlinear programs. *Discrete Optimization*, *5*(2), 186–204.

Brouer, B. D., Alvarez, J. F., Plum, C. E., Pisinger, D., & Sigurd, M. M. (2014). A base integer programming model and benchmark suite for liner-shipping network design. *Transportation Science*, *48*(2), 281–312.

Chang, X., Xu, Y., Sun, H., & Khan, I. (2021). A distributed robust optimization approach for the economic dispatch of flexible resources. *International Journal of Electrical Power & Energy Systems*, *124*, 106360.

Charnes, A., & Cooper, W. W. (1959). Chance-constrained programming. *Management Science*, *6*(1), 73–79.

Chen, K., Yi, X., Xin, X., & Zhang, T. (2023). Liner shipping network design model with carbon tax, seasonal freight rate fluctuations and empty container relocation. *Sustainable Horizons*, *8*, 100073.

Chen, W., & Sim, M. (2009). Goal-driven optimization. *Operations Research*, *57*(2), 342–357.

Chen, W., Sim, M., Sun, J., & Teo, C.-P. (2010). From CVaR to uncertainty set: Implications in joint chance-constrained optimization. *Operations Research*, *58*(2), 470–485.

Chen, X., Sim, M., & Sun, P. (2007). A robust optimization perspective on stochastic programming. *Operations Research*, *55*(6), 1058–1071.

Chen, Z., Kuhn, D., & Wiesemann, W. (2024). Data-driven chance constrained programs over Wasserstein balls. *Operations Research*, *72*(1), 410–424.

Cho, S.-C., & Perakis, A. N. (1996). Optimal liner fleet routeing strategies. *Maritime Policy and Management*, *23*(3), 249–259.

Christiansen, M., Fagerholt, K., Nygreen, B., & Ronen, D. (2013). Ship routing and scheduling in the new millennium. *European Journal of Operational Research*, *228*(3), 467–483.

Christiansen, M., Hellsten, E., Pisinger, D., Sacramento, D., & Vilhelmsen, C.

(2020). Liner shipping network design. *European Journal of Operational Research*, *286*(1), 1–20.

Chua, Y. J., Soudagar, I., Ng, S. H., & Meng, Q. (2023). Impact analysis of environmental policies on shipping fleet planning under demand uncertainty. *Transportation Research Part D: Transport and Environment*, *120*, 103744.

Delage, E., & Ye, Y. (2010). Distributionally robust optimization under moment uncertainty with application to data-driven problems. *Operations Research*, *58*(3), 595–612.

Du, Y., Xu, Y., & Chen, Q. (2010). A feedback procedure for robust berth allocation with stochastic vessel delays. *2010 8th World Congress on Intelligent Control and Automation*, Jinan, China.

Feng, C.-M., & Chang, C.-H. (2010). Optimal slot allocation with empty container reposition problem for Asia ocean carriers. *International Journal of Shipping and Transport Logistics*, *2*(1), 22–43.

Fletcher, R., & Leyffer, S. (1994). Solving mixed integer nonlinear programs by outer approximation. *Mathematical Programming*, *66*, 327–349.

Gabrel, V., Murat, C., & Thiele, A. (2014). Recent advances in robust optimization: An overview. *European Journal of Operational Research*, *235*(3), 471–483.

Galambos, J. (1977). Bonferroni inequalities. *The Annals of Probability*, 577–581.

Gao, R., & Kleywegt, A. (2023). Distributionally robust stochastic optimization with Wasserstein distance. *Mathematics of Operations Research*, *48*(2), 603–655.

Gao, S., Xin, X., Li, C., Liu, Y., & Chen, K. (2022). Container ocean shipping network design considering carbon tax and choice inertia of cargo owners. *Ocean & Coastal Management*, *216*, 105986.

Gelareh, S., & Meng, Q. (2010). A novel modeling approach for the fleet deployment problem within a short-term planning horizon. *Transportation Research Part E: Logistics and Transportation Review*, *46*(1), 76–89.

Gelareh, S., Nickel, S., & Pisinger, D. (2010). Liner shipping hub network design in a competitive environment. *Transportation Research Part E: Logistics and Transportation Review*, *46*(6), 991–1004.

Ghaoui, L. E., Oks, M., & Oustry, F. (2003). Worst-case value-at-risk and robust portfolio optimization: A conic programming approach. *Operations Research*, *51*(4), 543–556.

Givens, C. R., & Shortt, R. M. (1984). A class of Wasserstein metrics for probability distributions. *Michigan Mathematical Journal*, *31*(2), 231–240.

Golias, M. M. (2011). A bi-objective berth allocation formulation to account for vessel handling time uncertainty. *Maritime Economics & Logistics*, *13*(4), 419–441.

Guo, L., Zheng, J., Du, H., Du, J., & Zhu, Z. (2022). The berth assignment and allocation problem considering cooperative liner carriers. *Transportation Research Part E: Logistics and Transportation Review*, *164*, 102793.

Han, K., Liu, H., Gayah, V. V., Friesz, T. L., & Yao, T. (2016). A robust optimization approach for dynamic traffic signal control with emission considerations. *Transportation Research Part C: Emerging Technologies*, *70*, 3–26.

Ho-Nguyen, N., Kilinç-Karzan, F., Küçükyavuz, S., & Lee, D. (2023). Strong formulations for distributionally robust chance-constrained programs with left-hand side uncertainty under Wasserstein ambiguity. *INFORMS Journal on Optimization*, *5*(2), 211–232.

Ho-Nguyen, N., Kılınç-Karzan, F., Küçükyavuz, S., & Lee, D. (2022a). Distributionally robust chance-constrained programs with right-hand side uncertainty under Wasserstein ambiguity. *Mathematical Programming*, 1–32.

Ho-Nguyen, N., Kılınç-Karzan, F., Küçükyavuz, S., & Lee, D. (2022b). Distributionally robust chance-constrained programs with right-hand side uncertainty under Wasserstein ambiguity. *Mathematical Programming*, *196*, 641–672.

Hota, A. R., Cherukuri, A., & Lygeros, J. (2019). Data-driven chance constrained optimization under Wasserstein ambiguity sets. *2019 American Control Conference (ACC)*, Philadelphia, USA.

Jaramillo, D., & Perakis, A. N. (1991). Fleet deployment optimization for liner shipping Part 2. Implementation and results. *Maritime Policy and Management*, *18*(4), 235–262.

Jia, S., Li, C.-L., & Xu, Z. (2020). A simulation optimization method for deep-sea vessel berth planning and feeder arrival scheduling at a container port. *Transportation Research Part B: Methodological*, *142*, 174–196.

Jiang, N., & Xie, W. (2025). The Terminator: An integration of inner and outer approximations for solving Wasserstein distributionally robust chance constrained programs via variable fixing. *INFORMS Journal on Computing*, *37*(2), 381–412.

Kim, K. H., & Moon, K. C. (2003). Berth scheduling by simulated annealing. *Transportation Research Part B: Methodological*, *37*(6), 541–560.

Ksciuk, J., Kuhlemann, S., Tierney, K., & Koberstein, A. (2023). Uncertainty in maritime ship routing and scheduling: A Literature review. *European Journal of Operational Research*, *308*(2), 499–524.

Küçükyavuz, S., & Jiang, R. (2022). Chance-constrained optimization under limited distributional information: A review of reformulations based on sampling and distributional robustness. *EURO Journal on Computational Optimization*, *10*, 100030.

Lemesre, J., Dhaenens, C., & Talbi, E. G. (2007). Parallel partitioning method (PPM): A new exact method to solve bi-objective problems. *Computers & Operations Research*, *34*(8), 2450–2462.

Li, W., Cai, L., He, L., & Guo, W. (2024a). Scheduling techniques for addressing uncertainties in container ports: a systematic literature review. *Applied Soft Computing*, 111820.

Li, Z., Wang, L., Wang, G., Xin, X., Chen, K., & Zhang, T. (2024b). Investment and subsidy strategy for low-carbon port operation with blockchain adoption. *Ocean & Coastal Management*, *248*, 106966.

Liang, J., Li, L., Zheng, J., & Tan, Z. (2023). Service-oriented container slot allocation policy under stochastic demand. *Transportation Research Part B: Methodological*, *176*, 102799.

Lim, A. (1998). The berth planning problem. *Operations Research Letters*, *22*(2–3), 105–110.

Lin, F., Fang, X., & Gao, Z. (2022). Distributionally robust optimization: A review on theory and applications. *Numerical Algebra, Control and Optimization*, *12*(1), 159–212.

Liu, C., Xiang, X., & Zheng, L. (2020). A two-stage robust optimization approach for the berth allocation problem under uncertainty. *Flexible Services and Manufacturing Journal*, *32*(2), 425–452.

Liu, D., & Yang, H. (2015). Joint slot allocation and dynamic pricing of container sea–rail multimodal transportation. *Journal of traffic and transportation engineering (English Edition)*, *2*(3), 198–208.

Liu, K., Li, Q., & Zhang, Z.-H. (2019). Distributionally robust optimization of an emergency medical service station location and sizing problem with joint chance constraints. *Transportation research part B: methodological*, *119*, 79–101.

Liu, M., Lai, K.-h., Wong, C. W., Xin, X., & Lun, V. Y. (2025a). Smart ports for sustainable shipping: concept and practices revisited through the case study of China’s Tianjin port. *Maritime Economics & Logistics*, *27*, 50–95.

Liu, M., Xin, X., Wang, X., Zhang, T., & Chen, K. (2025b). Dual-channel slot sales strategy for container liner shipping companies with blockchain technology adoption. *Transport Policy*, *162*, 200–220.

Liu, Y., Xin, X., Yang, Z., Chen, K., & Li, C. (2021). Liner shipping network-transaction mechanism joint design model considering carbon tax and liner alliance. *Ocean & Coastal Management*, *212*, 105817.

Luedtke, J., Ahmed, S., & Nemhauser, G. L. (2010). An integer programming approach for linear programs with probabilistic constraints. *Mathematical Programming*, *122*(2), 247–272.

Luo, X., Ling, H., Xing, M., & Bai, X. (2024). A dynamic-static combination risk analysis framework for berthing/unberthing operations of maritime autonomous surface ships considering temporal correlation. *Reliability Engineering & System Safety*, *245*, 110015.

Lv, X., Jin, J. G., & Hu, H. (2020). Berth allocation recovery for container transshipment terminals. *Maritime Policy & Management*, *47*(4), 558–574.

Lv, Y., & Gao, Y. (2023). Time-based resilience enhancement with dual berth allocation strategies in bulk cargo terminals under machinery failure scenarios. *2023 7th International Conference on Transportation Information and Safety (ICTIS)*, Xi'an, China.

Maragos, S. A. (1994). *Yield management for the maritime industry.* Massachusetts Institute of Technology.

Meilijson, I., & Nádas, A. (1979). Convex majorization with an application to the length of critical paths. *Journal of Applied Probability*, *16*(3), 671–677.

Meng, Q., & Wang, S. (2012). Liner ship fleet deployment with week-dependent container shipment demand. *European Journal of Operational Research*, *222*(2), 241–252.

Meng, Q., Wang, S., Andersson, H., & Thun, K. (2014). Containership routing and scheduling in liner shipping: overview and future research directions. *Transportation Science*, *48*(2), 265–280.

Meng, Q., & Wang, T. (2010). A chance constrained programming model for short-term liner ship fleet planning problems. *Maritime Policy & Management*, *37*(4), 329–346.

Meng, Q., & Wang, T. (2011). A scenario-based dynamic programming model for multi-period liner ship fleet planning. *Transportation Research Part E:*

Logistics and Transportation Review, *47*(4), 401–413.

Meng, Q., Wang, T., & Wang, S. (2012). Short-term liner ship fleet planning with container transshipment and uncertain container shipment demand. *European Journal of Operational Research*, *223*(1), 96–105.

Meng, Q., Wang, T., & Wang, S. (2015). Multi-period liner ship fleet planning with dependent uncertain container shipment demand. *Maritime Policy & Management*, *42*(1), 43–67.

Mohajerin Esfahani, P., & Kuhn, D. (2018). Data-driven distributionally robust optimization using the Wasserstein metric: performance guarantees and tractable reformulations. *Mathematical Programming*, *171*(1), 115–166.

Moorthy, R., & Teo, C.-P. (2006). Berth management in container terminal: the template design problem. *OR Spectrum*, *28*, 495–518.

Mourão, M., Pato, M. V., & Paixão, A. (2002). Ship assignment with hub and spoke constraints. *Maritime Policy & Management*, *29*(2), 135–150.

Natarajan, K., Pachamanova, D., & Sim, M. (2009). Constructing risk measures from uncertainty sets. *Operations Research*, *57*(5), 1129–1141.

Ng, M. (2014). Distribution-free vessel deployment for liner shipping. *European Journal of Operational Research*, *238*(3), 858–862.

Ng, M. (2015). Container vessel fleet deployment for liner shipping with stochastic dependencies in shipping demand. *Transportation Research Part B: Methodological*, *74*, 79–87.

Ng, M., & Lin, D.-Y. (2018). Fleet deployment in liner shipping with incomplete demand information. *Transportation Research Part E: Logistics and Transportation Review*, *116*, 184–189.

Notteboom, T., Pallis, T., & Rodrigue, J.-P. (2021). Disruptions and resilience in global container shipping and ports: the COVID-19 pandemic versus the 2008–2009 financial crisis. *Maritime Economics & Logistics*, *23*, 179–210.

Perakis, A. N., & Jaramillo, D. (1991). Fleet deployment optimization for liner shipping Part 1. Background, problem formulation and solution approaches. *Maritime Policy and Management*, *18*(3), 183–200.

Pérez-Cañedo, B., Verdegay, J. L., Rosete, A., & Concepción-Morales, E. R. (2020). Fully fuzzy multi-objective berth allocation problem. In *International Conference on Hybrid Artificial Intelligence Systems* (pp. 261–272), Cham: Springer International Publishing.

Powell, B., & Perkins, A. (1997). Fleet deployment optimization for liner shipping: An integer programming model. *Maritime Policy & Management*, *24*(2), 183–192.

Qu, S., Li, X., Liu, C., Tang, X., Peng, Z., & Ji, Y. (2023). Two-stage robust programming modeling for continuous berth allocation with uncertain vessel arrival time. *Sustainability*, *15*(13), 10560.

Rahimian, H., & Mehrotra, S. (2022). Frameworks and results in distributionally robust optimization. *Open Journal of Mathematical Optimization*, *3*, 1–85.

Rockafellar, R. T., & Uryasev, S. (2000). Optimization of conditional value-at-risk. *Journal of Risk*, *2*, 21–42.

Rodrigues, F., & Agra, A. (2022). Berth allocation and quay crane assignment/scheduling problem under uncertainty: A survey. *European Journal of Operational Research*, *303*(2), 501–524.

Ruszczyński, A. (2002). Probabilistic programming with discrete distributions and precedence constrained knapsack polyhedra. *Mathematical Programming*, *93*, 195–215.

Scarf, H. E., Arrow, K., & Karlin, S. (1957). *A min-max solution of an inventory problem* (pp. 19–27). *Santa Monica: Rand Corporation*.

Segura, F. G., Segura, E. L., Moreno, E. V., & Uceda, R. A. (2017). A fully fuzzy linear programming model to the berth allocation problem. *2017 Federated conference on computer science and information systems (FedCSIS)*, Prague, Czech Republic.

Shahabi, M., Unnikrishnan, A., Jafari-Shirazi, E., & Boyles, S. D. (2014). A three level location-inventory problem with correlated demand. *Transportation* *research part B: methodological*, *69*, 1–18.

Sheikholeslami, A., & Ilati, R. (2018). A sample average approximation approach to the berth allocation problem with uncertain tides. *Engineering Optimization*, *50*(10), 1772–1788.

Shen, H., & Jiang, R. (2023). Chance-constrained set covering with Wasserstein ambiguity. *Mathematical Programming*, *198*(1), 621–674.

Snyder, L. V. (2006). Facility location under uncertainty: a review. *IIE transactions*, *38*(7), 547–564.

Stopford, M. (2008). *Maritime economics 3e*. Routledge.

Thorsen, A., & Yao, T. (2017). Robust inventory control under demand and lead time uncertainty. *Annals of Operations Research*, *257*, 207–236.

Ting, S.-C., & Tzeng, G.-H. (2004). An optimal containership slot allocation for liner shipping revenue management. *Maritime Policy & Management*, *31*(3), 199–211.

Wagner, M. R. (2008). Stochastic 0–1 linear programming under limited distributional information. *Operations Research Letters*, *36*(2), 150–156.

Wang, C., & Chen, S. (2020). A distributionally robust optimization for blood supply network considering disasters. *Transportation research part E: logistics and transportation review*, *134*, 101840.

Wang, C., Liu, K., Zhang, C., & Miao, L. (2024a). Distributionally robust chance-constrained optimization for the integrated berth allocation and quay crane assignment problem. *Transportation Research Part B: Methodological*, *182*, 102923.

Wang, C., Wang, Q., Xiang, X., Zhang, C., & Miao, L. (2025). Optimizing integrated berth allocation and quay crane assignment: A distributionally robust approach. *European Journal of Operational Research*, *320*(3), 593–615.

Wang, S., & Meng, Q. (2012a). Liner ship route schedule design with sea contingency time and port time uncertainty. *Transportation Research Part B: Methodological*, *46*(5), 615–633.

Wang, S., & Meng, Q. (2012b). Robust schedule design for liner shipping services. *Transportation Research Part E: Logistics and Transportation Review*, *48*(6), 1093–1106.

Wang, S., & Meng, Q. (2017). Container liner fleet deployment: A systematic overview. *Transportation Research Part C: Emerging Technologies*, *77*, 389–404.

Wang, S., Wang, T., & Meng, Q. (2011). A note on liner ship fleet deployment. *Flexible Services and Manufacturing Journal*, *23*, 422–430.

Wang, T., Meng, Q., & Tian, X. (2024b). Dynamic container slot allocation for a liner shipping service. *Transportation Research Part B: Methodological*, *179*, 102874.

Wang, T., Meng, Q., Wang, S., & Qu, X. (2021). A two-stage stochastic nonlinear integer-programming model for slot allocation of a liner container shipping service. *Transportation Research Part B: Methodological*, *150*, 143–160.

Wang, T., Meng, Q., Wang, S., & Tan, Z. (2013). Risk management in liner ship fleet deployment: a joint chance constrained programming model. *Transportation Research Part E: Logistics and Transportation Review*, *60*, 1–12.

Wang, T., Tian, X., & Wang, Y. (2020). Container slot allocation and dynamic pricing of time-sensitive cargoes considering port congestion and uncertain demand. *Transportation Research Part E: Logistics and Transportation Review*, *144*, 102149.

Wang, Y., Meng, Q., & Du, Y. (2015). Liner container seasonal shipping revenue management. *Transportation Research Part B: Methodological*, *82*, 141–161.

Wu, Y., & Miao, L. (2021). An efficient procedure for inserting buffers to generate robust berth plans in container terminals. *Discrete Dynamics in Nature and Society*, *2021*(1), 6619538.

Xiang, X., & Liu, C. (2021). An expanded robust optimisation approach for the berth allocation problem considering uncertain operation time. *Omega*, *103*, 102444.

Xiang, X., Liu, C., & Miao, L. (2017). A bi-objective robust model for berth allocation scheduling under uncertainty. *Transportation Research Part E: Logistics and Transportation Review*, *106*, 294–319.

Xiang, X., Liu, C., & Miao, L. (2018). Reactive strategy for discrete berth allocation and quay crane assignment problems under uncertainty. *Computers & Industrial Engineering*, *126*, 196–216.

Xiang, Z., Xin, X., Zhang, T., Chen, K., & Liu, M. (2025). Asia–Europe liner shipping network design model considering Arctic route and black carbon tax. *Ocean & Coastal Management*, *261*, 107492.

Xie, W. (2021). On distributionally robust chance constrained programs with Wasserstein distance. *Mathematical Programming*, *186*(1), 115–155.

Xie, W., Ahmed, S., & Jiang, R. (2022). Optimized Bonferroni approximations of distributionally robust joint chance constraints. *Mathematical Programming*, *191*(1), 79–112.

Xin, X., Wang, X., Zhang, T., Chen, H., Guo, Q., & Zhou, S. (2023). Liner alliance shipping network design model with shippers' choice inertia and empty container relocation. *Electronic Research Archive*, *31*(9), 5509–5540.

Xin, X., Zhang, T., Wang, X., He, F., & Wu, L. (2025a). Risk-averse distributionally robust optimization for construction waste reverse logistics with a joint chance constraint. *Computers & Operations Research*, *173*, 106829.

Xin, X., Zhang, T., Xiang, Z., & Liu, M. (2025b). Battery electric vehicle transportation network robust pricing-infrastructure location model with boundedly rational travelers. *Applied Energy*, *386*, 125606.

Xu, Y., Chen, Q., & Quan, X. (2012). Robust berth scheduling with uncertain vessel delay and handling time. *Annals of Operations Research*, *192*, 123–140.

Yu, J., Tang, G., Voß, S., & Song, X. (2023). Berth allocation and quay crane assignment considering the adoption of different green technologies. *Transportation Research Part E: Logistics and Transportation Review*, *176*, 103185.

Zeng, Q., Hu, X., Wang, W., & Fang, Y. (2011a). Disruption management model and its algorithms for berth allocation problem in container terminals. *International Journal of Innovative Computing, Information and Control*, *7*(5), 2130–2142.

Zeng, Q., Yang, Z., & Hu, X. (2011b). Disruption recovery model for berth and quay crane scheduling in container terminals. *Engineering Optimization*, *43*(9), 967–983.

Zhang, G., Jia, N., Zhu, N., He, L., & Adulyasak, Y. (2023). Humanitarian transportation network design via two-stage distributionally robust optimization. *Transportation Research Part B: Methodological*, *176*, 102805.

Zhang, Q., Zeng, Q., & Yang, H. (2016). A lexicographic optimization approach for berth schedule recovery problem in container terminals. *Transport*, *31*(1), 76–83.

Zhang, T., Wang, S., & Xin, X. (2025). Liner fleet deployment and slot allocation problem: A distributionally robust optimization model with joint chance constraints. *Transportation Research Part B: Methodological*, *197*, 103236.

Zhang, Z.-H., & Li, K. (2015). A novel probabilistic formulation for locating and sizing emergency medical service stations. *Annals of Operations Research*, *229*, 813–835.

Zhao, C., & Guan, Y. (2018). Data-driven risk-averse stochastic optimization with Wasserstein metric. *Operations Research Letters*, *46*(2), 262–267.

Zhao, Y., Chen, Z., Lim, A., & Zhang, Z. (2022). Vessel deployment with limited information: Distributionally robust chance constrained models. *Transportation Research Part B: Methodological*, *161*, 197–217.

Zhen, L. (2015). Tactical berth allocation under uncertainty. *European Journal of Operational Research*, *247*(3), 928–944.

Zhen, L., & Chang, D.-F. (2012). A bi-objective model for robust berth allocation scheduling. *Computers & Industrial Engineering*, *63*(1), 262–273.

Zhen, L., Lee, L. H., & Chew, E. P. (2011). A decision model for berth allocation under uncertainty. *European Journal of Operational Research*, *212*(1), 54–68.

Zhou, P., Kang, H., & Lin, L. (2006). A dynamic berth allocation model based on stochastic consideration. *2006 6th World congress on intelligent control and automation*, Dalian, China.

Zurheide, S., & Fischer, K. (2012). A revenue management slot allocation model for liner shipping networks. *Maritime Economics & Logistics*, *14*, 334–361.

Zurheide, S., & Fischer, K. (2015). Revenue management methods for the liner shipping industry. *Flexible Services and Manufacturing Journal*, *27*, 200–223.

Zymler, S., Kuhn, D., & Rustem, B. (2013). Distributionally robust joint chance constraints with second-order moment information. *Mathematical Programming*, *137*, 167–198.